



THE UNIVERSITY *of* EDINBURGH

This thesis has been submitted in fulfilment of the requirements for a postgraduate degree (e.g. PhD, MPhil, DClinPsychol) at the University of Edinburgh. Please note the following terms and conditions of use:

- This work is protected by copyright and other intellectual property rights, which are retained by the thesis author, unless otherwise stated.
- A copy can be downloaded for personal non-commercial research or study, without prior permission or charge.
- This thesis cannot be reproduced or quoted extensively from without first obtaining permission in writing from the author.
- The content must not be changed in any way or sold commercially in any format or medium without the formal permission of the author.
- When referring to this work, full bibliographic details including the author, title, awarding institution and date of the thesis must be given.

**Inner nuclear membrane
proteins:**
***Targeting and influence on
genome organization***

Nikolaj Zuleger



Thesis presented for the degree of Doctor of Philosophy

University of Edinburgh

February 2012

DECLARATION

I declare that this thesis has been composed by myself and the work presented herein is my own, except where stated otherwise. This research has not been submitted for any other degree except as specified.

Nikolaj Zuleger

Edinburgh

February, 2012

ACKNOWLEDGEMENTS

I would like to sincerely thank Eric, my Doktorvater, for his invaluable guidance and enthusiasm and for giving me the opportunity to start and develop exciting projects in the lab. Thank you for always making time for me and helping me to progress both personally and scientifically.

Thank you to my PhD committee, particularly Bill and Lea for their valuable advice and stimulating discussions.

Many thanks also to the Bickmore lab, in particular Wendy and Shelagh, for a great and productive collaboration.

I would also like to thank the members of the Schirmer and Earnshaw labs, past and present, for helpful suggestions and help and for being a fun and enjoyable company both in and beyond the lab.

Many thanks to the Sawin and Stancheva labs for sharing reagents.

Thank you to Dave and Al from the COIL facility for your help to analyze gigabytes of data.

Many thanks also to the Wellcome Trust for funding.

My warmest gratitude goes to my family, who has been always supportive through all these years.

Special thanks also to Olga for all her patience and support.

Thank you all

ABBREVIATIONS

ATP	adenosine-5'-triphosphate	min	minute(s)
bp	base pairs	mRFP	monomeric red fluorescent protein
BSA	bovine serum albumine	N	Asparagine
cDNA	complementary DNA	NE	nuclear envelope
ChIP	chromatin immunoprecipitation	NET	nuclear envelope transmembrane protein
CMV	cytomegalovirus	NLS	nuclear localization signal
D	Aspartate	NPC	nuclear pore complex
Da	Dalton	Nup	nucleoporin
DAPI	4',6'-diamidino-2-phenylindole	ONM	outer nuclear membrane
DNA	deoxyribonucleic acid	Q	Glutamine
dNTP	deoxynucleotide triphosphate	PA	(GFP-) Photoactivation
E	Glutamate	PBS	phosphate buffered saline
EDTA	ethylenediaminetetraacetic acid	PCR	polymerase chain reaction
ER	endoplasmic reticulum	pH	$-\log_{10}(a_{H^+})$
FISH	fluorescence <i>in situ</i> hybridization	RNA	ribonucleic acid
FRAP	Fluorescence recovery after Photobleaching	RNAi	RNA interference
GFP	green fluorescent protein	RT-PCR	reverse transcription PCR
HP1	heterochromatin protein 1	SDS	sodium-dodecyl sulfate
IF	immunofluorescence	SSC	saline sodium citrate
INM	inner nuclear membrane	siRNA	short interfering RNA
K	Lysine	SV40	simian virus 40
kb	kilobase(s)	U	enzyme units
L	Leucine	WB	Western blotting
lacO	lac operator		
lacI	lac repressor		
LBR	lamin B receptor		

LIST OF FIGURES

Fig.	Title	Page
1	<i>Schematic of the nuclear envelope (NE)</i>	3
2	<i>The lateral diffusion-retention hypothesis</i>	5
3	<i>ATP- and GP210-dependent translocation of INM proteins</i>	8
4	<i>Speculative models of classical NPC-mediated transport of INM proteins</i>	11
5	<i>NET translocation through the central channel of the NPC</i>	13
6	<i>The Rab1 configuration</i>	18
7	<i>Experimental testing of the two models for chromosome positioning in the interphase nucleus</i>	19
8	<i>Chromosomes in interphase nuclei occupy specific territories</i>	20
9	<i>Non-random and tissue-specific positions of chromosome territories within the nucleus</i>	21
10	<i>NE proteins interact with chromatin proteins</i>	23
11	<i>Chromatin can be tethered to the nuclear periphery by an affinity mechanism</i>	26
12	<i>Radial positioning of genes and their transcriptional activity during differentiation</i>	28
13	<i>Large-scale chromatin rearrangements during differentiation</i>	30
14	<i>Wide range of NET recovery rates in the NE</i>	58
15	<i>Mobile fractions of NETs in the NE and the ER as assessed by FRAP experiments</i>	59
16	<i>Schematic of the photoactivation (PA) experiment in order to distinguish NE-NE movement from ER-NE translocation</i>	61
17	<i>PA experiments distinguish NE-NE movement from the ER-NE translocation</i>	62
18	<i>ER-NE translocation is faster than NE-NE movement (Quantification of PA experiments as described in figures 17 and 18)</i>	64
19	<i>Electron microscopy reveals the ONM and INM distribution of exogenously expressed GFP-NETs</i>	67
20	<i>SUN2 and emerin require ATP for translocation</i>	69
21	<i>The nucleoplasmic domain of emerin is required for its ATP-dependent translocation</i>	70

22	<i>Emerin and SUN2 require ATP also for the mobility within the ER</i>	71
23	<i>Depletion of Ran function affects LBR translocation</i>	72
24	<i>ATP and Ran requirement pathways for NET translocation act independently from one another</i>	73
25	<i>Ran-mediated translocation is not dependent on <u>n</u>uclear <u>l</u>ocalization sequences (NLS)</i>	76
26	<i>NE distribution of Sec61β, NLS-Sec61β and LBR with and without Ran function depletion</i>	78
27	<i>Addition of Phenylalanine-Glycines (FGs) does not confer Ran-dependence for translocation of NETs into the INM.</i>	79
28	<i>Addition of FGs enhances translocation of INM proteins</i>	80
29	<i>FGs are enriched in NETs</i>	81
30	<i>Nucleoporin Nup35 affects translocation of some NETs</i>	83
31	<i>Screen for NETs that can reposition a marked interior locus to the nuclear periphery</i>	87
32	<i>Algorithm for unbiased determination of the lacO array position</i>	88
33	<i>Some NETs can reposition the lacO array-containing chromosome 5</i>	89
34	<i>Some NETs can reposition the lacO array-containing chromosome 13</i>	91
35	<i>Conformation of the lacO array repositioning effects by replicates of the positives against negative controls</i>	92
36	<i>Chromosome repositioning effects caused by NETs are not due to general chromatin distribution towards the nuclear periphery</i>	93
37	<i>Affirmation that the whole chromosome is moving to the nuclear periphery</i>	94
38	<i>Chromosome 5 repositioning towards the nuclear periphery is recapitulated in cells stably expressing the NETs but lacking the lacO array</i>	96
39	<i>Quantification of Chromosome 5 repositioning in cells stably expressing NETs but lacking the lacO array</i>	98
40	<i>Localization of chromosomes 1, 11, 13, 17 and 19 upon stable NET expression</i>	100
41	<i>3-dimensional (3D) erosion algorithm for determination of the spatial chromosome position</i>	102
42	<i>3D algorithm confirms the results of the 2D method</i>	104
43	<i>Chromosome repositioning NETs can co-immunoprecipitate a chromatin fraction - NET-mediated repositioning of chromosomes is likely direct</i>	106
44	<i>Soluble fragments of NETs that reposition chromosomes</i>	107
45	<i>Soluble fragments of chromosome-tethering NETs fail to reposition</i>	108

	<i>chromosome 5 to the nuclear periphery</i>	
46	<i>NETs that reposition chromosomes are tissue-specific</i>	113
47	<i>Chromosome 5 is more peripheral in human liver than in kidney</i>	114
48	<i>Knockdown of liver-specific proteins NET45 and NET47 in HepG2 liver cells</i>	115
49	<i>Peripheral localization of chromosome 5 is reduced in HepG2 liver cells depleted from liver-specific NET45 and NET47</i>	116
50	<i>Up- and down-regulated genes in cell lines stably expressing the chromosome-repositioning NETs</i>	119
51	<i>Overlap with a hepatic differentiation system in up-regulated genes is strong for NET47, intermediate for NET29 and weak for NET39</i>	122
52	<i>Strong enrichment of differentially expressed genes associated with aspects of development and differentiation was observed in cells stably expressing chromosome repositioning NETs</i>	123
53	<i>Stable cell lines of soluble NET fragments do not recapitulate gene changes caused by the full-length proteins</i>	124
54	<i>Artificial chromosome 5 tethering mimics only partially the expression profile of chromosome tethering NET cell lines</i>	125
55	<i>Different mechanisms target NETs to the INM</i>	136
56	<i>Are NETs using peripheral or central NPC channels to translocate into the INM?</i>	141
57	<i>NETs that bind transport receptors could be “seeded” into the future INM during mitosis</i>	142
58	<i>Hypothetical models of chromosome repositioning</i>	148
59	<i>Simple model of chromosome position regulation by NETs</i>	149
60	<i>Speculative affinity mechanism to establish spatial chromosome organizational patterns</i>	152
61	<i>Possible mechanisms for gene regulation by the NE</i>	158

LIST OF TABLES

Table	Title	Page
1	<i>Primary antibodies used in this study</i>	37
2	<i>Secondary antibodies used in this study</i>	38
3	<i>Whole chromosome paints used in this study</i>	39
4	<i>Commercial Kits used in this study</i>	40
5	<i>Primers used in this study</i>	41
6	<i>Parameters of previous FRAP studies on NE protein mobility of emerin, LAP2β and MAN1</i>	55
7	<i>NE FRAP $t_{1/2}$s and $t_{1/2}$s for ER-NE translocation and NE-NE movement as measured by PA</i>	65
8	<i>NET51, NET55 and emerin NLS scores before and after fusion to LBR-NLS or SV40 NLS</i>	74
9	<i>The top ten down-regulated genes upon knockdown of NET45 and NET47 in HepG2 liver cells are linked to liver function</i>	120
10	<i>Distinct pools of NETs</i>	130-131

ABSTRACT

The nuclear envelope is a complex double membrane system that separates the activities of the nuclear and cytoplasmic compartments. A recent explosion in the number of proteins associated with this subnuclear organelle together with it now being linked to over 2 dozen diseases indicates the importance of better understanding its functional organisation. This thesis addresses two important questions for this: how do integral proteins of the nuclear envelope get to their sites of function and do any of these proteins direct genome organisation? To address the first question I used FRAP and photoactivation methods to find that different proteins use at least 4 distinct mechanisms to reach the inner nuclear membrane. Some appeared to be translocated by simple unaided lateral diffusion in the membrane while others needed Ran GTPase activity, others ATP, some others were aided by phenylalanine/glycines (FGs). Both Ran and FG mechanisms required the nucleoporin Nup35, albeit the mechanisms appeared to be completely independent of one another. To investigate the role of the nuclear envelope in genome organization, I screened for nuclear envelope proteins that reposition particular chromosomes to the nuclear periphery, finding five with this function. Interestingly, all of the proteins with this effect are tissue-specific. Depletion of two liver-specific nuclear envelope proteins reversed their effects on a specific chromosome for positioning with respect to the nuclear periphery. Finally, exogenous expression of these proteins in tissue culture cells caused induction of genes involved in differentiation pathways.

CONTENTS

DECLARATION.....	II
ACKNOWLEDGMENTS.....	III
ABBREVIATIONS.....	IV
LIST OF FIGURES.....	V-VII
LIST OF TABLES.....	VIII
ABSTRACT.....	IX

Chapters

Chapter 1 - Introduction.....	1-34
1.1 The nuclear envelope architecture	1-3
1.2 Trafficking of nuclear membrane proteins to the INM.....	3-16
1.2.1 The lateral diffusion-retention mechanism	5-6
1.2.2 ATP and temperature dependence for INM translocation/ gated diffusion into the INM	7-8
1.2.3 A classical NPC-mediated pathway	8-13
1.2.4 Involvement of nucleoporins in targeting of INM proteins.....	14-16
1.3 Genome organization from the NE?	17-34
1.3.1 Nuclear periphery and genome organization.....	17-22
1.3.2 NE proteins can interact with chromatin components – Implication for NE-mediated chromosome organization.....	22-24
1.3.3 What are the mechanisms that direct cell-type specific chromosome organization patterns?	24-26

1.3.4	Gene regulation as a consequence of radial chromosome repositioning	27-28
1.3.5	Differentiation, chromosome/gene repositioning and gene activity – The bigger picture.....	28-34
1.4	Preview	34
Chapter 2 - Material and Methods		35-53
2.1	Materials	35-40
2.2	Methods.....	41-53
2.2.1	Nucleic acid methods	41-44
2.2.1.1	Polymerase chain reaction.....	41-42
2.2.1.2	Sequencing of plasmid DNA	42
2.2.1.3	Isolation of total cellular RNA	42-43
2.2.1.4	Reverse transcriptase PCR	43
2.2.1.5	Biotin labelling of total RNA and microarray analysis	44
2.2.2	Protein techniques.....	44-46
2.2.2.1	Western blotting.....	44-45
2.2.2.2	Chromatin IP (ChIP) procedure.....	45-46
2.2.3	Tissue culture methods.....	46-48
2.2.3.1	Mammalian cell maintenance and transfection	46
2.2.3.2	Establishment of stable cell lines	46
2.2.3.3	ATP depletion in HeLa cells	46-47
2.2.3.4	Ran function depletion in HeLa cells.....	47

2.2.3.5	Nup35 depletion in HeLa cells.....	47
2.2.3.6	Knockdown of NET45 and NET47 in HepG2 liver cells	47-48
2.2.4	Microscopy methods, image processing and analysis	48-53
2.2.4.1	Fluorescence recovery after photobleaching (FRAP)	48
2.2.4.2	GFP-photoactivation (GFP-PA)	49
2.2.4.3	Indirect immunofluorescence techniques and imaging analysis.....	49-50
2.2.4.4	Fluorescence <i>In Situ</i> Hybridization (FISH)	50-51
2.2.4.5	FISH on human biopsy tissue sections.....	51-52
2.2.4.6	Image generation, image processing and statistics.....	52
2.2.4.7	Algorithm for dividing the nuclear area into 5 concentric rings	52
2.2.4.8	2D and 3D chromosome positioning analysis algorithms	53

Chapter 3 - Targeting of membrane proteins to the INM is mediated by multiple mechanisms..... 54-84

3.1	How to study membrane protein translocation into the nucleus.....	55-59
3.2	FRAP in the NE is predominantly measuring ER-INM translocation	60-68
3.3	Distinct translocation requirements for distinct NETs.....	68-73
3.4	Ran-mediated translocation is independent of NLSs or FGs	74-79

3.5	FGs are enriched in INM proteins and facilitate their translocation	80-81
3.6	Ran- and FG-mediated pathways require Nup35	82-83
3.7	Summary of chapter 3	84

Chapter 4 - NETs can reposition chromosomes to and from the nuclear periphery 85-109

4.1	A screen to identify NETs that reposition chromosomes	86-94
4.2	Recapitulation of NET-mediated chromosome tethering in cells lacking the lacO array and repositioning analysis of additional chromosomes.....	95-104
4.3	NETs can precipitate a chromatin fraction and only full-length NETs can reposition chromosomes - Further proof of NET-mediated chromosome repositioning	105-108
4.4	Summary of chapter 4	109

Chapter 5 - Tissue-specific NETs can mediate a spatial chromosome positioning that correlates with that in tissues 110-117

5.1	Chromosome repositioning NETs are tissue-specific.....	111-113
5.2	Chromosome positioning correlates with tissue-specificity of NETs	114
5.3	NET-mediated tissue-specific chromosome positioning is reversible.....	115-116

5.4	Summary of chapter 5	117
Chapter 6 - NET-mediated chromosome repositioning promotes tissue-specific gene gene expression		118-127
6.1	NET-mediated chromosome repositioning affects global gene expression	118-120
6.2	Differentially expressed genes in NET cell lines partly overlap with gene changes in differentiation systems.....	121-123
6.3	Transcriptome changes mediated by the full-length NETs are not recapitulated by their soluble fragments	123-124
6.4	Artificial <i>versus</i> NET-mediated chromosome repositioning.....	124-125
6.5	Summary of chapter 6	126-127
Chapter 7 - Discussion.....		128-159
7.1	What determines the steady state levels of NETs in FRAP and PA experiments?.....	129-133
7.2	Multiple independent mechanisms co-exist for translocation of NETs into the INM.....	133-136
7.3	The Ran-mediated mechanism is independent of NLSs	137
7.4	The FG-facilitated mechanism suggests that INM proteins can act as their own transport receptors	138-139

7.5	What determines which pathway is utilized?.....	139-140
7.6	Peripheral versus central channel translocation.....	140-143
7.7	Tissue-specific NETs mediate chromosome repositioning	144-146
7.8	Direct versus indirect NET-chromosome interaction.....	146-150
7.9	Does chromosome repositioning occur in mitosis or interphase.....	150-153
7.10	Changes in gene activity upon chromosome and gene repositioning.....	153-156
7.11	Functional consequences of NET-mediated gene repositioning – tissue-specific genes are regulated	156-158
7.12	Final remarks	159
REFERENCES.....		160-171
APPENDIX.....		172-184

Chapter 1

Introduction

1.1 The nuclear envelope architecture

The Nuclear Envelope (NE) is the landmark that is used to distinguish eukaryotes from prokaryotes. It forms the physical barrier between the nucleus and the cytoplasm. Our ability to distinguish this feature emerged from advances in microscopy. In 1931 the German physicist Ernst Ruska developed the electron microscope which revolutionized the field of cell biology as with the help of this device one was able to study cellular structures at a super magnification. So it was in 1950 that Callan and Tomlin performed electron microscopy on amphibian oocytes to reveal that the NE is a double membrane system (Callan and Tomlin, 1950). The 2 membranes, the outer (ONM) and inner nuclear membrane (INM), are connected at sites where the nuclear pore complexes (NPCs) are inserted (Figure 1). NPCs mediate directional transport between the cytoplasm and the nucleus for soluble molecules larger than ~40 kDa [reviewed in (D'Angelo and Hetzer, 2006; D'Angelo and Hetzer, 2008)]. The ONM is continuous with the endoplasmic reticulum (ER) and is studded with ribosomes (Franke et al., 1981; Gerace and Burke, 1988; Watson, 1955). Many proteins reside in both ONM and the ER; however there is evidence that some proteins localize uniquely to the ONM but not the ER [reviewed in (Schirmer and Foisner, 2007)]. The ONM and INM are separated by a uniformly thick (30-50 nm) luminal compartment, called the perinuclear space. Some proteins that stretch from the ONM and the INM into the perinuclear space interact with each other, thus forming a connection between the cytoplasm and the

nucleoplasm (Figure 1). The INM contains a unique set of membrane-associated and integral proteins most of which have been identified only recently in several separate proteomic studies (Dreger et al., 2001; Korfali et al., 2010; Schirmer et al., 2003; Wilkie et al., 2011). Some of these specific INM proteins interact with the lamin polymer and with chromatin [reviewed in (Mattout-Drubezki and Gruenbaum, 2003)].

Underlying the INM is the nuclear lamin polymer (Figure 1). The nuclear lamina is operationally defined as the intermediate filament lamin polymer together with those proteins integral to the membrane that resist biochemical extraction when the lipid membrane is removed with detergent (Dwyer and Blobel, 1976). Mutations in both lamins and several NE transmembrane proteins (NETs) cause a variety of human diseases, each with distinct and restricted tissue pathologies [reviewed in (Worman and Bonne, 2007)]. As the proteins linked to such diseases are widely expressed, it has been proposed that partner proteins with more restricted tissue distribution contribute to pathology (Schirmer and Gerace, 2005; Wilkie and Schirmer, 2006). The loss of interaction between NE proteins and those partner proteins could result in aberrant signalling leading to gene misregulation and subsequent cellular deficits that ultimately lead to tissue pathologies.

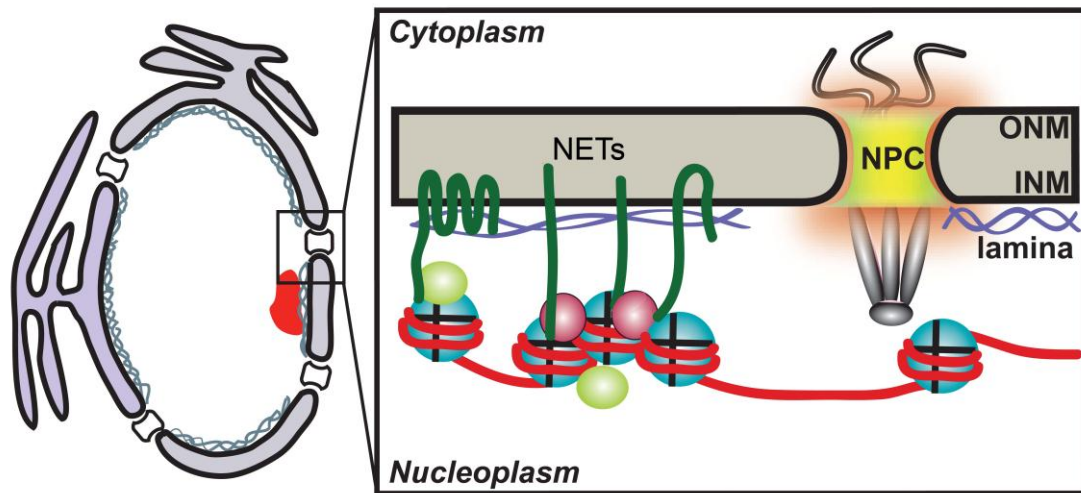


Figure 1. Schematic of the nuclear envelope (NE). The NE consists of the outer (ONM) and inner (INM) nuclear membranes both of which are connected in spots where nuclear pore complexes (NPCs) are inserted. The NPCs regulate the nucleo-cytoplasmic transport of macromolecules. An intermediate polymer consisting of lamin proteins (blue) underlines the INM. The INM harbours a unique set of membrane proteins (NETs), which together with the lamin polymer are referred to as the lamina. Lamins, NETs and nucleoplasmic NPC proteins are known to interact with chromatin components such as histone proteins. (Figure adapted from Zuleger and Schirmer, 2011)

1.2 Trafficking of nuclear membrane proteins to the INM

The transport of soluble cargos from the cytoplasm into the nucleoplasm has been extensively studied [reviewed in (Gorlich and Kutay, 1999; Stewart, 2007)]. This process occurs through the central channel of the NPC and involves transport receptors termed karyopherins or importins which are interacting with both cargos and phenylalanine/glycine(FG)-containing proteins of the NPC (nucleoporins). This process additionally involves the small GTPase Ran. Protein cargos containing a classical nuclear localization signal (NLS) are imported through the central channel of the NPC by the transport receptor importin- β , which binds the cargos through the adaptor protein importin- α . In the nucleus, cargo-bound importin- β interacts

with RanGTP resulting in dissociation of the import complex and release of the cargo. Importin- β and importin- α are recycled back to the cytoplasm separately both being bound to RanGTP. Once back in the cytoplasm RanGTPase is generating RanGDP resulting in dissociation of the importins making them available for a new import cycle.

In contrast to soluble cargo transport, nuclear transport of nuclear envelope transmembrane proteins (NETs) remains less understood. The surface area of the nucleus doubles during interphase (Fry, 1976; Maul et al., 1972; Steen and Lindmo, 1978), but the density of proteins in the nuclear membrane remains largely the same. For example, the distance between the NPCs essentially does not change because new NPCs are inserted into the membrane to match the growth of the membrane (D'Angelo et al., 2006; Maul et al., 1972). This means that NETs must be continuously synthesized in the ER and translocated into the INM *via* the NPC throughout interphase. But how does this happen? The nuclear membrane is continuous with the ER but covers the whole surface of the nucleoplasm, thus forming a diffusion barrier. However, the ONM and INM fuse with each other at the pore membrane where the NPCs are inserted (Prunuske and Ullman, 2006). Electron microscopy revealed that there are ~10nm peripheral channels between the NPC and the pore membrane (Hinshaw et al., 1992; Reichelt et al., 1990) that could allow NETs to move between the INM and ONM by simple lateral diffusion. These channels have been estimated to allow transit of proteins of up to 60kDa (Hinshaw et al., 1992; Reichelt et al., 1990).

1.2.1 The lateral diffusion-retention mechanism

The development of the diffusion-retention mechanism emerged from three key findings: 1) observations that viral transmembrane proteins could diffuse freely between ER/Golgi and INM (Torrissi et al., 1987), 2) the fact that an INM protein could move between nuclei in fused heterokaryons while protein synthesis was blocked (Powell and Burke, 1990) and 3) the discovery of peripheral channels between the NPC and the pore membrane (Hinshaw et al., 1992; Reichelt et al., 1990). The diffusion-retention hypothesis postulates that INM and ER proteins rapidly diffuse between INM and ER at equilibrium, but proteins of the INM are accumulated in the INM because of their ability to bind to lamins and/or chromatin (Figure 2).

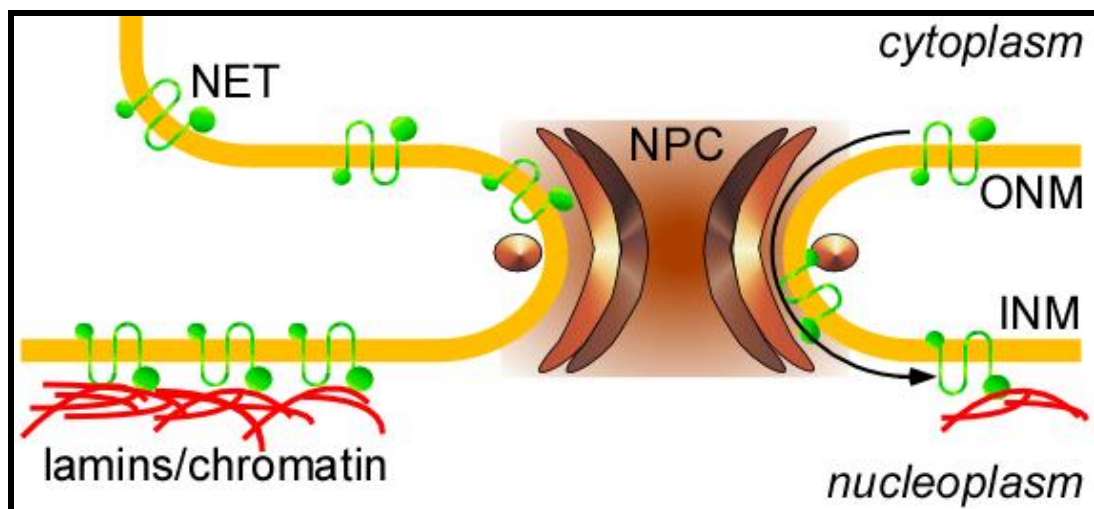


Figure 2. The lateral diffusion-retention hypothesis. After their synthesis in the ER, NETs translocate through the outer nuclear membrane (ONM) into the inner nuclear membrane (INM) using the peripheral channels of the nuclear pore complexes (NPCs). Diffusion can occur in both directions (ONM-to-INM or INM-to-ONM) but directionality is achieved through interaction of NETs with nucleoplasmic components such as lamins and/or chromatin and NETs are thus retained in the INM. (Figure adapted and modified from Malik et al., 2009)

It was Bruno Soullam and Howard Worman (Soullam and Worman, 1993) who brought these three previous findings together by phrasing and

testing this hypothesis. They used fusion proteins of the INM protein lamin B receptor (LBR), so termed because of its ability to bind to lamin B (Worman et al., 1988). The aminoterminal domain of LBR that contains the lamin binding region (Ye and Worman, 1994) was fused to the transmembrane portion of the chicken hepatic leptin, a Type II transmembrane protein that resides normally in the ER and the plasma membrane (Chiacchia and Drickamer, 1984). After fusion, the chimeric protein accumulated in the INM meaning that the ER protein diffused between the INM and ONM but asymmetry in the diffusion equilibrium in favour of INM residency was achieved through binding of the LBR portion of the chimera to lamins in the nucleoplasm. This observation was confirmed by two further studies using lamin binding sequences from the INM proteins LAP2 β (Furukawa et al., 1998) and MAN1 (Wu et al., 2002). The retention part of the model was also supported by the fact that when performing FRAP on INM membrane proteins fused to GFP pre-bleach levels were never achieved after recovery of the fluorescence (Ellenberg et al., 1997; Rolls et al., 1999; Shimi et al., 2004; Wu et al., 2002). This observation implied that a portion of the protein must be highly immobile due to interaction with nuclear components such as lamins or chromatin. Even stronger support for the retention-hypothesis came from observations that the INM protein emerin was more mobile in cells lacking its binding partner, lamin A (Ostlund et al., 2006).

1.2.2 ATP and temperature dependence for INM translocation/ gated diffusion into the INM

The Gerace laboratory demonstrated that translocation of their artificial construct (described below) was both ATP- and temperature-dependent (Ohba et al., 2004). This opened the possibility that either the diffusion-retention mechanism is not as simple as previously thought or implied the observation of a completely novel mechanism for INM protein translocation.

In this study they cloned 2 portions (the transmembrane domain and the soluble lamin-binding domain) of the NET LAP2 β and fused these portions with FRB and FKBP, respectively, both of which are interacting with each other when the drug rapamycin is present. The LAP2 β membrane domain fused to FRB could freely diffuse between the ER and the INM as it did not contain the lamin and chromatin binding portion of LAP2 β . The cells were then co-transfected with the soluble FKBP-fused LAP2 β portion containing the lamin binding site. Upon addition of the drug rapamycin the FRB and FKBP fragments interacted and the transmembrane reporter accumulated rapidly in the INM due to the gained lamin binding ability. Further, the accumulation of this construct was strongly inhibited by reduction of temperature and depletion of ATP. Also, injected antibodies against the nucleoporin GP210 restricted INM accumulation of the construct, suggesting that the translocation process into the INM could also be NPC-dependent. This also raised the possibility that GP210 being a nucleoporin that localizes in the periphery of the NPC could act as a “gatekeeper”, which would allow NETs translocate into the INM upon ATP hydrolysis.

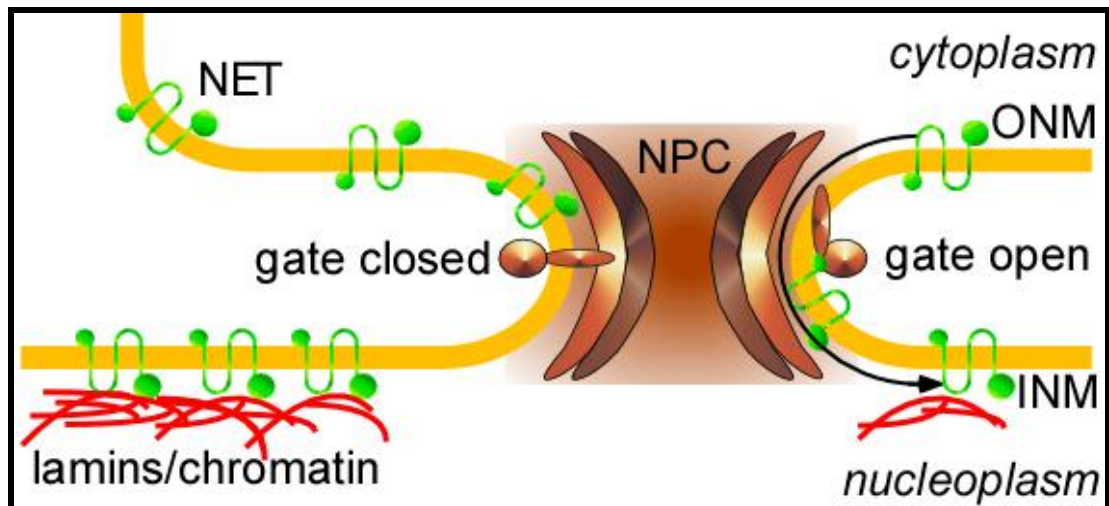


Figure 3. ATP- and GP210-dependent translocation of INM proteins. After their biogenesis in the ER INM proteins are traversing through the peripheral channels of the NPC utilizing a mechanism that requires ATP and the presence of GP210. GP210 is likely to act as a “gate” that allows some molecules to pass but blocks others from translocation. (Adapted and modified from Malik et al., 2009)

1.2.3 A classical NPC-mediated pathway

The Summers laboratory found that viral and mammalian INM proteins are integrated into the membrane co-translationally and that viral and mammalian INM proteins occupy different sites at the translocon than other membrane proteins that are not destined for the INM. This suggested that the sorting of membrane proteins begins in the ER immediately after their synthesis (Braunagel et al., 2007). More importantly, they also found that importin- α -16/KPNA-4-16, an isoform of a nuclear import receptor protein, is interacting with the INM proteins already in the ER. Together with the findings of the Gerace laboratory that the nucleoporin protein GP210 was involved in INM targeting, this finding suggested a potential involvement of the NPC and soluble transport machinery in the translocation of membrane proteins into the INM.

The Blobel laboratory followed up on these findings and specifically tested for NPC function in INM protein transport (King et al., 2006). Using yeast as a model organism, the Blobel laboratory found that disruption of the Ran cycle inhibited the targeting of NLS-containing INM proteins Heh1 and Heh2 (human homologues are MAN1 and LEM2/NET25 respectively). The effect was reversible since restoring the Ran cycle resulted again in proper targeting of the proteins to the INM. Intriguingly, they also found that transport receptors, similar to the nuclear transport of soluble proteins, were involved in the targeting of Heh1 and Heh2. This was done by demonstrating that both importin- α and importin- β 1 were responsible for the translocation of the NETs Heh1 and Heh2 as depletion of both receptors resulted in decreased localization in the INM of both NETs. Involvement of importin- α and importin- β 1 seemed to be specific for these proteins as depletion of other known transport receptors had no effect on INM targeting of Heh1 and Heh2. Intriguingly, *in vitro*, a direct interaction between importin- α and Heh2 was demonstrated whilst *in vivo* the transport was shown to be also NLS-dependent, since a mutant version of Heh2 lacking the NLS failed to localize to the INM.

Are NLSs really the determinants of the classical NPC translocation pathway for membrane proteins?

Subsequently, the Kutay laboratory found in HeLa cells that the INM protein SUN2 also harbours an NLS and had the ability to bind importin- α and importin- β *in vitro* (Turgay et al., 2010). This finding further supported the presence of a classical NPC-mediated transport of INM proteins. However, unlike in the yeast study of Heh1 and Heh2, mutation of the SUN2 NLS did not inhibit the protein targeting to the INM, suggesting that SUN2 could use an alternative pathway independent from the one involving Ran and transport receptors.

Additionally, the SUN2 study discovered another signal, a stretch of arginines that retrieved SUN2 from the Golgi-apparatus. Mutation of this

signal resulted in strong SUN2 accumulation in the Golgi. This added yet another layer of complexity to the already known mechanisms of NET INM targeting.

Are NETs translocating through the central or peripheral channels of the NPC?

The involvement of classical nuclear transport components (transport receptors and Ran) reported in the Summers, Kutay and Blobel lab studies also opened room for speculation that instead of the peripheral NPC channels (as previously assumed) NETs could actually use the central NPC channels to translocate into the INM.

A translocation of NETs through the central channel of the NPC would make sense from the point that there would be enough space in the central channel to accommodate transport receptors and Ran bound to the translocated protein. However, this scenario would most likely also involve an extraction of the NET from the membrane (Figure 4, B). Extraction would require a lot of energy and a complex system of proteins to both prevent aggregation of the hydrophobic membrane spans of the NET and to insert the NET after NPC transit (Figure 4, B).

Translocation through the peripheral channel of the NPC would make more sense from the point of energy requirement since the NET would not have to be extracted from the membrane upon hydrolysis of ATP. However, if NETs really bind transport receptors to allow their translocation, the peripheral channels could not possibly accommodate this comparatively large receptor-NET complex.

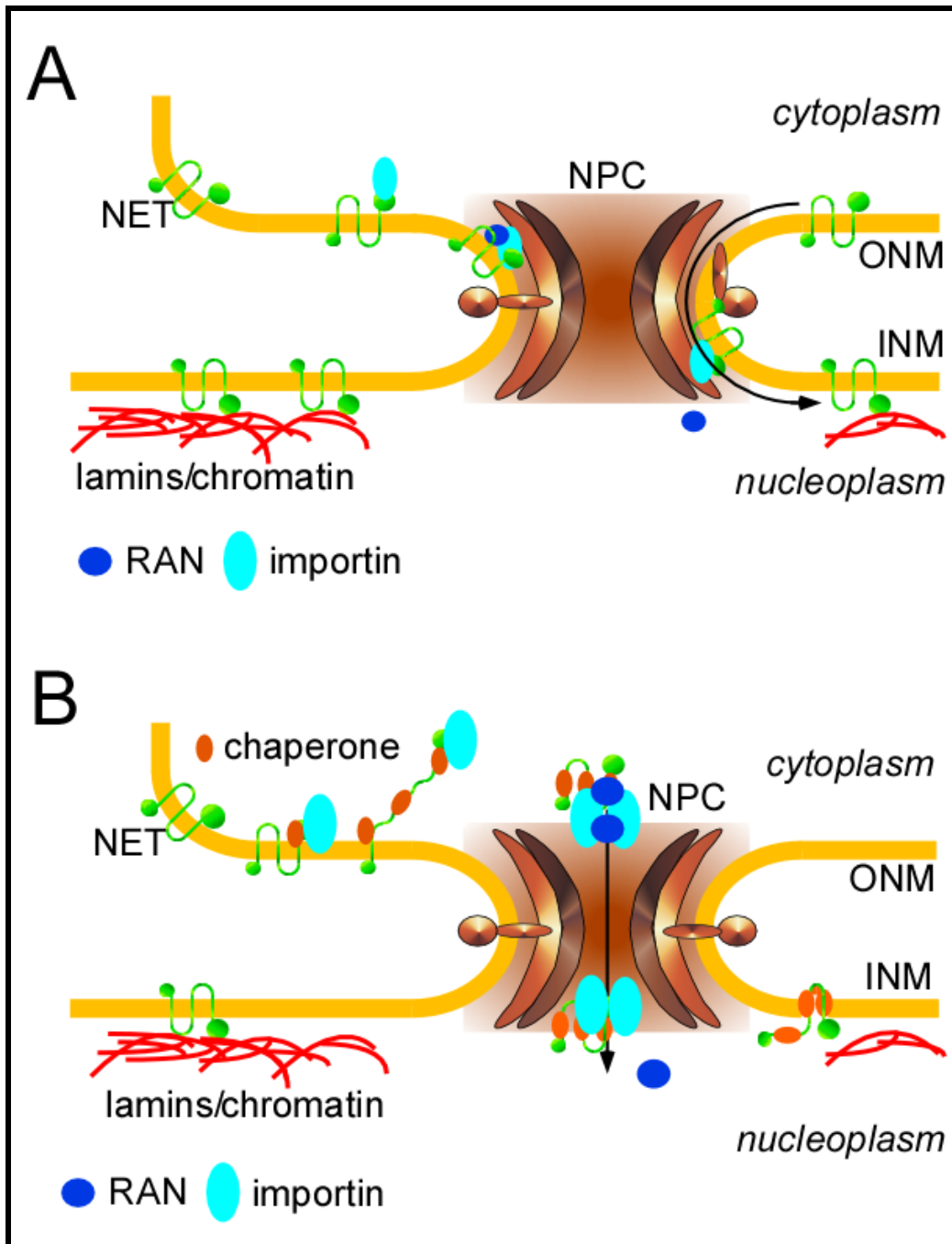


Figure 4. Speculative models of classical NPC-mediated transport of INM proteins. (A) After their synthesis in the ER NETs form a complex with transport receptor proteins (importins) and Ran, which is then traversing into the INM via the peripheral channels of the NPC. (B) After the biogenesis NETs are recognized by importins and Ran and are extracted from the lipid bi-layer with the help of chaperones to prevent aggregation of the membrane segments. The complex is then transiting into the nucleus through the central channel of the NPC. Once in the nucleus NETs are inserted into the INM. (Adapted and modified from Malik et al., 2009)

The two most recent studies from the Starr and Veenhoff laboratories argue for a scenario that seems to be in-between the two described above. Analysing the yeast INM protein Heh2 (Meinema et al., 2011) and the drosophila INM protein UNC84 (Tapley et al., 2011) both studies suggest that the NETs remain in the membrane during transport with their C-terminal portion whereas the N-terminal portion perforates the central channel of the NPC where it binds to transport receptors and Ran (Figure 5). Even though both studies claimed the scenario of using the central channels, only the yeast study (Meinema et al., 2011) addressed this question through direct experiments. In this study they fused a central channel nucleoporin and their NET construct with FRB and FKBP, respectively, both of which bind to one another when the drug rapamycin is present. After addition of rapamycin the NET construct accumulated around the nuclear pores suggesting that it localized in the central channels. Unfortunately the study did not test the specificity of the system by testing if a peripheral channel nucleoporin, like Nup35 for example, would not be able to trap the translocating NET construct.

The Drosophila study from the Starr laboratory additionally describes an INM sorting motif of UNC84 that is bound by the membrane associated truncated importin- α homologue (Figure 5), a mechanism that was earlier described by the Summers laboratory (Braunagel et al., 2007).

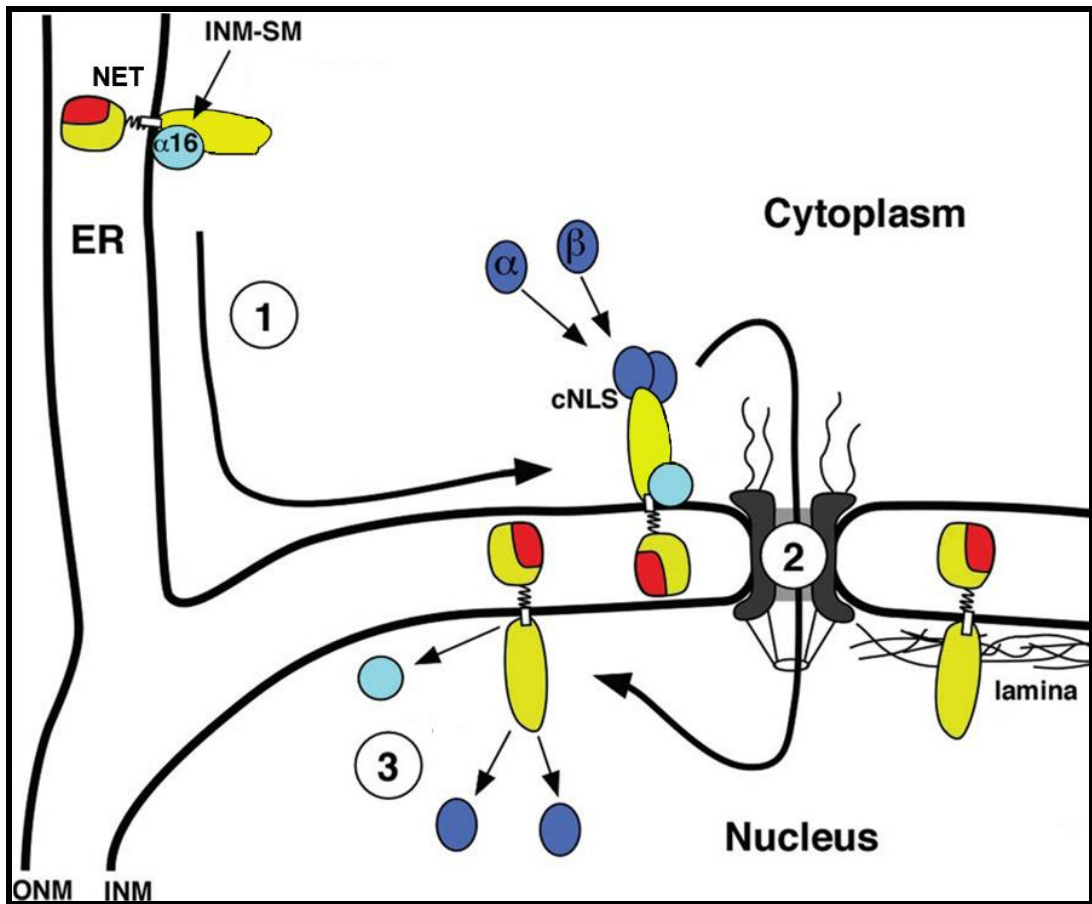


Figure 5. NET translocation through the central channel of the NPC. (1) After the synthesis in the ER NLS-containing NETs are recognized by importin- α -16, which localises the INM protein to the cytoplasmic face of the NPC. Here the transport receptors importin- α and importin- β are complementing the complex. (2) The transport receptor-bound soluble domain of the NET is then translocating through the central channel of the NPC while the membrane segment is retained at the membrane. (3) Once in the INM receptor proteins dissociate from the NET. (Figure adapted from Tapley et al., 2011)

1.2.4 Involvement of nucleoporins in targeting of INM proteins

All mechanisms for transport of NETs into the INM described above have one thing in common: they all involve passage of the NET across the NPC. It is then not surprising that several studies found specific NPC proteins, or nucleoporins, to be involved in translocation of NETs into the INM. The earlier mentioned study from the Gerace laboratory found that injection of antibodies against the nucleoporin GP210 in HeLa cells blocked transport of the INM protein and that the effect was reversible when the GP210 peptides used for the generation of this antibody were introduced into the cells (Ohba et al., 2004). GP210 is considered to locate at the peripheral channel of the NPC and sticks into the lumen that is surrounded by the ONM and INM. Thus, it was proposed that GP210 might have a gating function for INM proteins when they diffuse into or out of the nucleus.

Rick Wozniak's laboratory made the observation that when another nucleoporin, Nup155, was depleted in HeLa cells, the targeting of tested inner INM proteins like LBR, LEM2 and LAP2 β was strikingly impaired whereas the nuclear non-membrane protein lamin B was still targeting to the INM upon the Nup155 knockdown (Mitchell et al., 2010). Thus Nup155 seemed to be an additional player that regulates transport of INM proteins.

In other organisms nucleoporins were also shown to impact the import of NETs into the INM. Whilst in HeLa cells knockdown of GP210 and Nup155 was inhibiting targeting of INM proteins, in *Xenopus* egg extracts depletion of another nucleoporin, Nup188, enhanced the translocation of NETs into the INM (Theerthagiri et al., 2010). Subsequent depletion of Nup188 was also shown to promote the passage of NETs into the INM in mammalian HeLa cells (Antonin et al., 2011). These findings suggested either a direct role for Nup188 to facilitate the passage of INM proteins along the NPC or that depletion of Nup188 destabilizes the NPC, potentially resulting in enlarged peripheral channels which in turn ease translocation of NETs.

In yeast it was shown that two INM proteins, Heh1 and Heh2, required the NPC protein Nup2 but not Nup188 or Pom152 for translocation into the INM (King et al., 2006). But when the Hochstrasser lab analyzed the INM translocation requirements for another INM protein, Doa10, they found that Nup2 was not required but Nup188 and Pom152 were (Deng and Hochstrasser, 2006). This discrepancy strengthened the possibility that distinct mechanisms function for translocation of NETs to the INM. The distinct characteristics of different INM proteins are possibly the determinants that decide which pathway is utilized for transport into the nucleus. In fact this idea was supported by the fact that both Heh1 and Heh2 possess a classical NLS but Doa10 does not.

While of course the nucleoporins mentioned above could really play a specific role in the transport of at least some NETs, the transport effects, both facilitation and inhibition upon manipulation of these Nups, could also be due to general disruption of the NPC. This scenario is very likely, because the NPC is a big complex and it is not difficult to imagine that depletion of some Nups, many of which are NPC core components [for review see (Lusk et al., 2007)], from the NPC would actually destabilize the structure of this complex protein transport machine. Hence studies which manipulate Nups while testing if they are necessary for transport of NETs should also test for the specificity of the effect, for example by showing that transport of one protein is affected but another is not. Many of the studies described above were lacking these controls.

Which mechanism is correct or do several mechanisms co-exist?

Recent years have seen an explosion of players and mechanisms that could be involved in the targeting of NETs into the INM. It is, however, not clear if different independent mechanisms work in parallel or whether they are all part of a complex unifying mechanism. The existence of multiple mechanisms, for example, would enable essential NETs to reach the INM

when a favoured mechanism is inhibited or overloaded. All studies described above were also only investigating one or two proteins, hence a reliable conclusion concerning the total pool of NETs and their requirement for a particular mechanism cannot be made. Clearly, a more systematic study sampling a large number of proteins under the same experimental conditions and testing for different requirements would resolve this question.

In the last 20 years we have learned a lot about translocation of NETs into the INM but also several new key questions appeared, many of which will be addressed in this study. Discovering all the details of this translocation process is particularly important since improper targeting of many NETs has been associated with several human inherited diseases.

1.3 Genome organization from the NE?

Once the NETs are in the INM they orchestrate several crucial cellular functions one of which is the organization of chromatin. Thus the second part of my thesis will deal with NET-mediated spatial genome organization.

1.3.1 Nuclear periphery and genome organization

Chromatin organization within the interphase nucleus is not random. Early electron microscopy revealed darker stained areas of dense chromatin within the interphase nucleus (Moses, 1956), that were termed heterochromatin. These areas tend to be proximal to the NE in most cell types although this dense chromatin is also present at nucleoli and centromeres. In contrast to the centromeric heterochromatin, the amount of which varies very little between different cell types, the amount of dense chromatin at the NE differs substantially from one cell type to another (Milner, 1969). These observations implied a non-random organization of chromatin. In fact, the phenomenon of non-random organization of chromatin was already observed by Carl Rabl long before the electron microscopy era over a century ago. Studying salamander larvae he found that centromeres are located at one side of the nucleus, usually close to the centrosome (Figure 6, left), even though the centrosome localized outside the nucleus (Rabl, 1885). This special chromatin configuration was later coined after its discoverer. The Rabl configuration also ascribes the phenomenon where telomeres are associated with one side of the nucleus (Figure 6, right).

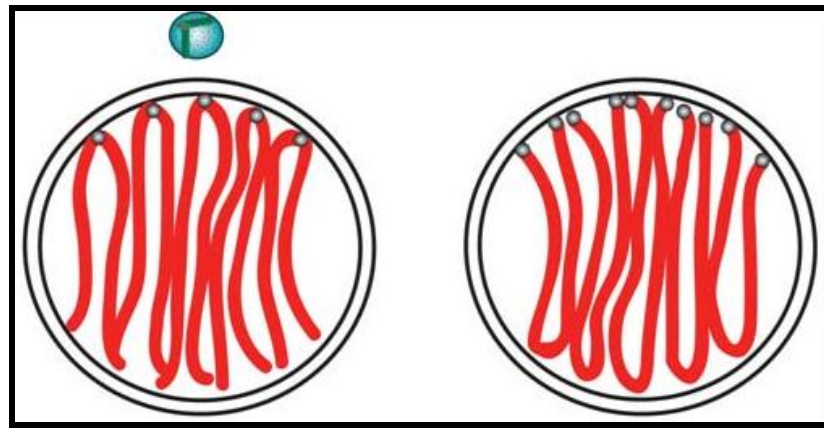


Figure 6. The Rabl configuration. Centromeres are accumulating at the pole of the nucleus where the centrosome is proximal (left) or telomeres localize to one side of the nucleus (right). (Figure adapted from Zuleger and Schirmer, 2011)

Also work from Theodor Boveri suggested that the genome is not randomly organized. He made the first observation that chromosomes occupy specific conformations within the interphase nucleus (Boveri, 1909) and thus proposed the concept of distinct chromosomal territories within the interphase nucleus. It was only 70 years later when a definitive study performed by Thomas and Christoph Cremer provided experimental evidence that chromosomes are not randomly organized within the interphase nucleus (Zorn et al., 1979). In this study DNA damage was induced with a microlaser in a small part of the cell nucleus under the experimental rationale that, if chromosomes are randomly organized and thus strongly intermingled with each other with no defined territories, then the laser will damage many or possibly all chromosomes (Figure 7, left). However, if organized in isolated non-overlapping territories, the laser will damage only a few chromosomes (Figure 7, right). The study found that only very few chromosomes were damaged by the laser, implying that indeed chromosomes are occupying compact regions within the interphase nucleus, the chromosome territories.

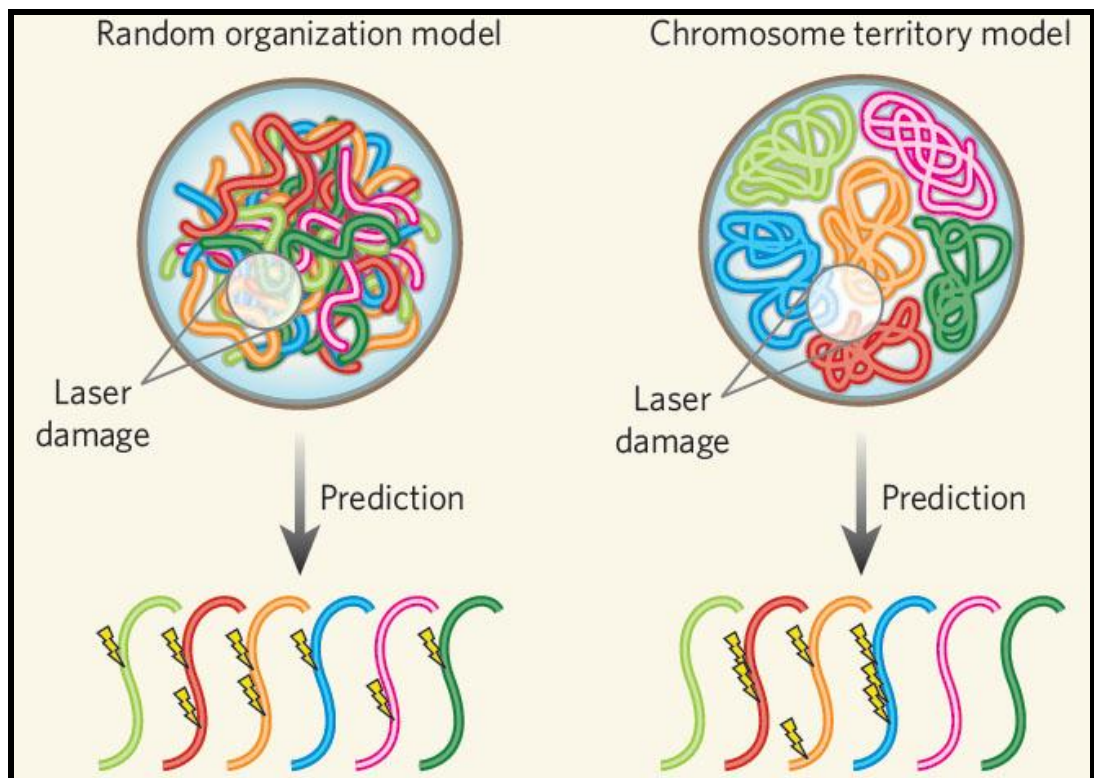


Figure 7. Experimental testing of the two models for chromosome positioning in the interphase nucleus. A laser pulse is damaging a small region of the nucleus. If the chromosomes in the nucleus are randomly organized and strongly intermingled, many of them or even all will be damaged by the laser (left). If chromosomes are organized in distinct non-overlapping territories, the laser will damage only few chromosomes (right). (Image adapted from Meaburn and Misteli, 2007)

However, the visualization of such chromosome territories could only be realized later when high resolution microscopy combined with fluorescence *in situ* hybridization (FISH) techniques were developed [(Schardin et al., 1985); Figure 8].

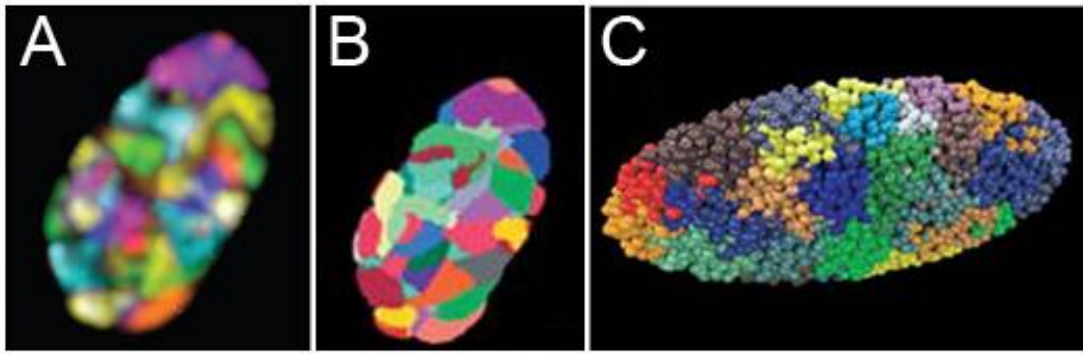


Figure 8. Chromosomes in interphase nuclei occupy specific territories. (A) Micrograph of a nucleus where all individual chromosomes are visualized. (B) False colour image of all chromosomes in a nucleus. (C) Modelling of the chromosome territories by a computer algorithm. (Panel A adapted from Hubner and Spector, 2010 and is originally from Andreas Bolzer and Irina Solovei; panel B and C adapted from Bolzer et al., 2005)

But are these territories themselves randomly organized within the nucleus or do chromosomes occupy particular regions within the 3-dimensional nuclear framework? This question was addressed by the Bickmore laboratory in a study which demonstrated that in human fibroblasts chromosome 18 tends to locate to the nuclear periphery while chromosome 19 tends to be internal [Figure 9, A; (Croft et al., 1999)]. Intriguingly, since the peripheral chromosome 18 was gene-poor and the interior chromosome 19 gene-rich it was proposed that gene-density might play a role in determining whether a chromosome is located in the nuclear interior or at the nuclear periphery. Later, the Misteli laboratory confirmed this non-random organization of the chromosome territories when they demonstrated that chromosomes that are most commonly involved in tissue-specific tumor translocations tend to be adjacent to one another in these particular tissues (Parada et al., 2002).

Later, spatial positions of chromosome territories were shown to vary between different tissues (Parada et al., 2004; Stadler et al., 2004), showing that in mouse, for example, chromosome 5 is at the nuclear periphery in lung cells but in the interior in liver cells [Figure 9, B; (Parada et al., 2004)].

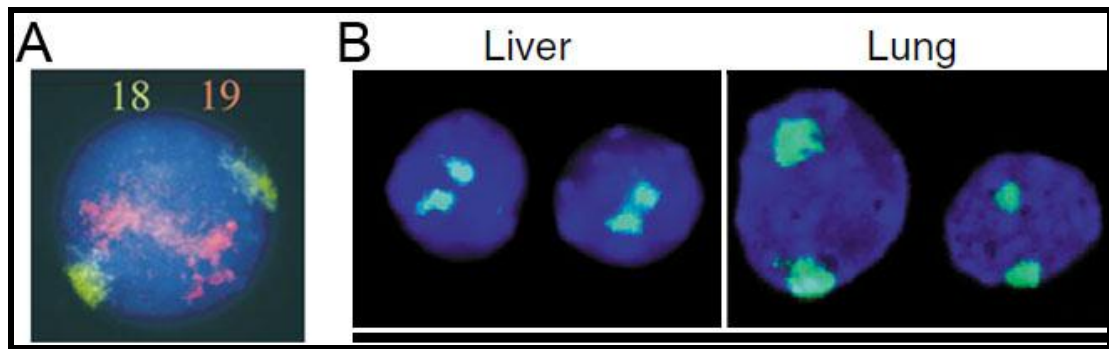


Figure 9. Non-random and tissue-specific positions of chromosome territories within the nucleus. (A) In human cells chromosome 18 (green) tends to reside at the nuclear periphery while chromosome 19 localizes in the nuclear interior. **(B)** In mouse chromosome 5 is in the interior in liver cells but peripheral in lung cells. (panel A is adapted from Croft et al., 1999; panel B is adapted from Parada et al., 2004)

Moreover, it seems that tissue-specific chromosome patterning is established during differentiation since repositioning of chromosomes was observed in adipogenesis (Kuroda et al., 2004; Szczerbal et al., 2009), erythroid (Galiova et al., 2004) and T-cell differentiation (Kim et al., 2004). Furthermore, the idea that specific chromosome patterning is established during differentiation is also coherent with general assumption that chromatin is generally less specifically organized in undifferentiated cells. Interestingly, the observations that chromosome positions differ between cell-types and also change during differentiation questioned the previously established proposal that gene-density determines the chromosomes' 3-dimensional position. Since gene-density of a chromosome is a factor that remains constant during differentiation, clearly other factors, likely being tissue-specific themselves, must be involved in the tissue-specific spatial organization of chromosomes.

With the evidence of non-random chromosome positioning clearly established, the question arose:

How do chromosomes find their specific place within the nucleus?

1.3.2 NE proteins can interact with chromatin components – Implication for NE-mediated chromosome organization

Previous studies have shown that a small portion of an internal chromosome can stretch out to interact with the nuclear periphery (Kupper et al., 2007), indicating that NE components could contribute to particular organizational patterns of chromosomes within the interphase nucleus. It was not surprising since several NE proteins *can* bind chromatin and chromatin related components [Figure 10; reviewed in (Mattout-Drubezki and Gruenbaum, 2003)]. Lamins, for example, bind chromatin structures like telomeres and centromeres (Baricheva et al., 1996; Shoeman and Traub, 1990) and interact with core histones H2A and H2B (Goldberg et al., 1999; Hoger et al., 1991; Taniura et al., 1995).

NETs can also bind DNA directly. LAP2 β binds DNA *via* its N-terminal domain (Cai et al., 2001) while another NET, MAN1, binds DNA by its C-terminus (Caputo et al., 2006). The vast majority of NET interactions reported thus far have been with chromatin proteins or chromatin associated components. The lamin B receptor binds core histones H3 and H4 (Polioudaki et al., 2001) and can bind heterochromatin *via* heterochromatin proteins HP1 α and γ (Ye and Worman, 1996). LEM domain-containing proteins LAP2 β (Furukawa, 1999), emerin (Lee et al., 2001) and MAN1 (Mansharamani and Wilson, 2005) bind to chromatin *via* BAF (barrier-to-autointegration factor), which itself is a chromatin binding protein.

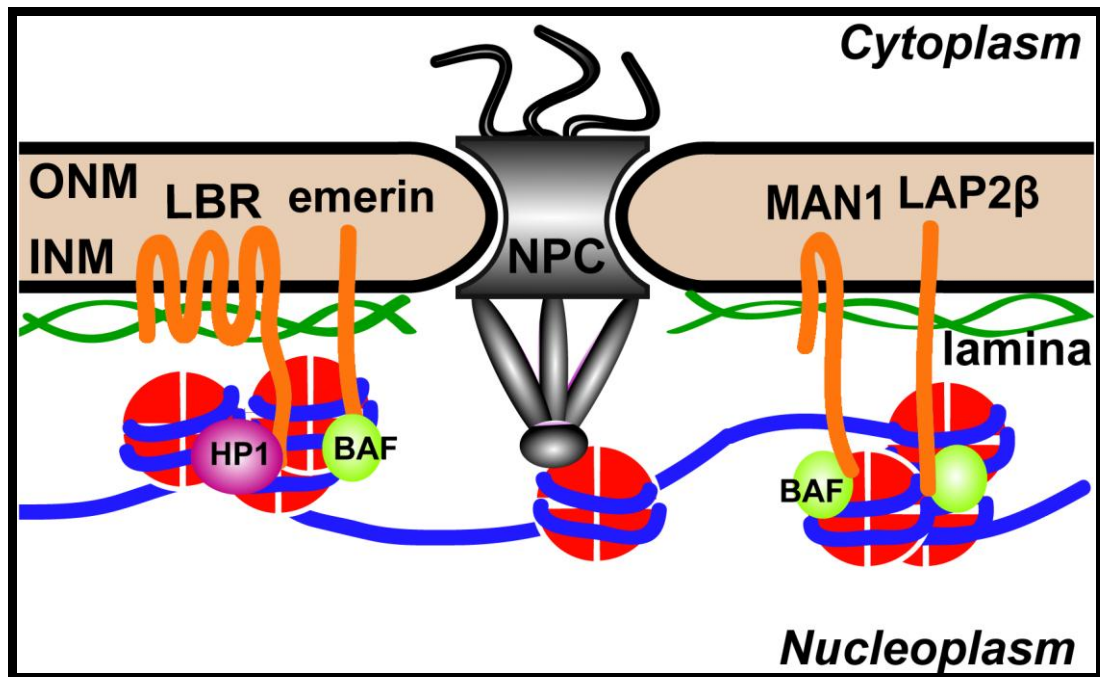


Figure 10. NE proteins interact with chromatin proteins. The INM of the NE possesses a specific set of NETs (orange), which together with the lamins are referred to as the lamina. Lamins, NPCs and NETs can all interact with DNA directly or via chromatin components like barrier-to-autointegration factor (BAF), heterochromatin protein 1 (HP1) and histones (red).

Also NE protein interactions with epigenetic marks and enzymes involved in epigenetic modifications have been reported. For example, chromatin that co-immunoprecipitated with LBR was enriched in silent epigenetic marks (Makatsori et al., 2004). LBR also interacts with the methylcytosine binding protein MeCP2 (Guarda et al., 2009) while other NETs LAP2 β and SUN1 bind to histone deacetylase HDAC3 (Somech et al., 2005) and acetyl transferase hALP1 (Chi et al., 2007), respectively. Apart from chromatin binding enzymes that can modify chromatin NETs have also been shown to interact with several transcriptional regulators [reviewed in (Heessen and Fornerod, 2007)]. Emerin, for example, binds to Lmo7 (Holaska et al., 2006), Btf (Haraguchi et al., 2004) and germ cell-less [GCL; (Holaska et al., 2003)] whilst MAN1 binds Smad proteins (Osada et al., 2003; Pan et al., 2005) and LAP2 β binds GCL (Nili et al., 2001).

Many novel NETs have been discovered recently (Dreger et al., 2001; Korfali et al., 2010; Nili et al., 2001; Schirmer et al., 2003; Wilkie et al., 2011), many of which are likely to bind chromatin proteins, chromatin modifying enzymes or DNA. Indeed a recent study, which ran visual screens on ten of these novel NETs, found that some of these proteins could reposition a gene locus to the nuclear periphery (Korfali et al., 2010).

1.3.3 What are the mechanisms that direct cell-type specific chromosome organization patterns?

Despite the assumption that the NE could be one of the major players in the establishment of tissue-specific chromosome positioning, direct testing of this hypothesis has proven difficult. First attempts involved the observations that a truncated form of lamin B1 caused a release of the peripheral chromosome 18 into the nuclear interior (Malhas et al., 2007). Similarly, disease-linked mutations of lamin A caused chromosome 13 and 18 to move away from the nuclear periphery (Meaburn et al., 2007; Mewborn et al., 2010). Indeed, these lamin associated effects could also be indirect since targeting of many NETs is lamin-dependent [reviewed in (Schirmer and Foisner, 2007)]. Therefore it is reasonable to assume that NETs could be the actual mediators of chromosome positioning effects.

The hypothesis that NE proteins could mediate specific chromosome positioning patterns emerges from the observation that the NETs emerin and LBR bind to distinct positions on chromosomes during mitosis (Haraguchi et al., 2000) and accordingly establish chromosome attachment points, which potentially could lead to the establishment of specific chromosome organization patterns once the NE is reformed. The above studies all describe widely expressed NE proteins and it is therefore also difficult to envision that they are the main drivers of tissue-specific chromosome positioning patterns. Moreover, the studies also provide only correlative observations that NE can mediate specific positioning patterns of

chromosomes and do not provide direct evidence that NE proteins are tethering chromosomes to the nuclear periphery.

The first evidence that a chromosome can be tethered to the NE was provided independently by three laboratories, which made use of an artificial high affinity system to tether chromosomes in a controlled fashion to the nuclear periphery (Finlan et al., 2008; Kumaran and Spector, 2008; Reddy et al., 2008). In all three studies, bacterial lac operator (lacO) sequences were integrated into the mammalian genome into a locus that tended to be in the nuclear interior. Additionally the lac repressor (lacI) was fused to either a GFP reporter alone or to both a reporter and a NE protein and expressed in these cell lines. While the expression of the lacI-reporter fusion (not bound at the NE) had no effect on chromosome positioning, the NE protein-fused lacI moved the lacO array, and also the according chromosome as tested in the Finlan et al. study (the other two studies did not test whether the lacO array containing chromosome was also moving), to the nuclear periphery (Figure 11).

Notably, though all three studies used different NE proteins they all found that tethering of the chromosome required a full mitotic cell division (Figure 11, B) suggesting that large-scale chromosome arrangements are less likely to occur during interphase.

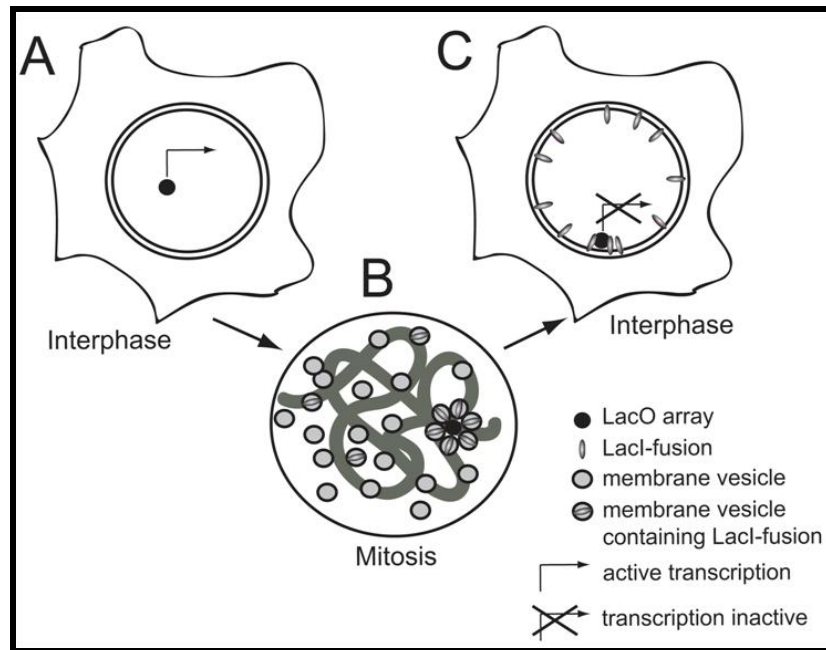


Figure 11. Chromatin can be tethered to the nuclear periphery by an affinity mechanism. (A) A bacterial *lacO* array locus is integrated into the genome of a mammalian cell. This locus tends to be in the nuclear interior and is transcriptionally active. **(B)** The *lac* repressor (*lacI*), a bacterial protein with a high affinity to the *lacO* array is fused to a NE protein and introduced into the cell. When the cell goes through mitosis, the NE breaks down into small vesicles, some of which contain the *lacI*-NE fusion protein. These vesicles bind to the *lacO* array. **(C)** When the NE is reformed after mitosis *lacI*-fusion is captured at the nuclear periphery together with the *lacO* array. The array containing locus becomes transcriptionally inactive at the NE. (Figure adapted from Zuleger and Schirmer, 2011)

The findings of the three studies advanced our understanding of chromosome organization enormously as they all provided first proof that a chromosome *can* be recruited to the nuclear periphery *via* a NE tether. But even though the proof of principle is provided, endogenous proteins that could tether chromosomes to the nuclear periphery have yet to be found. The three *lacO* studies also tested for transcriptional changes of the locus/chromosome upon its tethering to nuclear periphery and the findings will be presented in the next section.

1.3.4 Gene regulation as a consequence of radial chromosome repositioning

It is reasonable to assume that repositioning of a particular chromosome will have transcriptional consequences on the genes located on this chromosome. For instance, if a chromosome would move from the interior to the nuclear periphery, which as mentioned earlier is a predominantly silent environment, the genes of this chromosome adjacent to the NE should be silenced. In fact, in the previously mentioned lacO studies the activities of genes proximal to the lacO array were tested. And indeed in two of the studies a preference for gene silencing was observed (Finlan et al., 2008; Reddy et al., 2008). In the third study the transcriptional activity of the tethered locus was not affected (Kumaran and Spector, 2008). These discrepancies might reflect the usage of different tether proteins which in turn recruit different transcriptional regulators, or are due to differences in the cell lines. Another possible explanation for the difference is also the use of the very strong promoter (early SV40 promoter) in the Kumaran and Spector study, the activity of which could likely override any positioning effects.

Additionally, inconsistencies have been observed in systems where no artificial tethering systems were used. For instance, some genes were reported to move from the periphery into the interior when activated; others however, remained at the periphery after activation. For example, the *C-maf* (Hewitt et al., 2004), *IgH* (Kosak et al., 2002), *β -globin* (Ragoczy et al., 2006) and *Mash1* [Figure 12, A; (Williams et al., 2006)] genes are all repressed at the nuclear periphery but become activated and move into the nuclear interior when the cells are differentiating into T-cells, B-cells, erythroid cells or neural cells, respectively. Other genes like the *PLP* [Figure 12, B; (Nielsen et al., 2002)], *IFN- γ* (Hewitt et al., 2004), *ERBB-2* (Park and De Boni, 1998) and the *COL1A1* (Johnson et al., 2000), however remain at the nuclear periphery upon their activation.

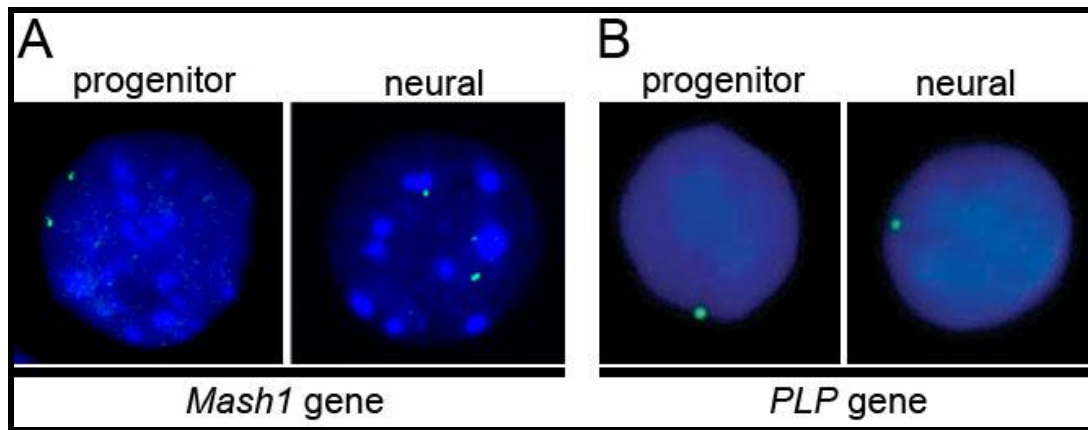


Figure 12. Radial positioning of genes and their transcriptional activity during differentiation. (A) The *Mash1* gene (green spots) is inactive and localizes at the nuclear periphery in neural progenitor cells (left). During neuron differentiation the *Mash1* gene becomes transcriptionally active and moves into the nuclear interior (right). (B) In contrast, the *PLP* gene (green spot) is at the nuclear periphery in progenitor cells (left) and in differentiated nerve cells (right) even though it becomes activated during neurogenesis. (panel A adapted from Williams et al., 2006; panel B adapted from Nielsen et al., 2002)

1.3.5 Differentiation, chromosome/gene repositioning and gene activity – The bigger picture

Though the studies mentioned above observed a radial change in chromosome and gene positioning during differentiation, they were only testing for few genes and chromosomes and there was a clear need for a more systematic study that would address the interplay of chromosome organization and the functional readout of it. There are three recent reports all of which show the large scale chromatin re-organizations during differentiation in the light of a functional output. The first study studied the change in the nuclear architecture during the differentiation of rod photoreceptor cells of nocturnal and diurnal mammals and revealed that the nuclear architecture of these cells is adapting to vision (Solovei et al., 2009). The study found that whereas the nuclear architecture of rod photoreceptor cells of diurnal mammals matched that found in most eukaryotic cells with having most of heterochromatin located at the nuclear periphery and the

euchromatin in the nuclear interior. However, whilst the same organization was found in progenitor photoreceptor cells of nocturnal mammals, in differentiated rod photoreceptor cells of nocturnal mammals a completely inverted chromatin organization was observed in which heterochromatin localized in the nuclear interior surrounded by the euchromatin which lined to the nuclear periphery (Figure 13, A). It was proposed that the functional consequence of the inverted organization of rod nuclei was to allow them to act as collecting lenses and thus enhance the night vision of nocturnal mammals.

The second study used the whole organism *Caenorhabditis elegans* to study the radial position of developmentally controlled tissue-specific promoters during differentiation (Meister et al., 2010). This study revealed that these promoters were not specifically organized in embryos but shifted robustly to the nuclear interior upon activation only in tissues the promoters were specific for (Figure 13, B).

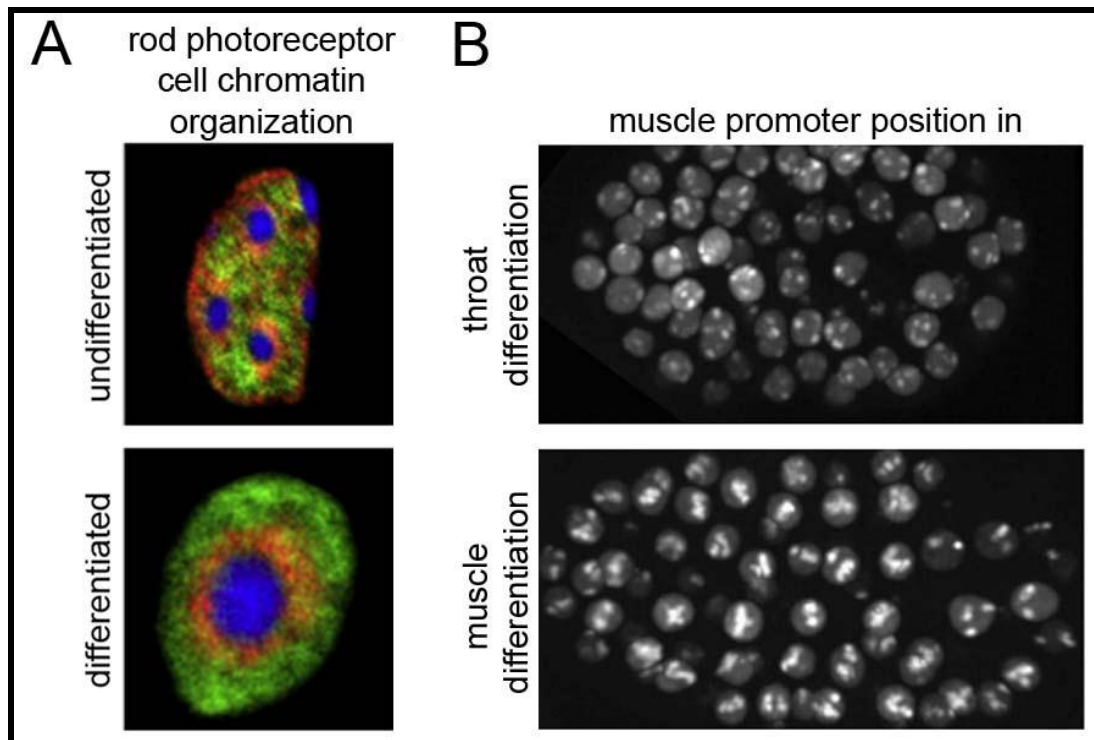


Figure 13. Large-scale chromatin rearrangements during differentiation. (A) Arrangement of euchromatin (green), L1-rich heterochromatin (red) and heterochromatin of chromocenters (blue) in undifferentiated (top) and differentiated (bottom) rod photoreceptor nuclei. Most heterochromatin is peripheral and most of the euchromatin interior in undifferentiated cells while after the differentiation the arrangement is completely inverted. (B) Position of a muscle-specific promoter (*myo-3*) in throat differentiation (top) and muscle differentiation (bottom). The muscle promoter has no preferred position during throat differentiation but shifts robustly into the nuclear interior in muscle-differentiating cells. (panel A adapted from Solovei et al., 2009; panel B adapted from Meister et al., 2010)

The last study investigated the dynamics of gene positioning with respect to the nuclear periphery during neurogenesis (Peric-Hupkes et al., 2010). This study mapped all genes in contact with the nuclear periphery in embryonic stem cells, lineage-committed neural precursor cells and completely differentiated astrocytes and found that many genes changed their positioning in respect to the nuclear periphery during the differentiation process. More importantly, genes becoming activated during the differentiation process often moved into the nuclear interior whilst being at the nuclear periphery when being inactive. Hence this study also provided

evidence on a large-scale level for functional consequences of radial gene repositioning during differentiation.

Do large-scale chromosome reorganizations occur in mitosis or interphase?

Many labs have studied chromatin movements in living insect and mammalian cells and reported gene movements of up to 10 μm in interphase cells (Chuang et al., 2006; Gunawardena and Rykowski, 2000; Solovei et al., 2004) but for bigger chromosome domains and whole chromosomes reported movements did normally not exceed the 2 μm mark (Abney et al., 1997; Bornfleth et al., 1999; Edelmann et al., 2001; Marshall and Wilson, 1997; Thomson et al., 2004; Walter et al., 2003). It is therefore difficult to imagine that the huge chromosome re-organization patterns observed during differentiation could possibly occur during interphase, a rather more plausible explanation would be a establishment of a different chromosome organization during mitosis as also reported by the three lacO studies, where artificial high affinity tethering of an internal chromosome to the periphery required a mitotic cycle (Finlan et al., 2008; Kumaran and Spector, 2008; Reddy et al., 2008). Despite growing evidence that mitosis could be the prerequisite for large-scale chromosome reorganization, a recent study demonstrated that chromosomes can move large distances in post-mitotic cells in a step that required activity of cellular motors (Mehta et al., 2010).

To directly test if mitosis is preceding large-scale chromosome rearrangements several studies followed the interphase chromosome organization of mother cells and the respective daughter cells. Though the individual studies all agree that chromosome territories are maintained during interphase, their results regarding chromosome organization after the cell went through mitosis differ. Some report an organization that is inherited to the daughter cells (Essers et al., 2005; Gerlich et al., 2003) while others report that the radial positioning of chromosome territories in interphase differs significantly from mother to daughter cells (Cvackova et al., 2009;

Strickfaden et al., 2010; Thomson et al., 2004; Walter et al., 2003). Looking at the latter studies more closely one can recognize that even though huge re-arrangements seem to occur, minor radial positioning is preserved to daughter cells. For example, if mother cells had some chromosome portions at the nuclear periphery, then also daughter cells had at least some of the portions still at the nuclear edge (i.e. Figure 4A in Strickfaden et al., 2010). This would mean that some chromosomes are still at the periphery though their neighbours might have changed the position.

What are the proteins that mediate chromosome positioning?

AND

Can these proteins mediate tissue-specific chromosome organization?

We will only be able to work out the molecular mechanisms of chromosome repositioning once all the proteins responsible are discovered. Despite of growing evidence that the NE could be involved in chromosome repositioning, no study thus far has systematically manipulated the protein composition of the NE and then tested for possible effects on chromosome positioning. The number of NE proteins has increased from just a dozen to more than 100 within the last 10 years (Dreger et al., 2001; Korfali et al., 2010; Schirmer et al., 2003; Wilkie et al., 2011). Given this enormous number it is reasonable to deduce that at least some could play a role in chromosome organization. Many of these novel NE proteins were isolated from specific tissues and thus could be tissue-specific. The more interesting it is to test, if some of them play a role in global chromosome organization since large-scale chromosome re-arrangements occur also during differentiation (when many of the tissue-specific NETs are expressed).

Another important question is whether tethering of genes from one chromosome to the nuclear periphery causes the chromosome to change its

radial position respectively or whether the chromosome repositioning itself is the cause for gene repositioning. Furthermore, it is not completely clear whether change in transcriptional activity is cause or consequence for radial repositioning of genes and chromosomes i.e. are genes that are silent at the nuclear periphery released into the nuclear interior in order to get activated or are they activated at the periphery first and move to the nuclear interior as a consequence of it? For example, strong transcriptional activation could change epigenetic marks to lower affinity for the periphery so transcription could drive the gene away from the periphery. Alternatively, release from the periphery could move the gene into a transcriptionally active environment, for example in proximity to PML bodies, which would promote the activation of this gene.

An increasing amount of reports argues for the latter scenario where repositioning of the gene preceded its activation (Andrulis et al., 1998; Chambeyron and Bickmore, 2004; Chambeyron et al., 2005; Yao et al., 2011). This scenario is also supported by the discovery of so called “transcription factories” or “expression hubs” (Jackson et al., 1993). These transcription factories are nuclear foci of many active genes with high concentrations of polymerases and transcription factors and the fact that many active genes must be concentrated in such a factory follows from the observation that the number of active genes in the cell is by far exceeding the number of these transcription factories. Hence, a repressed gene is more likely to move first in order to reach such a transcription factory in order to be subsequently activated.

Answering all of the questions mentioned above will only be possible once the players responsible for the chromosome and gene re-arrangements are identified. Only then one can manipulate these players and test the effects on chromosome organization. We propose that many of these chromosome organizing proteins reside in the NE. The NE contains more than 100 NETs some of which have already been shown to alter chromatin organization (Korfali et al., 2010). Many of these proteins were isolated from

specific tissues and therefore it is reasonable to deduct that they might play a potential role in tissue-specific chromosome organization.

1.4 Preview

This chapter focused on the important questions in the field of NE membrane protein targeting and nuclear periphery mediated genome organization. The answers to some of these questions are presented in the following chapters. For example, we are able to show that translocation of NETs is mediated by distinct mechanisms, which are independent from each other. Our further findings in this area also argue for the use of the peripheral rather than the central channels of the NPC for translocation of NETs into the INM.

The following chapters will also give a possible explanation for how tissue-specific chromosome organization is established. We found tissue-specific NETs, which could reposition chromosomes to the nuclear periphery upon their overexpression and release chromosomes from the periphery upon their depletion. Intriguingly, the expression of these chromosome repositioning NETs caused a differential expression of genes specific to the tissue in which these NETs were preferentially expressed.

Chapter 2

Materials and Methods

2.1 Materials

All standard reagents and chemicals if not otherwise stated were obtained from Sigma, Merck or Fisher Scientific. TRIzol reagent was obtained from Invitrogen. Formaldehyde was from Electron Microscopy Sciences.

Bacterial strains

DH5alpha

F⁻ endA1 glnV44 thi-1 recA1 relA1 gyrA96 deoR nupG Φ 80d/lacZ Δ M15 Δ (lacZYA-argF)U169 hsdR17(r_K⁻ m_K⁺) λ -

StrataClone SoloPack Competent Cells (Stratagene, from kit 240207)

F⁻ creC510 Φ 80d/lacZ Δ M15 recA1 endA1 tonA rpsL20 (StrR) hsdR17(r_K⁻ m_K⁺) λ -

Buffers and solutions

Denaturation buffer (FISH)	70% v/v Formamide in 2xSSC, pH7.2
Hybridization buffer (FISH)	provided with STARFISH probes
LB	1% tryptone; 0.5% yeast extract; 10mM NaCl; pH7.4
PBS	65mM Na ₂ PO ₄ ; 8.8mM KH ₂ PO ₄ ; 137mM NaCl; 2.7mM KCl; pH7.4

SSC, 20x	3M NaCl; 300mM Sodium Citrate; pH7.2
TAE	40mM Tris-acetate; 1mM EDTA
Tfbl buffer	30mM KAc; 100mM RbCl ₂ ; 10mM CaCl ₂ ; 50mM MnCl ₂ ; 15% glycerol; pH 5.8
TfbII buffer	10mM MOPS; 75mM CaCl ₂ ; 10mM RbCl ₂ ; 15% glycerol; pH 6.5
SDS-page buffer	25 mM Tris; 192 mM glycine; 0.1% SDS; pH 8.3
Transfer-Buffer	80% SDS-page buffer; 20% methanol
Crosslinking solution 10x	500 mM Hepes pH 7.9; 1.5 mM NaCl; 10 mM EDTA; 5 mM EGTA
Buffer L1 (ChIP)	50 mM Hepes pH 7.9; 140 mM NaCl; 1 mM EDTA; 10% glycerol; 0.5% NP-40; 0.25% Triton X-100
Buffer L2 (ChIP)	10 mM Tris pH 8.0; 200 mM NaCl; 1 mM EDTA; 0.5 mM EGTA
Buffer L3 (ChIP)	10 mM Tris pH 8.0; 1 mM EDTA; 0.5 mM EGTA
ChIP dilution buffer	20 mM Tris pH 8.0; 150 mM NaCl; 2 mM EDTA; 1% Triton X-100
Wash buffer 1 (ChIP)	20 mM Tris pH 8.0; 150 mM NaCl; 2 mM EDTA; 1% Triton X-100; 0.1 % SDS
Wash buffer 2 (ChIP)	20 mM Tris pH 8.0; 500 mM NaCl; 2 mM EDTA; 1% Triton X-100; 0.1 % SDS
DMEM	Dulbecco's Modified Eagle's Medium (Lonza, 12-604F)

Antibodies

Primary Antibodies

Table 1. Primary antibodies used in this study

Antibody/host	Application/ Dilution	Source
acetyl histone H3/rabbit	WB/1:500	Millipore (06-911)
β -actin/mouse	WB/1:5000	Sigma (A1978-200UL)
Digoxigenin/mouse	FISH/1:300	Roche (11333062910)
GFP/rabbit	IF and FISH/1:200 WB/1:1000	Invitrogen (A11122)
GFP/rabbit	IP/1:100	Rabbit polyclonal generated against the whole protein (antigen purified by Dzmityr Batrakou)
NET5/rabbit	WB/1:250	Millipore (06-1013)
NET29/rabbit	WB/1:250	Millipore (06-1018)
NET39/rabbit	WB/1:250	Millipore (06-1025)
NET45/mouse	WB/1:500	Monoclonal made to a protein fragment by Dr. Glenn E. Morris and Natalie Randals
NET47/rabbit	WB/1:250	Millipore (06-1026)
NET55/rabbit	WB/1:250	Millipore (06-1029)
Nup35/mouse	WB/1:1000	Tebu-Bio (157H00129401-B01)
Porin/rabbit	WB/1:500	Abcam (ab15895)
Ran/mouse	WB/1:5000	BD Biosciences (610341)
tri-methyl hist. H3/rabbit	WB/1:500	Millipore (07-523)
α -tubulin/mouse	WB/1:5000	Sigma (T6074-200UL)

Secondary antibodies

Secondary antibodies for IF/FISH were anti rabbit or anti mouse Alexa dye conjugates (Molecular Probes, Invitrogen). For Western blotting horseradish peroxidase conjugated highly cross-absorbed anti rabbit or anti mouse antibodies were applied. All secondary antibodies used are listed in the table below.

Table 2. Secondary antibodies used in this study

Antibody	Conjugate	Application/ Dilution	Source
Anti-mouse	Alexa 568	IF/FISH/1:200	Invitrogen (A11031)
Anti-rabbit	Alexa 594	IF/FISH/1:200	Invitrogen (A21207)
Anti-mouse	HRP	WB/1:3000	Promega (W4021)
Anti-rabbit	HRP	WB/1:5000	GE Healthcare (NA9340-1ML)

Avidin conjugates

Avidin (A21370) or Streptavidin (S32356) were used conjugated to Alexa dyes (Molecular Probes/Invitrogen) at a working concentration of 1:200.

Chromosome paints

StarFISH whole chromosome paints were obtained from Cambio (Cambridge, UK) and are listed in the table below.

Table 3. Whole chromosome paints used in this study

Chromosome paint	Cat. Nr.
concentrated Human Chromosome 1 paint	1066-1B-02
concentrated Human Chromosome 5 paint	1066-5B-02
concentrated Human Chromosome 11 paint	1066-11B-02
concentrated Human Chromosome 13 paint	1066-13B-02
concentrated Human Chromosome 17 paint	1066-17B-02
concentrated Human Chromosome 19 paint	1066-19B-02

Cells

HeLa, HT1080 and HepG2 cells were obtained from ATCC. HT1080 cells stably expressing GFP-NETs were established during the course of this study. 293T cells stably expressing BAF-GFP were obtained from Dr. Nadia Korfali, Wellcome Trust Centre for Cell Biology, Edinburgh, UK. HT1080 cells with stably integrated lac operator (lacO) repeats and stably expressing the lac repressor-GFP (lacI) were a gift from Professor Wendy Bickmore (MRC Human Genetics Unit, Edinburgh). In short, the 128mer lacO array plasmid was linearized and co-transfected with a selection plasmid into HT1080 cells. Cells were selected with 5 g/ml blasticidin S. For visualization of the lacO array integration these cells were further transfected with a linearized vector containing lacI-GFP. Cells were selected for this plasmid with 100 g/ml hygromycin (Chubb et al., 2002).

Commercial Kits

Table 4. Commercial Kits used in this study

Kit	Provider
QIAprep Spin Miniprep Kit (27106)	Qiagen
QIAfilter Plasmid Midi Kit (12243)	Qiagen
QIAquick Gel Extraction Kit (28704)	Qiagen
StrataClone Blunt PCR Cloning Kit (240207)	Stratagene
Illumina® TotalPrep™ RNA Amplification Kit (AMIL1791)	Ambion
Fugene HD transfection reagent (04709691001)	Roche
Nucleofection Kit R (VCA-1001)	Lonza
Nucleofection Kit V (VCA-1003)	Lonza

RNAi oligos

ON-TARGETplus Smartpool siRNA oligos against transcripts of human NET45 (DAK; L-006808-00-0020) and human NET47 (TM7SF2; L-005744-00-0020) were obtained from Dharmacon. For Nup35 siRNA-mediated knockdown following RNA oligos were used as a duplex: 5'-UGCCAGUUCUUACCUGGATT-3' (sense) and 5'-UCCAGGUAAGAACUGGGCATT-3' (antisense). The bold marked "TT" symbolizes DNA overhangs. For live-cell imaging detection of Nup35 siRNA transfected cells the antisense oligo was conjugated to the Alexa-647 dye at the 5'-end.

Human tissue blots and human biopsy tissues

A ready-to-use polyvinylidene fluoride (PVDF) membrane containing lysates from eleven human tissues was obtained from IMGENEX (IMB-103). Human biopsy liver and kidney tissue sections were provided by Professor David J. Harrison (Western General Hospital, Edinburgh, UK) in line with University of Edinburgh Ethics protocols.

2.2 Methods

2.2.1 Nucleic acid methods

Standard Cloning techniques involving transformation of plasmid DNA into bacteria, amplification of plasmid DNA in bacteria and plasmid isolation, restriction of DNA plasmids, agarose gel electrophoresis were performed as described by Sambrook and Russell (2001) and applied to obtain the expression plasmids used in this study. Plasmids not designed in this study are clearly indicated. The quality and concentration of the isolated plasmid DNA or RNA was assessed using the spectrophotometer NanoDrop 2000c (Thermo Scientific).

2.2.1.1 Polymerase chain reaction

Phusion High-Fidelity DNA Polymerase (Finnzymes) was used to amplify the genes of interest using the appropriate primers. The primers used are listed in the table below:

Table 5. Primers used in this study

Primer	Sequence (5'-3')	Restriction site
NET5_1stSol_fw	AAGCTTTACGGAGGATGAAGCCAACG	HindIII
NET5_1stSol_rv	GTCGACCTTCACGGCGGAGGAGAAG	Sall
NET5_2ndSol_fw	AAGCTTTAAGGAAGGCAACGGGC	HindIII
NET5_2ndSol_rv	GTCGACACGACCTCTCCAGGTG	Sall
NET39_Sol_fw	AAGCTTTAATGCCAGCTTCCCAGAG	HindIII
NET39_Sol_rv	GTCGACGGAGCGGGCACTGG	Sall
NET47_Sol_fw	AAGCTTTAAAGGCGCAGGTAGCC	HindIII
NET47_Sol_rv	GTCGACCCCGTCATGTGTGATATCCATG	Sall

Sol = soluble fragment; fw = forward primer; rv = reverse primer

The total reaction volume of 20µl contained 0.4U Phusion Polymerase enzyme, 200 µM of each dNTP, 0.5µM of each primer, 100ng of the template

DNA, 4 µL of the 5x Phusion buffer (provided with the enzyme) and double distilled water. PCR reactions were run on the G-STORM GS1 cyclor.

The PCR reaction had following cycling parameters:

- 1) 2 min at 95°C (denaturation)
- 2) 20 sec at 95°C (denaturation)
- 3) 30 sec at 58°C (primer annealing)
- 4) 72°C for 1min/1kb target sequence (extension)

Step 2 to 5 was repeated 25-30 times followed by a 5 min extension step at 72°C.

Final PCR products were analysed by means of agarose gel electrophoresis and cloned into the intermediate vector using the StrataClone Blunt PCR Cloning Kit (240207) from Stratagene following the manufacturer's instructions.

2.2.1.2 Sequencing of plasmid DNA

The entire sequence of the cDNAs cloned into the expression vectors was verified by sequencing. Sequencing was performed by the GenePool sequencing facility (University of Edinburgh). Provided chromatograms were analyzed using the freeware program FinchTV (Geospiza).

2.2.1.3 Isolation of total cellular RNA

Cells from a sub-confluent 10 cm culture dish were trypsinized with 2 ml trypsin/PBS solution and the trypsinization was stopped by adding 4 ml of fresh complete medium containing 10% serum to inactivate the trypsin. Cells were then pelleted and harshly resuspended in 1ml TRI-reagent (Invitrogen) and incubated at RT for 5 min. 200 µl chloroform was added and the mixture vigorously shaken for 20 sec and then let to incubate at room temperature for 10 min. The mixture was then spun at 12,000xg for 12 min at 4°C. After centrifugation the supernatant was removed and put into 500 µl isopropanol, mixed and incubated for 5 min at room temperature. A subsequent spin for

10 min at 12,000 xg and 4°C was performed to pellet the RNA. The supernatant was discarded and the pellet washed in 70% ethanol. After a 2 min spin at 6,000xg at 15°C the supernatant was removed and the pellet was resuspended in 50 µl molecular grade RNase-free water and used for RT-PCR or biotin labelling for microarrays. RNA that was not subsequently processed was stored at -80 °C.

2.2.1.4 Reverse transcriptase PCR

For the reverse transcriptase PCR reaction the Titan kit (Roche, 11855476001) was used. For the reaction following components and their according amounts were pipetted:

total RNA (50ng/ µl)	2 µl
primer1/primer2 mix (2.5µM each)	4 µl
dNTPs (25mM)	0.2 µl
RT-PCR buffer	2 µl
MgCl ₂	0.6 µl
DTT	0.5 µl
Reverse transcriptase	0.2 µl
H ₂ O	0.5 µl

RT-PCR Program:

- 1) 45 min 48°C
- 2) 2 min 95°C
- 3) 20 sec 95°C
- 4) 25 sec 56°C
- 5) 1 min 68°C
- 6) cycle 25x [step 3-5]

2.2.1.5 Biotin labelling of total RNA and microarray analysis

Total RNA preparations were transcribed into cDNA and then subsequently into biotin labelled cRNA using the Illumina® TotalPrep™ RNA Amplification Kit (Applied Biosystems, AMIL1791) following the manufacturer's instructions (This work was performed by Dzmitry Batrakou). Labelled cRNA was hybridized to Illumina HumanHT-12 v3 bead arrays containing 48803 probes covering UniGene and RefSeq annotated genes (performed by the Wellcome Trust Clinical Research Facility, Western General Hospital, Edinburgh, UK). The subsequent microarray data were normalized using the free statistics package R (R Development Core Team (2011); R: A language and environment for statistical computing. R Foundation for Statistical Computing, Vienna, Austria. ISBN 3-900051-07-0, URL <http://www.R-project.org/>). A low intensity filter was applied to eliminate samples that do not reach the $\log_2(\text{signal})$ of at least 6.5. Afterwards, all transcripts that exhibited small expression differences were eliminated using a cut-off of 1.4 ($\text{abs}(\log_2 \text{NET}/\text{ref})=0.5$) (this was done by Dr. Jose de las Heras).

2.2.2 Protein techniques

2.2.2.1 Western blotting

Cell lysates or purified proteins were separated on 8-12% SDS-Gels. Subsequently the gels were transferred onto a ImmobilonP membrane (Millipore) by means of semidry transfer (BIO-RAD). After transfer the membrane was blocked in 5% milk powder (in PBS with 0.05% Tween-20) for 60 min. Subsequently, the membrane was incubated with the primary antibody (1:500 in PBS/Tween20/5% milk) for 45 min. Six washes in PBS/Tween20/5% milk were followed by incubation with the secondary antibody conjugated to the horse-radish peroxidase (HRP, 1:10000 in PBS/Tween20/5% milk) for 30 min. After 6 washes in PBS/Tween20 the membrane was incubated with the ECL reagent (Amersham) to allow the

HRP to react with hydrogen peroxide and luminol to generate a fluorescent signal that was measured on an X-Ray film (CP-BU NEW, Agfa).

2.2.2.2 Chromatin IP (ChIP) procedure¹

Cells stably expressing GFP fusion proteins were grown to 90% confluence, trypsinized and counted. 10^7 cells were aliquoted and crosslinked in a total volume of 10 ml at 4°C for 10 min with 1x crosslinking buffer containing 1% formaldehyde. Crosslinking was stopped by adding glycine at a final concentration of 125 mM. Subsequently, cells were collected by centrifugation at 400xg for 6 min and washed twice with PBS containing freshly added protease inhibitors (Roche 11873580001). Pellets were resuspended in 5 ml of protease inhibitors-containing Buffer L1 and incubated at 4°C for 10 min with gentle rocking. Cells were again collected by centrifugation at 800xg for 10 min and subsequently resuspended at a concentration of 2×10^6 cells/ml in Buffer L2 (containing protease inhibitors) for an incubation at 4°C for 10 min. After collecting again by centrifugation, pellets were resuspended in 500 μ l of Buffer L3 and SDS was added to a final concentration of 0.01%. The mixture was then sonicated using a BioRuptor bath sonicator on high power for 20 pulses of 30 s each followed by a 30 s rest (so 10 min of actual sonication), adding fresh ice every 5 min. Roughly 1/10 volume of the sonicated lysate was removed and boiled in SDS sample buffer and used as input material on Western blots. Lysates were pre-cleared with a mixture of protein A (Millipore, LSKMAGA02) and protein G (Millipore, LSKMAGG02) magnetic beads for 1 h at 4°C. After removal of the beads samples were incubated with rabbit GFP antibodies (made to the whole protein) overnight at 4°C on a rotating wheel. On the next day 50 μ l of a mix of protein A and G magnetic beads (Millipore) was added followed by incubation for 3 h at 4°C on a rotating wheel. Beads were washed 5 times in

¹ the ChIP protocol was kindly provided by Dr. Irina Stancheva (Wellcome Trust Centre for Cell Biology, Edinburgh, UK); The ChIP procedure was performed by Dr. Nadia Korfali (Wellcome Trust Centre for Cell Biology, Edinburgh, UK)

500 µl Wash buffer 1 followed by 3 washes in 500 µl of Wash buffer 2. To remove the bound proteins from the beads SDS sample buffer was added followed by boiling. The eluted material was then analyzed by SDS-PAGE and western blotting.

2.2.3 Tissue culture methods

2.2.3.1 Mammalian cell maintenance and transfection

HeLa, HepG2 and HT1080 cells were grown in Dulbecco's modified Eagle's medium (DMEM) supplemented with 10% fetal calf serum, 100 units/ml penicillin, and 100 µg/ml streptomycin. HT1080 cells were additionally supplemented with 100µg/ml hygromycine and 5µg/ml blasticidin S to keep them selected for the stably integrated lacO amplifications and the lacI-GFP coding sequence. Cells were plated onto 10 mm coverslips (VWR International) in 24-well plates. Once they had achieved 20% confluency, they were transfected with 0.5 µg reporter using Fugene HD (Roche).

2.2.3.2 Establishment of stable cell lines

To establish stable cell lines plasmids carrying the gene of interest and the geneticin resistance cassette were linearized and transfected into HT1080 cells using Fugene HD (Roche) following the manufacturer's instructions. At two days post-transfection Geneticin (Invitrogen) was added at 500 µg/ml and maintained for two weeks to select for stable transfectants. These cells were subsequently sorted by FACS to select for cells with similar expression levels. After sorting cells were maintained in 100 µg/ml Geneticin.

2.2.3.3 ATP depletion in HeLa cells

HeLa cells were depleted for ATP by exchanging regular culture medium for glucose-free medium containing 10mM sodium azide and 6 mM 2-deoxyglucose, 25mM HEPES-KOH and 10% FBS. FRAP experiments were

initiated 10 min after the medium exchange. Cells were discarded 40 min after the medium exchange to avoid pleiotropic effects from ATP depletion.

2.2.3.4 Ran function depletion in HeLa cells

To inhibit Ran function during FRAP experiments a plasmid encoding the dominant negative mutant of Ran was co-transfected with GFP-NETs. This mutant has a glutamine to leucine substitution at amino acid position 69 (Q69L). Because Ran function is impaired by Ran fusion to ectopic tags the plasmid also contained monomeric RFP, expression of which was driven by a separate CMV promoter enabling visualization of Ran mutant expressing cells. For Ran depletion this construct was co-transfected with NET-GFP constructs and cells were analysed 24h post-transfection. A Ran antibody was used to detect increased Ran levels in the total population by western blotting and in individually transfected cells (as determined by expression of monomeric RFP) by immunofluorescence.

2.2.3.5 Nup35 depletion in HeLa cells

The nucleoporin Nup35 was depleted from HeLa cells by means of siRNA. RNAi duplexes designed to target the 5'-UGCCCAGUUCUUACCUGGA-3' region of the human Nup35 mRNA. Cells were used for experiments 48-60h post nucleofection of 7µg siRNA oligos into one million cells using nucleofection kit R and program I-013. The siRNA duplexes were conjugated to Alexa647 dye in order to visualize transfected cells. The extent of Nup35 knockdown was assessed by western blotting using an anti-human Nup35 polyclonal antibody.

2.2.3.6 Knockdown of NET45 and NET47 in HepG2 liver cells

Smartpools were obtained from Dharmacon for NET45 (DAK; L-006808-00-0020) and NET47 (TM7SF2; L-005744-00-0020). 3 µg of each oligo mix was combined and transfected into 1.5×10^6 HepG2 cells using nucleofection (Lonza, Kit V, protocol T-28). The control siRNA was a random scrambled

sequence (sense strand: 5'-CGUACGCGGAAUACUUCGA-3'; antisense strand 5'-UCGAAGUAUUCCGCGUACG-3'). Cells were taken for RNA at 48 h or fixed at the indicated time points post-transfection. Peptidylprolyl Isomerase A (PPIA) was used as a loading control.

2.2.4 Microscopy methods, image processing and analysis

2.2.4.1 Fluorescence recovery after photobleaching (FRAP)

FRAP experiments were performed on a wide-field microscope (DeltaVision, Applied Precision; IX70 microscope, Olympus and CoolSNAP HQ camera, Photometrics) with an attached 488 nm laser using a 60x Plan-Apochromat oil 1.4 NA objective lens. HeLa cells were analyzed 16-24 h post transfection with NET-GFP fusions in a 37°C heated chamber containing complete culture medium with 25mM HEPES-KOH. Five pre-bleach images were taken before cells were bleached with a $\sim 5.5 \mu\text{m}^2$ laser spot at full laser intensity leaving subsequent fluorescence levels of 20-40%. Fluorescence recovery was then measured every 3.5s until a recovery plateau was reached. Image data were collected with SoftWoRx software (version 3.5) and processed with Image-Pro Plus Analyzer 6 (Media Cybernetics). A Visual Basic based "in house" algorithm (written by Dr. David Kelly, Wellcome Trust Centre for Cell Biology, Edinburgh, UK) was applied to Image Pro Plus in order to normalize the fluorescence recovery and to calculate the $t_{1/2s}$ as previously described (Phair and Misteli, 2001). Briefly, one region of interest was measured in the background, the whole cell and the bleached area. Those three regions were measured for each time frame to be able to correct for photobleaching compared to the five prebleach images taken. If the imaged cell moved the measured region of the bleached area was adapted manually in xy position for each frame. Recovery halftimes were calculated from normalized fluorescence values, while the immediate post-bleach value was set to 0% and the average of the ten last points of recovery curve to 100%.

2.2.4.2 GFP-photoactivation (GFP-PA)

GFP-PA experiments were performed on the confocal microscope SP5 (Leica) using a 60× 1.4 NA objective lens and a 405 nm UV laser. HeLa cells were co-transfected with PA-GFP-NET fusion and monomeric RFP tagged NET20 in order to visualize the NE and the ER (observations from our lab indicate that NET20 is not likely to interact with NE components). During PA experiments cells were maintained in a 37°C heated chamber containing complete culture medium and gassed with a mix of 5%CO₂ and 95% air. The region to be activated was chosen according to the NET20-mRFP signal (about one third of the NE was activated for NE measurements and for ER measurements all of the ER, which was at least 2 microns away from NE was activated to avoid cross-activation of the NE). Activation was performed with 8% laser power (UV laser, 405 nm) for 0.5s and distribution of the activated GFP fluorescence was measured at 1% laser power (Argon laser 488 nm line) every 10s. Image data were collected with the SP5 application suite (Leica) and processed with Image-Pro Plus 7 software (Media Cybernetics). Briefly, after activation of either the NE or the ER area the fluorescence total intensity of the non-activated NE portion was measured for each frame. The initial value of the non-activated NE part was set to 100 and the intensities of the subsequent frames adjusted accordingly. Normalized intensities for each frame were averaged from different experiments and plotted.

2.2.4.3 Indirect immunofluorescence techniques and imaging analysis

Three days post-transfection cells were washed once with PBS and fixed in 4% formaldehyde (in PBS) for 7 min. Subsequently cells were washed three times with PBS and then incubated 5 min with 0.1% Triton-X100 (in PBS) to permeabilize the cell membrane for antibody access. After 3 washes with PBS cells were blocked with 5% BSA in PBS for 20 min followed by a 45 min incubation with the primary antibody (in PBS/5%BSA) against the corresponding antigen. Three washes with PBS were followed by a 30 min incubation with the respective secondary antibody (in PBS/5%BSA). After

incubation cells were washed with PBS and mounted with Fluoromount-G (EM Sciences) onto glass slides and used for microscopy.

2.2.4.4 Fluorescence *In Situ* Hybridization (FISH)

For fluorescence *in situ* hybridization (FISH) all cells were fixed in 4% paraformaldehyde/PBS and then aged for 2 days in the fridge. After aging cells were pre-permeabilized in 0.2% Triton-X-100/PBS for 5 min, washed 3 times in PBS and then blocked with blocking buffer (2% BSA/0.1% Tween20/PBS) for 20 min at room temperature. Primary antibody incubations were then performed at 37°C for 1 h and secondary antibody incubations for 45 min in blocking buffer. After 3 washes in PBS cells were again fixed with 2% formaldehyde for 5 min to fix antibodies prior to denaturing FISH steps. After antibody fixations cells were permeabilized with 0.5% Triton X-100/PBS for 5 min and subsequently washed 3 times with PBS.

Further, cells were pre-equilibrated in 2x SSC and treated with RNase (100 µg/ml) at 37°C for 1 h. After washing in 2x SSC cells were dehydrated with a 70%, 90% and 100% ethanol series. Slides were backed at 70°C in an oven for 5 min and then submerged in pre-heated (80°C) 70% formamide/2x SSC (pH 7.2) for 20 min followed by a incubation in ice cold 70% ethanol for 2 min and another ethanol dehydration series. Slides were air dried and pre-heated to 37°C on a heating block. For 22x22mm coverslip scale hybridizations (Thermo Fisher Scientific, MNJ-350-020H) 5µg salmon sperm DNA (Sigma, D7656) and 10µg human Cot1 DNA (Invitrogen, 15279-011), which were previously mixed in 30µl 100% EtOH and dried with the DNA Speed Vac (DNA 110, Savant), were dissolved in 8µl hybridization buffer (CamBio, provided with chromosome paints) and the mixture vortexed for 10sec 3 times every 5 min before 2.5 µl chromosome paints were added. The complete hybridization mix was vortexed for 10 sec 3 times every 5 min and then put into the 80°C water bath for 5 min in order to denature the DNA. The denatured hybridization mix was placed into a 37°C waterbath for 15 min. Preheated cell-containing slides were hybridized to biotin-labelled chromosome paints (in the hybridization mix) on a 37°C heating block. The

coverslip was sealed on the slide with Fixogum rubber cement (Marabu GmbH & Co. KG, Germany, 290110000) and the slide was placed into an aluminium foil covered metal plate floating in the 37°C water bath for 48h.

After two days of hybridization the rubber cement was carefully removed from the coverslips and the slides were put into 37°C preheated 2x SSC for 5 min so that the coverslip would come off. Slides were then washed 4x 3 min in 2x SSC at 45°C then 4x 3 min in 0.1x SSC at 60°C with slight shaking once every minute, then pre-equilibrated in 4x SSC, 0.1% Tween-20 and blocked in 2%BSA/4xSSC/0.1 Tween20/PBS for 10 min at room temperature before incubating with avidin or digoxigenin antibody (Roche). DNA was visualized with DAPI (4,6-diamidino-2 phenylindole, dihydrochloride) and coverslips mounted in Fluoromount G (EM Sciences).

2.2.4.5 FISH on human biopsy tissue sections²

Human tissue sections were provided by Professor David J. Harrison (Western General Hospital, Edinburgh, UK) and obtained according to University of Edinburgh Ethics protocols. Tissues were formalin fixed, paraffin embedded and sectioned at 5-6 µm thickness onto slides. Sections were subsequently prepared for whole chromosome painting as below.

For deparaffinization, tissues were heated in the oven at 70°C to melt the wax. After heating, sections were put straight into 100% Xylene for 10 min at 45°C, followed by 3 additional incubations in 100% Xylene for 10 min each at 37°C. After the Xylene steps sections were put 4x10 min into 100% Ethanol, followed by 2x 5 min incubations in 95% Ethanol and 2x 5 min in 70% Ethanol at room temperature, respectively. For complete rehydration tissue sections were put into deionized water for 5 min. Cells were then permeabilized with 1 M Na isothiocyanate (in H₂O) at 80°C for 30 min followed by 50 µg/ml pepsin (Sigma P-6887) in 0.01 N HCl at 37°C for 45

² *The FISH protocol for human tissue sections was modified from Cremer et al., 2008*

min. Cells were then dehydrated with an EtOH series and whole chromosome painting was performed as above.

2.2.4.6 Image generation, image processing and statistics

TIFF files were generated using Metamorph (Molecular Devices) or SP5 application suite (Leica) and exported into ImageProPlus at 12 bit for further analysis. Images were also directly imported into Adobe Photoshop CS for figure preparation, reducing them to 8 bit.

To determine if two datasets compared are different from one another the Kolmogorov-Smirnov test (KS-test) was applied.

2.2.4.7 Algorithm for dividing the nuclear area into 5 concentric rings

The algorithm that divides nuclear area into 5 concentric rings is based on an erosion script originally written by Paul Perry (Human Genetics Unit, MRC, Edinburgh) for IPLab Software. The principal of sequentially eroding from all edges 20% of the nuclear area was used for a new script written by Dr. David Kelly (Wellcome Trust Centre for Cell Biology, UK) to allow analysis with the ImageProPlus Software (Media Cyberkinetics, USA). For this script the total nuclear area must first be manually established by setting a threshold based on DAPI staining. The detailed script for this algorithm is provided in the Appendix section.

2.2.4.8 2D and 3D chromosome positioning analysis algorithms³

The 2D algorithm erodes the area of the nucleus based on the DAPI signal into 5 concentric rings of roughly same area. Subsequently this algorithm loads the image of the chromosome staining for the same nucleus and the total signal intensity of the chromosomes in this nucleus is set to 100%. Subsequently, the algorithm allocates the proportion of the chromosome signals in each of these rings and gives an output of the percentage of the total chromosome signal for each ring.

The 3D algorithm works basically like the 2D version, except that it erodes the nuclear volume from 3-dimensional reconstructions of the cell nucleus from z-stacks. This algorithm erodes the nuclear volume into 6 shells of roughly same volume and allocates the signal proportion of the chromosome in each individual shell. The detailed scripts for both algorithms are provided in the Appendix section.

³ *The 2D and 3D chromosome position analysis algorithms were written in ImageProPlus by Dr. David Kelly (Wellcome Trust Centre for Cell Biology, UK)*

Chapter 3

Targeting of membrane proteins to the INM is mediated by multiple mechanisms

Historically INM proteins were considered to move from the ER, where they are synthesized, to the ONM from where they further diffuse laterally through the peripheral channels of the NPC into the INM (Soullam and Worman, 1995). Later, separate findings suggested ATP- or Ran-dependence for translocation of INM proteins. These studies, however, did not distinguish whether there was one complex mechanism that utilizes both Ran and energy or if the two function in separate translocation pathways because the substrates and organisms used were so different. This chapter aimed to test this by analyzing a wider range of INM proteins and comparing their dependence on these requirements using FRAP as the method of choice.

3.1 How to study membrane protein translocation into the nucleus?

Many previous studies using FRAP to investigate transport of NETs have yielded distinct results. This could mean that several distinct mechanisms function for different cargoes that were used in each study. Furthermore, these differences in results could be due to the fact that the mechanism is just too complex and the many steps included have not been worked out. Another possibility is that each individual study used different variable parameters such as cell lines and imaging settings (some parameters of previous studies on NETs emerin, LAP2 β and MAN1 are summarized in table 6).

Table 6. Parameters of previous FRAP studies on NE protein mobility of emerin, LAP2 β and MAN1

NET studied	t _{1/2} [s]	Cell line used	% NE Area bleached (2D)	Reference
emerin	~60	COS-7	~30%	(Ostlund et al., 1999)
	~90	BHK	~20%	(Rolls et al., 1999)
	~60	HeLa	~2%	(Shimi et al., 2004)
LAP2 β	~100	BHK	~20%	Rolls et al., 1999
	~55	HeLa	~2%	Shimi et al, 2004
MAN1	~100	BHK	~20%	Rolls et al., 1999
	~50	COS-7	~20%	(Wu et al., 2002)

I also used FRAP to study translocation of NETs into the INM. Earlier, my supervisor made the observation that when bleached in the NE, fluorescence from GFP-tagged NETs was recovering slower in cells with little NET protein in the ER but fast in cells that had high NET accumulation in the ER. This observation argued that fluorescence recovery in the NE during

FRAP experiments was mainly due to NETs coming from the ER rather than from NETs that diffused from unbleached parts of the NE. While this observation was also suggesting that FRAP in the NE is likely to predominantly measure ER to INM translocation but it needed to be tested first as done by GFP-photoactivation and immunoelectron microscopy as described later in this chapter.

To circumvent variability due to imaging and other experimental parameters I conducted a study where 15 INM proteins⁴ were investigated by means of FRAP using constant parameters. For FRAP, the fluorescence recovery was measured before, during and after the laser bleach in the NE (Figure 14, A, upper panel) to generate fluorescence recovery curves (Figure 14, A, lower panel). Recovery halftimes were calculated from normalized fluorescence values, while the immediate post-bleach value was set to 0% and the average of the ten last points of recovery curve to 100%. Within this mobile fraction range of the recovery curves the $t_{1/2}$ was generated (please see Methods Chapter for details) as a measure for protein mobility in the NE.

The tested NETs displayed a wide range of mobilities in the NE suggesting the possibility that different translocation mechanisms can apply for individual NETs (Figure 14, B). I also assessed NET mobilities in the ER, all of which were higher than the ones when bleached in the NE. A faster mobility of NETs in the ER is expected as in theory diffusion of NETs in the ER should be completely unhindered and match that of completely free diffusion in a membrane. In contrast, NE mobility should be slowed because of a potential gating process for translocation and NET interactions with nuclear components after the translocation. Though the mobilities in the ER were faster than in the NE for all proteins the ER mobilities between NETs varied suggesting that free membrane diffusion does not apply to all of them

⁴ *LAP1-L, LAP1-S, LAP2 and emerin GFP fusion constructs were cloned by Dr. Eric Schirmer, the SUN2 GFP construct was a gift from Dr. Didier Hodzic*

thus arguing that NETs with slower mobility in the ER could exhibit additional functions in the ER.

Indication for measuring translocation of NETs by NE FRAP is provided by the fact that a known ER resident protein, Sec61 β , displays similar mobility rates in both ER and NE as most of this protein is expected to reside in the ER or in the ONM (evidence for this will be provided later in this chapter) and accordingly no gating process into the INM during translocation or binding in the INM, which is the case for actual INM proteins, should slow the mobility of Sec61 β in the NE (Figure 14, B, inset).

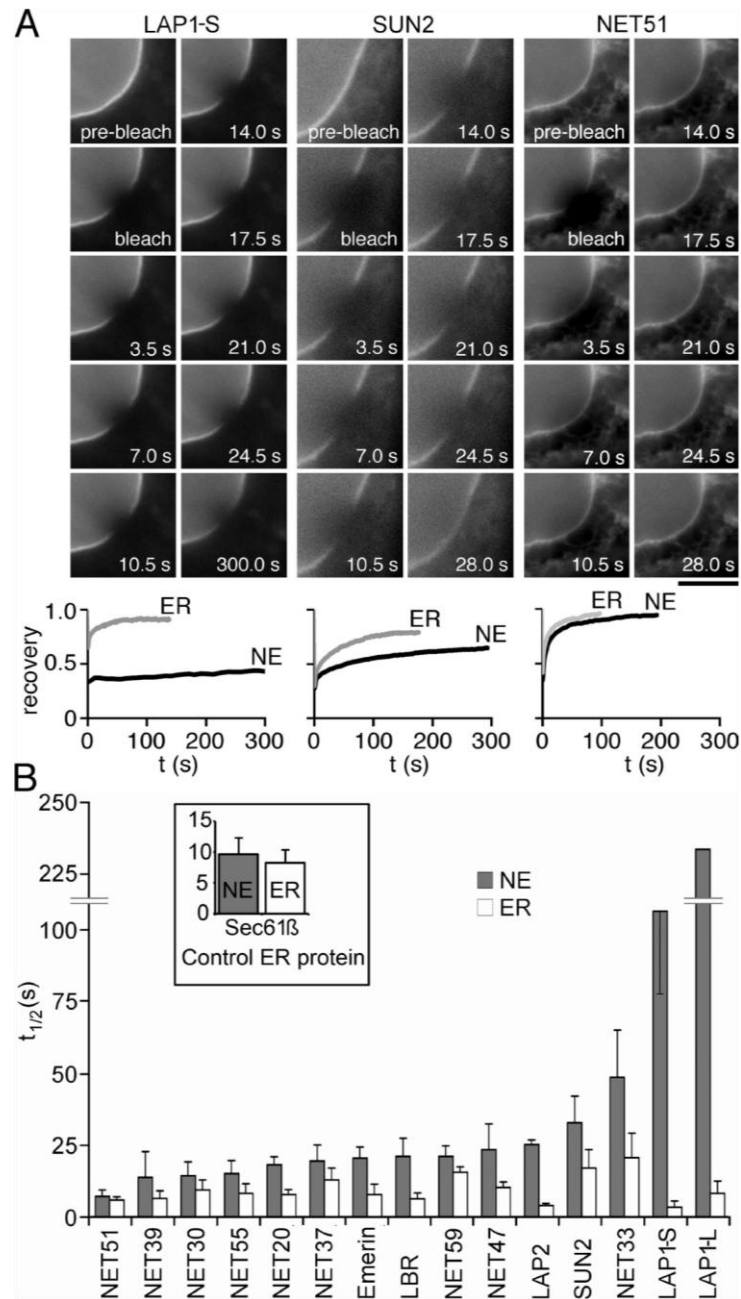


Figure 14. Wide range of NET recovery rates in the NE. (A) HeLa cells expressing NETs fused to GFP are bleached in the NE and the fluorescence recovery in the bleached area is monitored. Displayed are three NETs with different recovery rates: LAP1, SUN2 and NET51. Recovery was very slow LAP1, medium for SUN2 and fast for NET51. The recovery curves for ER and NE FRAP are displayed below. (B) The recovery half times for all tested NETs were calculated. NETs displayed a wide range of recovery rates. The ER protein Sec61 β (inset) displayed similar recovery rates in both NE and the ER. Error bars indicate standard deviation from at least 8 individual experiments. (Figure adapted from Zuleger et al., 2011a)

In addition to the recovery half-times I also assessed the mobile fractions of NETs in ER and NE (Figure 15). In FRAP experiments the fluorescence is often not recovering completely to pre-bleach levels. Assuming there is no protein aggregation or photobleaching during the recovery, the immobile fraction is due to a portion of the protein pool that is tightly bound and therefore highly immobile. The mobile fraction can be calculated by subtracting the % immobile fraction from the pre-bleach levels (100%). In the NE the NETs tested show a wide range of mobile fractions with LAP1-L being the most immobile NET while other NETs show more mobility with mobile fractions of 50-95%. It is striking that the five NETs with lowest mobile fraction (LAP1-L, LAP2, SUN2, LBR and LAP1-S) are widely characterized proteins that are known to have a wide range of binding partners in the nucleus. As expected, the mobile fractions in the ER were higher for all tested NETs (Figure 15).

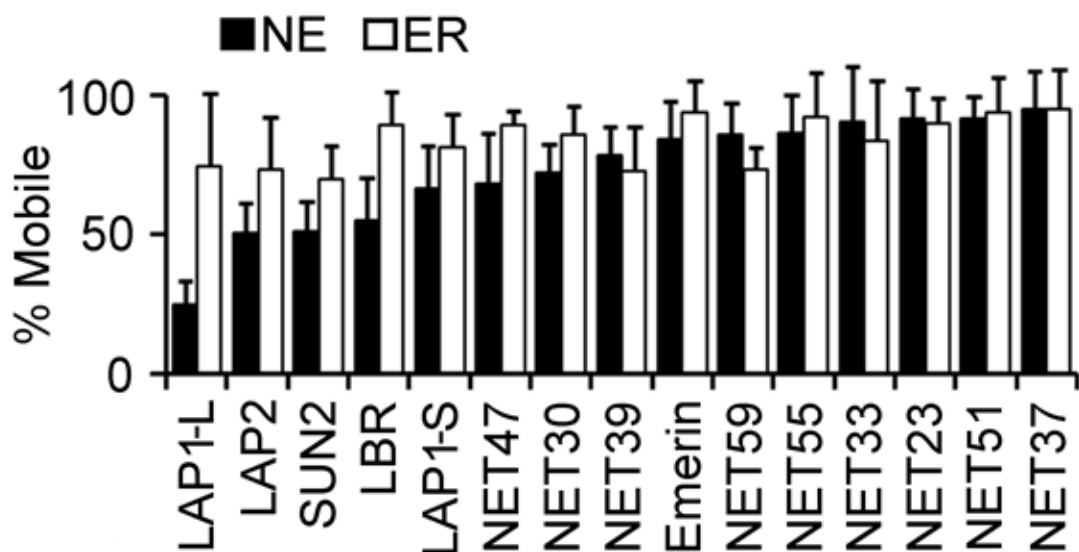


Figure 15. Mobile fractions of NETs in the NE and the ER as assessed by FRAP experiments. The tested NETs display a wide range of mobile fractions. In the NE LAP1-L shows very low levels of mobility (~25%) while all other tested NETs have mobile fractions between 50 and 95%. In the ER all NETs display higher mobility than in the NE. (Figure adapted from Zuleger et al., 2011a)

The results up to this point were generated during my Master's work and all remaining results reported are part of my PhD work.

3.2 FRAP in the NE is predominantly measuring ER-INM translocation

To further investigate whether the observed recovery in the NE during NE FRAP is not primarily due to general protein movement within the NE but rather movement from the ER into the NE the two possibilities were dissected by means GFP photoactivation (PA). The application of PA-GFP allows visualizing particular parts in the living cell and to detect the movement of this visualized protein pool. Hence, we can photoactivate a section of the NE and measure whether the protein stays tethered or moves and we can photoactivate in the ER and see if the protein accumulates in the NE. For this 5 NETs were fused to PA-GFP and cells expressing these fusions were analyzed. To discriminate the NE-NE movement NETs were activated in one part of the NE and the fluorescence accumulation in the non-activated part was detected (Figure 16, left). If the fluorescence recovery in FRAP experiments was primarily due to movement of protein within the NE, then the activated material must relatively quickly distribute from the activated part of the NE into the non-activated part of the NE. For measuring the ER-NE translocation step NETs were activated in the ER and the fluorescence accumulation in the NE was observed (Figure 16, right). If the fluorescence recovery in FRAP experiments was due to ER-NE translocation, then in PA experiments material activated in the ER should quickly accumulate in the NE and these accumulation kinetics should be similar to the NE FRAP recovery and should be much faster than movement within the NE during PA in the NE.

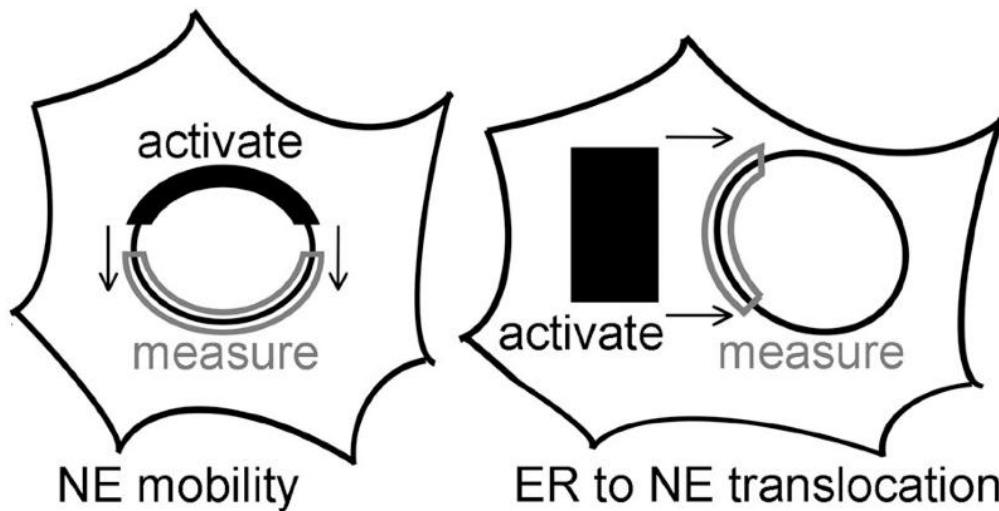


Figure 16. Schematic of the photoactivation (PA) experiment in order to distinguish NE-NE movement from ER-NE translocation. HeLa cells expressing PA-GFP-NET fusions were photoactivated in particular regions and the dispersion of the fluorescence monitored. Left: NETs were activated in one portion of the NE and the fluorescence distribution into the non-activated part of the NE was measured. Right: NETs were photoactivated in the ER and the fluorescence dispersion into the adjacent part of the NE was measured. (Figure adapted from Zuleger et al., 2011a)

Intriguingly, when activated in the NE only, NET37 and LAP2 exhibited extremely slow movement towards the non-activated part of the NE suggesting extremely low mobility within the NE *per se* (Figure 17, first and third column). This also means that in FRAP experiments in the NE the fluorescence recovery cannot be due to movement within the NE. When photoactivated in the ER, however, a quick accumulation of both NET37 and LAP2 in the NE was observed (Figure 17, second and fourth column) meaning that in NE FRAP the recovery is likely mainly due to movement from the ER into the NE. Hence, NE FRAP is likely to measure ER-NE translocation rather than NE-NE movement.

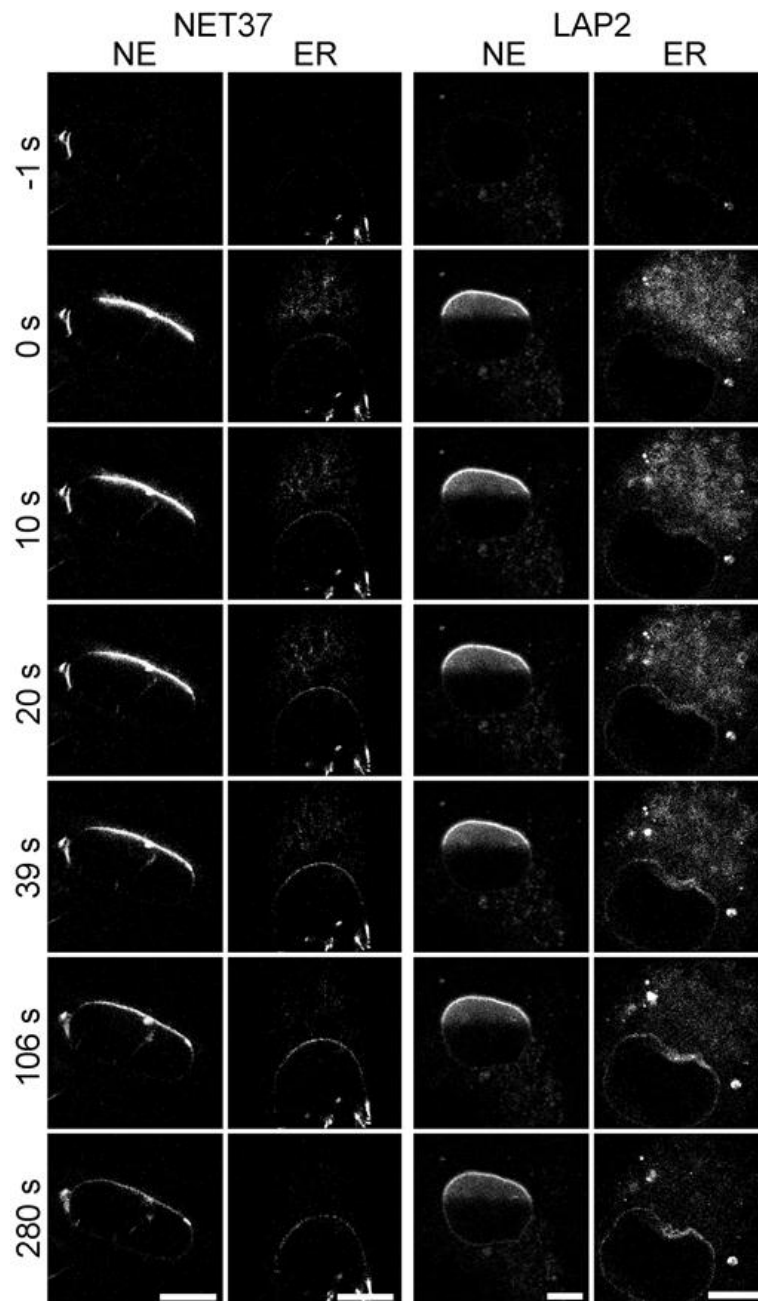


Figure 17. PA experiments distinguish NE-NE movement from the ER-NE translocation. NETs were fused to a photoactivatable version of GFP and expressed in HeLa cells. PA-GFP-LAP2 or NET37 fusions were activated in one portion of the NE (first and third column) and fluorescence intensity was measured in the non-activated portion of the NE. Additionally NETs were activated in the ER and the fluorescence was measured in the non-activated NE portion proximal to the activated ER area (second and fourth column). While the distribution of fluorescence (and therefore NETs) was very slow when activated in the NE (first and third column), the fluorescence accumulation in the NE was very fast when NETs were activated in the ER (second and fourth column). Scale bars are 5 μ m. (Figure adapted from Zuleger et al., 2011a)

In addition to NET37 and the LAP2 same PA experiments were performed on NET51, NET55 and emerlin and the measurements from several repeats quantified and averaged (Figure 18). The results again indicated that NET movement within the NE is minimal (black line; after the activation of one portion of the NE the signal accumulation in the non-activated NE portion is small as indicated by the small slope); however the mobility of NETs during translocation from the ER into the NE was high (grey line; the NE signal accumulation after the activation in the ER is high as indicated by the comparatively large slope). This result strongly supports the idea that most of the recovery during FRAP experiments is not due to movement within the NE itself but rather due to translocation of NETs from the ER into the NE.

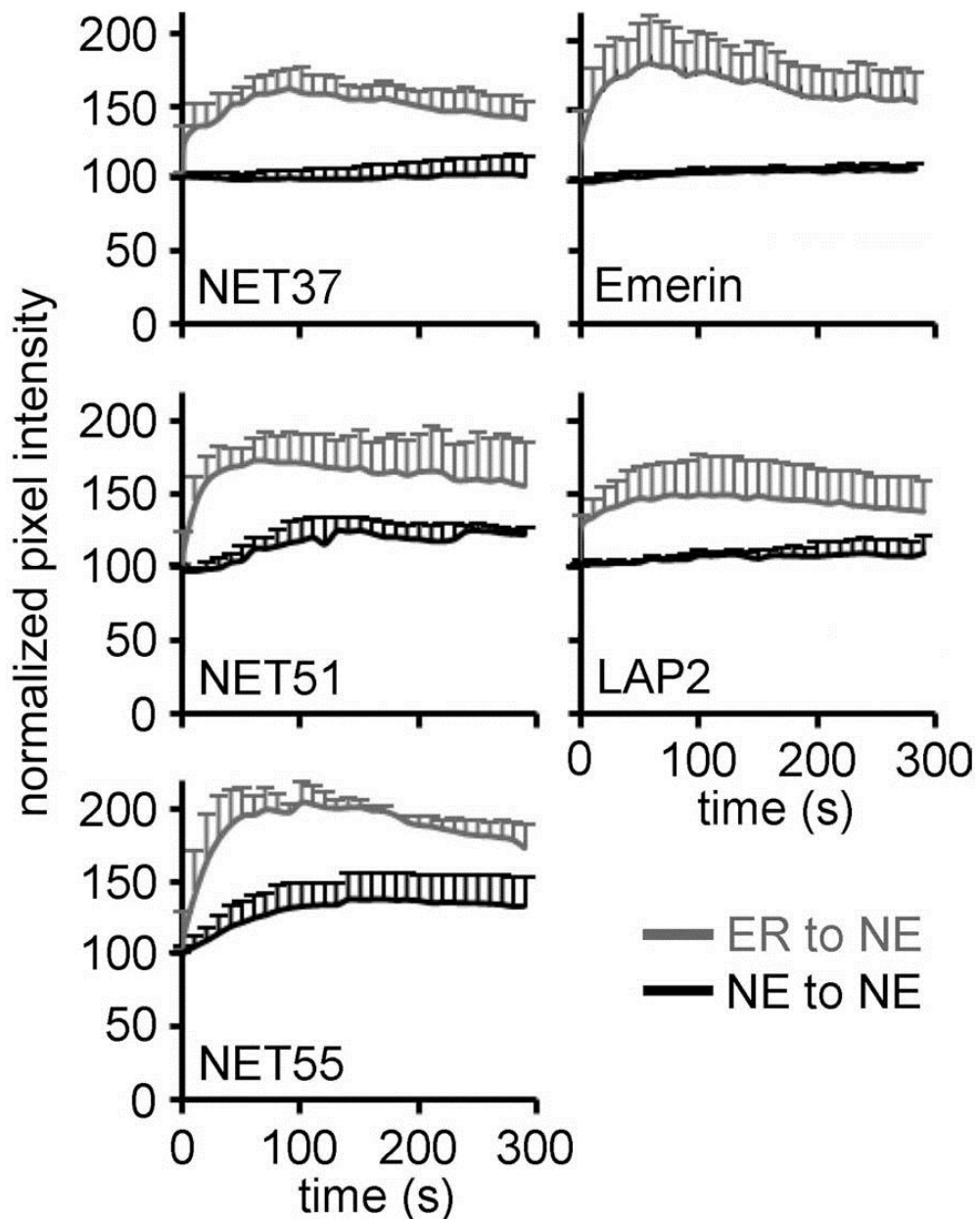


Figure 18. ER-NE translocation is faster than NE-NE movement (Quantification of PA experiments as described in figures 16 and 17). Fluorescence accumulation was measured in the non-photoactivated NE area after photoactivation in either the NE (black) or the ER (grey) (see figure 16 for details). While fluorescence accumulation in the NE was very rapid and intense after PA in the ER (grey), the NE-NE fluorescence movement was barely evident for all tested NETs (black). Fluorescence values are in arbitrary units and are normalized. Error bars indicate standard deviations from 3-7 individual experiments. (Figure adapted from Zuleger et al., 2011a)

The table below summarizes the $t_{1/2}$ s of slow NET diffusion within the NE in PA experiments and the much faster recovery kinetics of the same NETs in the NE during FRAP experiments. The $t_{1/2}$ s for ER-NE translocation as measured by PA are also presented and are roughly matching the kinetics in NE-FRAP again supporting that NE FRAP is predominantly measuring ER-NE translocation.

Table 7. NE FRAP $t_{1/2}$ s and $t_{1/2}$ s for ER-NE translocation and NE-NE movement as measured by PA

NET	FRAP: NE $t_{1/2}$ [s]	PA: ER-to-NE $t_{1/2}$ [s]	PA: NE-to-NE $t_{1/2}$ [s]
NET37	19.3 ± 5.5	27.8 ± 5.0	NA*
NET51	7.1 ± 2.2	7.0 ± 2.1	70.9 ± 32.2
NET55	14.9 ± 4.6	17.7 ± 9.0	47.6 ± 18.5
emerin	20.3 ± 3.8	12.0 ± 4.2	56.8 ± 23.0
LAP2	25.0 ± 1.6	14.6 ± 6.1	70.2 ± 52.9
* No $t_{1/2}$ could be calculated for NET37 in NE-NE photoactivation because it exhibited too little movement			

Given the results above I am reasonably confident that most of the recovery in FRAP experiments in the NE is mainly due to ER-NE translocation rather than redistribution within the NE. However, it should be noted that due to the fact that the NET proteins are exogenously overexpressed in FRAP experiments, several additional pools are likely to impact the recovery behaviour in the NE. One such pool, for instance, is the mobile pool in the INM membrane, which arises from saturation of binding sites for the NET in the INM due to NET overexpression. There is also the highly immobile pool in the INM, which is the reason for the immobile fraction. This immobile pool is blocking the diffusion of molecules from the ER to the INM. There is another NET pool that is diffusing from the ER into the ONM and one more pool that is translocating from the ONM into the INM. Our PA results indicate that the pools, both bound and unbound, in the INM can be

neglected as there is hardly any movement within the NE but in NE FRAP experiments recoveries for most NETs exceed the 80% pre-bleach intensities meaning that recovery must be principally due to ER-NE translocation. Thus only the ER-ONM pool can skew our INM translocation measurements by FRAP. As explained in the following example. If most NET molecules are in the ONM rather than INM and we see over 80% fluorescence recovery after the photobleach for most NETs in the NE, than what we would measure by NE FRAP is movement from the ER in to the ONM but not translocation from the ER over the ONM into the INM. However, when most of the NET molecules are in the INM but not the ONM then high fluorescence recoveries in the NE after bleaching could not possibly be due to ER-ONM movement but must be due to translocation from the ER over the ONM into the INM. Thus, I needed to test whether most of the NET material is in the INM or ONM.

The spatial resolution of FRAP and PA is not sufficient to distinguish between the INM and ONM, thus I measured the distribution of NET-GFP fusions between the INM and ONM by immunogold labelling of the NETs with GFP antibodies and subsequent analysis by electron microscopy⁵. This revealed that the INM harboured the majority of material for all NETs tested (Figure 19). We also tested the INM/ONM distribution of the ER control protein Sec61 β ⁶, which as expected, had most of its material (93%) in the ONM and only 7% in the INM, also meaning that exogenous overexpression of an ER protein does not result in its subsequent accumulation in the INM. The high proportion (~55-80%) of NET accumulation in the INM also meant that the fluorescence recovery in FRAP experiments cannot be due solely to ER-ONM movement because in that case NETs would not recover to 80% (and higher) pre-bleach fluorescence levels but would recover to maximally

⁵ *The immuno-gold labelling was performed by Christine Richardson in the laboratory of Dr. Martin Goldberg, Durham University, UK. I did the electron microscopy and performed the quantification of the obtained micrographs*

⁶ *Sec61 β plasmid obtained from Rapoport laboratory, Harvard Medical School, Boston, USA*

45% as this is the maximum percentage of molecules in the ONM we measure for GFP-NETs.

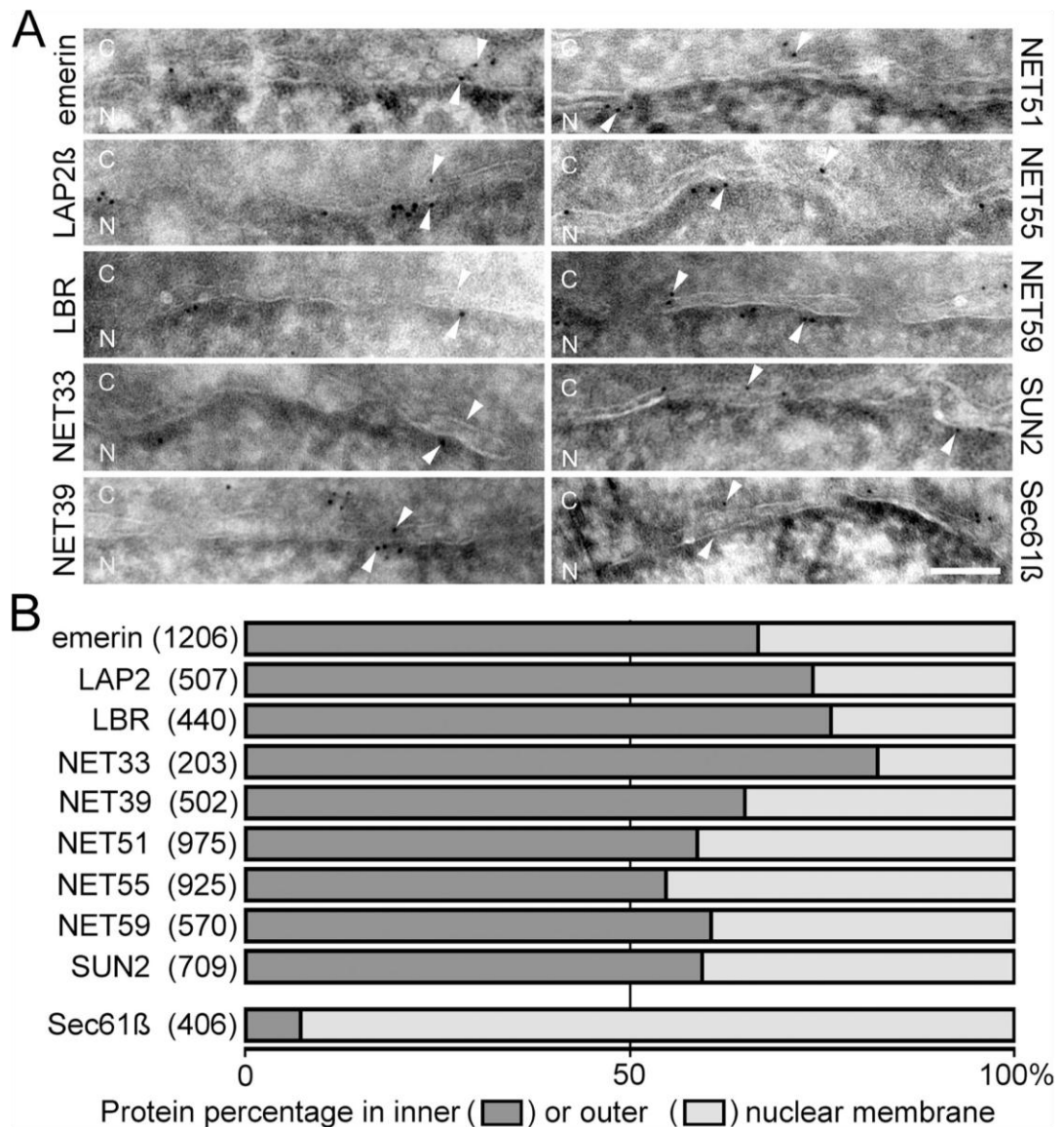


Figure 19. Electron microscopy reveals the ONM and INM distribution of exogenously expressed GFP-NETs. (A) Electron micrographs of NET fusion proteins labelled by 5nm gold particles (black spots). NETs display a bigger proportion of gold particles in the INM compared to the ONM whereas the ER control protein Sec61β has more gold particles in the ONM than in the INM. Downward arrowheads mark the ONM and upward arrowheads mark the INM. The nucleoplasmic and cytoplasmic faces are indicated with N and C, respectively. Scale bar is 100nm. (B) Quantification of the gold particle counts in the inner (dark grey) or outer (light grey) nuclear membrane for each NETs tested. The numbers of total gold particles counted for each protein are indicated next to each sample. (Figure adapted from Zuleger et al., 2011a)

Based on the above observations, I will be using the term “translocation” for movement from the ER into the INM of the NE even though I acknowledge that NE FRAP (and likewise PA in the ER and the subsequent accumulation of the signal in the NE) is measuring the translocation predominantly but not exclusively.

3.3 Distinct translocation requirements for distinct NETs

Having determined that FRAP in the NE for this set of NETs was principally measuring the translocation step from the ER-INM, we could use this method to further test the different requirements reported for the translocation of NETs. These experiments will also determine whether the different requirements reported previously apply to all of our NETs. For testing specific requirements of NET translocation by FRAP we reduced the number of NETs to six. These six NETs were representing proteins with different characteristics such as total protein size, size of the nucleoplasmic domain, NLS prediction score and total number of transmembrane spans.

First, we tested if ATP is a requirement for NET translocation as reported by the Gerace laboratory (Ohba et al., 2004). For this cells were depleted of ATP and analyzed by FRAP in the NE (Figure 20). Cells not depleted for ATP served as controls. Among the six tested NETs only translocation of SUN2 and emerin was impaired by ATP depletion. The mobile fraction of SUN2 decreased so much that an accurate $t_{1/2}$ could not be calculated (asterisks). For emerin the mobile fraction also decreased by more than 2-fold resulting in the doubling of the $t_{1/2}$. All of the other four NETs tested were unaffected by ATP depletion.

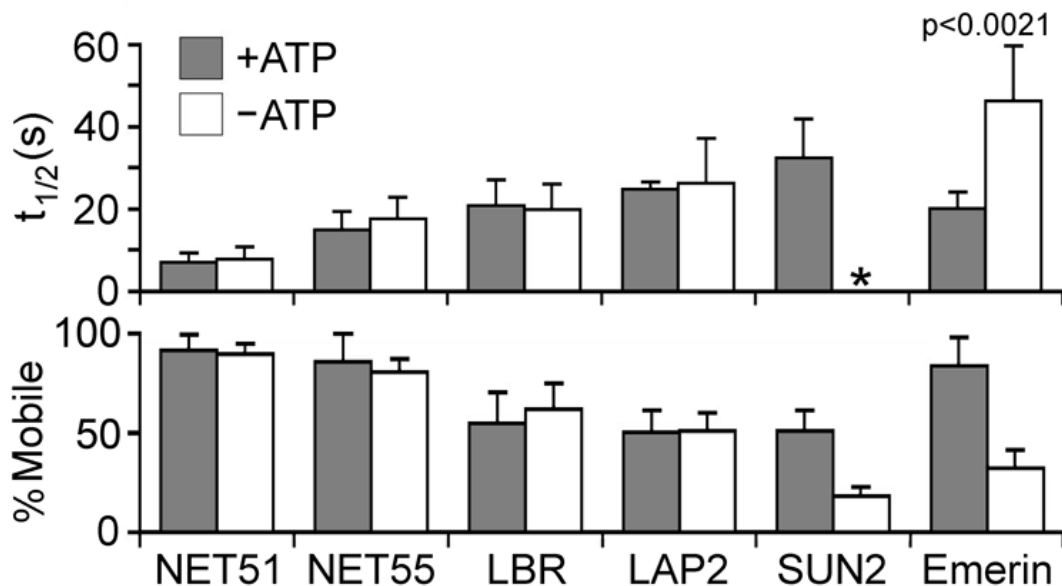


Figure 20. SUN2 and emerlin require ATP for translocation. FRAP experiments in the NE were performed in medium depleted for ATP and compared to non-depleted control cells. The $t_{1/2}$ s are presented in the top panel and the mobile fractions in the bottom panel. The mobility of NET51, NET55, LBR and LAP2 were not affected by ATP depletion but both SUN2 and emerlin had a visibly inhibited mobility under depletion conditions. For emerlin the $t_{1/2}$ doubled and the mobile fraction dropped by 2-fold whereas for SUN2 the mobile fraction dropped to such an extent that a $t_{1/2}$ value could not be accurately determined (asterisks). Error bars indicate standard deviation from at least 8 individual experiments. (Figure adapted from Zuleger et al., 2011a)

We next aimed to test if the nucleoplasmic region of emerlin (1-224aa) is required for its ATP-dependent translocation into the INM. This was the most likely case since this region is the most accessible (more accessible than the luminal region) for proteins and other binding factors. For this the nucleoplasmic emerlin region was fused to NET51 and LBR, two proteins that did not required ATP as wild-type counterparts. Wild-type emerlin and NET55 were used as positive and negative controls, respectively. The proteins were analyzed by FRAP in the NE with and without ATP depletion. Like wild-type emerlin also NET51 and LBR acquired ATP dependence when fused to the nucleoplasmic region of emerlin meaning that the nucleoplasmic domain of emerlin is required its ATP-dependent translocation. NET55 served as negative control since it was not affected by ATP depletion in previous experiments (Figure 21).

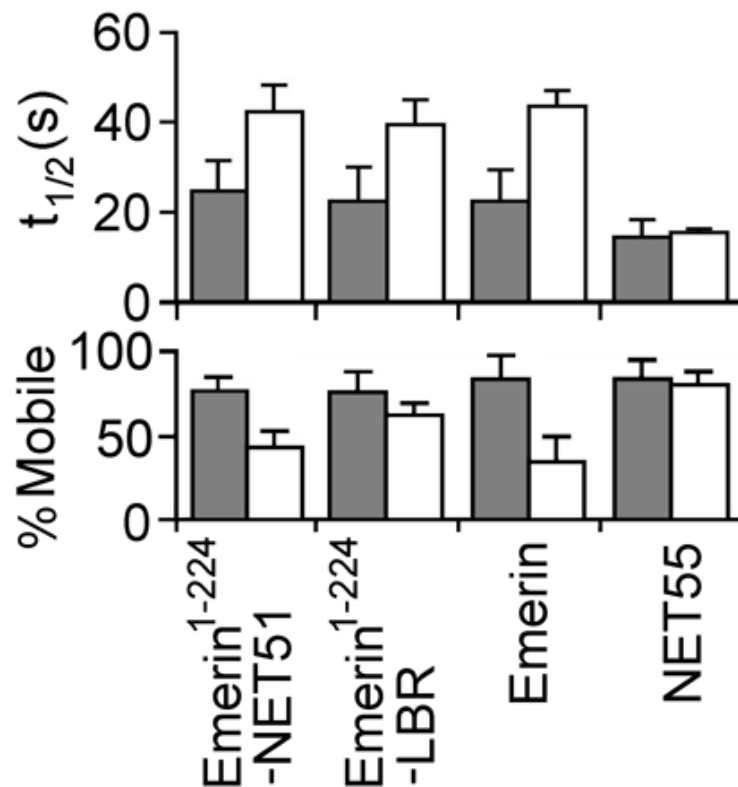


Figure 21. The nucleoplasmic domain of emerin is required for its ATP-dependent translocation. The nucleoplasmic region of emerin (1-224aa) was fused to NET51 and LBR, two proteins that do not require ATP for nuclear translocation. These chimeric constructs were tested by FRAP in the NE upon ATP depletion and compared to wild-type emerin and NET55. The $t_{1/2}$ s are presented at the top and the mobile fractions at the bottom. When fused to the nucleoplasmic region of emerin both NET51 and LBR are conferring ATP dependence to a similar extent as the wild-type emerin although the mobile fractions for both chimeric constructs are higher than that of wild-type emerin. Wild-type NET55 served as a negative control and was not affected by ATP depletion. Error bars indicate standard deviation from at least 8 individual experiments. (Figure adapted from Zuleger et al., 2011a)

Importantly, we also tested if ATP was required for NET mobility within the ER as the recovery in the NE could potentially also be impaired due to slower protein movement in the ER. To answer this, FRAP experiments upon ATP depletion were performed on emerin and SUN2 in the ER and compared to ATP non-depleted control cells (Figure 22). NET51 served as a negative control. Like in the NE, emerin and SUN2 displayed ATP dependence in the ER while NET51 was unaffected. Thus ATP in some way facilitates ER diffusion of emerin and SUN2.

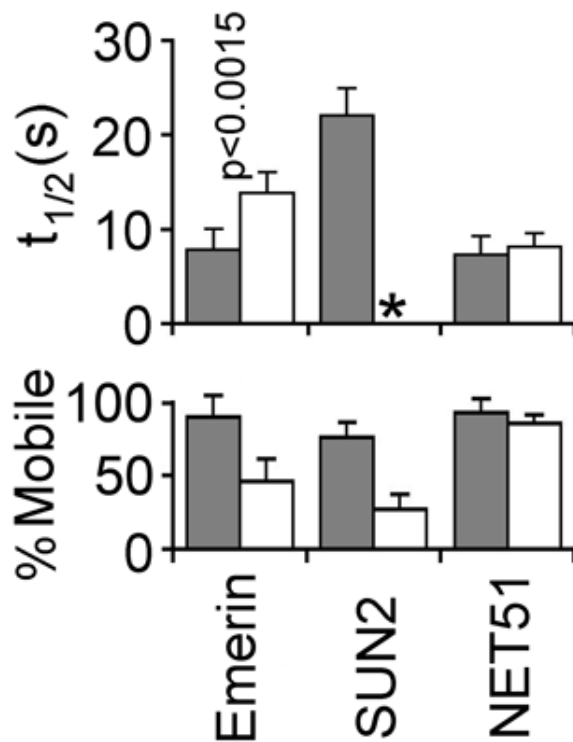


Figure 22. Emerin and SUN2 require ATP also for the mobility within the ER. Fluorescence recovery for emerin, SUN2 and NET51 was measured after photobleaching in the ER with and without ATP depletion. Both emerin and SUN2 were affected by depletion whereas NET51, which served as a negative control, was not. Error bars indicate standard deviation from at least 8 individual experiments. (Figure adapted from Zuleger et al., 2011a)

Next, we tested if Ran-GTPase activity is required for NET translocation from the ER into the INM, a requirement that was suggested by the Blobel laboratory (King et al., 2006). For this, a dominant negative RanQ69L mutant of Ran was co-transfected with GFP-NETs and cells were analyzed by FRAP in the NE (Figure 23). Since Ran is small, only ~25 kDa, it is likely to lose its function when fused to a big fluorescent tag like GFP. Thus, we created a plasmid construct that was coding for untagged Ran and additionally for an mRFP reporter that was driven by a separate promoter. The expression of the Ran mutant was confirmed by both Western blotting and indirect immunofluorescence (Figure 23, A). Of the six proteins tested only LBR was significantly ($p < 0.001$) affected by Ran activity depletion

(Figure 23, B). The $t_{1/2}$ of LBR more than doubled compared to Ran non-depleted control cells (Figure 23, B upper panel). Interestingly, the mobile fraction of LBR was hardly affected by Ran function depletion (Figure 23, B bottom panel).

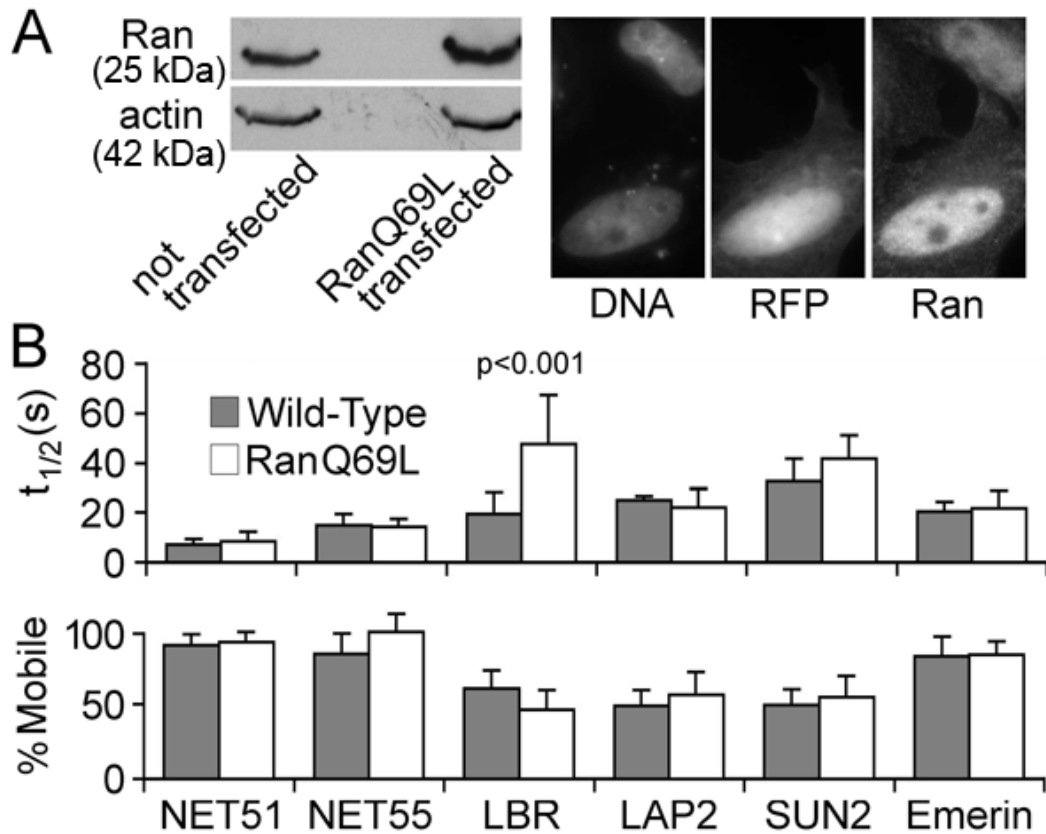


Figure 23. Depletion of Ran function affects LBR translocation. FRAP experiments were performed in HeLa cells expressing NETs upon Ran GTPase function depletion and compared to non-depleted control cells. Ran function was depleted by co-expression of the dominant negative mutant RanQ69L. **(A)** Left panel: Confirmation of the Ran mutant expression by western blotting, actin was used as a loading control. Right panel: Confirmation of the Ran mutant expression by immunofluorescence. The bottom cell expresses the mRFP as an expression marker for the Ran mutant. The mRFP gene is on the same plasmid as the Ran mutant but driven from a separate promoter because Ran function is sensitive to ectopic tags. The bottom cell showing the mRFP expression also confirms higher Ran staining compared to the untransfected control cell. **(B)** Only LBR fluorescence recovery after photobleaching is affected when Ran function is depleted. The recovery half time of LBR doubled compared to the wild-type control. Error bars indicate standard deviation from at least 8 individual experiments. (Figure adapted from Zuleger et al., 2011a)

There is a possibility that proteins that were neither affected by ATP nor by Ran function depletion are actually able to use both pathways and in the case of depletion of one mechanism the other pathway would rescue the depletion effect. To test this we depleted both ATP and Ran function simultaneously (Figure 24). Like with depletion of ATP or Ran alone translocation was affected only for LBR, SUN2 and emerin. Interestingly, depletion of ATP and Ran together yielded no greater reduction in translocation than either alone for any of the three proteins that required one or the other for translocation. This indicates that ATP- and Ran-dependent translocation pathways occur separately from each other. ATP and Ran function double-depletion did not affect translocation of NET51, NET55 and LAP2. Thus for these three proteins we can exclude the scenario that upon single depletion of the ATP pathway, for example, the Ran pathway is rescuing the translocation.

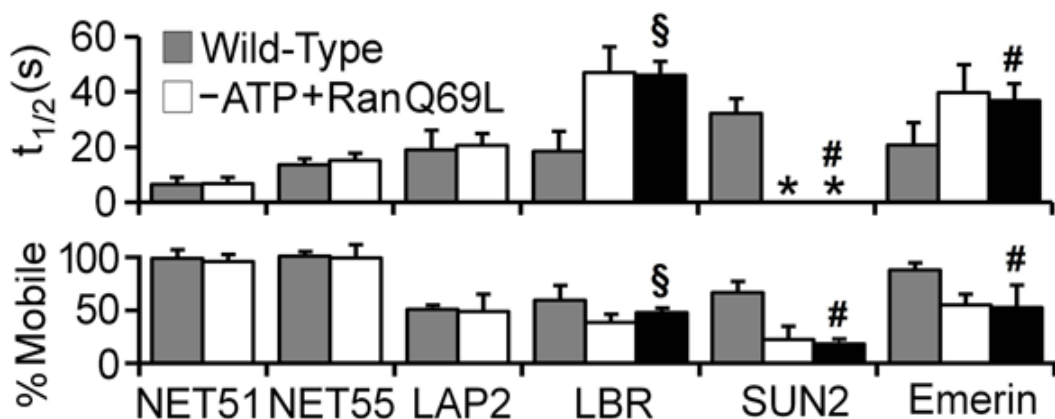


Figure 24. ATP and Ran requirement pathways for NET translocation act independently from one another. HeLa cells were subjected to FRAP upon depletion of both ATP and Ran and compared to untreated control cells. NET51, 55 and LAP2 were not affected by the double depletion. Depletion of ATP and Ran did not affect the LBR translocation stronger than depletion of Ran function alone (black bar, §). SUN2 and emerin were affected by double depletion to the same level as by ATP depletion alone (black bars, #). No accurate $t_{1/2}$ could be calculated for SUN2 due to a strong drop in the mobile fraction (asterisks). Error bars indicate standard deviation from at least 8 individual experiments. (Figure adapted from Zuleger et al., 2011a)

3.4 Ran-mediated translocation is independent of NLSs or FGs

Since LBR was the only tested NET affected by Ran we searched for specific LBR characteristics that distinguish it from the other tested NETs, because these characteristics could be the determinants for Ran function requirement during translocation. One such striking characteristic of LBR was the presence of many nuclear localization sequences, short NLSs. The three strongest NLSs out of four are located between 1-128 aa of the LBR (as predicted by the pSORTII algorithm, the NLS prediction score for this LBR region is 1.19). Testing if NLSs are determinants of the Ran pathway could be done either by fusing the LBR-NLSs to proteins that do not have any or by mutating the NLSs in the LBR sequence. Since the latter is likely to result in the disruption of the LBR's structure we went ahead with the first option. Therefore we fused this LBR-NLS region to NET51, NET55 and emerin, all of which did not confer Ran function dependence. Additionally these three proteins were separately fused to the classical SV40NLS. The NLS prediction scores before and after fusion to the NLSs are provided in the table 8.

Table 8. NET51, NET55 and emerin NLS scores before and after fusion to LBR-NLS or SV40 NLS

NET	wild-type	NET+ LBR-NLSs	NET+ SV40-NLS
NET51	-0.22	1.20	1.52
NET55	-0.47	0.94	1.27
emerin	0.02	1.44	1.76

Note: The NLS prediction score for LBR is 1.19

All these fusions were analyzed by FRAP upon Ran function depletion (Figure 25, A). None of the NLS-fusion NETs were affected by Ran function depletion, while inhibition was observed for wild-type LBR being a positive control.

As the wild-type NETs were unaffected by Ran depletion they must have other mechanisms for translocation and these mechanisms might allow for translocation even if the additional NLSs contributed a possible Ran component. Thus a better experiment would be to fuse an NLS to a non-INM protein, for example an ER protein, and test then if Ran function depletion would interfere with translocation into the INM. To do this we fused the classical SV40NLS to the ER protein Sec61 β . While the wild-type Sec61 β localized strongly to the ER and to some minor extent also to the NE, the NLS-fused version of this protein localized mainly to the NE as shown by immunofluorescence (Figure 25, B upper panel). At higher resolution Immuno-EM confirmed that wild-type Sec61 β is accumulating preferentially in the ONM while the SV40NLS-fused version resides mainly in the INM (Figure 25, B lower panel). However, when analyzed by FRAP neither wild-type Sec61 β nor Sec61 β -NLS were affected by Ran function depletion (Figure 25, C) while wild-type LBR being a positive control displayed inhibition.

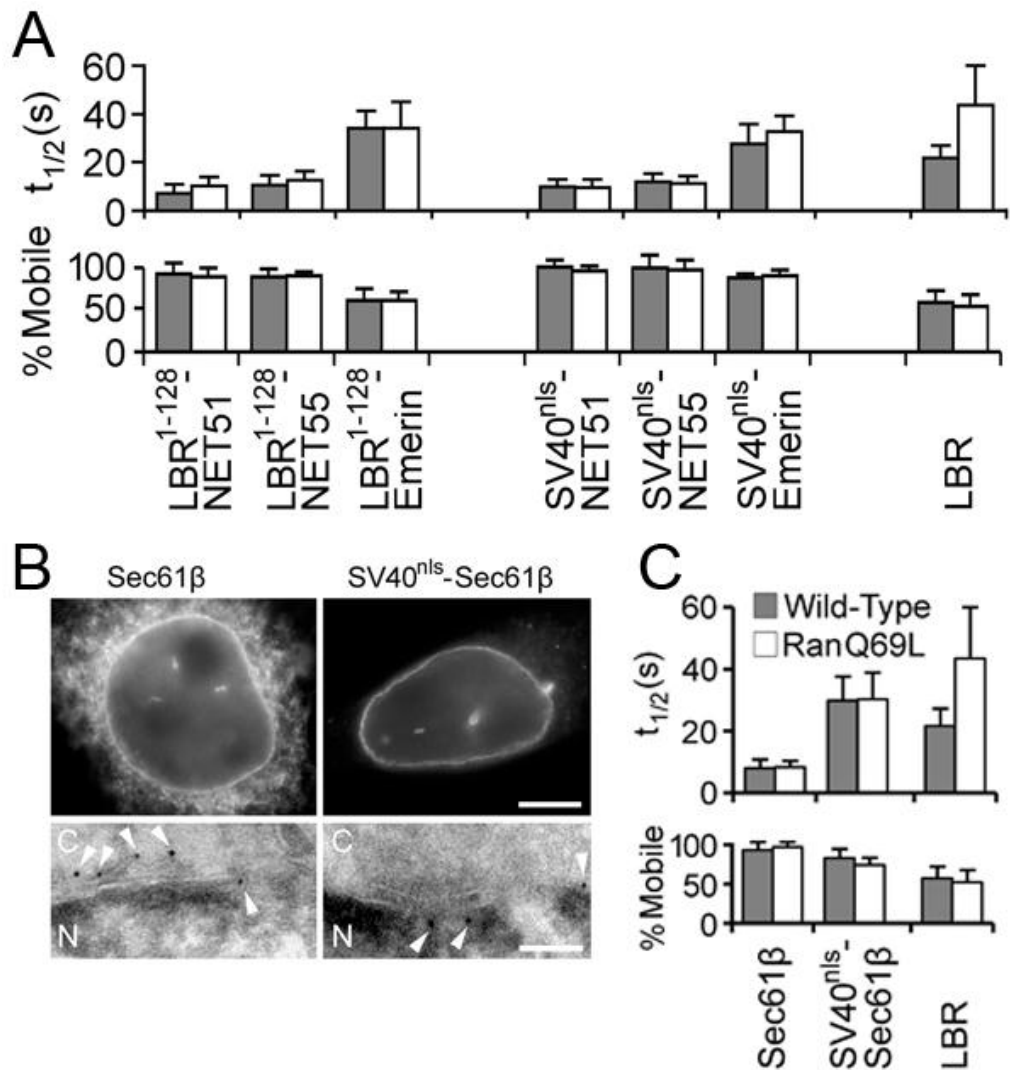


Figure 25. Ran-mediated translocation is not dependent on nuclear localization sequences (NLS). (A) The first 128 amino acids of LBR containing three putative NLSs (as predicted by the NLS prediction algorithm pSORTII) or the SV40NLS were fused to NET51, 55 and emerlin, three proteins that did not require Ran function as wild type counterparts. When tested upon Ran depletion conditions none of the chimeric fusion proteins confirmed inhibition in translocation. LBR serving as a positive control did show an inhibited translocation. (B) Localization of the ER protein Sec61 β wild-type and its counterpart, which was fused to the classical SV40NLS by immunofluorescence (top panel) and electron microscopy (bottom panel). Wild-type Sec61 β localizes exclusively to the ER membranes and the ONM whereas the SV40NLS-Sec61 β localizes mainly to the INM. (C) Sec61 β wild-type and SV40NLS-Sec61 β were analysed by FRAP upon depletion of Ran. No inhibition in translocation was observed for either protein while the positive control LBR was affected in its translocation. Error bars indicate standard deviation from at least 8 individual experiments. (Figure adapted from Zuleger et al., 2011a)

Even though the translocation kinetics of the Sec61 β -NLS construct were not affected by Ran depletion, the distribution of molecules between the ONM and INM might have changed under this condition making an effect invisible by FRAP. Therefore we used immunoelectron microscopy to check for the potential change in the distribution of the constructs with and without Ran function depletion (Figure 26). As already described wild-type Sec61 β had about 95% of its material in the ONM, but when fused to the classical SV40NLS this protein accumulated about 80% of its material in the INM. Ran depletion only slightly reduced the INM accumulation to ~75%. The same observation was made for LBR. About 75% of LBR molecules reside in the INM under normal conditions but when Ran function is depleted the INM accumulation slightly drops to ~70%. Together with the previous observations of NLS-chimeras upon Ran function depletion this data suggests that NLSs do not confer Ran-dependent NET translocation into the INM.

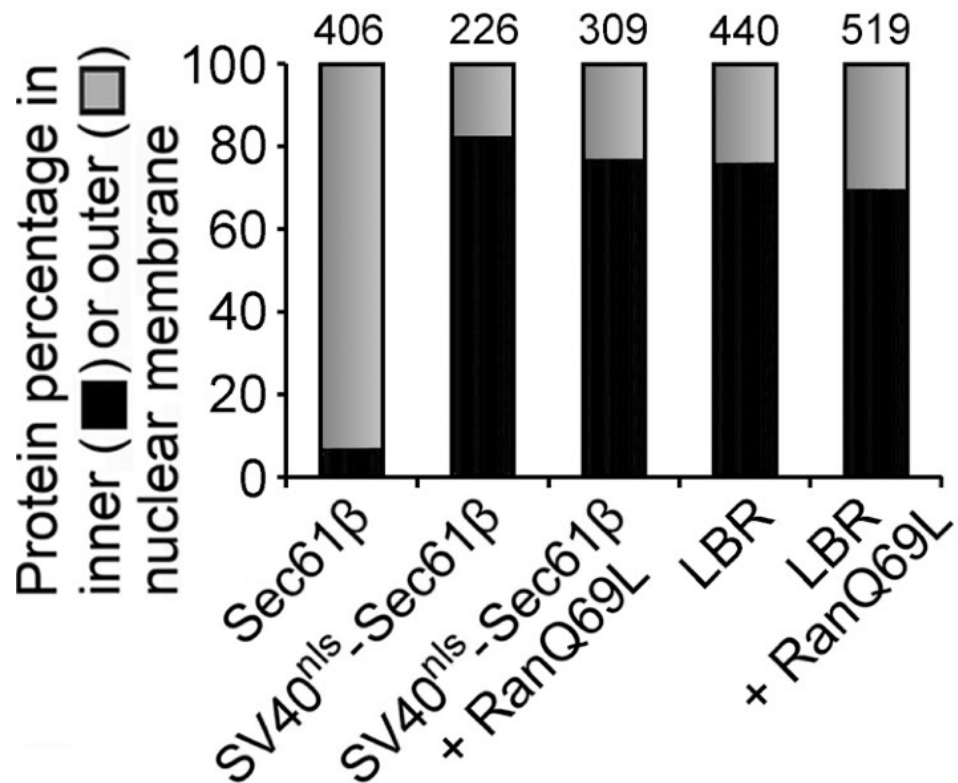


Figure 26. NE distribution of Sec61β, NLS-Sec61β and LBR with and without Ran function depletion. The INM and ONM distribution of the Sec61β, NLS-Sec61β and LBR was assessed by electron microscopy micrographs of 30-50 individual cells. The amount of total gold particles counted is indicated on top of each sample. The percentage of gold particles in the INM is labelled in black and percentage in the ONM in gray. About 5% of Sec61β are residing in the INM whereas when the SV40NLS is added to this protein the gold particle percentage goes up to ~80%. Upon Ran function depletion the percentage of NLS-Sec61β goes slightly down to ~75%. About 75% of LBR reside in the INM under non-depleted conditions but when Ran function is depleted, this percentage goes also slightly down to ~70%. (Figure adapted from Zuleger et al., 2011a)

Since NLSs did not confer Ran-dependent INM protein translocation we searched for further LBR characteristics that distinguish it from the other NETs. One such characteristic was a high number of phenylalanine/glycine (FG)-repeats in the LBR sequence. This amino-acid pairing is not very common as only 1.5% of all human proteins possess six or more FGs (Zuleger et al., 2011a). FGs occur in nucleoporins and transport receptors (for example importin-α and importin-β) and these FGs are believed to facilitate

the transport of soluble cargoes into the nucleus *via* the central channel of the NPC (Rexach and Blobel, 1995) though clear experimental data for this hypothesis is still missing. LBR has six FGs while NET51 has one and NET55 has four. Since both NET51 and NET55 did not show any Ran depletion dependence both were fused to a short artificial sequence containing four FGs (MFGHTFGFGQSVFG) and these constructs were tested by FRAP with and without Ran function depletion⁷ (Figure 27). LBR serving as a positive control exhibited Ran dependence while neither NET51 nor NET55 when fused to the FG-sequence were affected. Thus, Ran function dependence does not seem to depend on FGs either.

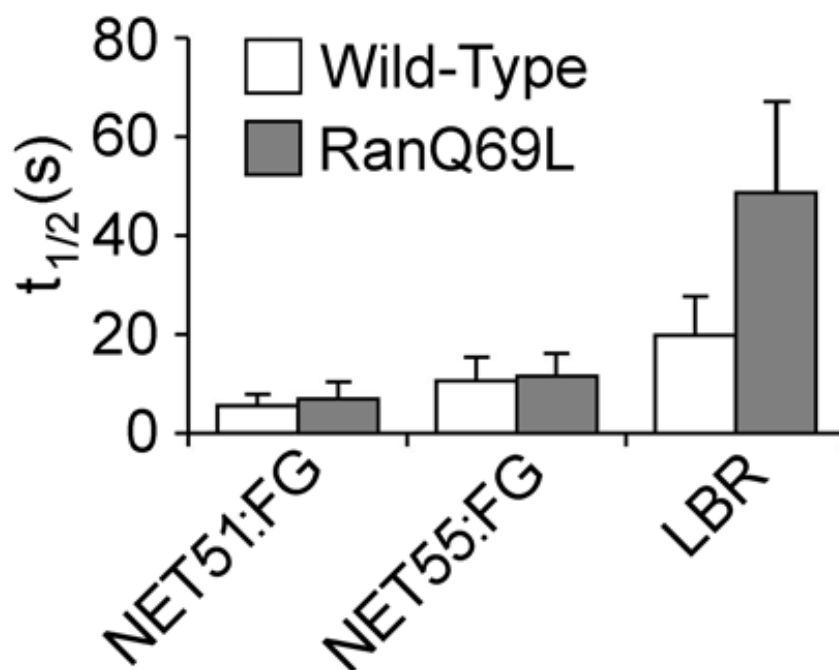


Figure 27. Addition of Phenylalanine-Glycines (FGs) does not confer Ran-dependence for translocation of NETs into the INM. An FG-containing sequence (MFGHTFGFGQSVFG) was fused to NET51 and NET55. These constructs were analyzed by FRAP in the NE with and without Ran function depletion. Neither NET51:FG nor NET55:FG was inhibited by Ran function depletion unlike LBR, which was used as a positive control. Error bars indicate standard deviation from at least 8 individual experiments. (Figure adapted from Zuleger et al., 2011a)

⁷ An alternative way to test for FG-facilitated Ran dependence would be to mutate all the FGs in LBR. We decided not to do this as it would likely result in the change of the protein conformation

3.5 FGs are enriched in INM proteins and facilitate their translocation

Though FGs did not confer Ran-dependent INM translocation, we observed that when NET51 and NET55 were fused to the four FG-containing sequence, the translocation occurred significantly faster than that of their wild-type analogues (Figure 28) suggesting that FGs could play a role in translocation of NETs into the INM.

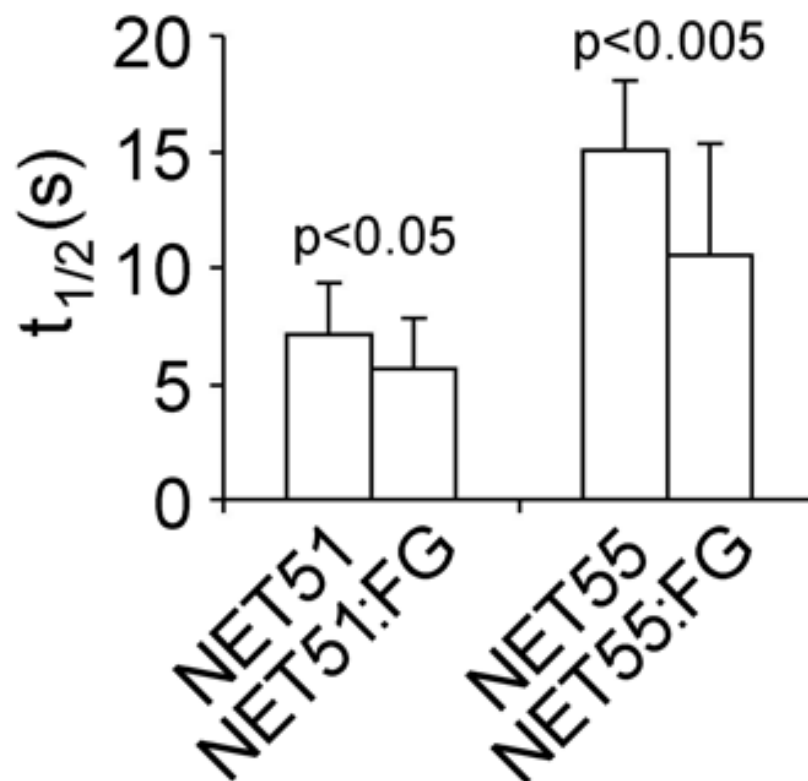


Figure 28. Addition of FGs enhances translocation of INM proteins. FRAP dynamics in the NE were tested for wild-type NET51 and NET55 and their FG-containing sequence fused counterparts. Both NET51:FG and NET55:FG had faster recovery kinetics than their wild-type analogues and therefore translocate faster into the INM. Error bars indicate standard deviation from at least 12 individual experiments. The p-values are indicated on top of each pair. (Figure adapted from Zuleger et al., 2011a)

As mentioned above FGs are not very common in protein sequences *per se*, thus we wanted to inspect if FGs were a common characteristic of

NETs in general. We searched 199 predicted NETs found in a proteomic data set from rat liver (Schirmer et al., 2003) and compared them with all transmembrane proteins coded by the rat genome⁸ (Figure 29, A). Strikingly, the occurrence of 12 or more FGs in the NE dataset was enriched compared to the total membrane protein set (Figure 29, A). The enrichment of FGs was also highly significant when comparing the same NE membrane protein data set with all membrane proteins found in a different organelle, the mitochondrion (Figure 29, B) indicating that presence of FGs is a special characteristic of membrane proteins destined for the nucleus but not membrane proteins of other organelles.

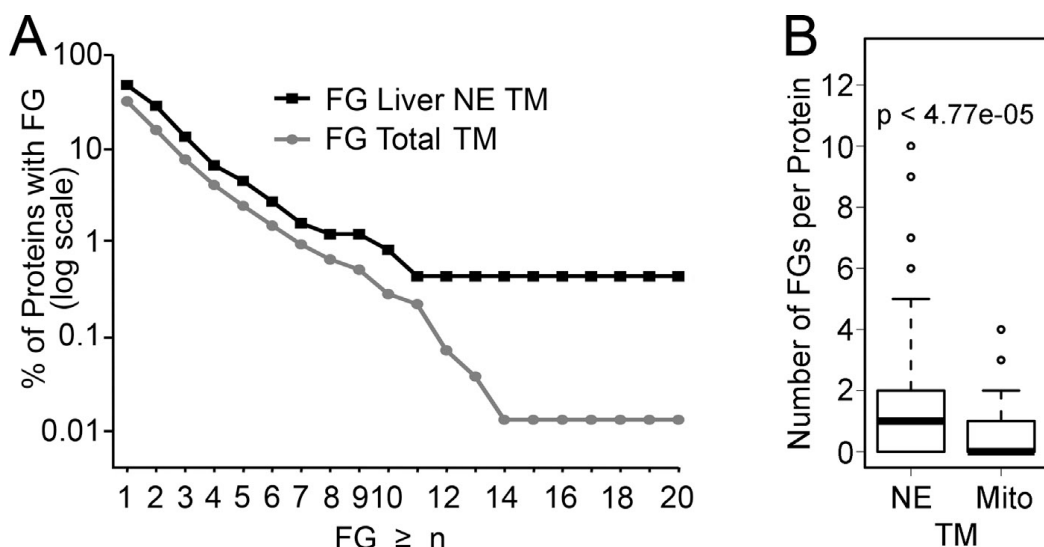


Figure 29. FGs are enriched in NETs. (A) 199 predicted NETs from a rat liver proteomic study were searched for FGs in their soluble domains (predicted membrane domains were excluded) and compared to soluble domains of all membrane proteins encoded by the rat genome. These two data sets were plotted for their occurrence of FGs. It is evident that the percentage of membrane proteins having 12 or more FGs in the NE data set is higher than in the total membrane protein set. (B) Occurrence of FGs was compared between the 199 predicted NETs from the same rat liver proteomic study and all membrane proteins found in mitochondria. The NET dataset is more enriched for multiple FG-containing proteins than the mitochondrial membrane protein dataset. The p -value for the difference significance is indicated. (Figure adapted from Zuleger et al., 2011a)

⁸ This analysis was done by Dr. Alastair Kerr (Wellcome Trust Centre for Cell Biology, Edinburgh, UK)

3.6 Ran- and FG-mediated pathways require Nup35

The ability of the FGs to increase the translocation rates of NETs together with the observation that FGs are enriched in NETs opened the possibility that FGs in NETs might interact with FGs in nucleoporins to navigate the NPC channel as this is the proposed model for soluble proteins during nuclear transport (Rexach and Blobel, 1995). Recent structural refinements of the NPC suggest that some FG-containing nucleoporins reside in the peripheral channel of the NPC (Alber et al., 2007). One such nucleoporin is Nup35 (mammalian Nup35 is the homologue of yeast Nup53). To test if Nup35 is involved in INM translocation of NETs we depleted HeLa cells of Nup35 by means of siRNA (Figure 30, B) and analyzed NET translocation under the Nup35 depletion (Figure 30, A). Similar to Ran function depletion, only LBR translocation was significantly inhibited upon depletion of Nup35 (Figure 30, A). This result indicated that Ran and Nup35 both might function in the same translocation pathway. To test this possibility LBR was subjected to simultaneous depletion of both Ran and Nup35 (Figure 30, C). Upon double depletion LBR translocation was not more strongly inhibited than upon depletion of either Ran or Nup35 alone (Figure 30, C). This result is consistent with that both Ran and Nup35 might be part of the same NET translocation pathway.

We further tested if the FG-facilitated pathway also depends on Nup35 based on the previously mentioned hypothesis that FG Nups facilitate transport of FG-containing proteins. For this we analyzed wild-type NET51 and NET51 fused to the FG-sequence with and without Nup35 depletion (Figure 30, D). Translocation of wild-type NET51 was not affected by Nup35 depletion; however, when fused to FGs NET51 exhibited a decrease in translocation kinetics to levels of wild-type NET51 (Figure 30, D). This data suggests that the FG-facilitated translocation pathway is also dependent on the FG-containing nucleoporin Nup35.

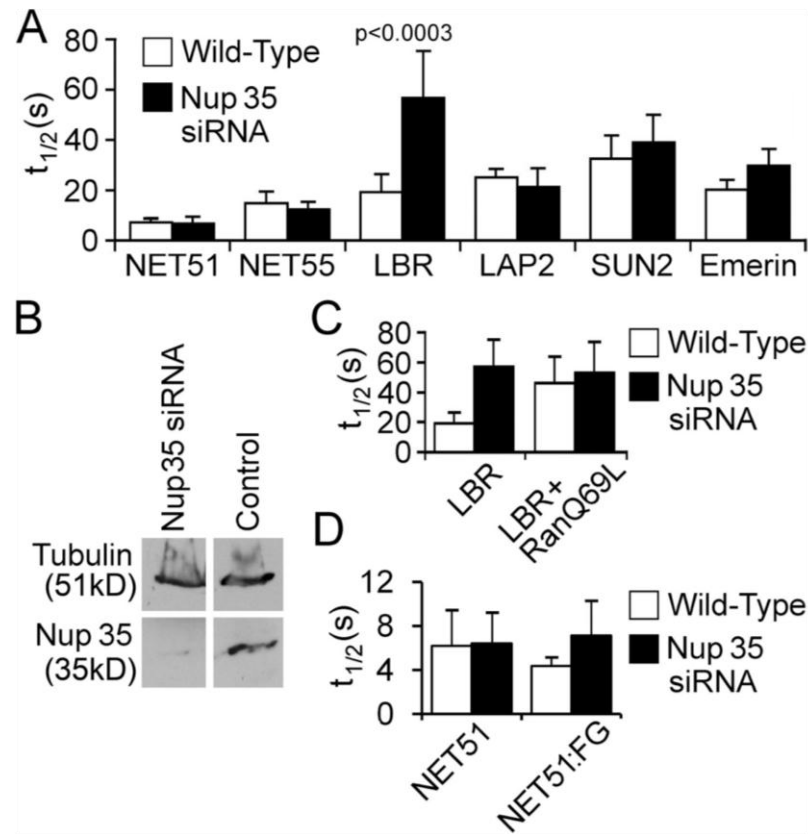


Figure 30. Nucleoporin Nup35 affects translocation of some NETs (A) NET translocation kinetics were analyzed by FRAP with and without depletion of the nucleoporin Nup35. LBR was the only heavily affected protein upon Nup35 depletion (*p*-value indicated). **(B)** Western blot confirming efficient Nup35 depletion. Tubulin was used as a loading control. **(C)** LBR was tested with and without Nup35 depletion. Depletion of Nup35 affected LBR translocation to a similar extent as the depletion of Ran function alone. LBR was not further affected when both Ran and Nup35 were depleted. **(D)** NET51 and its NET51:FG were tested in the Nup35 depletion background. While NET51 wild-type was not affected by Nup35 depletion, NET51:FG translocation was inhibited. Error bars indicate standard deviation from at least 8 individual experiments. (Figure adapted from Zuleger et al., 2011a)

3.7 Summary of chapter 3

In this chapter I used FRAP and GFP-PA to study the transport of NETs to the INM. By means of GFP-PA I was able to show that NET movement within the INM is restricted, however ER-NE translocation was rapid. This finding revealed that the relatively rapid recovery of NETs in the NE as measured by FRAP must be predominantly due to ER-NE translocation rather than NE-NE movement. Therefore I used FRAP as a method to study the translocation of NETs into the INM. I found that there was a wide range of translocation rates within 15 tested NETs. I went on to test 6 out of these 15 in further detail subjecting them to different conditions. I found that out of six NETs only emerlin and SUN2 required ATP for translocation. Further, when Ran function was depleted only LBR translocation was impaired. Thus the possibility that all NETs require ATP and Ran in order to negotiate the NPC diffusion barrier could be excluded. I also found that both pathways are independent of one another. A further assumption previously established was that NLS-containing NETs require Ran function to translocate into the INM. Here I fused the classical SV40-NLS or the LBR-NLS to NETs and found that the addition of the NLSs did not establish a Ran dependence. However, I found a new mechanism for translocation in which phenylalanine/glycines (FGs) in the protein sequence of NETs facilitated their translocation into the INM. When we looked at a larger NET dataset an enrichment for FGs was revealed. Both the Ran and FG-facilitated pathways required a peripheral channel NPC protein Nup35 though both pathways were independent of one another. The use of the Nup35 strongly argues for translocation of NETs through the peripheral rather than the central channel of the NPC.

Chapter 4

NETs can reposition chromosomes to and from the nuclear periphery

It is known that chromosomes of interphase cells are not randomly organized but tend to occupy particular regions, called chromosome territories (Cremer and Cremer, 2001; Parada and Misteli, 2002; Scherthan et al., 1996). These chromosome territories themselves are also specifically organized within the nucleus with some chromosomes being preferentially at the nuclear edge and others in the nuclear interior. To understand how these 3D chromosome organizations are established, factors that can mediate such chromosome arrangements need to be identified. Because many chromosomes are close to the nuclear periphery it only follows logically that the NE could be one such factor. This idea was supported by recent findings where chromosomes could be tethered to the NE using exogenous high affinity systems (Finlan et al., 2008; Kumaran and Spector, 2008; Reddy et al., 2008). In this chapter I identified endogenous proteins that can organize chromosomes.

4.1 A screen to identify NETs that reposition chromosomes

We hypothesized that INM proteins could affect positioning of chromosomes in interphase cells. Many of these proteins are tissue-specific and thus this characteristic could also explain why a particular chromosome is at the nuclear periphery in one tissue, but not the other. To find NE proteins that can reposition chromosomes to and from the nuclear periphery, we expressed a large set of them in 2 distinct cell lines, each marked for a specific chromosome⁹. The first cell line has a lacO integration in a euchromatic region on chromosome 5, the second cell line has the lacO locus integrated in a heterochromatic region on chromosome 13. The locus on chromosome 5 tends to be in the nuclear interior whereas the locus integration on chromosome 13 tends to be at the nuclear periphery. Loci in both cell lines are visualized by a GFP-fused lacI. Both cell lines are derived from human fibrosarcoma HT1080 cells and we previously tested our NE proteins for targeting in the HT1080 cell line (Malik et al., 2010). Three days post-transfection the lacO cells were analyzed for whether the position of the array had changed upon the expression of a particular NET. Analysis was performed three days post transfection to give the cells enough time to express the NET first and to let the cells go through mitosis since the lacO study from the Bickmore laboratory demonstrated that a cell has to go through one cell division to reposition a chromosome to or away from the nuclear periphery (Finlan et al., 2008).

Images used for analysis were 2D planes from cell mid-sections. Only lacO array spots that were within the 2D plane midsections were counted. This allowed deducing with absolute confidence whether the lacO arrays were at the nuclear periphery or the nuclear interior (i.e. lacO spots on top of the nuclei at the NE would not appear in the mid-plane section). Since cells for this analysis were fixed in formaldehyde, the 3D structure of the cells was

⁹ both lines provided by Professor Wendy Bickmore, MRC Human Genetics Unit, Edinburgh, UK

maximally preserved allowing referring to the nuclear edge as the nuclear periphery (due to the preservation of the 3D structure lacO array signals on top of the nucleus are not captured by the 2D cell mid-section plane and therefore cannot appear as false-positive interior signals like it would be the case if the cells were fixed with Methanol/Acetic acid).

The schematic below outlines a possible output of the screen on the example of the chromosome 5 integration cell line (Figure 31).

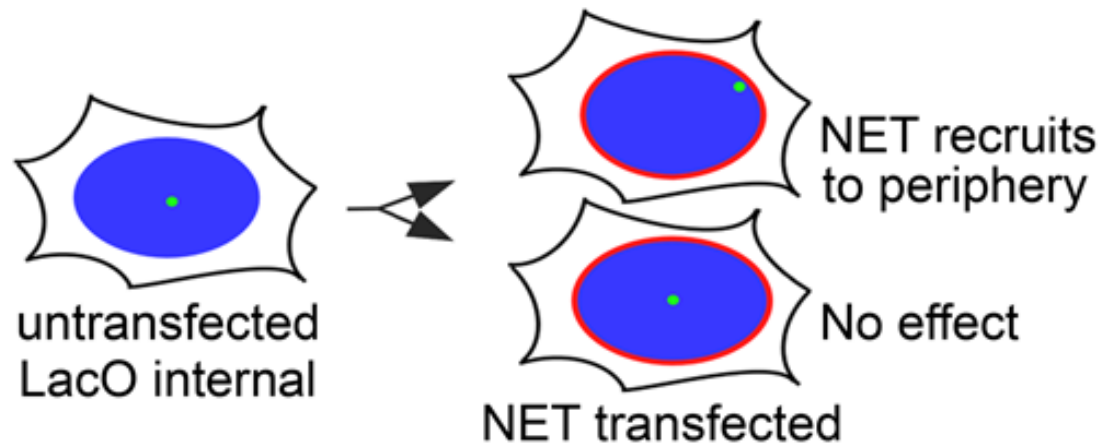


Figure 31. Screen for NETs that can reposition a marked interior locus to the nuclear periphery. A human HT1080 fibrosarcoma cell line contains a lacO array, a bacterial DNA sequence that does not occur in the mammalian genome. To visualize this array the cell line also expresses a bacterial lacI repressor (fused to GFP), which has a high affinity to the lacO array thus marking it as a green spot within the nucleus. The array is located in the nuclear interior in interphase cells (on the left). The cell line is transfected with NETs, which are fused to monomeric RFP (red ring around the nucleus). Three days after transfection the cells are subject to microscopy analysis to determine if any of the NETs repositioned the interior locus (green) to the nuclear periphery (upper cell on the right).

To prevent bias in scoring whether the locus is at the periphery or not an algorithm was applied, which erodes the nuclear area based on the DAPI signal into 5 shells (where shell 1 is the most peripheral shell and 5 the most

interior) of roughly equal areas¹⁰ allowing to score in which shell the lacO array is located for each individual cell nucleus (Figure 32).

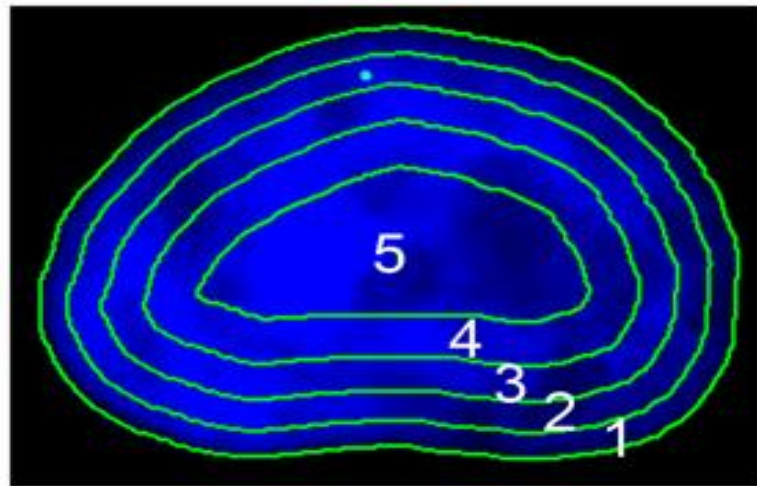


Figure 32. Algorithm for unbiased determination of the lacO array position. The algorithm recognizes the cell nucleus by the DAPI signal and erodes the nuclear area from the periphery towards the interior into 5 shells of roughly equal areas (1= most peripheral shell, 5= most interior shell), so that the lacO array (green spot) position can be allocated to a particular shell (in this case shell 2).

Twenty-three NETs were screened in the cell line with the lacO array integration on chromosome 5. For initial statistical confidence fifty cells expressing each NET were imaged and analyzed with the erosion algorithm. In untransfected and mRFP transfected control cells the lacO array was in the most peripheral shell in 20% of the cells. Though most of the NETs had no or minor effects, others like NET5 (~45% at periphery), 29 (~35% at periphery), 39 (~45% at periphery), 45 (~35% at periphery) and 47 (~35% at periphery) increased the incidence of the array at the nuclear periphery by roughly 2-fold (Figure 33).

¹⁰ this algorithm was originally designed by Paul Perry, MRC Human Genetics Unit, Edinburgh and adapted to ImageProPlus Image analysis software by Dr. David Kelly, Wellcome Trust Centre for Cell Biology, Edinburgh

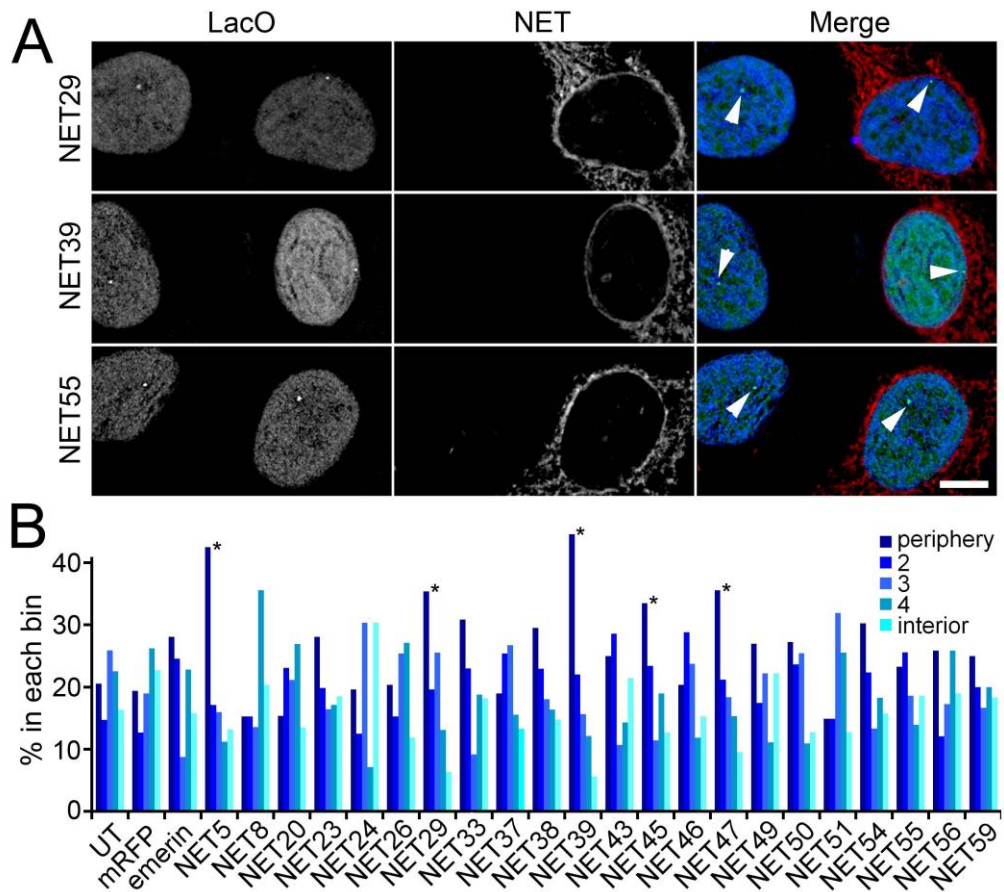


Figure 33. Some NETs can reposition the lacO array-containing chromosome 5. (A) NET29 and NET39 expressing cells show peripheral localization of the lacO array whereas in untransfected cells in the same micrograph the array remains in the interior (top and middle panel). The array location in the NET55 expressing cell is not altered compared to the untransfected cell in the same micrograph (bottom panel). Scale bar, 5 μ m (B) Quantification of the lacO array position using the algorithm described in Figure 32. Each bar represents the percentage of the lacO array scored in a particular radial shell in the nuclear area when analyzing 50 cells for each sample. The darkest blue bars represent the most peripheral shell with a gradient of lighter blue colours marking the more internal shells respectively. Quantification shows that NET5, 29, 39, 45 and 47 significantly increase the incidence of the lacO array at the nuclear periphery (~2-fold) compared to mRFP transfected and untransfected control cells. *P* values <0.0007 are marked by the asterisks and represent the confidence that the asterisks marked samples are different from the untransfected and the mRFP transfected controls as measured by the KS test.

To test whether different NETs would have specificity for distinct chromosomes we tested the same set of NETs in a cell line where another chromosome, chromosome 13, was marked by the lacO array. In this cell line the lacO array is peripheral in 50% of the cells (Figure 34, A). When

screening the NETs in this cell line three scenarios were observed. Proteins like NET5, and NET45 had no strong effect on the array position compared to mRFP transfected and untransfected controls. Others like NET24, NET47 and NET49 decreased the incidence of the array at the NE (~1.5-2-fold) and yet others like NET29 and NET39 increased (~1.2-fold) the incidence at the periphery (Figure 34, B). It is important to note that whereas proteins like NET29 and NET39 were both relocating chromosome 5 and 13 to the NE others had only effect on one chromosome (for example NET5 or NET45) and yet others like NET47 had opposite effects in the respective cell lines suggesting specificity of NETs for particular chromosomes.

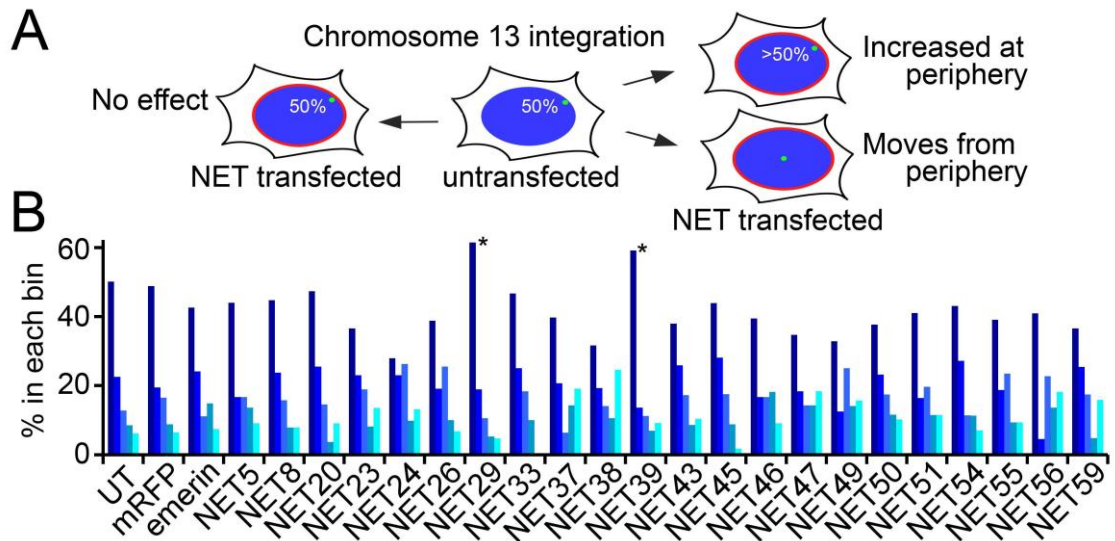


Figure 34. Some NETs can reposition the lacO array-containing chromosome 13. (A) Schematic of the visual screen in the cell line where chromosome 13 is marked by a lacO array. The array is located in at the nuclear periphery in 50% of the cells and overexpression of NETs could increase this incidence (right upper panel) or decrease this incidence (right, lower panel) or leave the array incidence in the peripheral bin unchanged (left). (B) Quantitative analysis of the visual screen when scoring 50 cells for each sample with the erosion algorithm described in Figure 32. The darkest blue bars represent the most peripheral shell with a gradient of lighter blue colours marking the more internal shells respectively. The analysis shows that NET29 and NET39 increase the incidence of the lacO array at the nuclear periphery. P values <0.078 are marked by the asterisks and represent the confidence that the asterisks marked samples are different from the untransfected and the mRFP transfected controls as measured by the KS test.

To obtain statistical confidence of array repositioning effects 5 NETs with strong effects and 2 NETs with no reposition effects were re-tested in both cell lines in two additional independent experiments along with the mRFP transfected and untransfected controls. The repositioning effects were reproducible confirming that NET5, 29, 39, 45 and 47 repositioned the array-containing chromosome 5 to the nuclear periphery (~2-fold compared to controls) whereas in the chromosome 13 labelled cell line only NET29 and NET39 increased (~1.2-fold) the peripheral localization of the array. NET47 decreased the peripheral localization in this cell line (~1.5-fold). NET37 and

NET55 as well as the mRFP transfected control cells did not alter the array position in either cell line (Figure 35).

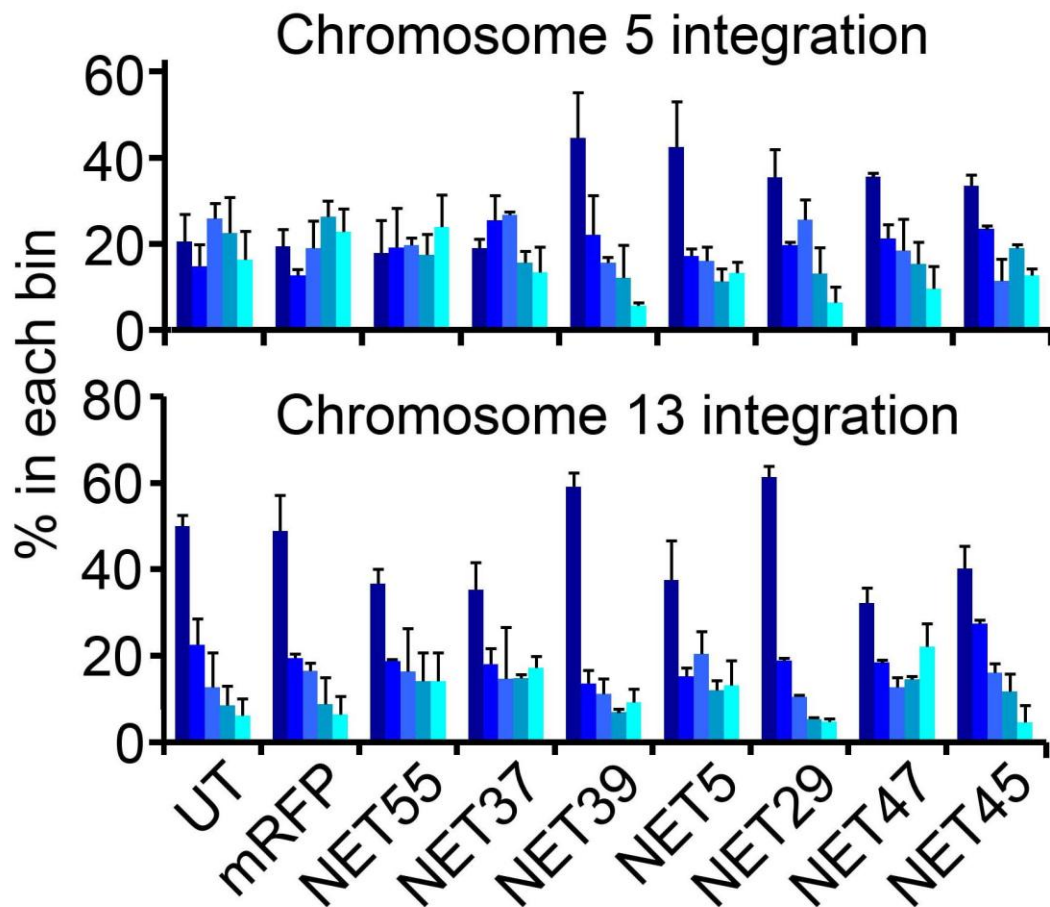


Figure 35. Confirmation of the lacO array repositioning effects by replicates of the positives against negative controls. NETs with the strongest effects from figures 34 and 35 were retested in 2 additional experiments (50 cells scored in each repeat) and the results averaged. The repositioning effects of proteins tested were reproducible for both cell lines with p values < 0.0001 for the chromosome 5 cell line and $p < 0.0322$ for the chromosome 13 cell line. The p -values represent the confidence that respective samples are different from the untransfected and the mRFP transfected controls as measured by the KS test.

Since the chromosome repositioning effect could be indirect due to general chromatin distribution towards the nuclear periphery we scored the DAPI signal distribution in the samples with the repositioning effect and compared them to those that did not reposition the chromosomes (Figure

36). The rationale behind it is that if array reposition effects are due to general chromosome distribution towards the nuclear periphery then the DAPI intensity in these cells would be stronger in the peripheral shells than in the interior shells. For this analysis the algorithm from Figure 32 was modified to measure the DAPI intensity in each shell. Fifty cells were analyzed for each sample. The distribution of the DAPI signal did not alter in the samples with tethering effects (NET29, 39 and 47) when compared to the control mRFP samples in both cell lines meaning that the array repositioning effects are not due to general chromatin distribution towards the nuclear periphery.

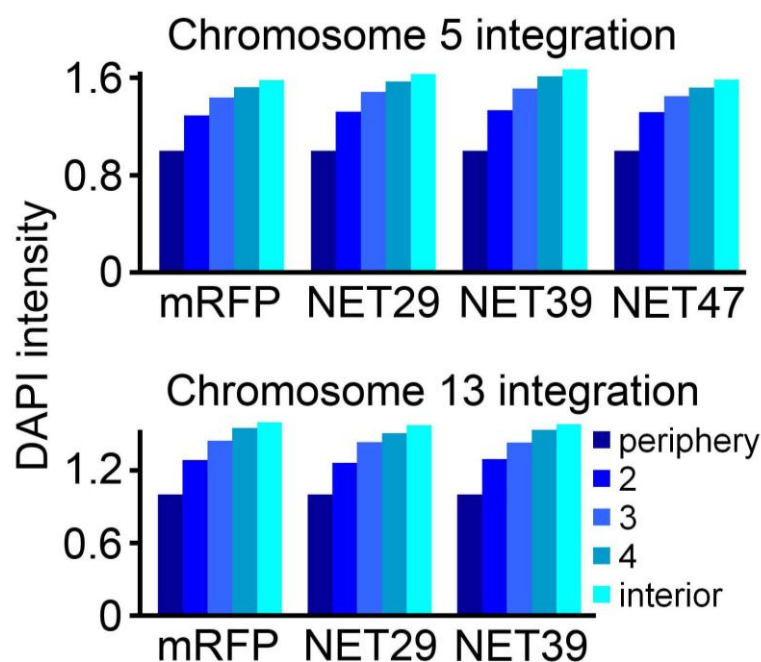


Figure 36. Chromosome repositioning effects caused by NETs are not due to general chromatin distribution towards the nuclear periphery. To test if the chromosome repositioning effects are due to general chromatin distribution towards the nuclear periphery the erosion algorithm from Figure 32 was adapted to measure the DAPI signal intensity in each shell. 50 samples for the tethering NETs (NETs 29, 39 and 47 in the chromosome 5 labelled cell line and NETs 29 and 39 in the chromosome 13 labelled cell line) were tested and no increase of the DAPI signal was observed at the nuclear periphery compared to the mRFP transfected control cells. The darkest blue bars represent the most peripheral shells with a gradient of lighter blue colours marking the more internal shells respectively. The DAPI intensity is presented in normalized arbitrary units. Note: The DAPI intensity decreases from the interior towards the periphery because the micrographs have not been deconvolved.

When performing the lacO array repositioning screen it was expected that when the lacO array repositions to the nuclear periphery then the lacO array-containing chromosome would also reposition together with the array since work from the Bickmore lab provided evidence for this (Finlan et al., 2008). In order to affirm that the whole lacO array-containing chromosome is also relocating upon overexpression of particular NETs fluorescence *in situ* hybridization (FISH) was performed to label both the lacO array and the chromosome 5 simultaneously (Figure 37). In control cells expressing the NET37 the lacO array-containing chromosome localized to the nuclear interior (Figure 37 upper panel), but in the NET39 expressing cells both the array and the chromosome localized to the nuclear periphery confirming that the array is moving together with the chromosome. Furthermore, it is important to note that in the case of NET39 both the array containing chromosome and the chromosome homologue without the array integration localize to the periphery suggesting that NET39 recruits chromosome 5 independently of the lacO array (Figure 37 lower panel). This is also supported by the fact that in the NET39 expressing cell the lacO array itself is not right at the nuclear periphery whereas chromosome 5 is.

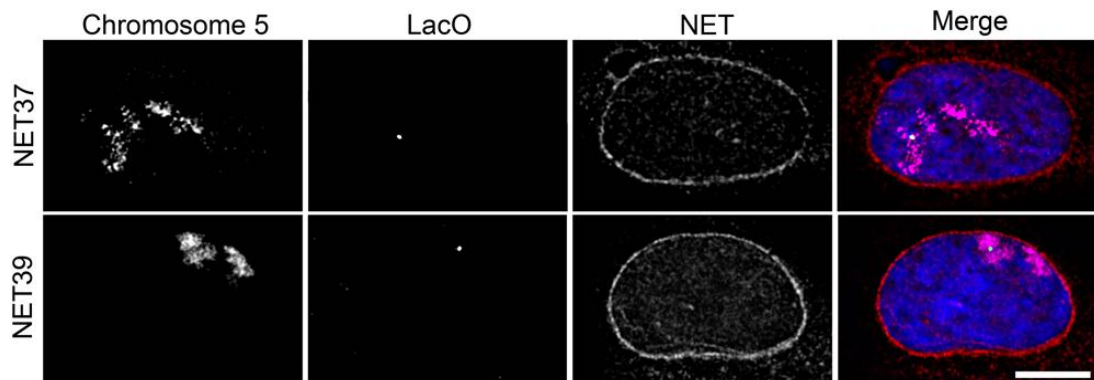


Figure 37. Affirmation that the whole chromosome is moving to the nuclear periphery. Both the lacO array and chromosome 5 were visualized simultaneously by means of fluorescence *in situ* hybridization (FISH). In the NET37 expressing cell both the array and the chromosome localize to the nuclear interior (upper panel) whereas in the NET39 expressing cell both array and chromosome are at the nuclear periphery (lower panel). Notably, both chromosome 5 copies are at the nuclear periphery, one that contains the lacO array and the other without the array integration suggesting that the tethering effect is independent of the lacO array.

4.2 Recapitulation of NET-mediated chromosome tethering in cells lacking the lacO array and repositioning analysis of additional chromosomes

To exclude repositioning effects due to possible NET-lacO array interactions HT1080 cell lines stably expressing the NETs but lacking the lacO array were generated. The NETs in those cell lines were fused to GFP because better antibodies are available for GFP than for mRFP¹¹. FISH analysis on chromosome 5 in these cell lines confirmed the chromosome repositioning effects seen previously in the lacO cell lines (Figure 38). Cell lines stably expressing NET5, 29, 39 and 47 tended to have the chromosome 5 at the nuclear periphery while cell lines expressing control proteins NET37 and NET55 tended to have a more internal chromosome 5 localization.

¹¹ *antibodies to the fluorescence tag have to be used because the fluorophore is destroyed during the FISH procedure*

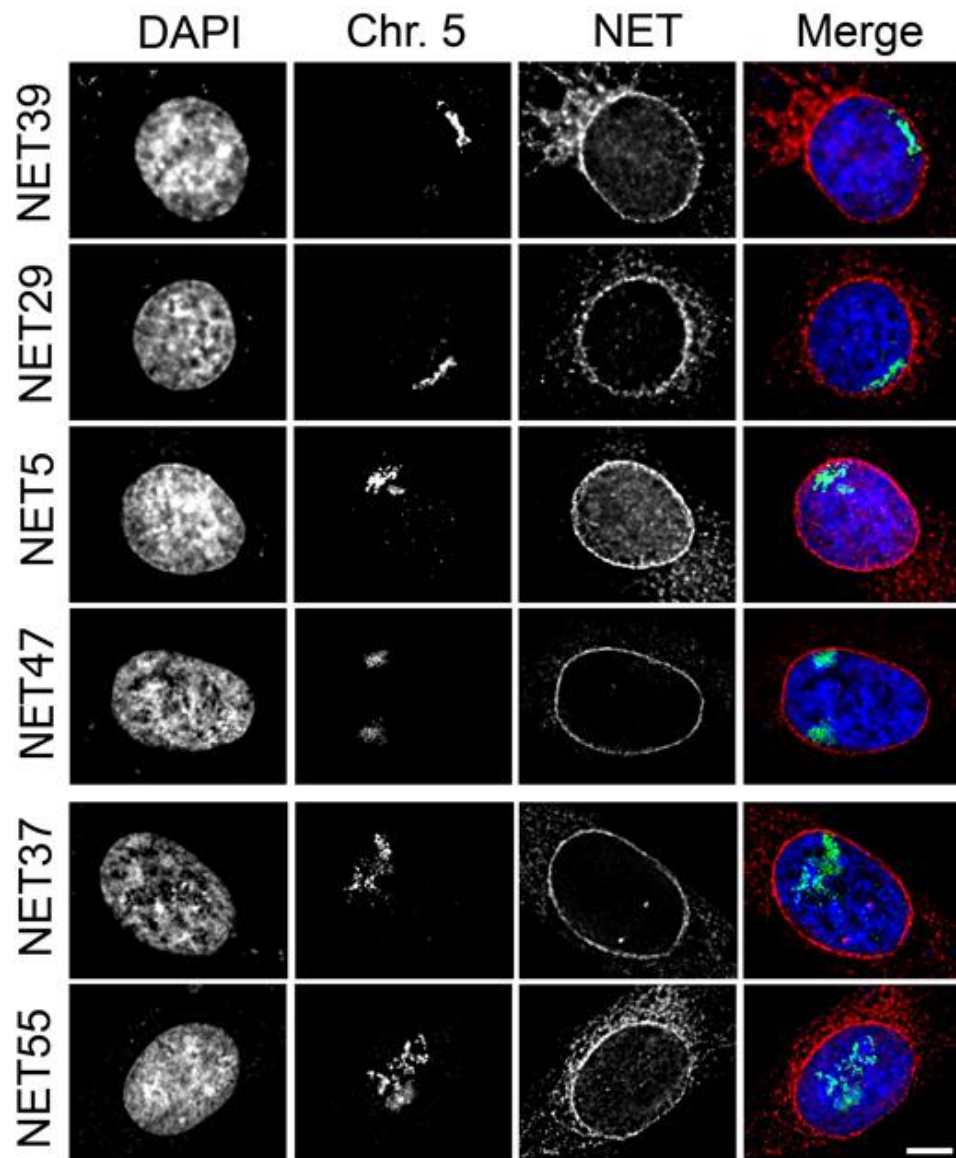


Figure 38. Chromosome 5 repositioning towards the nuclear periphery is recapitulated in cells stably expressing the NETs but lacking the lacO array. Cells lacking the lacO array but stably expressing the NETs were tested for chromosome 5 position by FISH. Cells expressing NET5, 29, 39 and 47 have all revealed more peripheral chromosome 5 localization whereas NET37 and NET55 serving as negative controls had a more internal localization of this chromosome.

To quantify the chromosome 5 repositioning effects in cells stably expressing the chromosome repositioning NETs the algorithm described in Figure 32 was modified to measure the total chromosome intensity in each erosion shell of the nucleus¹². Furthermore, since chromosomes are much bigger than the lacO array, the two most peripheral and two most interior shells were fused and are referred to as periphery and interior, respectively (Figure 39, A). In two independent experiments the chromosome 5 positions were determined by means of this algorithm. Again, NET5, 29, 39 and 47 revealed a more peripheral chromosome localization (~50-100% increase) compared to untransfected or GFP-NLS expressing control cells, while NET37 and NET55 had a similar chromosome 5 distribution as the untransfected and GFP-NLS transfected controls (Figure 39, B).

¹² *this 2D chromosome positioning algorithm was written by Dr. David Kelly (Wellcome Trust Centre for Cell Biology, Edinburgh, UK)*

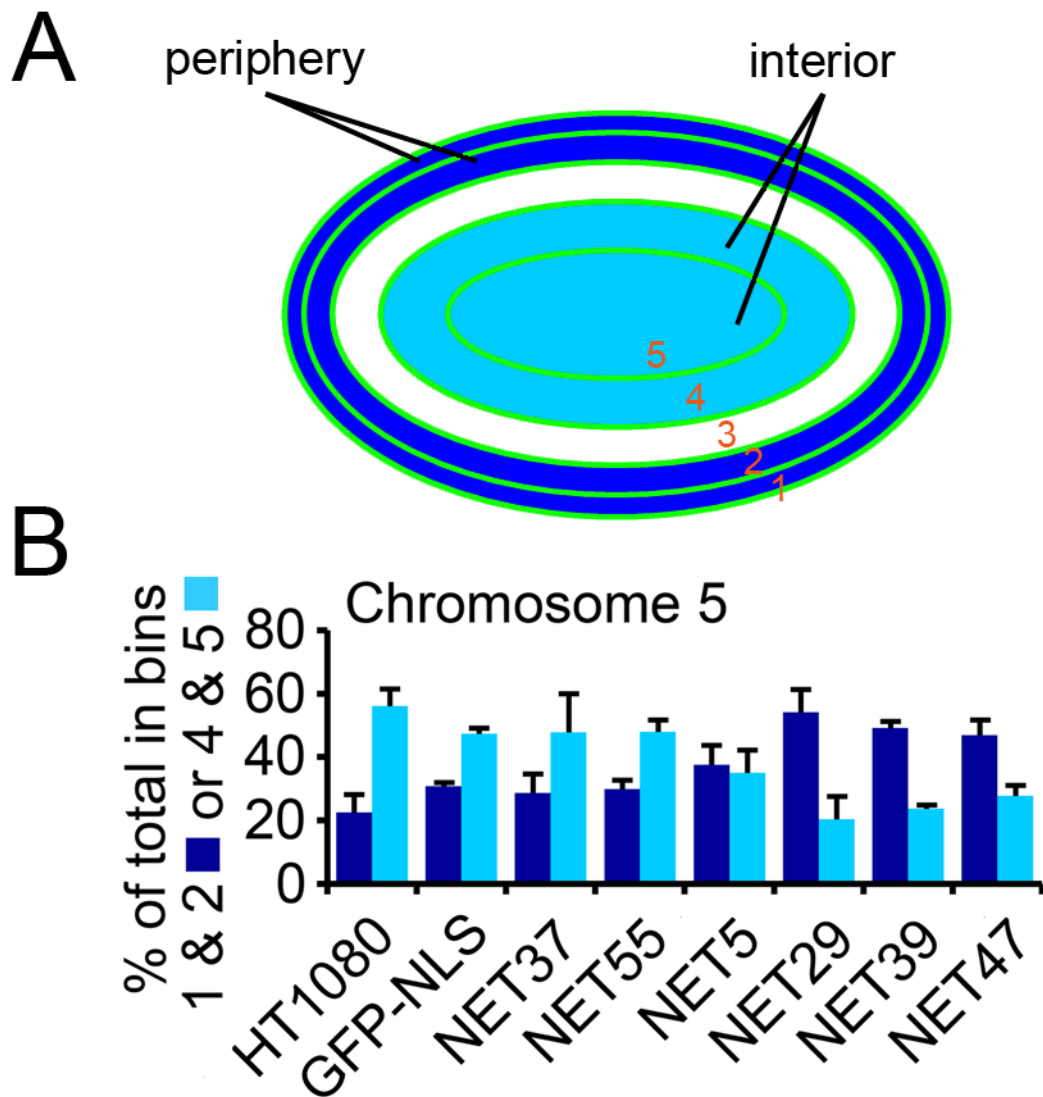


Figure 39. Quantification of Chromosome 5 repositioning in cells stably expressing NETs but lacking the lacO array. (A) The automated algorithm from Figure 32 was modified to measure the proportion of chromosome signal in each individual shell. Because the chromosomes occupy a much bigger area than the small lacO array the two most outer and two most inner shells were fused and called *periphery* and *interior* respectively. (B) Chromosome 5 localization was quantified in two individual experiments where a total of 100 cells were analyzed. NET5, 29, 39 and 47 all revealed a more peripheral localization of chromosome 5 (~2-fold compared to controls), while untransfected and GFP-NLS transfected control cells as well as NET37 and NET55 stable cells made a more internal localization of chromosome 5 evident thus confirming the results in Figure 38.

We tested if localization of additional chromosomes in respect to the nuclear periphery is affected by NETs, which are stably expressed in the

HT1080 cell line. Further chromosomes tested were chromosome 1, 11, 13, 17 and 19. For chromosome 13 the results from the lacO array visual screen were also recapitulated (Figure 40, A): NET29 and NET39 increased the incidence of this chromosome at the nuclear periphery (~1.2-fold) whereas upon NET47 expression this chromosome localized more internally (~2-fold) than in control samples (untransfected and GFP-NLS transfected cells). Also, like in the lacO screen, expression of NET5, 37 and 55 had no effect on the chromosome 13 localization.

Next, the localization of chromosome 19 was assessed (Figure 40, B). This chromosome is known to occupy a more internal localization in interphase cells, which was confirmed in this study. More than 80% of the chromosome signal was in the interior for all of the samples tested and none of the NETs was able to accumulate this chromosome at the nuclear periphery suggesting again that repositioning effects are chromosome specific.

Locations of chromosomes 1, 11 and 17 were tested in the NET39 and NET47 expressing cells and in GFP-NLS expressing control cells. For all these three chromosomes the effects were rather weak. NET39 and 47 expressing cells displayed a more internal localization of chromosome 1 (~10% decrease) compared to GFP-NLS expressing control cells (Figure 40, C). But both NET39 and NET47 revealed a more peripheral localization of chromosome 11 (~20% increase) compared to the GFP-NLS control (Figure 40, D). Chromosome 17 was much more internal than chromosome 1 and 11. Upon expression of NET 39 and NET47 its peripheral proportion increased slightly in comparison to the GFP-NLS control (Figure 40, E).

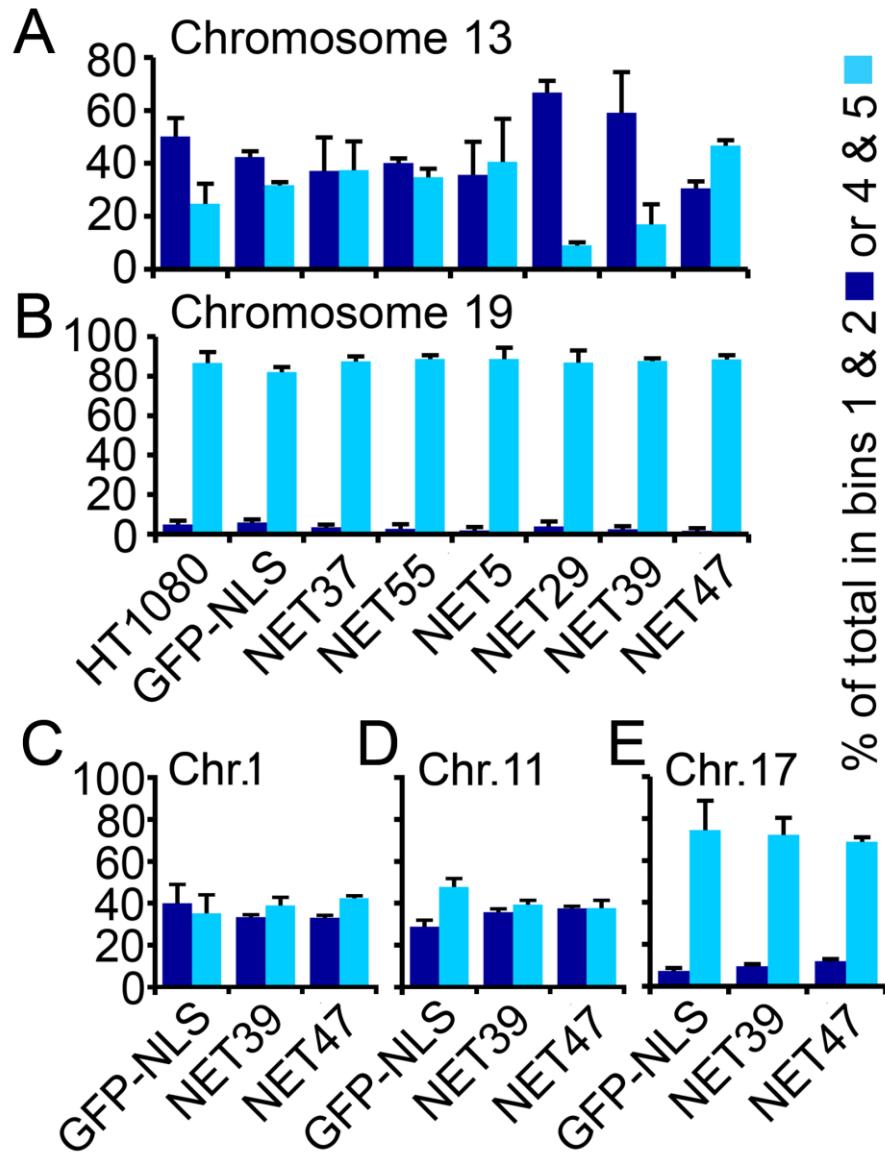


Figure 40. Localization of chromosomes 1, 11, 13, 17 and 19 upon stable NET expression. Cells stably expressing the NETs and control cells were analyzed by FISH scoring 100 cells in total for each sample in two individual experiments. **(A)** NET29 and NET39 expressing cells revealed a more peripheral localization of chromosome 13 than cells expressing NET5, 37, 47, 55 or control cells (untransfected and GFP-NLS transfected cells). **(B)** Chromosome 19 was very internal in all samples and no NET altered its position into a more peripheral configuration. **(C)** Both NET39 and NET47 slightly decreased the localization of chromosome 1 from the nuclear periphery compared to GFP-NLS control cells. **(D)** and **(E)** NET39 and NET47 slightly increased the incidence of chromosomes 11 and 17 at the nuclear periphery compared to GFP-NLS expressing control cells.

Since the 2D algorithm does not reflect the total nuclear volume we developed an algorithm that is analyzing the chromosome position within the complete 3-dimensional nuclear volume. Unlike the 2D algorithm, which erodes the nuclear area, the 3D algorithm erodes the nuclear volume from 3D reconstructions and scores the proportion of the chromosome in each 3D shell. Due to technical settings the 3D algorithm erodes the nuclear volume into 6 concentric 3D shells of roughly same volume¹³. An example from such a 3D reconstruction of the nucleus together with one chromosome pair is shown in Figure 41 A. The sequence of an erosion is shown in Figure 42 B where the chromosomes are shown after each erosion step.

¹³ the 3D algorithm was written by Dr. David Kelly (Wellcome Trust Centre for Cell Biology, Edinburgh, UK)

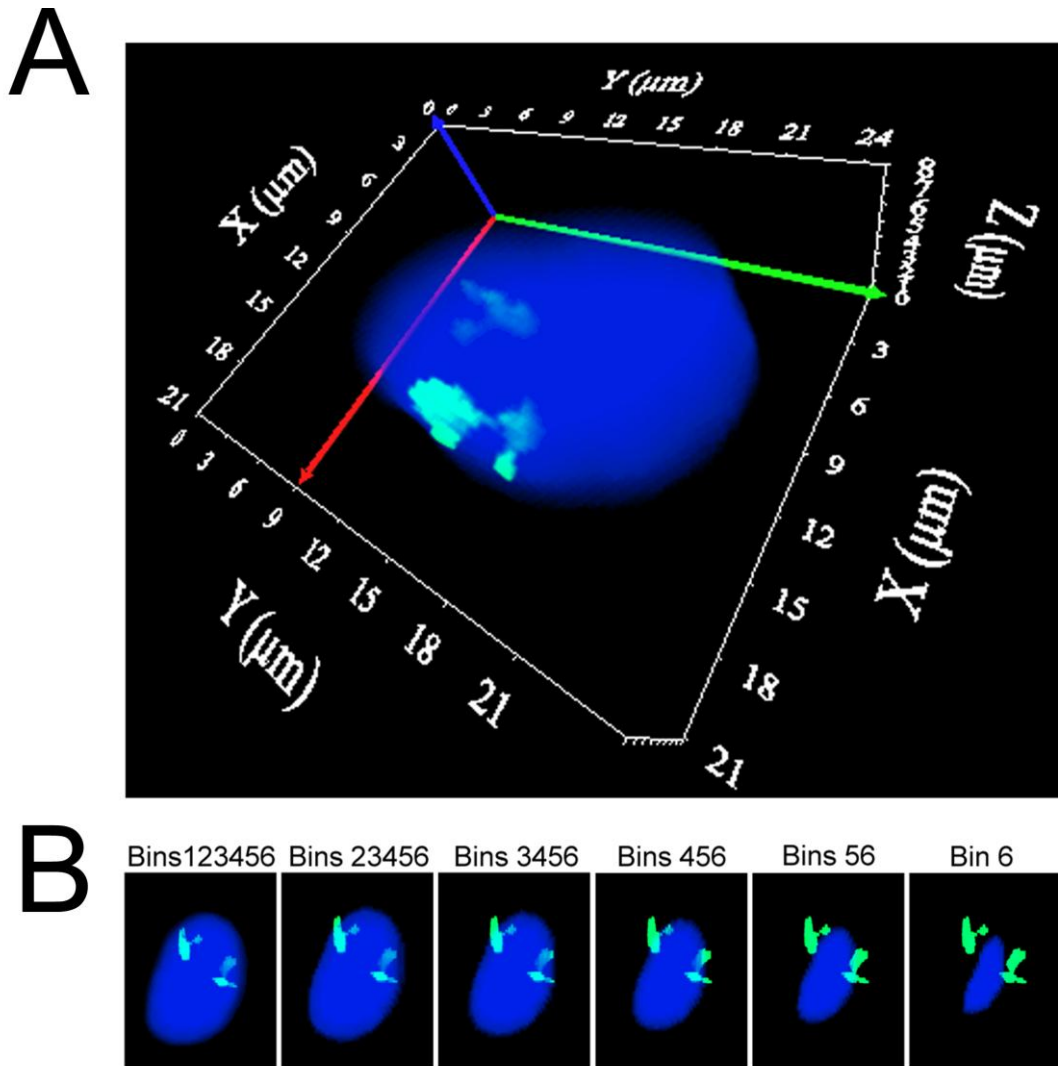


Figure 41. 3-dimensional (3D) erosion algorithm for determination of the spatial chromosome position. (A) 3D reconstruction of a nucleus with the chromosome from stacks. **(B)** The 3D algorithm erodes the reconstructed nuclear volume from the periphery to the interior into 6 concentric shells of roughly same volume. Erosion is shown stepwise shell by shell from left to right. The proportion of the chromosome is determined automatically by the algorithm in each individual shell.

Five chromosomes (1, 5, 11, 13 and 17) were re-tested for their spatial localization upon individual NET expression using the 3D erosion algorithm (Figure 42). Like in the 2D erosion algorithm the two most peripheral and most internal shells were fused and are referred to as periphery and interior, respectively. 3D reconstructions from 20 individual cells were used for

analysis for each sample. The results from the 2D erosion analysis were recapitulated. Cell lines expressing NET5, 29, 39 and 47 revealed a more peripheral localization of chromosome 5 (100-200% increase) compared to NET37, NET55 and the GFP-NLS control (Figure 42, A). NET29 and NET39 increased the incidence of chromosome 13 at the periphery (50% increase) compared to the control and to the other NETs tested (Figure 42, B). NET39 and 47 decreased (50% decrease) the peripheral localization of chromosome 1 (Figure 42, C) but increased (50-100% increase) the incidence of chromosome 11 (Figure 42, D) and 17 (100-200% increase) (Figure 42, E) at the nuclear periphery.

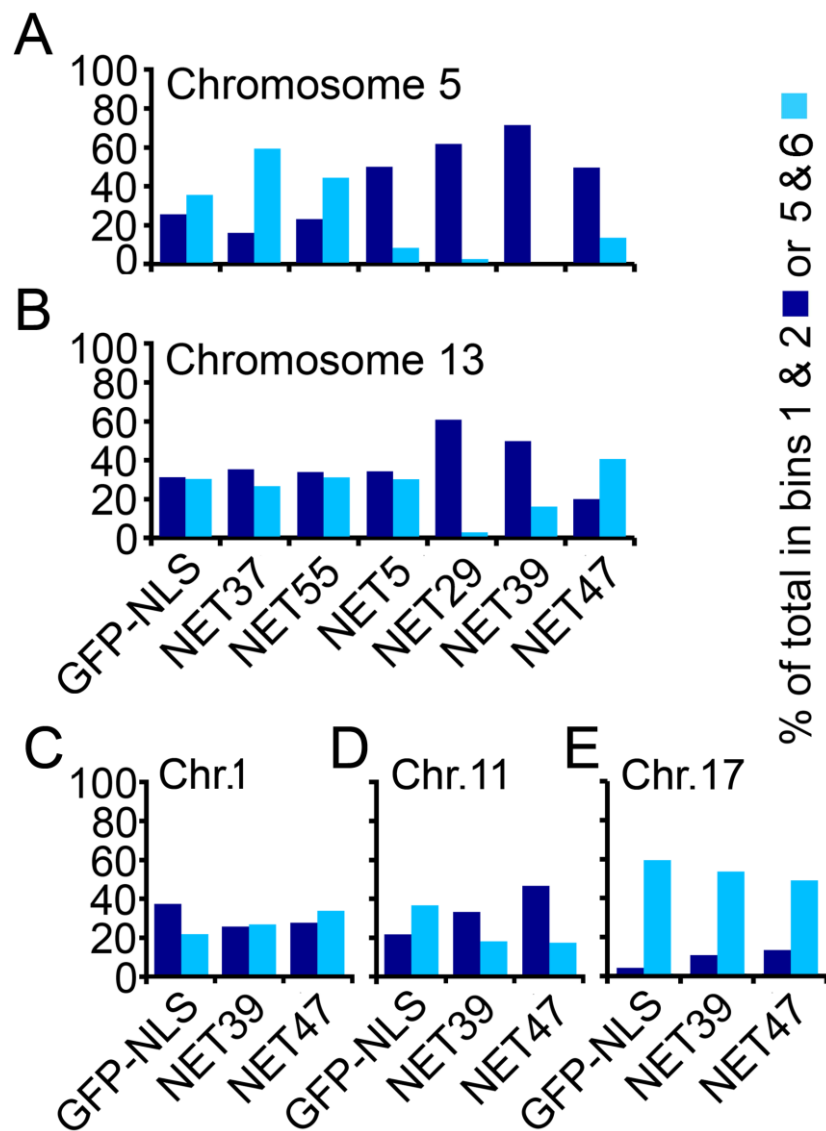


Figure 42. 3D algorithm confirms the results of the 2D method. The algorithm eroding the 3D reconstructed nuclei and scoring for the chromosome proportion in each eroded shell was applied to test the 3D localization of chromosomes 1, 5, 11, 13 and 17. Twenty nuclei were analyzed for each sample and the results averaged. The most two inner and the two most outer shells were fused and named periphery and interior, respectively. **(A)** Similar to the 2D analysis NET5, 29, 39 and 47 revealed a more peripheral localization of chromosome 5 compared to NET37, 55 and the controls (untransfected cells and GFP-NLS expressing cells). **(B)** NET29 and 39 expressing cells revealed a more peripheral chromosome 13 localization compared to the other NETs and the controls. Like in the 2D analysis NET47 decreased the chromosome 13 incidence at the periphery. **(C)** Chromosome 1 was less peripheral in NET39 and NET47 expressing cells compared to the GFP-NLS control. **(D)** and **(E)** Both NET39 and NET47 caused a more peripheral localization of chromosome 11 and 17 in comparison to the GFP-NLS control sample.

4.3 NETs can precipitate a chromatin fraction and only full-length NETs can reposition chromosomes - Further proof of NET-mediated chromosome repositioning

Though expression of some NETs resulted in the repositioning of some chromosomes to the nuclear periphery it was not clear if NETs can actually physically interact with chromatin. To test if NETs can bind chromatin a modified ChIP procedure was applied. GFP-fused NETs were precipitated after crosslinking with paraformaldehyde and then immuno-precipitated with an anti GFP antibody. The precipitate was probed for histone H3 as a general marker for chromatin. As a negative control NLS-GFP alone was used. Barrier-to-autointegration factor (BAF), a protein known to interact with chromatin was used as a positive control¹⁴. All NETs that caused chromosome 5 repositioning were able to precipitate the histone H3 whereas NET55, which did not reposition this chromosome, did not precipitate histone H3 (Figure 43). These results indicate that the NET-mediated effect of chromosome repositioning could be through a physical interaction with the chromosome. At this point, however, it is unclear whether the NET-chromatin interaction is direct or indirect.

¹⁴ Dr. Nadia Korfali (Wellcome Trust Centre for Cell Biology, Edinburgh, UK) performed the ChIP experiments and generated the BAF-GFP cell line

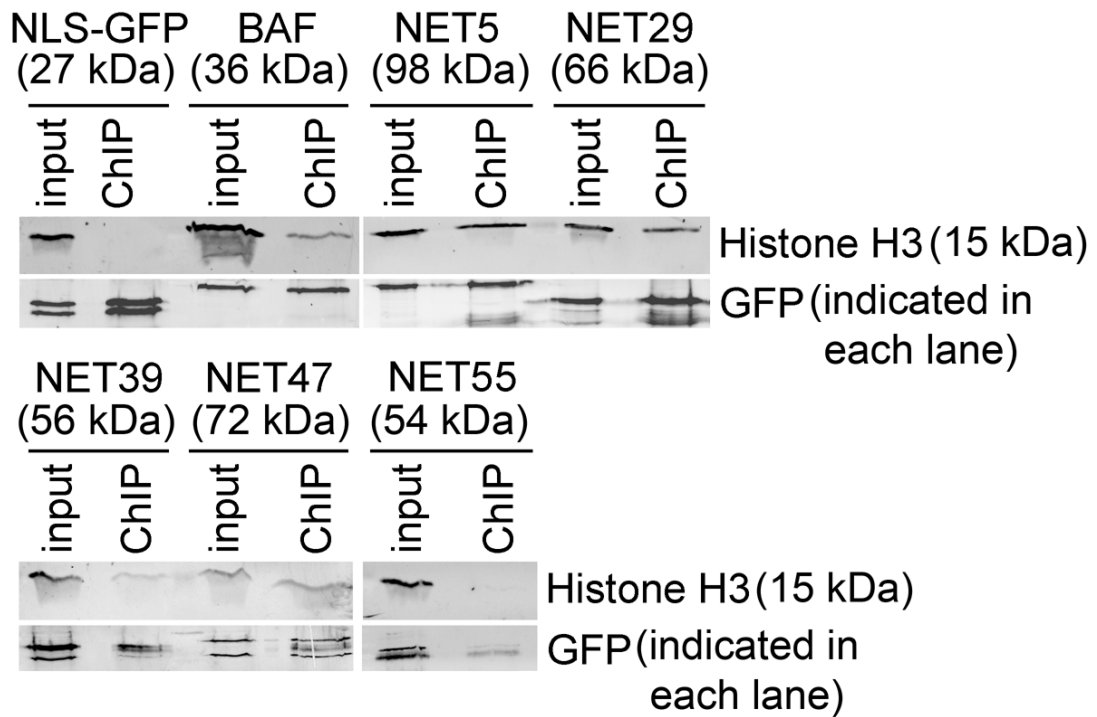


Figure 43. Chromosome repositioning NETs can co-immunoprecipitate a chromatin fraction - NET-mediated repositioning of chromosomes is likely direct. Cell lines stably expressing chromosome 5 repositioning NETs were subject to a modified ChIP procedure where GFP-NETs were precipitated with an anti GFP antibody after cells were crosslinked. The precipitates were probed for histone H3 as marker for chromatin to test if NETs are able to precipitate chromatin. NLS-GFP alone was used as a negative control and BAF, a known chromatin protein served as a positive control. NET5, 29, 39 and 47 as well as BAF were all able to precipitate histone H3 whereas the GFP alone and NET55 were not.

To further test if the tethering effect of NETs is direct or indirect stable cell lines expressing soluble fragments of the tethering NETs were generated (Figure 44). The rationale here is that if full-length NETs are modulating chromosome position through an enzymatic function or by initiating a signalling cascade then also soluble fragments of those NETs should reposition chromosomes to the nuclear periphery. However, if full-length NETs are robustly interacting with the chromosome to capture it at the nuclear periphery, then soluble fragments of these NETs would not be able to promote chromosome repositioning.

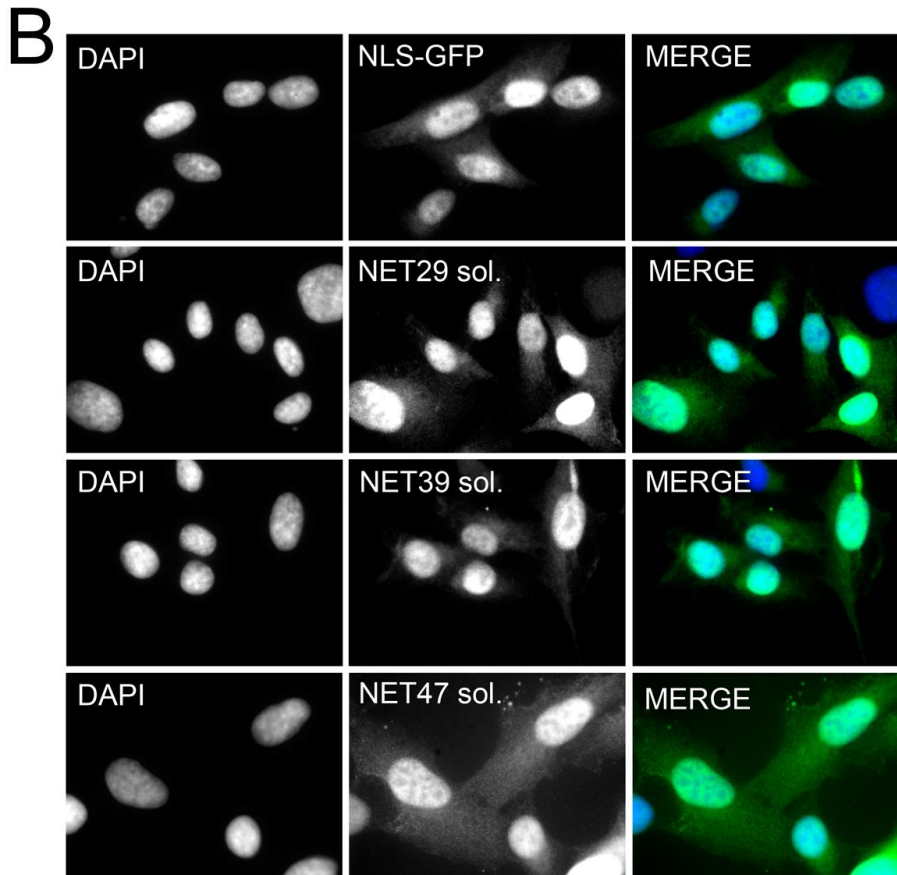
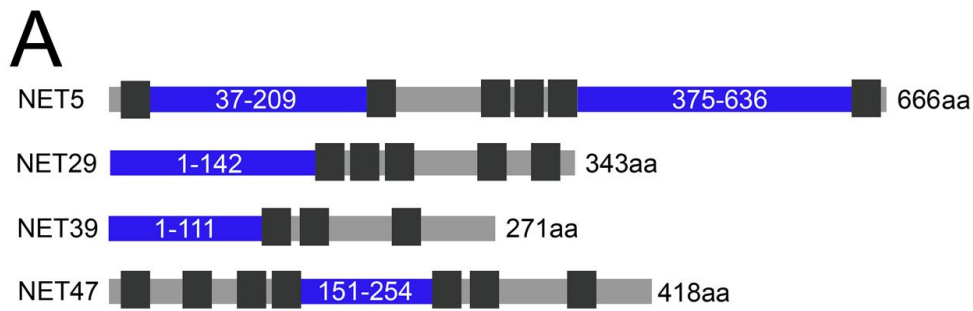


Figure 44. Soluble fragments of NETs that reposition chromosomes. (A) Soluble portions of NETs (blue) that were able to reposition chromosomes were cloned and fused to the classical SV40 NLS to ensure their nuclear localization. We designed two soluble constructs for NET5, because it contained two large soluble portions. Dark grey boxes indicate membrane domains of the corresponding NETs. **(B)** The localization of depicted soluble constructs was tested by immunofluorescence. All fragments localized to the nucleus, as did the NLS-GFP control.

To test if cells stably expressing the soluble fragments of NETs are also able to reposition chromosomes like their full length counterparts, three

soluble NET cell lines were subjected to quantification of the chromosome 5 localization by the 2D algorithm (Figure 45). A total of 100 cells were analyzed for each sample. Soluble NET29 had comparable chromosome 5 distribution patterns like the GFP-NLS control. For soluble NET39 and NET47 the chromosome localization tended to be slightly higher at the nuclear periphery compared to the control but the effect was not as striking as with full-length NET39 and NET47 (see Figure 39) suggesting that the chromosome repositioning to the periphery depends likely on direct interaction of the NET with the chromosome at the nuclear periphery rather than an enzymatic function of the NET.

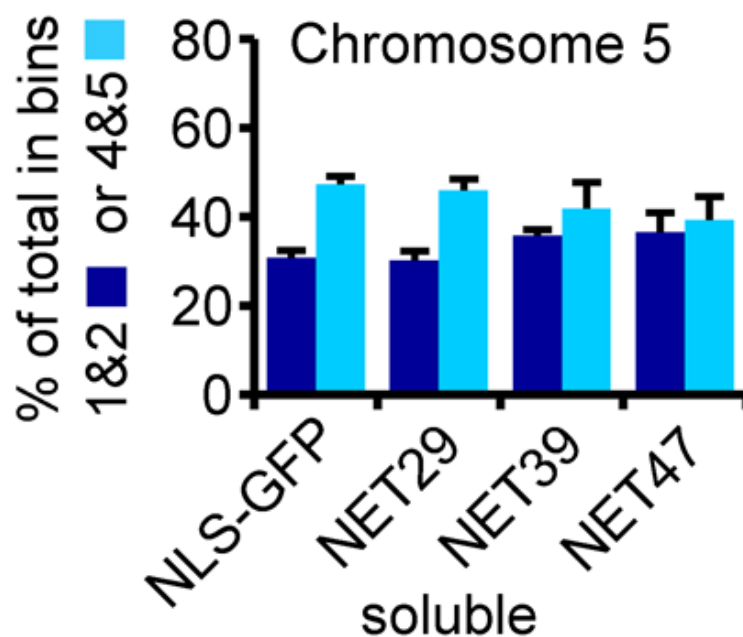


Figure 45. Soluble fragments of chromosome-tethering NETs fail to reposition chromosome 5 to the nuclear periphery. Soluble fragments of NETs 29, 39 and 47 were checked for their chromosome 5 localization to test if they can also cause a repositioning of the chromosome to the nuclear periphery like their full-length counterparts. A total of 100 cells were analyzed by the 2D algorithm for each sample. None of the soluble fragments were able to increase the incidence of chromosome 5 at the NE to such a striking extend as their wild-types analogues. Chromosome 5 distribution for NET29 was very similar to the NLS-GFP control whereas both NET39 and NET47 had a very slight increase of the chromosome at the nuclear periphery. Still the effect was much weaker than that from their full-length equivalents.

4.4 Summary of chapter 4

In this chapter I conducted a screen for NETs that can reposition chromosomes to the nuclear periphery. For this I initially used two cell lines in which chromosome 5 and 13 were visualized by a GFP labelled lacO array. These cell lines were transfected with RFP-fused NETs and the array-containing chromosome position was determined by a computer algorithm. I found several NETs that were changing the position of the array-containing chromosome in respect to the nuclear periphery. Furthermore, I confirmed the chromosome repositioning results in cell lines lacking the lacO array and stably expressing GFP-tagged NETs. We further demonstrated that NETs can co-immunoprecipitate histone H3 as a general marker for chromatin. Together with the finding that soluble portions of chromosome-repositioning NETs were not able to tether chromosomes to the nuclear periphery this observation suggested that the NET-chromosome interaction could be direct and not just caused by a NET-mediated signalling cascade.

Chapter 5

Tissue-specific NETs can mediate a spatial chromosome positioning that correlates with that in tissues

In previous studies some components of the NE were already shown to reposition chromosomes to and from the nuclear periphery. For example, a truncation mutant of the ubiquitously expressed lamin B1 in human cells was shown to cause repositioning of chromosome 18 from the nuclear periphery to the nuclear interior (Malhas et al., 2007). But since lamin B1 is a widely expressed protein it is unlikely to be a driver of tissue-specific chromosome positioning. We hypothesized that tissue-specific chromosome organization is likely to be mediated by proteins that are tissue-specific themselves. Therefore we tested the chromosome repositioning NETs whether they are preferentially expressed in particular tissues or not. For this we obtained and probed ready-to-use western blots containing several human tissues (Imgenex) with NET antibodies¹⁵ (Figure 46, A).

¹⁵ this was done by Dr. Nadia Korfali (Wellcome Trust Centre for Cell Biology, Edinburgh, UK)

5.1 Chromosome repositioning NETs are tissue-specific

I will refer to NETs being tissue-specific even though some of them are preferentially expressed in more than one tissue. Thus the meaning of tissue-specific here indicates that a NET is expressed in only very few tissues out of the many tested.

Indeed, in line with our hypothesis, all of the chromosome repositioning NETs were tissue-specific. NET5 had strong tissue preference for brain skeletal muscle and testis. Though the bands for NET5 were differently sized it can be explained by the presence of splice variants. NET29 has also several splice variants and was extremely liver-specific with detectable levels in brain and NET39 had extremely strong accumulation in brain, liver and muscle although moderate expression in heart, small intestine and kidney were also evident. Both NET45 and 47 were extremely liver-specific and NET55 was relatively ubiquitously expressed throughout all tested tissues (Figure 46, A).

We sought independent confirmation for NET tissue-specificity by using a publicly available transcriptome database (BioGPS), which is a microarray transcriptome comparison between more than 80 human tissues (Figure 46, B). Transcript levels of NET29, 39, 45, 47 and 55 were extracted from the database for adipose, bone marrow, heart, kidney, liver, lung, skeletal muscle, skin, small intestine and brain tissue. No data for NET5 were available in this database. The transcript levels for NETs were normalized against the median of more than 80 tissues sampled in the entire database. NET29 transcript levels were highest in heart, but were also high in liver. NET39 was preferentially expressed in heart tissue. NET45 was highly expressed in liver and the small intestine whereas NET47 was expressed in

similar amounts in both liver and heart. NET55 confirmed ubiquitous expression throughout all tissues. Though the transcriptome database basically confirmed the tissue-specificity of the NETs there were also some differences compared to the protein level results (human tissue immunoblots). Those can be explained by factors like differences in stability of mRNA or difficulty in processing of the human tissue for RNA preparation resulting in degradation of some transcripts.

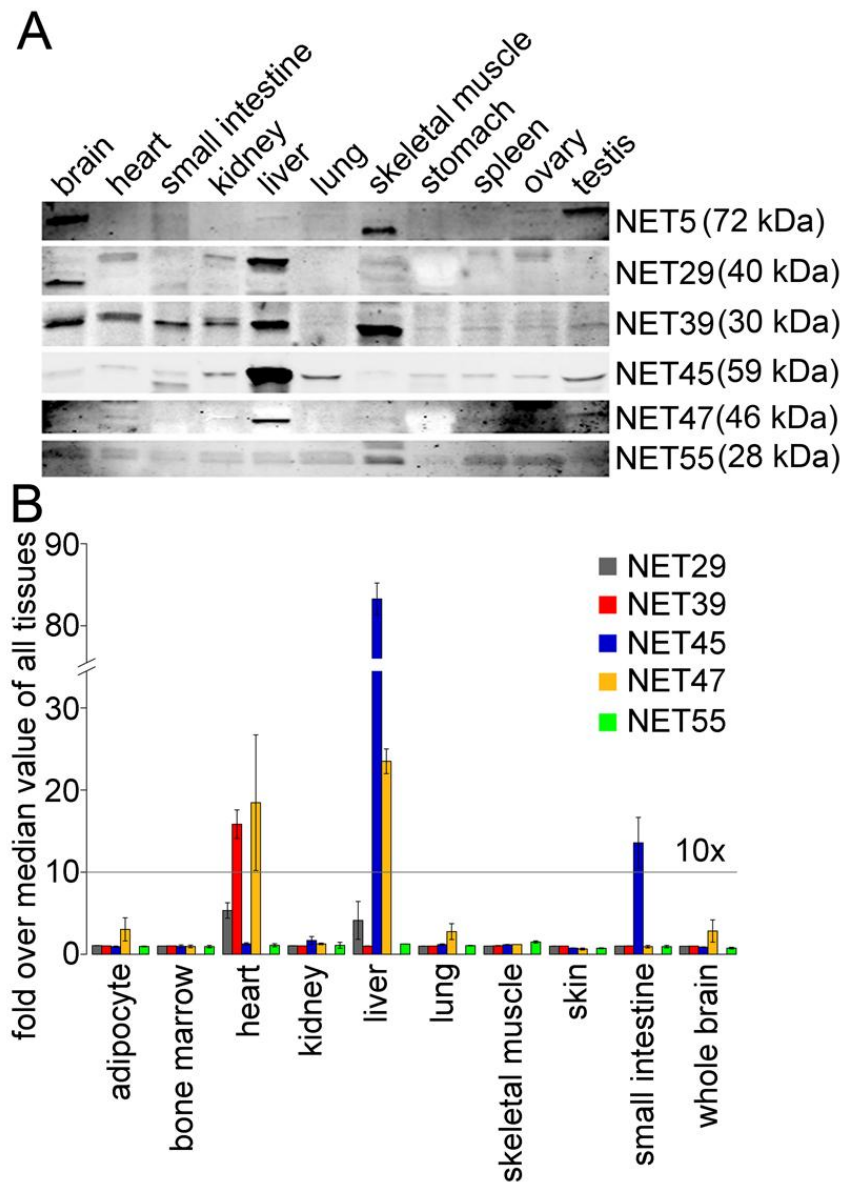


Figure 46. NETs that reposition chromosomes are tissue-specific. (A) Human tissue western blots were probed with antibodies against NETs. NET5 has several splice variants (bands with different apparent molecular weights) and was preferentially expressed in brain, skeletal muscle and testis. NET29 protein levels were highest in liver and brain. Although strongly expressed in liver and skeletal muscle NET39 could also be detected in brain, heart, small intestine and kidney. NET45 and NET47 were extremely liver-specific and NET55 was widely expressed. **(B)** NET transcript levels were accessed from a transcriptome database (BioGPS) in particular tissues. Transcript levels are shown as fold-difference over median from a total of more than 80 tissues of the database. NET29 transcript levels were up in liver and heart. NET39 was heart specific. NET45 levels were highest in liver but were also high in the small intestine and NET47 was high in both liver and heart. NET55 was ubiquitously expressed.

5.2 Chromosome positioning correlates with tissue-specificity of NETs

To test the potential link between tissue-specific preferred positions of interphase chromosomes and the tissue-specific expression of NETs the chromosome 5 location was compared between human liver and kidney biopsy tissues. As shown in Figure 46 out of the NETs that repositioned chromosome 5 NET45 and NET47 were highly expressed in liver but none of them was expressed in kidney. Hence, together with the knowledge that all of the chromosome-tethering NETs were identified from liver tissue, we hypothesized that in liver, where these chromosome 5 tethering NETs are naturally up-regulated, chromosome 5 should be more at the periphery than in kidney, where none of these NETs are expressed. To test this hypothesis human tissue sections from liver and kidney tissue were obtained and subjected to FISH and quantitative analysis with the 2D erosion algorithm. Indeed, in liver¹⁶ chromosome 5 had a more peripheral localization than in kidney¹⁷ (Figure 47, A). Quantitative analysis of both tissues scoring 100 cells in total confirmed this trend (Figure 47, B).

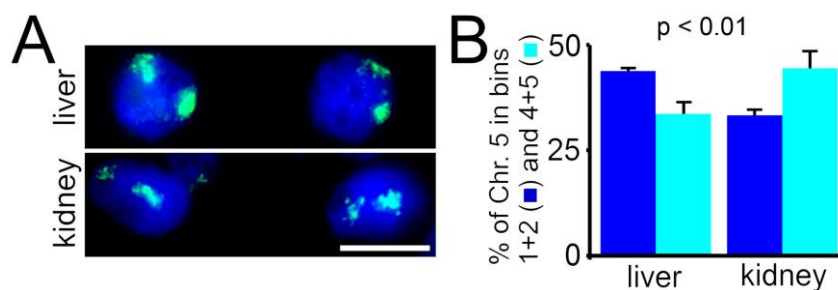


Figure 47. Chromosome 5 is more peripheral in human liver than in kidney. Human biopsy liver and kidney tissues were stained for chromosome 5 by FISH. (A) In liver chromosome 5 had a more peripheral configuration than in kidney tissue. (B) Quantitative analysis scoring 100 cells in total for both tissues confirms the trend that chromosome 5 is more peripheral in liver than in kidney (p -value < 0.01).

¹⁶ Within the liver section hepatocytes, which comprise ~80% of the liver tissue, were imaged.

¹⁷ Within the kidney section proximal and distal tubule cells and collecting duct cells of the renal medulla were imaged.

5.3 NET-mediated tissue-specific chromosome positioning is reversible

To further test if tissue-specific NETs could mediate tissue-specific spatial chromosome organizations we depleted two liver-specific NETs in the liver-derived cancer cell line HepG2. The rationale behind this is that if liver-specific NET45 and 47¹⁸, both naturally expressed in this cell line, are tethering chromosome 5 to the nuclear periphery in these cells, then depletion of these NETs should result in the release of chromosome 5 from the nuclear periphery. By reducing the levels of these two proteins by means of RNAi (Figure 48) chromosome 5 should be released from the periphery at least partially since its tethering points at the periphery are reduced.

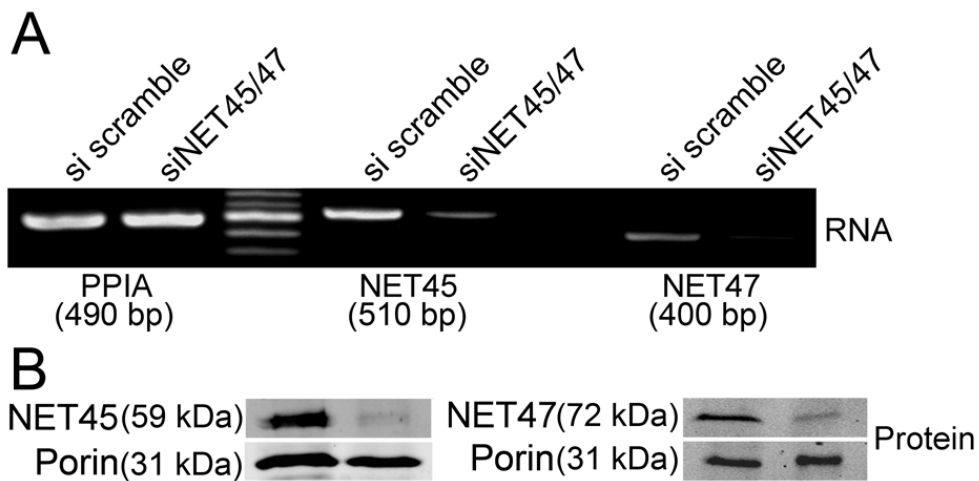


Figure 48. Knockdown of liver-specific proteins NET45 and NET47 in HepG2 liver cells. (A) Semi-quantitative RT-PCR shows efficient transcript reduction for both NET45 and NET47 in HepG2 cells treated with NET45 and NET47 siRNA oligos compared to scramble siRNA oligo treated control cells. PPIA was used as a loading control. (B) Reduction of protein levels of NET45 and NET47 is assessed by western blotting in cells treated with siRNA oligos against the two proteins. NET45 was detected with a NET45 antibody in HepG2 cells. NET47 was detected as a GFP fusion with an anti GFP antibody because the anti NET47 antibody was not working on HepG2 lysates (even though it worked on the human tissue western blots). Porin was used as a loading control.

¹⁸ from here on I will refer to NET47 being liver-specific because in human tissue western blots, i.e. on the protein level, it was highly expressed only in liver but in the transcriptome database, i.e. at the RNA level, it was up-regulated in both liver and heart

After depletion of the liver-specific NETs 45 and 47 in HepG2 cells FISH was performed to test the chromosome 5 localization (Figure 49). In control cells chromosome 5 localized mainly to the nuclear periphery (Figure 49, A left), however, in cells depleted for NET45 and NET47 the chromosome lost its peripheral localization in many cells (Figure 49, A right). This observation was confirmed when the chromosome 5 localization was quantified in both samples (Figure 49, B). Four days after siRNA treatment the peripheral localization of chromosome 5 was reduced with significant p-values and this effect increased over time.

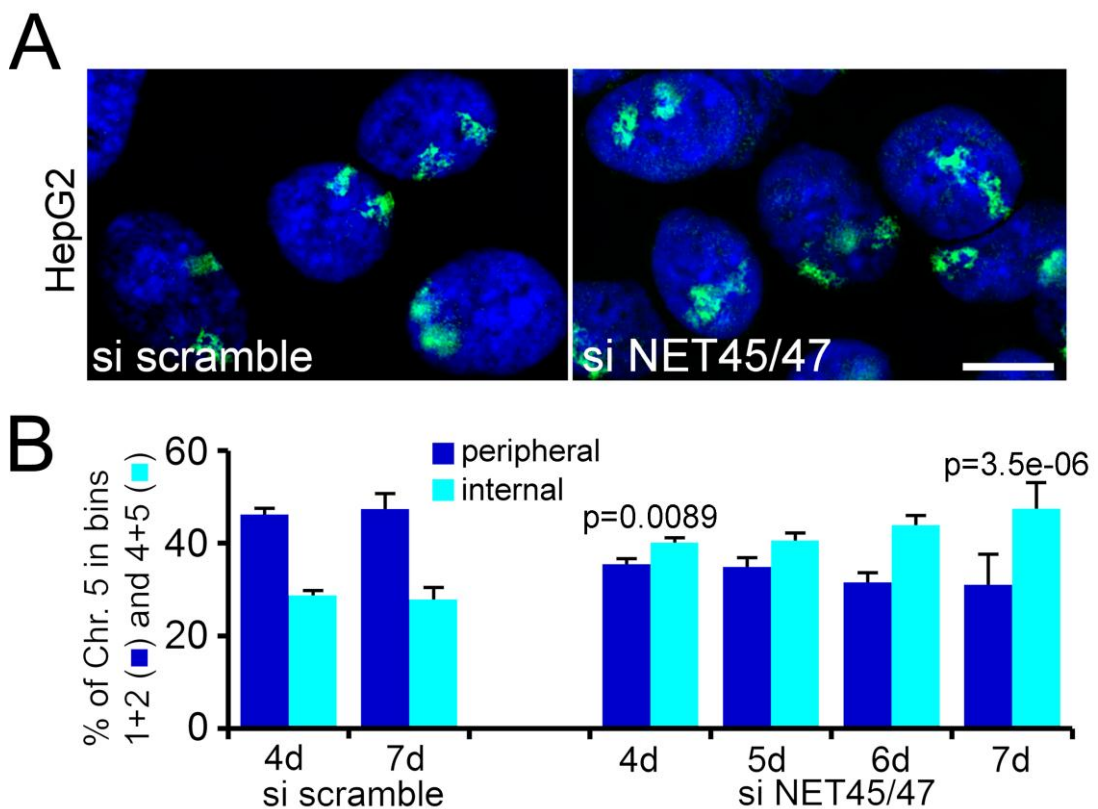


Figure 49. Peripheral localization of chromosome 5 is reduced in HepG2 liver cells depleted from liver-specific NET45 and NET47. (A) In scramble siRNA treated cells chromosome 5 localizes mainly to the nuclear periphery (left) but is found more internal in cells depleted from NET45 and NET47. (B) Quantitative analysis using the 2D erosion algorithm confirms the trend. Chromosome 5 localization is significantly reduced in NET45 and NET47 depleted cells after 4 days of RNAi treatment compared to scramble oligo treated control cells. The reduced peripheral localization of chromosome 5 persists even after 7 days of siRNA treatment.

5.4 Summary of chapter 5

In this chapter we analyzed the expression patterns of the chromosome-tethering NETs in human tissues and found that all of these NETs were highly tissue-specific with some of them being specific to liver. In line with this finding I found that chromosome 5 was more peripheral in liver than in kidney, a tissue in which most of tethering NETs were not expressed. Based on this finding we tested if depleting of two liver-specific proteins would release chromosome 5 from the nuclear periphery and indeed knock-down of these proteins by RNAi caused the chromosome to become more internal.

Chapter 6

NET-mediated chromosome repositioning promotes tissue-specific gene expression¹⁹

6.1 NET-mediated chromosome repositioning affects global gene expression

Spatial chromosome and gene repositioning has been linked with modulations of the respective gene activities. That is why having identified several novel tissue-specific nuclear proteins that can alter the position of chromosomes we searched for gene expression changes that have occurred in coherence with the chromosome repositioning. This was done by means of microarray analysis. Differentially expressed genes in HT1080 cells stably expressing chromosome-tethering NETs were normalized against the differentially expressed genes in the GFP-NLS cells. The normalized differentially expressed genes from the NET cell lines were then divided into two groups. The first group represents all genes that were up-regulated (Figure 50, left) upon the overexpression of the according NET and the

¹⁹ *The bioinformatics gene expression analysis in this chapter was performed by Dr. Jose de las Heras (Wellcome Trust Centre for Cell Biology, Edinburgh, UK)*

second group shows all down-regulated genes (Figure 50, right) upon particular NET expression. Figure 50 represents those two groups in a Venn diagram with numbers of genes for each individual NET, which are specific to the NET and are shared with other NETs. Notably for both up- and down-regulated genes is the high overlap between the NET29 and the NET39 cell line. On the contrary the overlap for NET5 and NET47 was minimal. This observation makes sense from the point of view that both NET29 and NET39 had very similar chromosome repositioning patterns since both increased the incidence of chromosome 5 and 13 at the nuclear periphery whereas NET5 and NET47 were tethering chromosome 5 to the NE but not chromosome 13. When looking at differentially expressed genes shared between all of the NETs the overlap was minimal suggesting differences in mechanisms of chromosome repositioning between the NETs.

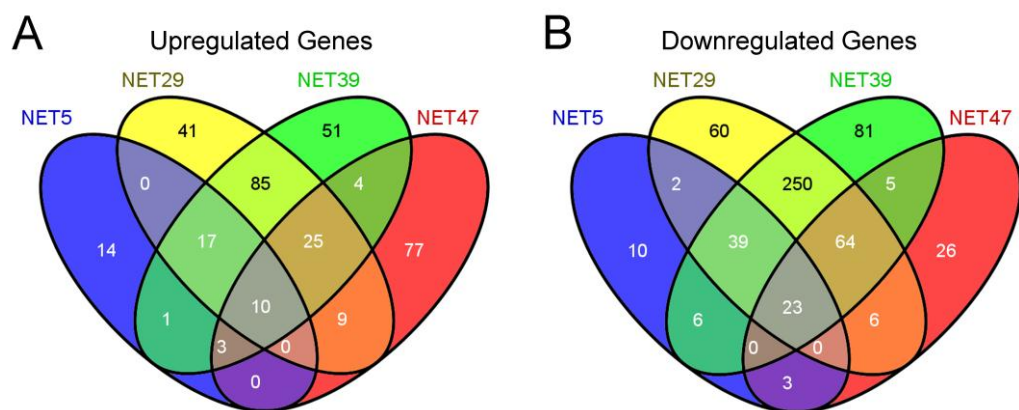


Figure 50. Up- and down-regulated genes in cell lines stably expressing the chromosome-repositioning NETs. The transcriptome of cells expressing the chromosome-repositioning NETs was assessed by microarrays and all genes that were changed in the according cell lines were clustered into two groups. The first group represents all genes that were up-regulated (left), the other group shows the number of genes that were down-regulated (right). Furthermore, the Venn diagram displays regulated genes, which were unique for each NET and those that were shared between the analyzed NET cell lines. NET29 and NET39 cell lines had a notable overlap of genes that were either up- or down-regulated. In contrast, the overlap between NET5 and NET47 was much smaller. The total overlap between all NET cell lines was moderate for both up- and down-regulated genes.

To check if NET-mediated differential expression of genes would correlate with the tissue-specificity of the particular NETs we analysed the

transcription profile of HepG2 cells upon knockdown of liver-specific proteins NET45 and NET47. The table below (Table 9) lists the 10 most down-regulated genes upon the NET45 and NET47 knockdown. Indeed, of the 10 most down-regulated genes seven were associated with liver function.

Table 9. The ten most down-regulated genes upon knockdown of NET45 and NET47 in HepG2 liver cells are linked to liver function

Rank	Gene	Function
1	<i>DAK</i>	NET45
2	<i>IGFBP1</i>	Highly induced in LIVER regeneration
3	<i>ACOX2</i>	LIVER metabolism
4	<i>APOM</i>	LIVER enriched, cholesterol transport
5	<i>LOX</i>	Crosslinks collagen in LIVER, cirrhosis
6	<i>SOAT2</i>	LIVER enriched, fatty acid metabolism
7	<i>EGR1</i>	Induced during LIVER regeneration
8	<i>SELM</i>	Perinuclear localization
9	<i>THAP4</i>	Widely expressed
10	<i>MIF4GD</i>	RNA metabolism, highest in placenta, LIVER, pancreas

6.2 Differentially expressed genes in NET cell lines partly overlap with gene changes in differentiation systems

We further investigated if NET induced chromosome repositioning results in tissue-specific gene expression profiles. For this we compared the differentially expressed genes in the NET cell lines with genes up-regulated in a hepatic differentiation system. The transcriptome of a hepatic differentiation system was obtained from a public database (<http://www.ncbi.nlm.nih.gov/projects/geo/query/acc.cgi?acc=GSE14897>) and plotted (differentiated vs. undifferentiated). On this plot we introduced a line to mark a threshold demarcating genes that were at least 2-fold up-regulated during hepatic differentiation (all genes above the line). We then compared the differentially expressed genes of the NET cell lines with the hepatic differentiation system by overlaying the differentially expressed genes in the NET cell lines with the up-regulated genes in the hepatic differentiation system (Figure 51). Genes that were up-regulated in both, the NET cell lines and the hepatic differentiation system, were colour coded in red. Genes that were down-regulated in the NET cell lines but up-regulated in the hepatic differentiation system were colour coded in blue (enlarged blue spots).

Many genes that were up-regulated in the cell line expressing the liver-specific protein NET47 were also up-regulated during hepatic differentiation (Figure 51, NET47). In contrast, the muscle- and heart-specific protein NET39 had very little overlap since most of genes that were up-regulated during hepatic differentiation were down-regulated (Figure 51, NET39) in the NET39 stable cell line. NET29 that was relatively liver-specific (but not as much as NET47) had an intermediate overlap with the hepatic differentiation system (Figure 51, NET29). These data suggest that tissue-specific NETs can induce regulation of tissue-specific genes.

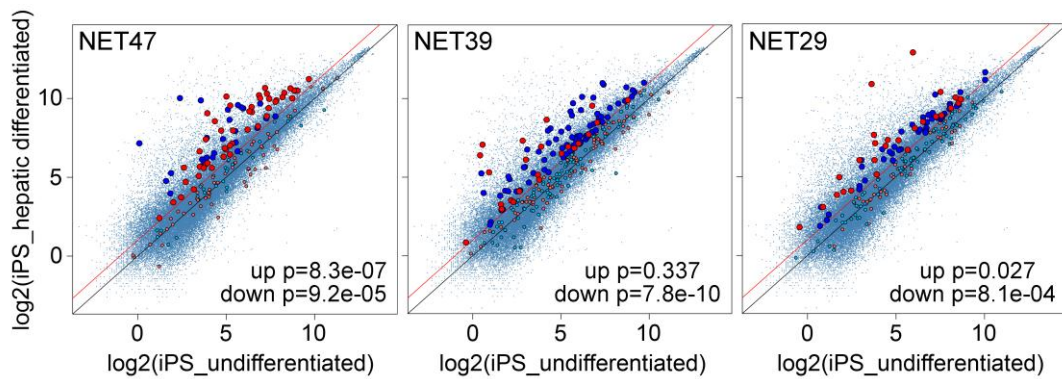


Figure 51. Overlap with a hepatic differentiation system in up-regulated genes is strong for NET47, intermediate for NET29 and weak for NET39. Transcriptome data from a hepatic differentiation system was assessed and genes that were up- or down-regulated in the HT1080 cell lines stably expressing NET29, NET39 and NET47 were overlaid. Colour coded in red are genes that were up-regulated in the NET expressing cell line and the enlarged blue colour coded spots are genes that are down-regulated in the stable NET cell line. When defining a confidence threshold for genes that were up-regulated in the hepatic differentiation system (red line) one can see that many genes that were up-regulated during hepatic differentiation were also up-regulated in the liver-specific NET47 expressing cell line. In contrast, for NET39, which is more muscle-specific, the overlap with the hepatic differentiation system is minimal as many genes that are up-regulated during hepatic differentiation are down-regulated in the NET39 cell line. NET29, which is expressed in both liver and heart, displays an intermediate overlap with the hepatic differentiation system.

We further tested if differentially expressed genes in the NET cell lines are enriched for those involved in differentiation. For this we performed gene ontology analysis using the GOstats package (Bioconductor.org). We tested if functions associated with aspects of differentiation are enriched in the cell lines stably expressing the chromosome repositioning NETs 29, 39 and 47 (Figure 52, NET samples) using the total genome (Figure 52, ALL) as a reference. Cell lines stably expressing the chromosome repositioning NETs displayed an enrichment of functions implicated in differentiation. This data suggests that overexpression of NETs can indeed cause an enrichment of genes involved in differentiation.

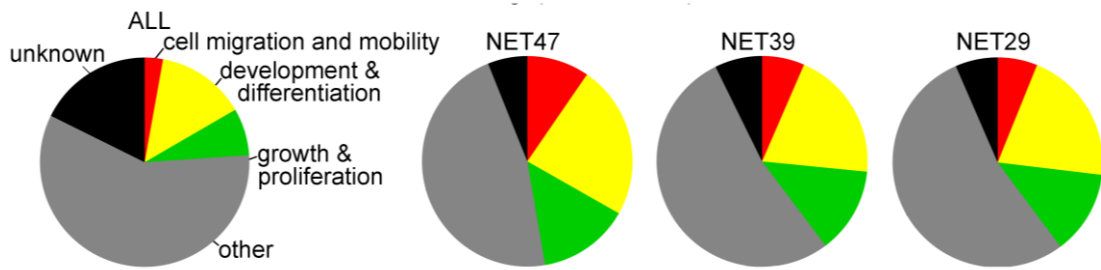


Figure 52. Strong enrichment of differentially expressed genes associated with aspects of development and differentiation was observed in cells stably expressing chromosome repositioning NETs. The gene expression profiles of the NET cell lines were divided into GO-terms according to particular cell functions. The whole genome served as a control (ALL). Specific NET expression profiles revealed strong enrichment for genes implicated in differentiation with cellular functions such as cell migration and mobility, development and differentiation and growth and proliferation when compared to the whole genome control (ALL).

6.3 Transcriptome changes mediated by the full-length NETs are not recapitulated by their soluble fragments

To investigate if NETs can alter gene expression only when they localize to the NE or if the soluble parts of NETs can also induce a specific expression pattern we have compared the expression profiles derived from cell lines expressing full length NETs and from cells expressing only the soluble NET domains (Figure 53). Genes that were up-regulated (compared to the GFP-NLS transfected control) were colour coded in red and genes down-regulated in blue. For the three NETs tested (NET47, NET39 and NET29) the soluble fragments could not recapitulate the expression patterns of their full length counterparts.

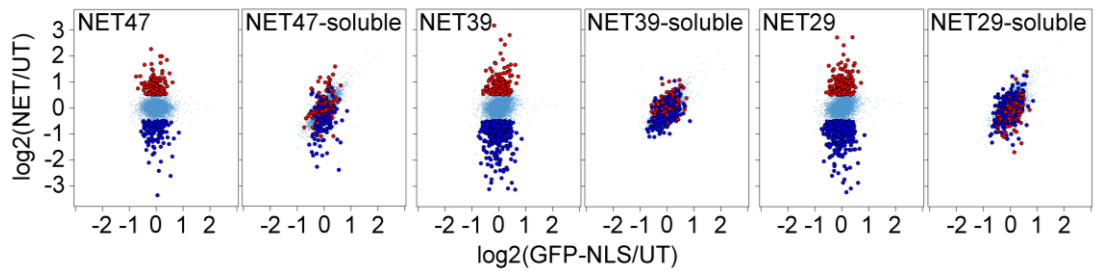


Figure 53. Stable cell lines of soluble NET fragments do not recapitulate gene changes caused by the full-length proteins. Expression profiles in cells expressing full-length chromosome-repositioning NETs were assessed and compared to the expression profiles of cells expressing only the soluble domains of the according NETs. The colour coded red spots represent genes that were up-regulated and blue spots genes that were down-regulated in the NET cell lines compared to the GFP-NLS transfected control cells. Neither for NET47 nor for NET39 and NET29 could the expression profile of the soluble fragment recapitulate the expression profile of the full-length NET.

6.4 Artificial versus NET-mediated chromosome repositioning

The final interesting question to answer was if artificially mediated chromosome repositioning (for example using the lacO-lacI system) or NET-mediated chromosome repositioning was necessary to induce changes in gene expression. To test this we compared the expression profiles of the chromosome-repositioning NETs with the expression profile of a cell line where a bacterial lacO array integrated into chromosome 5 and a lacI-LAP2 construct was expressed simultaneously in order to artificially tether the chromosome 5 to the NE (Figure 54). When looking at genes that were uniquely regulated by the particular NETs then there was about 20-35% overlap with the lacI-LAP2 cell line (Figure 54, left). The overlap with the lacI-LAP2 cell line increased to about 30-50% when total genes (not unique for particular NET) were compared. This data suggests that roughly two-thirds of genes are specifically altered by a particular NET and about one-third of altered genes are due to general effects of peripheral positioning. This indicated that both the general positioning effect and the specific mechanism

by which the chromosome is repositioned have an impact on gene expression.

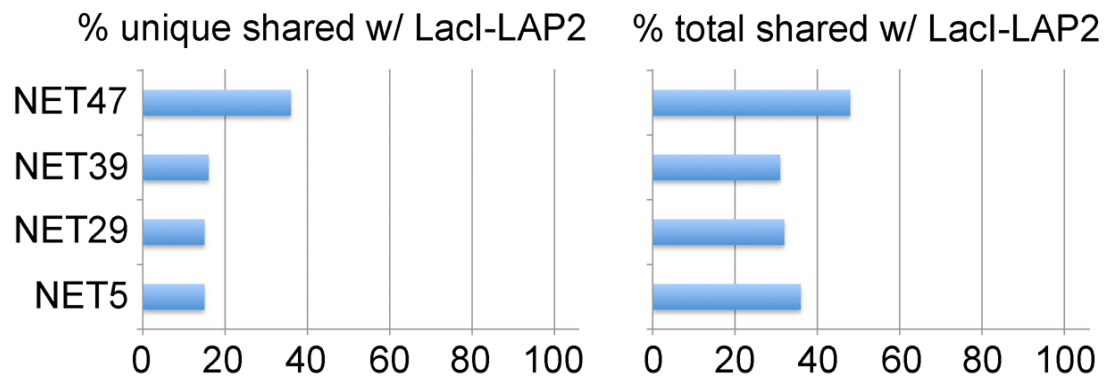


Figure 54. Artificial chromosome 5 tethering mimics only partially the expression profile of chromosome tethering NET cell lines. Gene expression profiles of cells stably expressing NETs that are relocating chromosome 5 to the NE and cells in which chromosome 5 was repositioned to the NE by an artificial high affinity tether were compared. The artificial high affinity tethering of chromosome 5 was accomplished through a lacO array integration into chromosome 5 and simultaneous expression of lacI-LAP2. LacI has a high affinity to the lacO array, thus tethering the whole chromosome 5 to the nuclear periphery. When looking at genes that were uniquely changed upon NET overexpression around 20% of genes were shared with the lacI-LAP2 cell line for NET5, NET29 and NET39. NET47 shared around 40% of differentially expressed genes with the lacI-LAP2 cell line. When taking genes into account that were not unique in the NET expressing cell lines then the proportion of genes shared with the lacI-LAP2 cell line increased for NET5, NET29 and NET39 to roughly 30% whereas for NET47 it increased to roughly 50%.

6.5 Summary of chapter 6

After having found that tissue-specific NETs help to achieve a tissue-specific chromosome patterning within the nucleus the next logical step was to test if specific gene expression patterns are established upon the up-regulation of these chromosome-repositioning NETs. In this chapter the expression profiles were assessed by means of microarrays. We found that there was a general tendency towards down-regulation of genes supporting the general hypothesis that genes are silent at the NE. We observed a strong overlap of differentially expressed genes between the NET29 and the NET39 samples coherent with the fact that both proteins had similar effects on chromosome positioning. When comparing all NETs together, the general overlap of differentially expressed genes was small suggesting different mechanisms at work.

When I further knocked down liver-specific chromosome-tethering NETs 45 and 47 in HepG2 liver cells we observed that 7 out of the top 10 down-regulated genes were related to liver function. This led us to compare the genes regulated by NETs with a hepatic differentiation system. We found that liver-specific NET47 had a strong overlap with the hepatic differentiation system while heart specific NET39 had only minimal overlap. NET29, which is expressed in both liver and heart, had an intermediate overlap with the hepatic differentiation system. These findings suggested a potential contribution of NETs to differentiation. Therefore we tested if differentially expressed genes in the NET cell lines could show enrichment for functions related to differentiation. Indeed this enrichment was observed.

We also tested if expression profiles of cells expressing full-length NETs would match those expressing soluble NET portions, which were distributed throughout the nucleus and failed to recruit chromosomes to the nuclear periphery. We found no correlation suggesting that a particular gene expression profile can only be caused when the NET and its interacting chromosome are both the nuclear periphery.

Last we tested if artificial chromosome repositioning (using the lacO system) would match the gene expression profile of NET-mediated chromosome repositioning. For this we used a cell line that had a lacO integration on chromosome 5 and we tethered this chromosome by a lacI construct which was located at the NE. The gene expression profiles of this cell line were compared to the expression profiles of cell lines stably expressing the chromosome 5 tethering NETs. We discovered that though there was some overlap (~ 1/3) within these systems, the majority (~ 2/3) of the genes did not overlap. This suggested that the particular repositioning mechanism (most likely involving specific interaction partners) is dominant but also the repositioning effect *per se* plays also a role for gene expression.

Chapter 7

Discussion

The present work provides the most comprehensive insight on transport of NETs to the INM to date and resolves a previous dispute showing that several mechanisms co-exist for INM protein translocation. The results presented here are in disagreement with the previously established hypothesis that NLSs are the main requirements for the use of the Ran-dependent pathway. In fact, looking further our data suggests that a novel mechanism where FGs in NET sequences facilitate translocation into the INM is a much more commonly used pathway than the one involving Ran. Furthermore, while the debate of whether NETs translocate *via* the central or the peripheral channels of the NPC has just started, our data strongly argue for translocation through the peripheral channels.

This work additionally describes a completely new layer of genome regulation from the NE that fuses chromosome positioning in a tissue-specific manner with regulation of gene expression. This fine-tuning mechanism is likely to optimize transcriptional regulatory cascades, for example in differentiation. This transcriptional optimization could occur by sequestering a transcriptional repressor together with the gene to be shut off at the predominantly silent environment of the nuclear periphery, thus achieving a more efficient silencing of the gene as the volume of the NE is about 1/40th of the total nuclear volume and the local concentration of the transcriptional repressor would therefore be dramatically increased. This mechanism would allow shutting off alternate differentiation pathways during commitment into a particular tissue more efficiently. Alternatively, bringing a gene to the

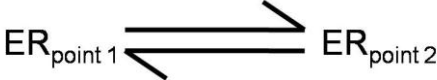
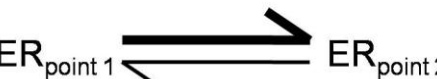
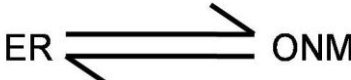
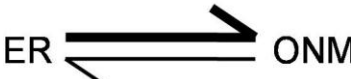
periphery together with a transcriptional activator could effectively enhance the concentration of the activator resulting in boosted transcription.

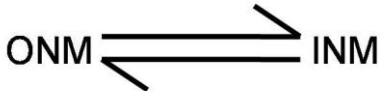

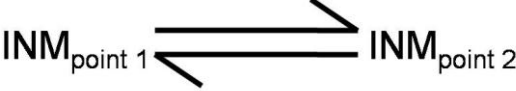

Though we appreciate that transcription factors remain the major drivers of tissue-specific gene expression during differentiation, our findings advance the understanding of a mechanism by which a particular gene expression profile can be optimized by the spatial organization of chromosomes and the according genes located on them through tissue-specific NETs. This hypothesis is supported by a recent study, which mapped the NE-chromatin interactions during differentiation of embryonic stem cells *via* neural precursor cells into astrocytes. This study was able to correlate the progressive differential expression of genes with their spatial repositioning from the NE (Peric-Hupkes et al., 2010). As shown in our study this repositioning can be mediated by the tissue-specific NETs, the variety of which is likely to match the release and capture of the plethora of genes during differentiation.

7.1 What determines the steady state levels of NETs in FRAP and PA experiments?

NETs, like all membrane proteins are synthesized in the ER. To reach their actual functional destination, the INM, NETs have to move within the ER towards the ONM in order to finally translocate into the INM *via* the NPCs. The dynamic NET exchange between these cellular compartments creates several NET pools all of which determine the steady state levels of NETs in FRAP and PA experiments. These pools are outlined in table 10:

Table 10. Distinct pools of NETs

NET Pool	Specifics of the pool
ER pool	<p>The ER NET pool is constantly “fed” by nascent NET molecules, which are synthesized in the ER. NET molecules that do not have any interaction partners within the ER move without any directionality (a). Other NETs that do interact with other proteins within the ER could partly require ATP to form and break these interactions. Some of these NET interaction partners within the ER could be proteins that provide directionality (i.e. proteins of the licensing machinery) therefore forcing NETs to move within the ER towards the NE (b).</p> <div style="text-align: center;"> <p>a</p>  <p>b</p>  </div>
ER-ONM pool	<p>Some NETs of the ER-ONM pool have no directionality, thus these NET molecules can diffuse from the ER into the ONM or <i>vice versa</i> (c). This will not apply to NETs that are bound to licensing proteins, however, as their diffusion equilibrium will be favoured towards the direction of the NE (d).</p> <div style="text-align: center;"> <p>c</p>  <p>d</p>  </div>

<p>Translocation pool</p>	<p>The translocation pool should not have any directionality for NETs that move by free diffusion, thus these NETs should be able to translocate between the ONM and the INM in either direction (e). Directionality will only be provided to NETs that use Ran and the active classical nuclear transport machinery for translocation. That means, for example, that if these NETs are bound to Ran and potentially also import receptors they will be forced to translocate into the nucleoplasm (f).</p> <div style="text-align: center;"> <p>e</p>  <p>f</p>  </div>
<p>INM pool</p>	<p>The INM NET pool is composed of two sub-pools. The first sub-pool harbours the minority of NETs, which are mobile in the INM. Consequently, this NET pool can either move within the INM (g) or even translocate back into the ONM. The second INM sub-pool harbours the majority of NET molecules. These NETs are highly immobile within the INM (h) because they are tightly bound to nuclear components in the nucleoplasm like lamins and chromatin. Thus their mobility depends on the abundance and strength of interactions with nucleoplasmic components. During the interaction the NET cannot move within the INM or translocate back into the ONM.</p> <div style="text-align: center;"> <p>g</p>  <p>h</p>  </div>

In this study I show that binding of NETs in the INM is very strong (since NETs photoactivated in the NE are not very mobile), which in turn

indicated that the fast fluorescence recovery in the NE in FRAP experiments depended stronger on exchange of NETs between ER and the INM rather than on movement of the NETs within the INM itself. This was also supported by the PA experiments where NETs photoactivated within the ER quickly accumulated in the NE.

Nevertheless, the corresponding contributions of the NET populations (table 10) to the measured mobilities during FRAP and PA experiments cannot be easily separated and therefore we applied computational modeling for ER-NE dynamics of 3 NETs (LAP1L, LAP2 and NET55) in an attempt to better understand the contributions of the pools to the steady state levels of NETs (Zuleger et al., 2011a; modeling performed by Dr. Andrew Goryachev, Centre for Systems Biology, Edinburgh, UK). The modeling took into account particular parameters such as mobilities of NETs in NE and ER FRAP experiments, mobilities during PA experiments in both the ER and the NE and the distribution of NETs between the ONM and INM (as determined by EM). The modeling was based on the assumption that NETs can freely diffuse between the NE and the ER in both directions (i.e. NETs that have particular translocation requirements such as ATP or Ran are not covered by the modeling²⁰).

The mathematical ER-NE protein dynamics modeling also indicated that there is substantial exchange between the ER and the INM. In addition modeling suggested that differences in the FRAP $t_{1/2}$ s (Figure 14B) of NETs are not due to different times needed to traverse the NPC (according to the modeling the translocation kinetics of all three NETs were similar) but rather reflect their binding affinities in the INM. That means, for example, that the large $t_{1/2}$ value of LAP1L can be explained by it having high affinity interactions in the INM while NET55 having a comparatively small $t_{1/2}$ value

²⁰ *We did not attempt to model NETs that have special requirements for translocation such as ATP or Ran. Such modelling would be far more complex and would have required large amounts of additional data, which the current content of my work did not provide*

has interactions of lesser affinity within the INM compared to LAP1L. This finding is also supported by the literature as LAP1 is known to have many nucleoplasmic interactors (for review see Schirmer and Foisner, 2007), while NET55 has no known interactors in the nucleus to date.

Finally, the modeling further suggests that there is no directionality in the actual translocation step, meaning that once in the pore membrane (the membrane portion where the ONM fuses to the INM) NETs can equally translocate between the INM and the ONM. However, after the translocation step some NET molecules are entrapped in the INM due to interactions with lamins and/or chromatin components. The abundance of lamin- ($\sim 3 \times 10^6$ lamin molecules in an average mammalian nucleus) and chromatin binding sites can never be saturated by NETs as even when overexpressed NETs are not likely to match the plethora of binding sites provided by the INM.

7.2 Multiple independent mechanisms co-exist for translocation of NETs into the INM

By directly comparing six NETs I was able to demonstrate that several distinct pathways co-exist whereas previous studies could not make this discrimination, because they only tested one or two proteins.

Considering the wide range of characteristics among the NETs identified to date it logically follows that they are very likely to use different mechanisms for translocation dependent on their individual NET characteristics. The idea of several independent mechanisms is also supported by the involvement of different nucleoporins in NET translocation described to date (Antonin et al., 2011; Deng and Hochstrasser, 2006; King et al., 2006; Ohba et al., 2004; Theerthagiri et al., 2010). Although it should be noted that in most of the previous studies nucleoporins were simply depleted or blocked by antibodies and it was not tested whether the

translocation effects were simply due to disruption of the NPC structure (or just sterical blocking) rather than due to a specific interaction effect of the NET with the Nup. In our study, however, the Nup35 depletion effect seems specific since depletion of Nup35 only affects FG-containing proteins [Figure 55, D; (Zuleger et al., 2011a)] and not other NETs. Furthermore, inferring from our data the previously proposed ATP- [Figure 55, B; (Ohba et al., 2004)] and Ran-dependent [Figure 55, C; (King et al., 2006)] mechanisms are used by the minority of NETs tested and thus most NETs are likely to traverse the NPC barrier by either simple lateral diffusion [Figure 55, A; Soullam and Worman, 1993; Soullam and Worman, 1995)] or by yet undiscovered mechanisms.

Our finding that two out of six NETs tested (emerin and SUN2) require ATP also for their ER mobility argues that previous assumptions that ATP is required for the structural modification of the NPC structure to accommodate the translocating NETs (Ohba et al., 2004) might be incorrect. A more plausible explanation would be that ATP is needed for a potential chaperone step just prior to translocation in which ER partners are dissociated to reduce the complex mass and so enable translocation through the size-limited peripheral channels (Figure 55, B). In turn this would ultimately result in the reduction of NET mobility in the NE and this is exactly what was observed. In addition to the ATP requirement in the penultimate moment prior to translocation, ATP seems to be also needed in the ER at significant distances from sites of translocation. This could indicate a requirement for at least some NETs to bind and release partner proteins in the ER upon ATP hydrolysis. Indeed, emerin, a NET that was affected by ATP depletion in this study, has previously been shown to interact with tubulin in the cytoplasm (Salpingidou et al., 2007). Similarly, SUN2, the other NET affected by ATP depletion is a known interactor of Nesprins, which are membrane proteins that reside on the cytoplasmic face of the NE (Padmakumar et al., 2005; Crisp et al., 2006).

Additional interaction partners in the ER could be proteins of the INM protein sorting machinery residing in the ER, which were discovered by the Summers laboratory (Braunagel et al., 2007). Furthermore, also some NETs, such as the SUN proteins, have been shown to dimerize (Wang et al., 2006), thus ATP could be required in the ER to form and break interactions between the NETs themselves.

It should be pointed out that inhibited mobility of NETs in the ER due to ATP depletion at significant distances from the site of translocation is very likely to ultimately also limit the rate of NET translocation into the INM. The depth of my data at this point, however, does not allow me to confidently deduce if the reduced translocation for emerin and SUN2 is due to inhibited mobility in the ER sites further away from sites of translocation or whether it is due to a ATP requirement in the penultimate moment prior to translocation or even due to a combination of both.

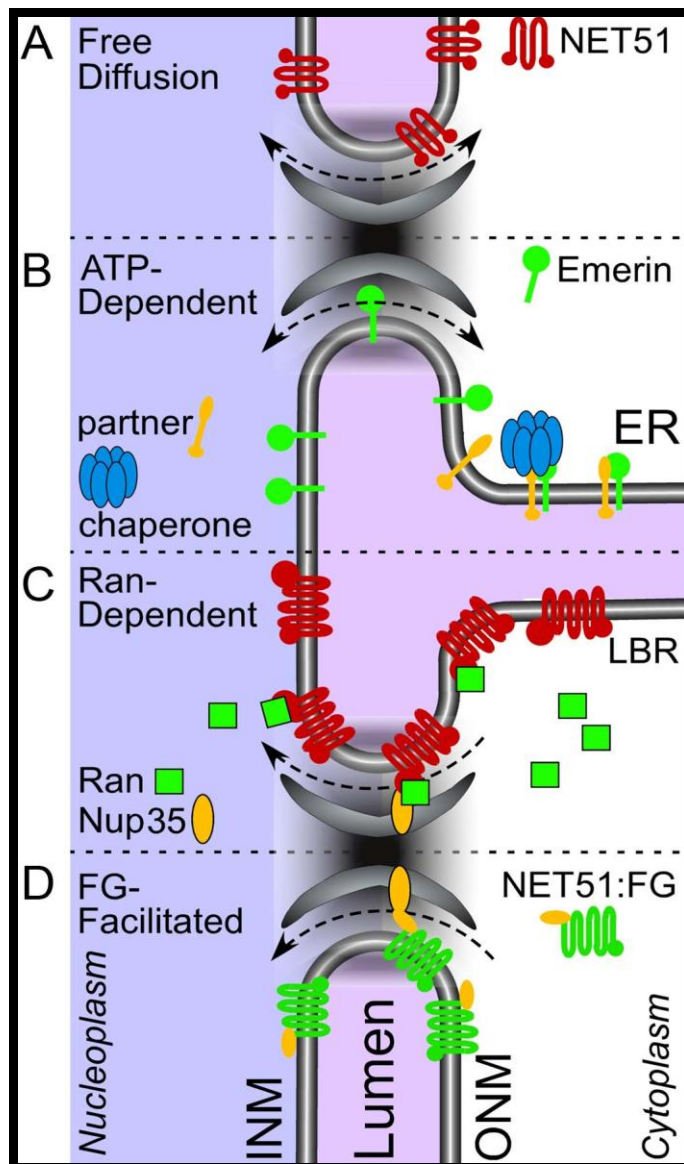


Figure 55. Different mechanisms target NETs to the INM. (A) Proteins like NET51 translocate into the INM via the peripheral channels of the NPC by simple lateral diffusion. (B) Proteins like emerlin and SUN2 require ATP for translocation into the INM. Since these proteins also require ATP for ER mobility we speculate that these proteins are bound to partner proteins and ATP is required to release emerlin and SUN2 from this interaction prior to translocation via the peripheral channels of the NPC. (C) Of the NETs tested, only LBR was dependent on the Ran GTPase for translocation, indicating that use of classical NPC components is not as common as previously suggested. Nup35 appears to also be required for Ran-mediated NET translocation. (D) Addition of FGs to the NET sequence facilitated translocation, indicating that a novel translocation mechanism exists. This mechanism also required Nup35 but was independent of the Ran-dependent translocation pathway.

7.3 The Ran-mediated mechanism is independent of NLSs

In contradiction to previous suggestions (Lusk et al., 2007) NLSs are clearly not the determinants for the Ran-dependent pathway according to our data. Although our finding that LBR translocation requires Ran function is in line with previous observations indicating that Ran can bind LBR (Ma et al., 2007) and importins are required for its licensing to translocate (Braunagel et al., 2007), the LBR-NLSs fused to other proteins did not show any Ran function dependence.

In addition to LBR several other NETs in our study contained NLSs (as predicted by the pSORTII algorithm) but did not show any Ran dependence, further arguing that a NLSs is not a determinant of the Ran-mediated translocation pathway. However, it should be noted that one of the classical NLSs is principally a stretch of basic residues and since many NETs have basic residues in their nucleoplasmic domains to interact with DNA (Ulbert et al., 2006) these could be predicted erroneously as NLSs.

Further support for a potential redundancy of NLSs for Ran-mediated INM protein targeting is provided by a recent study where an NLS on SUN2 bound to importin- α and importin- β in a Ran-dependent manner, but mutation of the NLS did not inhibit targeting of SUN2 in interphase cells (Turgay et al., 2010). Together with my finding that SUN2 targeting is not Ran-dependent, this supports that the NLSs in NETs are not conferring Ran-dependence.

7.4 The FG-facilitated mechanism suggests that INM proteins can act as their own transport receptors

Since the discovery that transport receptors might interact with NETs to facilitate their translocation across the NPC (King et al., 2006) a question has puzzled the NE community: How could these huge NET-receptor complexes (only the receptor importin- β is 97 kDa and often several receptors are bound to one cargo) be accommodated by the only 10 nm peripheral channels of the NPC, which in theory can fit a globular protein of only 60 kDa. Though a clear answer to this question cannot be given, and only translocation through the central channel seems possible in this case, my finding that FGs in NETs sequences can facilitate NET translocation into the INM suggests how this problem can be solved: NETs can act as their own transport receptors and thus facilitate their translocation through FG_{NET} - $FG_{nucleoporin}$ interactions just like it has been suggested for transport of soluble cargos where $FG_{receptor}$ - $FG_{nucleoporin}$ interactions facilitate the import into the nucleus (Rexach and Blobel, 1995). In fact, our bioinformatic analysis of 199 putative NETs shows a strong enrichment for FGs compared to mitochondrial membrane proteins arguing that this could be a general mechanism for INM protein transport. It should be noted, however, that the hypothesis that transport receptors mediate the transport of cargos into the nucleus through interaction of their FGs with FG-containing nucleoporins (Rexach and Blobel, 1995) is lacking direct experimental proof. Still, our findings regarding the FGs and the observation that the FG-containing Nup35 is involved in NET transport support this model.

When we found the accumulation of FGs in the LBR sequence we also noted that 4 out of the 6 FGs in the LBR sequence localize in or close to predicted transmembrane regions. This observation provides room for speculation that FG interactions between NETs and FG-Nups could not only occur in the peripheral channels but also in the membrane or the lumen. This idea is supported by the fact that GP210, a FG Nup that sticks from the peripheral channel into the lumen of the NE and contains most of its FGs in

the lumen, was found to be important for INM translocation of NETs (Ohba et al., 2004).

Importantly, the FG-facilitated mechanism could not only apply to membrane proteins. Many soluble proteins do not have a predicted NLS, yet localize to the nucleus. Thus one could imagine that these cargos could translocate through the NPC *via* interactions of their own FGs with the FG-Nups, just like suggested for the membrane proteins above. In fact this mechanism could be the preferred nuclear import pathway for many proteins lacking a NLSs. Therefore, future bioinformatic analyses should search large data sets of nuclear soluble and membrane proteins for whether there is a concentration of FGs in those that do not have predicted NLSs.

7.5 What determines which pathway is utilized?

The determinants driving the targeting by a particular mechanism still remain largely elusive but the use of a particular mechanism by a NET is most certain to depend on its particular properties. For example, in yeast the nucleoporin Nup170 is required for INM translocation of the NLS-containing NET Heh2 (King et al., 2006) but not for Doa10, which lacks an obvious NLS (Deng and Hochstrasser, 2006). The fact that testing for the same pathway while using different substrates and yielding different results really emphasizes that distinct determinants of NETs are likely to decide which translocation pathway to utilize. Supporting this idea, my study suggests that FGs in NETs are determinants of the FG-facilitated pathway.

To comprehensively determine which specific NET characteristics are defining the usage of particular translocation pathways future studies need to test a large number of NETs with different characteristics for different translocation pathways under the same experimental conditions. Once a

large group of NETs that uses a particular translocation pathway is identified one can search for specific characteristics of this NET group that distinguish it clearly from another.

7.6 Peripheral versus central channel translocation

The use of the NPC central channel for transport of most soluble cargoes is undisputed, however the possibility that membrane proteins could also translocate through the central channel was deemed unlikely because it would involve doubtful scenarios of either extraction of the membrane protein from the membrane or the slicing of the translocating membrane protein through the NPC. Two recent studies however, claim exactly the latter (Meinema et al., 2011; Tapley et al., 2011). They suggest that the complex NPC structure is highly elastic and so the NET can reach through this structure while still being bound to the membrane on one end and being in the central channel of the NPC associated with transport receptors on the other end. Our data on the other hand, suggests the use of the NPC peripheral channels (Figure 56, right panel), since two transport mechanisms in our study, the Ran and the FG-facilitated pathway, both required Nup35 (in yeast Nup53p), a nucleoporin that resides in the peripheral channel of the yeast NPC according to a recently published high resolution map of the NPC (Alber et al., 2007). Another study, in mammalian cells, argues that Nup35 interacts with lamins toward the nucleoplasmic face (Hawryluk-Gara et al., 2005), but also this study would be consistent with Nup35 being in the peripheral rather than in the central channels of the NPC.

Also previous studies, which increased the nucleoplasmic mass of a NET to more than 60 kDa (Ohba et al., 2004; Soullam and Worman, 1995), the size limit of the peripheral channels, and measured an inhibition of its translocation, support our results. If the NET would use the central channels for INM translocation, its size would be pretty much irrelevant since even the huge subunits of ribosomes are fitting through the NPC central channels

(Nissan et al., 2002). We also think that at least most of the NETs are using the peripheral channels as analysis from our lab on 199 predicted NETs shows that there is a clear size limit for NETs to have a nucleoplasmic domain of less than 60 kDa (Zuleger et al., 2011a), thus most of them would fit through the 60 kDa small peripheral channels.

An argument that speaks for use of the central channel (Figure 56, right panel) is the discrepancy of the suggested binding to transport receptors, at least for some NETs, during translocation (Braunagel et al., 2007; King et al., 2006; Meinema et al., 2011; Tapley et al., 2011; Turgay et al., 2010). Binding to these transport receptors would propel the NET nucleoplasmic mass to far more than 100 kDa, thus a translocation through the peripheral channels would only be possible when these channels changed shape to accommodate the large receptor-cargo complex.

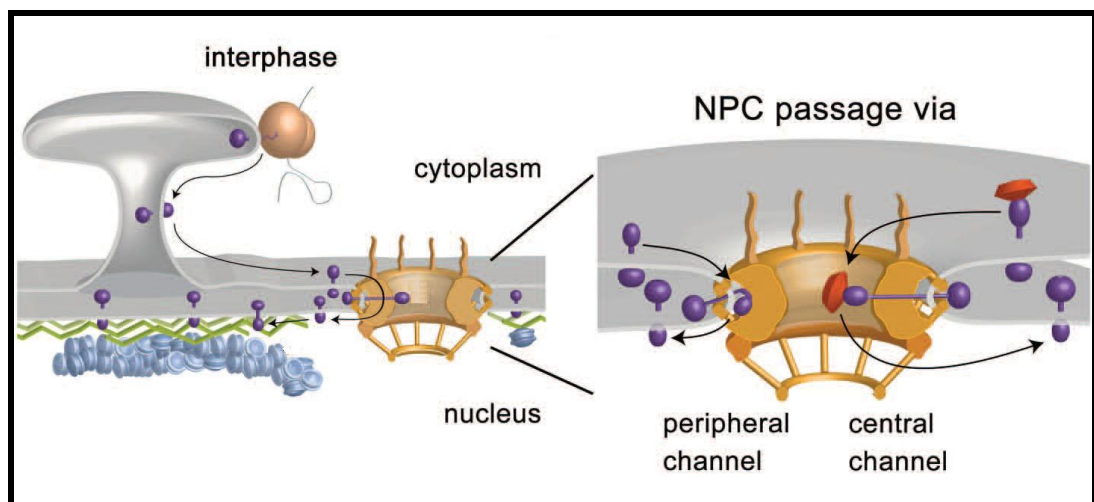


Figure 56. Are NETs using peripheral or central NPC channels to translocate into the INM? Two fundamentally distinct routes to reach the INM during interphase have been proposed for NETs: either through the peripheral NPC channels or through the central NPC channel aided by transport receptors (red). (Figure adapted from Antonin et al., 2011)

Although even possible that some NETs translocate through the peripheral and others through the central channels, the latter scenario would not account for the vast majority of NETs. This can be inferred from our data where FGs are enriched in large NET datasets arguing for the use of the peripheral channels through Nup35, while most of these NETs did not

contain a NLS (Zuleger et al., 2011a), a requirement claimed to be necessary for transport through the central channels (Meinema et al., 2011).

A thought to resolve the discrepancy of the central channel translocation paradigm is the possibility that the NLS-dependent binding of some NETs to transport receptors is occurring during mitosis and not in interphase. Several studies showing that some NETs are interacting with chromatin at the end of mitosis to enable the NE formation (Anderson and Hetzer, 2007; Anderson et al., 2009; Haraguchi et al., 2000) give space for that speculation. Thus these NETs might be “seeded” at the future INM with the help of bound transport receptors before the NE is formed (Figure 57). In this case size limitation, which plays a role during interphase, would be irrelevant.

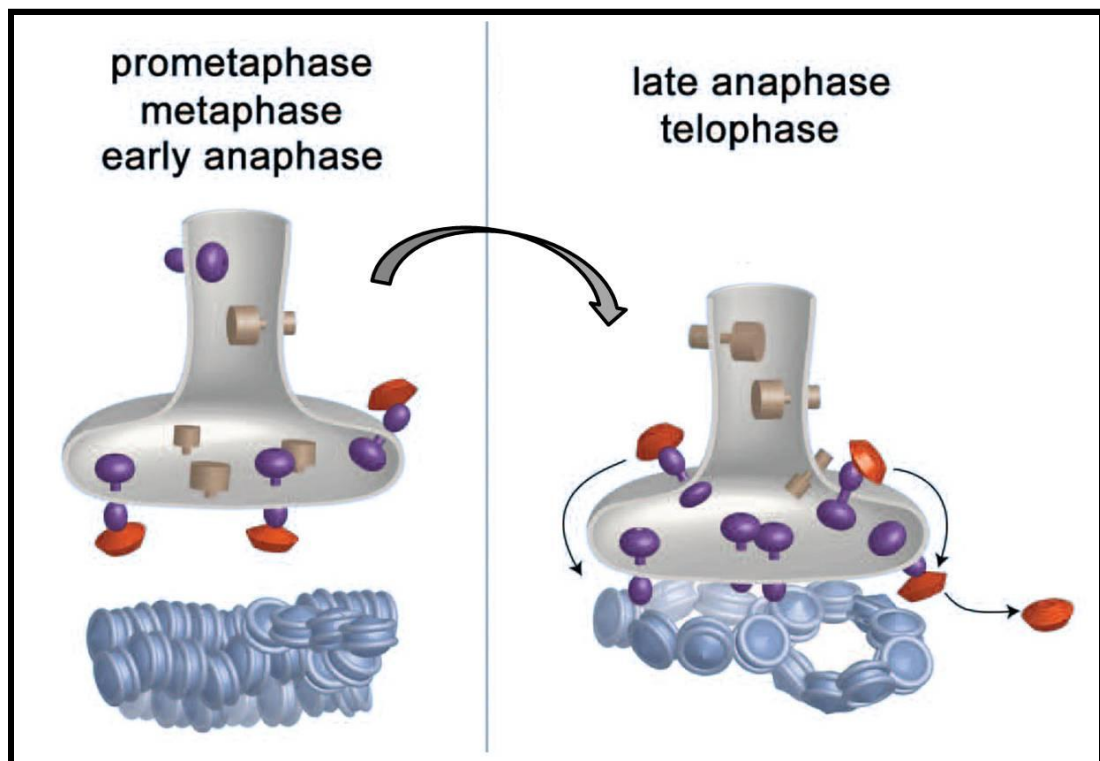


Figure 57. NETs that bind transport receptors could be “seeded” into the future INM during mitosis. Some NETs might be targeted to the future INM already during mitosis through binding to chromatin around which the NE is known to form. This process might involve interaction of transport receptors (red) with NETs. (Figure adapted from Antonin et al., 2011)

Clearly, future studies need to solve the dispute of whether the central or peripheral channels or even both are used simultaneously during interphase for NET INM targeting. The Veenhoff lab study implicated the use of the central channel by fusing both a central channel nucleoporin and a NET to protein fragments, which dimerize when the drug rapamycin is added. Doing this they were able to trap the NET construct at the NPC after adding the drug, assuming their NET is using the central channel for translocation (Meinema et al., 2011). However, it was not tested if trapping of the same NET could also be mediated in the peripheral channel by fusing one interaction fragment to one of the peripheral channel nucleoporins. If the NET is not trapped in the peripheral channels, this experiment would clearly demonstrate the specificity of the system and really prove the use of the central channels for at least some NETs. We are planning to do this experiment in future.

Also, the idea of potential NET targeting to the future INM during mitosis upon help of transport receptors needs to be pursued. The Blobel study that initially found the need of transport receptors for NET targeting (King et al., 2006) used temperature sensitive yeast strains to conditionally deplete the transport receptors. Upon receptor depletion NETs did not localize to the INM anymore but NET INM localization was restored upon subsequent expression of the receptors. Now repeating the same experiment, while having the cells blocked in interphase, would answer if the receptor-mediated targeting occurs in interphase or mitosis. If NET targeting is not restored upon subsequent receptor expression during the interphase block, we would know that receptor-mediated NET targeting occurs indeed during mitosis.

7.7 Tissue-specific NETs mediate chromosome repositioning

Tissue-specific 3-dimensional arrangements of chromosomes within the interphase nucleus are considered to be relevant but the function and consequence of this chromosome patterning remains largely unknown. Previous studies reported that some chromosomes reposition during differentiation (Galiova et al., 2004; Kim et al., 2004; Kuroda et al., 2004; Szczerbal et al., 2009) but the players that drive that repositioning remained obscure. Our findings provide an explanation for how tissue-specific chromosome positioning can be achieved and why this mechanism has not been discovered yet: the proteins that drive these cell type-specific chromosome arrangements are themselves tissue-specific.

Previously described NE-chromatin interactions involved ubiquitously expressed proteins [reviewed in (Mattout-Drubezki and Gruenbaum, 2003)]. These were mostly interactions with heterochromatin (Brown et al., 2008; Capelson et al., 2010; Kalverda et al., 2010; Makatsori et al., 2004; Pickersgill et al., 2006) or enzymes that add silencing marks (Somech et al., 2005). These interactions give a reason for why heterochromatin is located at the nuclear periphery but do not explain the tissue-specific patterns of chromosome positioning in relation to the nuclear periphery. Truncation mutants of lamin B1 have been shown to abolish peripheral localization of chromosome 18 (Malhas et al., 2007) but even this observation cannot explain the tissue-specific chromosome patterning since lamin B1 is also a widely expressed protein. Instead, lamin B1 might be required for the targeting of a tissue-specific NET that has a high affinity for chromosome 18. This hypothesis is supported by a recent study where the cardiomyopathy causing E161K mutation in lamin A promotes the release of chromosome 13 from the nuclear periphery while another mutation on lamin A, D596N, causing the same disease is not releasing chromosome 13 from the NE (Mewborn et al., 2010). This observation suggests that the chromosome tethering to the periphery in this case is likely to depend on other lamin-

interacting proteins like tissue-specific NETs. One such chromosome 13 tethering partner would not bind to the E161K lamin A mutant and therefore chromosome 13 is released from the NE. However, when lamin A is mutated in a different area then this partner is still able to bind to lamin and therefore chromosome 13 is maintained at the nuclear periphery.

Another study demonstrated that several other mutations in the *LMNA* gene caused a release of chromosome 13 and 18 from the nuclear periphery (Meaburn et al., 2007), but again, also lamin A is widely expressed in differentiated cells, thus a more tissue-specific binding partner of lamin A is likely to contribute to the release of these chromosomes from the NE. The idea of tissue-specific lamin binding partners is further supported by the fact that lamin mutations are not causing a chromosome repositioning in all cell types (Boyle et al., 2001; Meaburn et al., 2005). Future studies clearly need to answer the question of whether lamins are required for targeting of the novel tissue-specific NETs.

Even though we favour the hypothesis that tissue-specific NETs are the major drivers of tissue-specific chromosome arrangements it is actually also possible that A-type and B-type lamins can be drivers. Lamins are encoded by three different genes *LMNA*, *LMNB1* and *LMNB2*, all of which have several splice variants and the proportions of these proteins vary between cell-types (Broers et al., 1997). Also a study where different lamin sub-types were expressed in *Xenopus* oocytes revealed that lamin A assembles into a layer that is closer to the chromatin than the lamin B filament layer (Goldberg et al., 2008) implying a potential higher affinity of lamin A to chromatin proteins than lamin B. This scenario can be hypothesized as nobody has compared affinities of different lamins to same chromatin proteins. Thus the variety of lamin proteins, their proportions in each cell type and their potentially different affinities to chromatin proteins create a good combinatorial basis to achieve tissue-specific patterns of chromosome organization.

In addition, the combinatorial basis of lamins is also likely to impact differential targeting of different tissue-specific NETs. Distinct lamins could have different affinities to specific NETs, which in turn have preferences for particular chromosomes. This would result in a highly regulated cell type-specific 3D chromosome arrangement. The sum of all these differential lamin and NET interactions could really be the reason for switching of threshold interactions with chromosomes and thus resulting in tether of a particular chromosome and not another.

7.8 Direct versus indirect NET-chromosome interaction

We show in this study that chromosome repositioning NETs can co-precipitate a chromatin fraction but at this point we cannot distinguish whether NETs tether chromosomes *via* direct interactions to DNA or indirectly by binding to proteins which associate with DNA. It is clear that many NETs can interact with DNA directly (Cai et al., 2001; Caputo et al., 2006), however, the vast majority of identified NET interactions involved chromatin or chromatin binding proteins [reviewed in (Zuleger et al., 2011b)]. Thus we propose that rather than binding to DNA directly, the chromosome repositioning NETs are binding to tissue-specific chromatin binders like transcription factors or transcriptional repressors, proteins that are tightly bound to particular chromosome sequences. This hypothesis is sustained by the previous findings that NETs can indeed bind transcriptional regulators (Haraguchi et al., 2004; Holaska et al., 2003; Holaska et al., 2006).

This working model would outperform a model where for example general repetitive DNA sequences are directly bound by a NET, because it would prove more flexible as explained in the following example: If our tissue-specific NETs were to reposition chromosomes to the NE by direct interaction with DNA sequences, then the affected chromosome would be at the NE anytime when the NET is present. However, when the NET is tethering a

chromosome only when a specific regulator is present at a particular point in development, such as a kinase or phosphatase, which would modify the NET to either tether or release a particular chromosome or a NET-interacting transcriptional regulator, which is tightly bound to regions of the respective chromosome, then the NET could be present at any time and would tether the chromosome only when the transcriptional regulator is bound to the chromosome sequences. In fact, this model would also work for ubiquitously expressed NETs, which have been shown to bind chromatin [reviewed in (Zuleger et al., 2011b)] as the specificity for the chromosome/chromosome region would be provided by the tissue-specific DNA-binding protein (Figure 58, A). Though we favour the hypothesis mentioned above we cannot exclude a direct interaction of the chromosome-repositioning NETs found in this study and the respective chromosome. This possibility would be legitimate due to the fact that the NETs are tissue-specific. One could then imagine that a particular chromosome is in the nuclear interior but repositions to the NE only once a tissue-specific NET with a high affinity for this chromosome is expressed, for example during differentiation (Figure 58, B). A third possibility would involve a chromosome repositioning to the nuclear periphery by an interaction of a tissue-specific NET with a tissue-specific DNA binding protein, however in this scenario both proteins must be present in the cell at the same time and cannot be sequentially expressed (Figure 58, C).

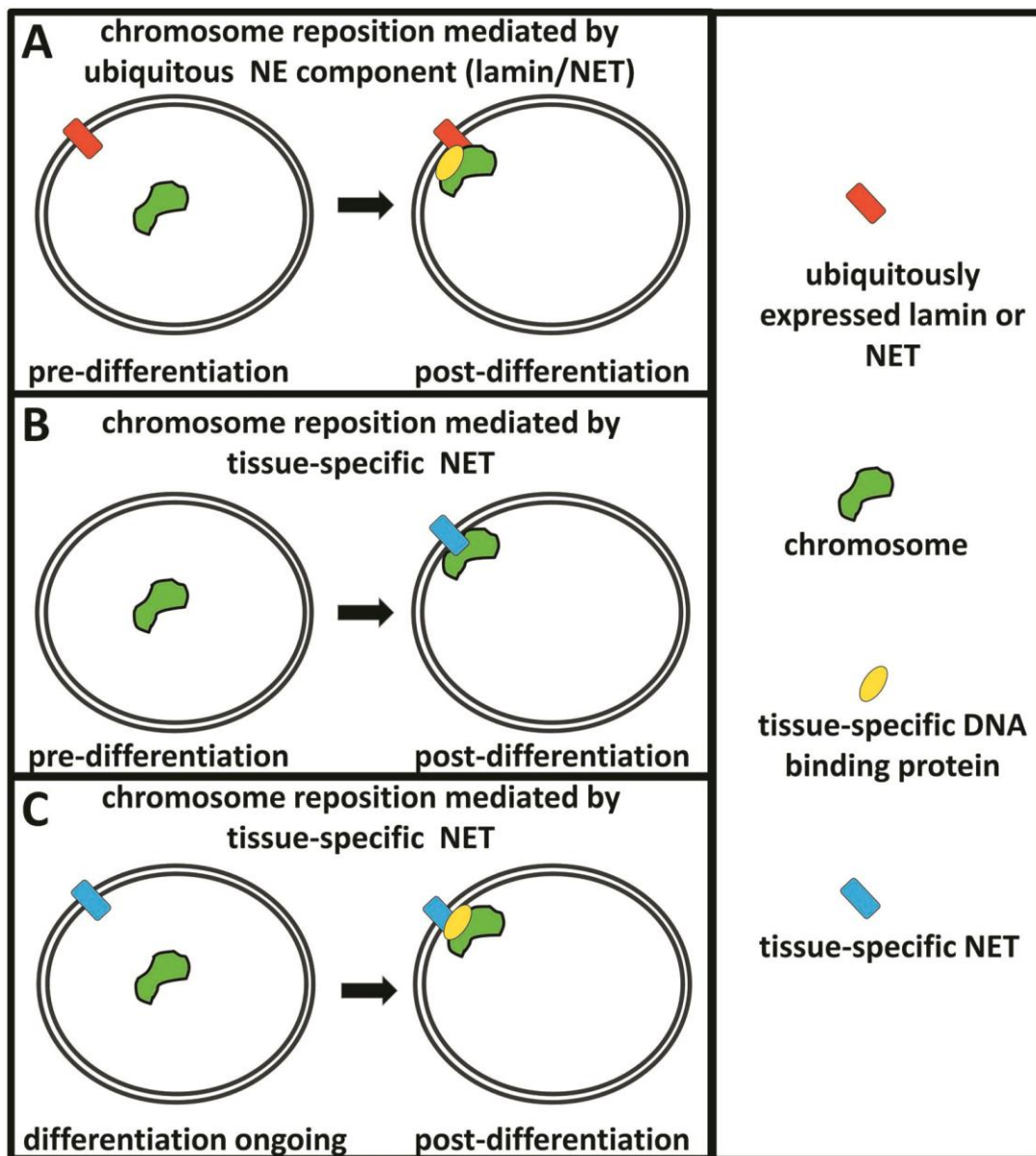


Figure 58. Hypothetical models of chromosome repositioning. (A) In the undifferentiated cell lamins and non-tissue-specific NETs are expressed and the chromosome resides in the nuclear interior (left). Upon differentiation a tissue-specific chromosome binding protein is expressed for which non-tissue-specific NETs/lamins have a high affinity for and thus the chromosome is repositioned towards the nuclear periphery (right). (B) In the undifferentiated cell the chromosome resides in the nuclear interior (left) but upon differentiation a tissue-specific NET is expressed that has a high affinity to the chromosome, thus the chromosome is tethered to the NE (right). (C) The cell is committed to differentiation and tissue-specific NETs are already expressed and the chromosome resides in the nuclear interior (left). With progressing differentiation a tissue-specific chromosome binding protein is expressed, which the tissue-specific NET has a high affinity for. This causes the chromosome to reposition to the nuclear edge (right).

Though these direct or indirect NET-chromosome affinity interactions are likely to be weaker than that of the lacO system, having many chromosome-NET tethers distributed at different points the chromosome would likely generate a more powerful tether than having them concentrated on one point of the chromosome like in the lacO system, which was previously shown to be able to recruit chromosomes to the NE (Finlan et al., 2008). Both models of direct and indirect NET interaction are consistent with my finding that in liver HepG2 cells chromosome 5 is partially lost from the nuclear periphery upon depletion of liver-specific NETs 45 and 47. Since the effect is not absolute it is likely that there are other additional NETs that contribute to the tether of chromosome 5 at the nuclear periphery and subsequently contribute to the generation of a specific chromosome positioning pattern (Figure 59).

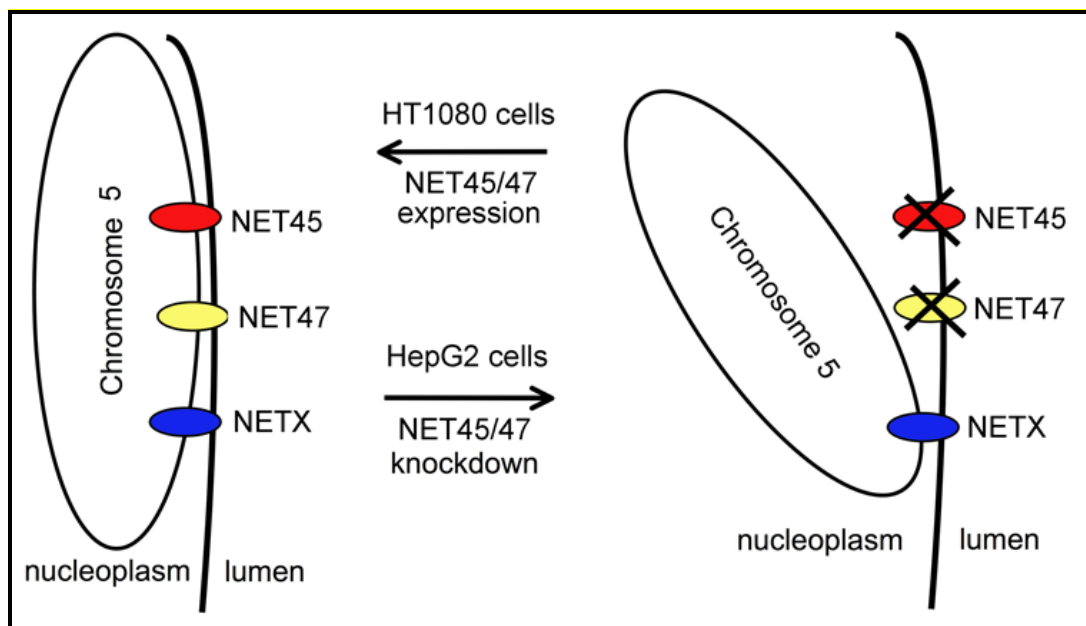


Figure 59. Simple model of chromosome position regulation by NETs. Upon expression of NETs that are tethering chromosome 5 the localization of this chromosome is secured at the nuclear periphery (left side). When the chromosome 5 tethering proteins NET45 and NET47 are depleted by siRNA, for example, chromosome 5 is released more into the nuclear interior but not completely as some yet unidentified proteins might still capture parts of this chromosome at the NE (right side). Upon renewed up-regulation/overexpression of NET45 and NET47 chromosome 5 is tethered to the nuclear periphery again.

Independent of whether these NET-chromosome interactions are direct or indirect another aspect that could drive specificity is epigenetics. This possibility gets strong support from studies that have found many NETs to interact with epigenetic marks or enzymes that can modify chromatin (Chi et al., 2007; Guarda et al., 2009; Makatsori et al., 2004; Somech et al., 2005) thus a NETs preference for a chromosome could not only be determined by a particular sequence but also by a specific epigenetic code, although it should be noted that there is no evidence for a large disparity in epigenetic modifications of chromosomes to date. But to test this idea one could investigate the chromosome regions that were found to be temporarily at the NE during differentiation of nerve cells (Peric-Hupkes et al., 2010) and test if their interaction with the NE correlates with a particular epigenetic state.

7.9 Does chromosome repositioning occur in mitosis or interphase?

In all of the studies where a chromosome was artificially tethered to the nuclear periphery by a high affinity mechanism (Finlan et al., 2008; Kumaran and Spector, 2008; Reddy et al., 2008), the chromosome tethering required the cells to go through a cell division. And although I have not tested in this study if NET-mediated chromosome repositioning actually requires mitosis, I do favour the hypothesis where mitosis precedes large-scale chromosome reorganization for the following reasons. The nucleus of the interphase cell is very crowded and chromosomes are comparatively large structures and trying to move a chromosome all the way from the interior to the periphery, a possible distance of several microns, would likely prove extremely difficult. In contrast, during mitosis the chromosomes are compact and the NE has broken down into vesicles²¹. These vesicles contain the

²¹ To date it is not entirely clear which form the NE takes after breaking down in mitosis. Some studies suggest it breaks down into vesicles (Buch et al., 2009; Hetzer et al., 2001; Salpingidou et al., 2008), others claim that it is streaming into the ER (Anderson and Hetzer, 2007; Ellenberg et al., 1997; Yang

chromosome repositioning NETs and could therefore bind to chromosomes for which the NETs have preference for (Figure 60, A). From the end of mitosis into interphase, when the NE is reformed, the NETs would have positioned the particular chromosome at the nuclear periphery (Figure 60, B-D). Evidence for this hypothesis derives from earlier mentioned observations where distinct emerin and LBR vesicles bind to different portions of chromosomes during mitosis (Haraguchi et al., 2000). Additional support for this hypothesis derives from our laboratory where the chromosome repositioning effect in 3T3-L1 cells was much smaller two days after the cells were transfected with chromosome repositioning NETs compared to the repositioning effect three days post transfection (observations were made in our laboratory by Eric Schirmer and Gerlinde Otti, unpublished). The rationale would be that cells would have to go through one round of mitosis so that the transfected NET DNA could reach the nucleoplasm²². After about 12 hours post transfection NET material is expressed. At this point, approximately 2d post transfection, the repositioning effects could already occur due to the presence of the NET but they did not. The strong chromosome repositioning effects were only observed after additional 24 hours suggesting that an additional round of mitosis was required to initiate the chromosome repositioning from the interior to the nuclear periphery.

et al., 1997). Here I will assume that the NE breaks down into vesicles, although the interaction with the chromosome would be virtually the same for both NE breakdown possibilities

²² *cells were transfected with a reagent that does not deliver plasmid DNA immediately into the nucleus*

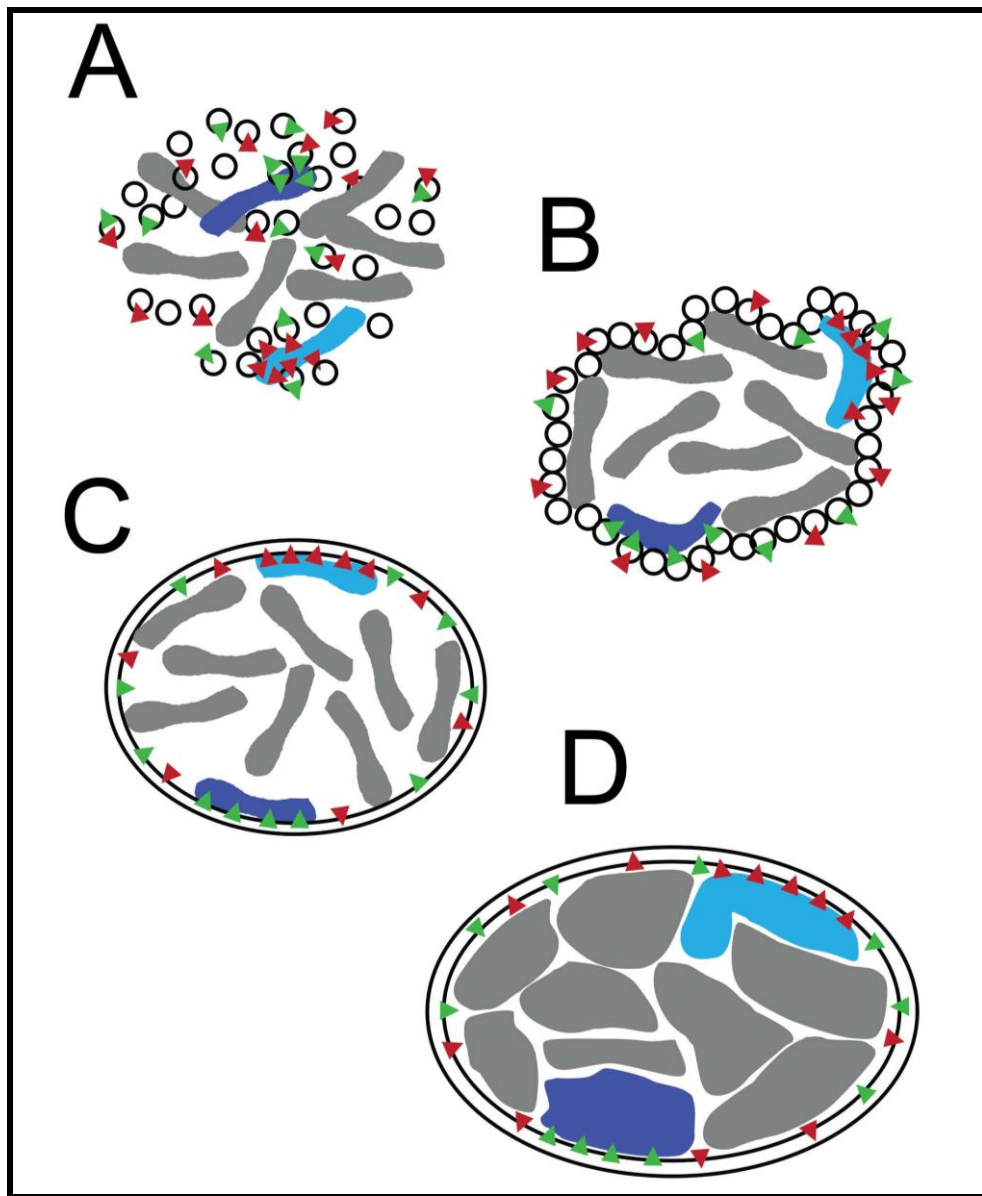


Figure 60. Speculative affinity mechanism to establish spatial chromosome organizational patterns. (A) The NE breaks down into ER/NE vesicles in mitosis. Distinct vesicles contain specific NE proteins (colored triangles). NETs of some vesicles bind to regions of specific condensed chromosomes. (B) The NE starts to reform from vesicles at the end of mitosis with some specific chromosomes still being attached to particular vesicles. (C) After the NE formation some chromosomes are trapped at the NE due to specific NETs that have a high affinity for these particular chromosomes. The chromosomes are still mainly condensed. (D) In interphase the chromosomes decondense completely and occupy distinct territories within the nucleus. (Figure adapted from Zuleger et al., 2011b)

Though the observations mentioned above indicate a requirement for mitosis there is a recent report that large-scale radial chromosome repositioning can occur in non-dividing cells (Mehta et al., 2010). Thus it is not entirely clear if large-scale radial chromosome arrangements are established in mitosis or interphase or even both and there is a need for future studies to clarify this.

7.10 Changes in gene activity upon chromosome and gene repositioning

If one chromosome is tethered to the nuclear periphery another chromosome must be released from the periphery to make space for the other. This can be inferred from our data where the DAPI signal in cells where chromosome tethering NETs were expressed did not alter from control cells meaning that chromosome repositioning is not a side effect of general distribution of chromatin towards the nuclear periphery but rather an equal redistribution of chromosomes. Therefore, apart from changes in gene expression that involve silencing through direct nuclear periphery association of the chromosomes I have tested, there are also likely to be repression of genes from other non-tested chromosomes that are tethered by the NETs and also up-regulation of genes from release of other chromosomes from the periphery and secondary changes due to some of the genes changing being transcriptional regulators themselves. And this is exactly what we encountered when analyzing the gene expression profiles of the NET cell lines, as we noticed up- and down-regulated genes not only on chromosomes we tested the position for.

While we noticed these gene changes in cells overexpressing chromosome-tethering NETs, it is reasonable to assume that depletion of these NETs would result in changes as considerable. In fact many genes are misregulated in laminopathies, diseases that arise from mutations in NE proteins, particularly lamins (Lai et al., 2010). Thus our results could also

explain this gene misregulation in laminopathies as targeting of many tissue-specific chromosome-tethering NETs is likely to depend on lamin binding, which would be possibly abolished when the lamins are mutated as already shown for other NETs (Ellis et al., 1998; Fairley et al., 1999; Reichart et al., 2004; Wheeler et al., 2007). This gene misregulation could thus be a consequence of a NET not tethering particular chromosomes when needed.

Most genes tested previously have been found to reposition from the nuclear periphery into the nuclear interior upon their activation (Hewitt et al., 2004; Kosak et al., 2002; Meister et al., 2010; Ragooczy et al., 2006; Williams et al., 2006; Yao et al., 2011). This type of repositioning may activate genes by moving them away from transcriptionally silent regions of heterochromatin, large proportions of which are lining the nuclear periphery of most differentiated cells. There is however significant variation in the amount of peripheral heterochromatin between different cell types (Milner, 1969) and therefore the gene positioning effect is also likely to vary from one cell type to another. It is therefore not surprising that even though most of the genes are activated upon their reposition from the NE into the nuclear interior others are activated at the nuclear periphery. For example, the *PLP* gene is activated at the NE during oligodendrocyte differentiation (Nielsen et al., 2002) and in other systems gene activation at the nuclear periphery was observed (Hewitt et al., 2004; Johnson et al., 2000; Park and De Boni, 1998).

In our study, when looking at all genes changed in the NET-overexpressing cell lines, we found a preference for silencing rather than activation. This is consistent with the general assumption that the NE is a preferentially silenced environment. But yet we have not determined whether the affected genes have actually altered their positions in respect to the nuclear periphery. Doing this, we will be able to correlate whether silencing really correlates with peripheral localization of the gene or, like in the few studies mentioned above, no repositioning of the genes occurs even upon change in its transcriptional activity. More importantly, determination of the potential repositioning of affected genes will enable us to tell whether the

summation of genes interacting with the nuclear periphery causes the according chromosome to move to the NE or if the chromosome is specifically tethered to the periphery and the according genes are just repositioning as a side-effect of it. In fact we anticipate that staining for both the chromosome that has been repositioned to the periphery and the affected genes that are located on this chromosome will be able to discriminate between the two scenarios mentioned above. For example, when all or at least most of the affected genes within the chromosome co-localize with the nuclear periphery, we can deduce that indeed these genes are the tether points and the chromosome relocates as a side effect of it. On the contrary if most genes are not co-localizing with the NE, but rather are distributed throughout the peripheral chromosome, then it follows that the affected genes are not the actual tether points and were repositioned along with the chromosome.

In most of the published studies mentioned above the position of the gene-containing chromosome was not determined to answer if the gene positioning corresponded to the position of the chromosome (i.e. is the chromosome changing its radial position together with the gene located on this chromosome or is the gene changing its radial position without affecting the radial position of the chromosome). A few recent studies addressed this question, however, and found that the gene moved within or even beyond the chromosome territory while the chromosome itself did not alter its position with respect to the nuclear periphery (Morey et al., 2008; Szczerbal et al., 2009). Nevertheless, in one of these studies that investigated the chromosome repositioning during adipogenesis, the *FABP4* gene moved from the periphery to the nuclear interior together with the corresponding chromosome (Szczerbal et al., 2009). Though the total of these observations is not giving a clear answer of whether individual gene repositioning causes the repositioning of the chromosome or *vice versa*, it is very likely that the summation of NE interactions with many individual gene sequences is forming a threshold for whether a chromosome is moving to the periphery or

not. More gene and chromosome data sampling will be required in future to give a clear answer to this interesting question.

7.11 Functional consequences of NET-mediated gene repositioning – tissue-specific genes are regulated

Our finding that the transcriptional profile of the liver-specific NET47 partly overlapped with that of a hepatic differentiation system supports the hypothesis that NET-mediated chromosome repositioning helps to establish tissue-specific gene expression patterns. This is supported by the fact that heart-specific NET39 had little overlap with the hepatic system and NET29, which is expressed in both heart and liver overlapped with the hepatic system to a level that was between that of NET47 and NET39. Even though we had a notable induction of tissue-specific genes upon ectopic expression of tissue-specific chromosome-tethering NETs in the HT1080 cell line one could imagine that the effect would be even greater when we used cells that are committed along a particular differentiation pathway, which the NETs are specific for. These cells would provide the tissue-specific NET interaction partners, which are not expressed in HT1080 cells. We are currently testing this by ectopically expressing tissue-specific NETs in differentiation systems and will investigate if more tissue-specific genes can be induced in these cells. I anticipate that in addition to getting better transcriptional correlations with differentiation paradigms these cells are also likely to provide the means of better separating the changes in differentiation from the positioning effects (for example by depleting the NET during the differentiation of the cell line).

The hypothesis that NET-mediated chromosome positioning could help to optimize the gene expression of a tissue that the NET is specific for gains further support by our finding that upon depletion of liver-specific NET45 and NET47 in the liver HepG2 cell line many liver-specific genes were down-regulated. This possibility suggests an additional mechanism to

optimize regulation of differentiation to the already known main drivers of differentiation like transcription factors.

Our observation that soluble fragments of chromosome repositioning NETs do not tether chromosomes to the periphery like their full-length membrane integrated counterparts and the fact that gene expression profiles of the two do not match each other suggest also that tethering of the chromosome to the NE is important to induce gene activity changes and also excludes the possibility that NETs cause chromosome repositioning indirectly through signalling cascades.

Even more important than the finding above, are our results of the comparison between NET-specific (chromosome 5 tethered by NET expression) and non-NET-specific (chromosome 5 tethered by lacO/lacI interaction) chromosome repositioning. These results indicate that bringing the chromosome to the nuclear periphery *per se* is not enough to induce a particular gene expression profile meaning that not only the positioning effect itself but also the specific mechanism by which a chromosome is positioned to the nuclear periphery is playing a crucial role.

Though the plethora of molecular determinants for gene regulation involving NETs is yet to be discovered, several possibilities can be proposed. Based on studies that found that NE components, including several widely expressed NETs, can sequester transcriptional regulators [reviewed in (Heessen and Fornerod, 2007)] one can imagine following working models: An active gene would be silenced when tethered to the nuclear periphery by a NET because a transcriptional repressor is sequestered at the NE (Figure 61, A left) or silencing would occur because the gene is tethered to the nuclear periphery and incorporated into the transcriptionally silent heterochromatin milieu at the NE (Figure 61, B). A third possibility would arise from the findings that widely expressed NETs can bind enzymes that can modify chromatin into a silent configuration (Guarda et al., 2009; Somech et al., 2005). The expression of a tissue-specific NET that has a high affinity to the gene would result in its tethering to the nuclear periphery where the

gene would be silenced by the activity of the enzymes that add silencing marks to the gene (Figure 61, C).

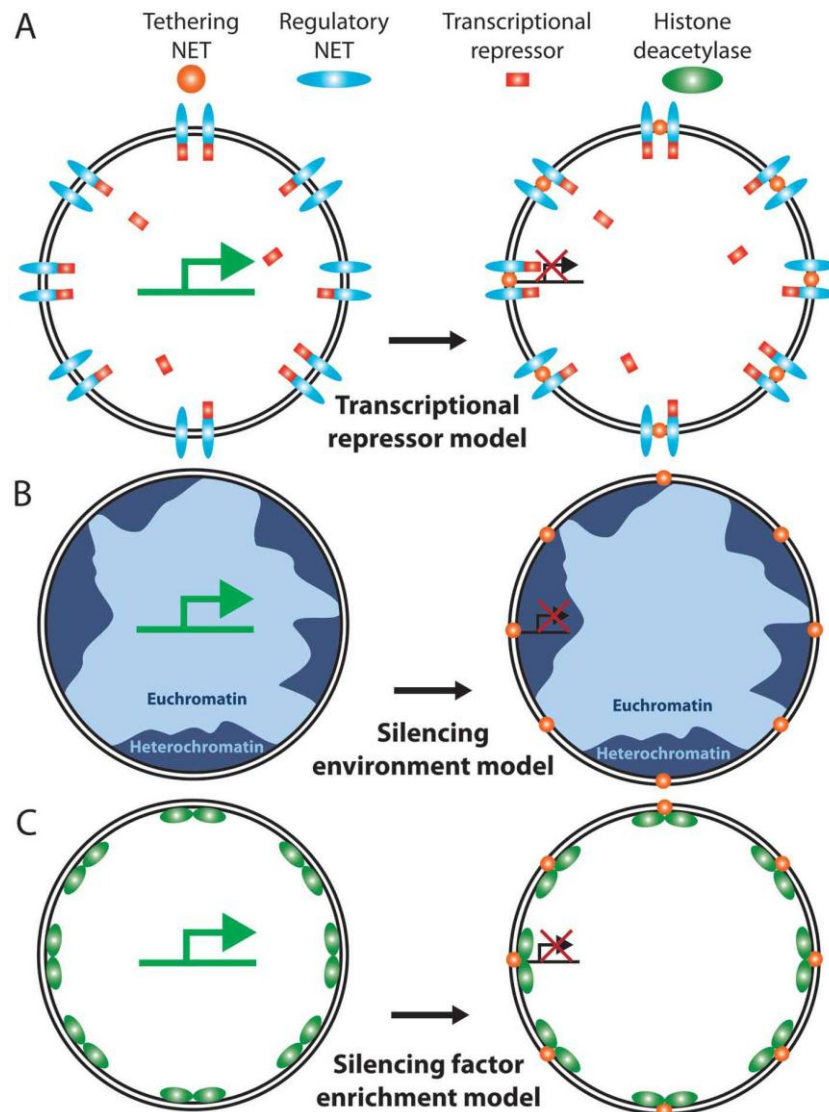


Figure 61. Possible mechanisms for gene regulation by the NE. (A) A widely expressed regulatory NET or lamin protein binds a transcriptional repressor to the nuclear periphery while a particular gene locus in the nuclear interior is transcriptionally active (left). Upon gradual expression of a tissue-specific NET with a high affinity for the gene, the locus moves to the NE where it is silenced due to the transcriptional repressor (right). (B) The gene is transcriptionally active in the interior (left) until a tissue-specific NET with a high affinity for this gene is expressed resulting in tethering of the gene to the nuclear periphery where it is silenced due to incorporation into heterochromatin (right). (C) The interior gene is transcriptionally active until a NET with a high affinity for it is expressed causing a repositioning of the gene to the NE where it is silenced due to chromatin silencing enzymes (i.e. histone deacetylase) trapped at the nuclear periphery. (Figure adapted from Zuleger et al., 2011b)

7.12 Final remarks

This work provides an advance in both the field of membrane protein targeting and the field of chromosome organization. Having found that several independent mechanisms co-exist for INM protein targeting, my work solves the inconsistencies of previous studies, which have reported distinct mechanisms but did not distinguish whether these are independent from one another or all part of a global and unifying mechanism. The discovery of the novel NET translocation mechanism (FG-facilitated mechanism) also gives rise to the anticipation that more additional mechanisms could be discovered in future. Once we discover all pathways we can systematically test the translocation of all NETs and determine which exact NET characteristics are determining which pathway to utilize.

As for the chromosome repositioning work, our finding that tissue-specific nuclear membrane proteins can change global chromatin organization and consequently impact gene expression supports the existence of a new layer of gene regulation, where gene activity is coupled to radial positioning of chromosomes. We do not argue that this regulatory layer dominates over other more traditional gene regulatory mechanisms, for example those mediated by transcription factors or epigenetics. Rather this repositioning-mediated gene regulatory mechanism is likely to fine-tune gene regulation mediated by epigenetics and transcription factors. Future studies will have to determine the exact mechanisms by which such NET-mediated nuclear organization changes occur. The fact that tissue-specific NETs promote the expression of tissue-specific genes is clearly asking for future studies to use manipulative differentiation models or even whole model organisms to gain the most complete picture of this fascinating regulation paradigm.

REFERENCES

- Abney, J.R., B. Cutler, M.L. Fillbach, D. Axelrod, and B.A. Scalettar. 1997. Chromatin dynamics in interphase nuclei and its implications for nuclear structure. *J Cell Biol.* 137:1459-1468.
- Alber, F., S. Dokudovskaya, L.M. Veenhoff, W. Zhang, J. Kipper, D. Devos, A. Suprpto, O. Karni-Schmidt, R. Williams, B.T. Chait, A. Sali, and M.P. Rout. 2007. The molecular architecture of the nuclear pore complex. *Nature.* 450:695-701.
- Anderson, D.J., and M.W. Hetzer. 2007. Nuclear envelope formation by chromatin-mediated reorganization of the endoplasmic reticulum. *Nat Cell Biol.* 9:1160-1166.
- Anderson, D.J., J.D. Vargas, J.P. Hsiao, and M.W. Hetzer. 2009. Recruitment of functionally distinct membrane proteins to chromatin mediates nuclear envelope formation in vivo. *J Cell Biol.* 186:183-191.
- Andrulis, E.D., A.M. Neiman, D.C. Zappulla, and R. Sternglanz. 1998. Perinuclear localization of chromatin facilitates transcriptional silencing. *Nature.* 394:592-595.
- Antonin, W., R. Ungricht, and U. Kutay. 2011. Traversing the NPC along the pore membrane: Targeting of membrane proteins to the INM. *Nucleus.* 2:87-91.
- Baricheva, E.A., M. Berrios, S.S. Bogachev, I.V. Borisevich, E.R. Lapik, I.V. Sharakhov, N. Stuurman, and P.A. Fisher. 1996. DNA from *Drosophila melanogaster* beta-heterochromatin binds specifically to nuclear lamins in vitro and the nuclear envelope in situ. *Gene.* 171:171-176.
- Bolzer, A., G. Kreth, I. Solovei, D. Koehler, K. Saracoglu, C. Fauth, S. Muller, R. Eils, C. Cremer, M.R. Speicher, and T. Cremer. 2005. Three-dimensional maps of all chromosomes in human male fibroblast nuclei and prometaphase rosettes. *PLoS Biol.* 3:e157.
- Bornfleth, H., P. Edelmann, D. Zink, T. Cremer, and C. Cremer. 1999. Quantitative motion analysis of subchromosomal foci in living cells using four-dimensional microscopy. *Biophys J.* 77:2871-2886.
- Boveri, T. 1909. Die blastomerenkerne von *Ascaris megaloccephala* und die Theorie der Chromosomen-individualitat. *Arch Zellforsch.* 3:181-268.
- Boyle, S., S. Gilchrist, J.M. Bridger, N.L. Mahy, J.A. Ellis, and W.A. Bickmore. 2001. The spatial organization of human chromosomes within the nuclei of normal and emerin-mutant cells. *Hum Mol Genet.* 10:211-219.
- Braunagel, S.C., S.T. Williamson, Q. Ding, X. Wu, and M.D. Summers. 2007. Early sorting of inner nuclear membrane proteins is conserved. *Proc Natl Acad Sci U S A.* 104:9307-9312.
- Broers, J.L., B.M. Machiels, H.J. Kuijpers, F. Smedts, R. van den Kieboom, Y. Raymond, and F.C. Ramaekers. 1997. A- and B-type lamins are differentially expressed in normal human tissues. *Histochem Cell Biol.* 107:505-517.

- Brown, C.R., C.J. Kennedy, V.A. Delmar, D.J. Forbes, and P.A. Silver. 2008. Global histone acetylation induces functional genomic reorganization at mammalian nuclear pore complexes. *Genes Dev.* 22:627-639.
- Buch, C., R. Lindberg, R. Figueroa, S. Gudise, E. Onischenko, and E. Hallberg. 2009. An integral protein of the inner nuclear membrane localizes to the mitotic spindle in mammalian cells. *J Cell Sci.* 122:2100-2107.
- Cai, M., Y. Huang, R. Ghirlando, K.L. Wilson, R. Craigie, and G.M. Clore. 2001. Solution structure of the constant region of nuclear envelope protein LAP2 reveals two LEM-domain structures: one binds BAF and the other binds DNA. *EMBO J.* 20:4399-4407.
- Callan, H.G., and S.G. Tomlin. 1950. Experimental studies on amphibian oocyte nuclei. I. Investigation of the structure of the nuclear membrane by means of the electron microscope. *Proc R Soc Lond. Series B, Containing Papers of a Biological Character.* 137:367-378.
- Capelson, M., Y. Liang, R. Schulte, W. Mair, U. Wagner, and M.W. Hetzer. 2010. Chromatin-bound nuclear pore components regulate gene expression in higher eukaryotes. *Cell.* 140:372-383.
- Caputo, S., J. Couprie, I. Duband-Goulet, E. Konde, F. Lin, S. Braud, M. Gondry, B. Gilquin, H.J. Worman, and S. Zinn-Justin. 2006. The carboxyl-terminal nucleoplasmic region of MAN1 exhibits a DNA binding winged helix domain. *J Biol Chem.* 281:18208-18215.
- Chambeyron, S., and W.A. Bickmore. 2004. Chromatin decondensation and nuclear reorganization of the *HoxB* locus upon induction of transcription. *Genes Dev.* 18:1119-1130.
- Chambeyron, S., N.R. Da Silva, K.A. Lawson, and W.A. Bickmore. 2005. Nuclear reorganisation of the *Hoxb* complex during mouse embryonic development. *Development.* 132:2215-2223.
- Chi, Y.H., K. Haller, J.M. Peloponese, Jr., and K.T. Jeang. 2007. Histone acetyltransferase hALP and nuclear membrane protein hsSUN1 function in de-condensation of mitotic chromosomes. *J Biol Chem.* 282:27447-27458.
- Chiacchia, K.B., and K. Drickamer. 1984. Direct evidence for the transmembrane orientation of the hepatic glycoprotein receptors. *J Biol Chem.* 259:15440-15446.
- Chuang, C.H., A.E. Carpenter, B. Fuchsova, T. Johnson, P. de Lanerolle, and A.S. Belmont. 2006. Long-range directional movement of an interphase chromosome site. *Curr Biol.* 16:825-831.
- Chubb, J.R., S. Boyle, P. Perry, and W.A. Bickmore. 2002. Chromatin motion is constrained by association with nuclear compartments in human cells. *Curr Biol.* 12:439-445.
- Cremer, M., F. Grasser, C. Lanctot, S. Muller, M. Neusser, R. Zinner, I. Solovei, and T. Cremer. 2008. Multicolor 3D fluorescence in situ hybridization for imaging interphase chromosomes. *Methods Mol Biol.* 463:205-239.
- Cremer, T., and C. Cremer. 2001. Chromosome territories, nuclear architecture and gene regulation in mammalian cells. *Nat Rev Genet.* 2:292-301.

- Crisp M, Liu Q, Roux K, Rattner JB, Shanahan C, Burke B, Stahl PD, Hodzic D. 2006. Coupling of the nucleus and cytoplasm: role of the LINC complex. *J Cell Biol.* 172(1):41-53.
- Croft, J.A., J.M. Bridger, S. Boyle, P. Perry, P. Teague, and W.A. Bickmore. 1999. Differences in the localization and morphology of chromosomes in the human nucleus. *J Cell Biol.* 145:1119-1131.
- Cvackova, Z., M. Masata, D. Stanek, H. Fidlerova, and I. Raska. 2009. Chromatin position in human HepG2 cells: although being non-random, significantly changed in daughter cells. *J Struct Biol.* 165:107-117.
- D'Angelo, M.A., D.J. Anderson, E. Richard, and M.W. Hetzer. 2006. Nuclear pores form de novo from both sides of the nuclear envelope. *Science.* 312:440-443.
- D'Angelo, M.A., and M.W. Hetzer. 2006. The role of the nuclear envelope in cellular organization. *Cell Mol Life Sci.* 63:316-332.
- D'Angelo, M.A., and M.W. Hetzer. 2008. Structure, dynamics and function of nuclear pore complexes. *Trends Cell Biol.*
- Deng, M., and M. Hochstrasser. 2006. Spatially regulated ubiquitin ligation by an ER/nuclear membrane ligase. *Nature.* 443:827-831.
- Dreger, M., L. Bengtsson, T. Schoneberg, H. Otto, and F. Hucho. 2001. Nuclear envelope proteomics: novel integral membrane proteins of the inner nuclear membrane. *Proc Natl Acad Sci U S A.* 98:11943-11948.
- Dwyer, N., and G. Blobel. 1976. A modified procedure for the isolation of a pore complex-lamina fraction from rat liver nuclei. *J Cell Biol.* 70:581-591.
- Edelmann, P., H. Bornfleth, D. Zink, T. Cremer, and C. Cremer. 2001. Morphology and dynamics of chromosome territories in living cells. *Biochim Biophys Acta.* 1551:M29-39.
- Ellenberg, J., E.D. Siggia, J.E. Moreira, C.L. Smith, J.F. Presley, H.J. Worman, and J. Lippincott-Schwartz. 1997. Nuclear membrane dynamics and reassembly in living cells: targeting of an inner nuclear membrane protein in interphase and mitosis. *J Cell Biol.* 138:1193-1206.
- Ellis, J.A., M. Craxton, J.R. Yates, and J. Kendrick-Jones. 1998. Aberrant intracellular targeting and cell cycle-dependent phosphorylation of emerin contribute to the Emery-Dreifuss muscular dystrophy phenotype. *J Cell Sci.* 111 (Pt 6):781-792.
- Essers, J., W.A. van Cappellen, A.F. Theil, E. van Drunen, N.G. Jaspers, J.H. Hoeijmakers, C. Wyman, W. Vermeulen, and R. Kanaar. 2005. Dynamics of relative chromosome position during the cell cycle. *Mol Biol Cell.* 16:769-775.
- Fairley, E.A., J. Kendrick-Jones, and J.A. Ellis. 1999. The Emery-Dreifuss muscular dystrophy phenotype arises from aberrant targeting and binding of emerin at the inner nuclear membrane. *J Cell Sci.* 112:2571-2582.
- Finlan, L.E., D. Sproul, I. Thomson, S. Boyle, E. Kerr, P. Perry, B. Ylstra, J.R. Chubb, and W.A. Bickmore. 2008. Recruitment to the nuclear periphery can alter expression of genes in human cells. *PLoS Genet.* 4:e1000039.
- Franke, W.W., U. Scheer, G. Krohne, and E.D. Jarasch. 1981. The nuclear envelope and the architecture of the nuclear periphery. *J Cell Biol.* 91:39s-50s.

- Fry, D.J. 1976. *The nuclear envelope in mammalian cells*. In *Mammalian Cell Membranes*. Vol. 2. G.A. Jameson and D.M. Robinson, editors. Butterworth, Woburn, Mass. 197-265.
- Furukawa, K. 1999. LAP2 binding protein 1 (L2BP1/BAF) is a candidate mediator of LAP2- chromatin interaction. *J Cell Sci*. 112:2485-2492.
- Furukawa, K., C.E. Fritze, and L. Gerace. 1998. The major nuclear envelope targeting domain of LAP2 coincides with its lamin binding region but is distinct from its chromatin interaction domain. *J Biol Chem*. 273:4213-4219.
- Galiova, G., E. Bartova, and S. Kozubek. 2004. Nuclear topography of beta-like globin gene cluster in IL-3-stimulated human leukemic K-562 cells. *Blood Cells Mol Dis*. 33:4-14.
- Gerace, L., and B. Burke. 1988. Functional organization of the nuclear envelope. *Annu Rev Cell Biol*. 4:335-374.
- Gerlich, D., J. Beaudouin, B. Kalbfuss, N. Daigle, R. Eils, and J. Ellenberg. 2003. Global chromosome positions are transmitted through mitosis in mammalian cells. *Cell*. 112:751-764.
- Goldberg, M., A. Harel, M. Brandeis, T. Rechsteiner, T.J. Richmond, A.M. Weiss, and Y. Gruenbaum. 1999. The tail domain of lamin Dm0 binds histones H2A and H2B. *Proc Natl Acad Sci U S A*. 96:2852-2857.
- Goldberg, M.W., I. Huttenlauch, C.J. Hutchison, and R. Stick. 2008. Filaments made from A- and B-type lamins differ in structure and organization. *J Cell Sci*. 121:215-225.
- Gorlich, D., and U. Kutay. 1999. Transport between the cell nucleus and the cytoplasm. *Annu Rev Cell Dev Biol*. 15:607-660.
- Guarda, A., F. Bolognese, I.M. Bonapace, and G. Badaracco. 2009. Interaction between the inner nuclear membrane lamin B receptor and the heterochromatic methyl binding protein, MeCP2. *Exp Cell Res*. 315:1895-1903.
- Gunawardena, S., and M.C. Rykowski. 2000. Direct evidence for interphase chromosome movement during the mid-blastula transition in *Drosophila*. *Curr Biol*. 10:285-288.
- Haraguchi, T., J.M. Holaska, M. Yamane, T. Koujin, N. Hashiguchi, C. Mori, K.L. Wilson, and Y. Hiraoka. 2004. Emerin binding to Btf, a death-promoting transcriptional repressor, is disrupted by a missense mutation that causes Emery-Dreifuss muscular dystrophy. *Eur J Biochem*. 271:1035-1045.
- Haraguchi, T., T. Koujin, T. Hayakawa, T. Kaneda, C. Tsutsumi, N. Imamoto, C. Akazawa, J. Sukegawa, Y. Yoneda, and Y. Hiraoka. 2000. Live fluorescence imaging reveals early recruitment of emerin, LBR, RanBP2, and Nup153 to reforming functional nuclear envelopes. *J Cell Sci*. 113:779-794.
- Hawryluk-Gara, L.A., E.K. Shibuya, and R.W. Wozniak. 2005. Vertebrate Nup53 interacts with the nuclear lamina and is required for the assembly of a Nup93-containing complex. *Mol Biol Cell*. 16:2382-2394.
- Heessen, S., and M. Fornerod. 2007. The inner nuclear envelope as a transcription factor resting place. *EMBO Reports*. 8:914-919.

- Hetzer, M., H.H. Meyer, T.C. Walther, D. Bilbao-Cortes, G. Warren, and I.W. Mattaj. 2001. Distinct AAA-ATPase p97 complexes function in discrete steps of nuclear assembly.[see comment]. *Nat Cell Biol.* 3:1086-1091.
- Hewitt, S.L., F.A. High, S.L. Reiner, A.G. Fisher, and M. Merckenschlager. 2004. Nuclear repositioning marks the selective exclusion of lineage-inappropriate transcription factor loci during T helper cell differentiation. *Eur J Immunol.* 34:3604-3613.
- Hinshaw, J.E., B.O. Carragher, and R.A. Milligan. 1992. Architecture and design of the nuclear pore complex. *Cell.* 69:1133-1141.
- Hoger, T.H., G. Krohne, and J.A. Kleinschmidt. 1991. Interaction of *Xenopus* lamins A and LII with chromatin in vitro mediated by a sequence element in the carboxyterminal domain. *Exp Cell Res.* 197:280-289.
- Holaska, J.M., K. Lee, A.K. Kowalski, and K.L. Wilson. 2003. Transcriptional repressor germ cell-less (GCL) and barrier to autointegration factor (BAF) compete for binding to emerin in vitro. *J Biol Chem.* 278:6969-6975.
- Holaska, J.M., S. Rais-Bahrami, and K.L. Wilson. 2006. Lmo7 is an emerin-binding protein that regulates the transcription of emerin and many other muscle-relevant genes. *Hum Mol Genet.* 15:3459-3472.
- Hubner, M.R., and D.L. Spector. 2010. Chromatin dynamics. *Annu Rev Biophys.* 39:471-489.
- Jackson, D.A., A.B. Hassan, R.J. Errington, and P.R. Cook. 1993. Visualization of focal sites of transcription within human nuclei. *EMBO J.* 12:1059-1065.
- Johnson, C., D. Primorac, M. McKinstry, J. McNeil, D. Rowe, and J.B. Lawrence. 2000. Tracking COL1A1 RNA in osteogenesis imperfecta. splice-defective transcripts initiate transport from the gene but are retained within the SC35 domain. *J Cell Biol.* 150:417-432.
- Kalverda, B., H. Pickersgill, V.V. Shloma, and M. Fornerod. 2010. Nucleoporins directly stimulate expression of developmental and cell-cycle genes inside the nucleoplasm. *Cell.* 140:360-371.
- Kim, S.H., P.G. McQueen, M.K. Lichtman, E.M. Shevach, L.A. Parada, and T. Misteli. 2004. Spatial genome organization during T-cell differentiation. *Cytogenet Genome Res.* 105:292-301.
- King, M.C., C.P. Lusk, and G. Blobel. 2006. Karyopherin-mediated import of integral inner nuclear membrane proteins.[see comment]. *Nature.* 442:1003-1007.
- Korfali, N., G.S. Wilkie, S.K. Swanson, V. Srsen, D.G. Batrakou, E.A. Fairley, P. Malik, N. Zuleger, A. Goncharevich, J. de Las Heras, D.A. Kelly, A.R. Kerr, L. Florens, and E.C. Schirmer. 2010. The leukocyte nuclear envelope proteome varies with cell activation and contains novel transmembrane proteins that affect genome architecture. *Mol Cell Proteomics.* 9:2571-2585.
- Kosak, S.T., J.A. Skok, K.L. Medina, R. Riblet, M.M. Le Beau, A.G. Fisher, and H. Singh. 2002. Subnuclear compartmentalization of immunoglobulin loci during lymphocyte development. *Science.* 296:158-162.
- Kumaran, R.I., and D.L. Spector. 2008. A genetic locus targeted to the nuclear periphery in living cells maintains its transcriptional competence. *J Cell Biol.* 180:51-65.

- Kupper, K., A. Kolbl, D. Biener, S. Dittrich, J. von Hase, T. Thormeyer, H. Fiegler, N.P. Carter, M.R. Speicher, T. Cremer, and M. Cremer. 2007. Radial chromatin positioning is shaped by local gene density, not by gene expression. *Chromosoma*. 116:285-306.
- Kuroda, M., H. Tanabe, K. Yoshida, K. Oikawa, A. Saito, T. Kiyuna, H. Mizusawa, and K. Mukai. 2004. Alteration of chromosome positioning during adipocyte differentiation. *J Cell Sci*. 117:5897-5903.
- Lai, F.P., R.A. Mutalif, S.C. Phua, and C.L. Stewart. 2010. Informatics-based analysis of mechanosignaling in the laminopathies. *Methods Cell Biol*. 98:323-335.
- Lee, K.K., T. Haraguchi, R.S. Lee, T. Koujin, Y. Hiraoka, and K.L. Wilson. 2001. Distinct functional domains in emerin bind lamin A and DNA-bridging protein BAF. *J Cell Sci*. 114:4567-4573.
- Lusk, C.P., G. Blobel, and M.C. King. 2007. Highway to the inner nuclear membrane: rules for the road. *Nat Rev Mol Cell Biol*. 8:414-420.
- Ma, Y., S. Cai, Q. Lv, Q. Jiang, Q. Zhang, Sodmergen, Z. Zhai, and C. Zhang. 2007. Lamin B receptor plays a role in stimulating nuclear envelope production and targeting membrane vesicles to chromatin during nuclear envelope assembly through direct interaction with importin beta. *J Cell Sci*. 120:520-530.
- Makatsori, D., N. Kourmouli, H. Polioudaki, L.D. Shultz, K. McLean, P.A. Theodoropoulos, P.B. Singh, and S.D. Georgatos. 2004. The inner nuclear membrane protein lamin B receptor forms distinct microdomains and links epigenetically marked chromatin to the nuclear envelope. *J Biol Chem*. 279:25567-25573.
- Malhas, A., C.F. Lee, R. Sanders, N.J. Saunders, and D.J. Vaux. 2007. Defects in lamin B1 expression or processing affect interphase chromosome position and gene expression. *J Cell Biol*. 176:593-603.
- Malik, P., N. Korfali, V. Srsen, V. Lazou, D.G. Batrakou, N. Zuleger, D.M. Kavanagh, G.S. Wilkie, M.W. Goldberg, and E.C. Schirmer. 2010. Cell-specific and lamin-dependent targeting of novel transmembrane proteins in the nuclear envelope. *Cell Mol Life Sci*. 67:1353-1369.
- Malik, P., N. Zuleger, and E.C. Schirmer. 2009. Transport of inner nuclear membrane proteins. In *Nuclear Transport*. R. Kehlenbach, editor. Landes Bioscience, Austin. 133-145.
- Mansharamani, M., and K.L. Wilson. 2005. Direct binding of nuclear membrane protein MAN1 to emerin in vitro and two modes of binding to barrier-to-autointegration factor. *J Biol Chem*. 280:13863-13870.
- Marshall, I.C.B., and K.L. Wilson. 1997. Nuclear envelope assembly after mitosis. *Trends Cell Biol*. 7:69-74.
- Mattout-Drubezki, A., and Y. Gruenbaum. 2003. Dynamic interactions of nuclear lamina proteins with chromatin and transcriptional machinery. *Cell Mol Life Sci*. 60:2053-2063.
- Maul, G.G., H.M. Maul, J.E. Scogna, M.W. Lieberman, G.S. Stein, B.Y. Hsu, and T.W. Borun. 1972. Time sequence of nuclear pore formation in phytohemagglutinin-stimulated lymphocytes and in HeLa cells during the cell cycle. *J Cell Biol*. 55:433-447.

- Meaburn, K.J., E. Cabuy, G. Bonne, N. Levy, G.E. Morris, G. Novelli, I.R. Kill, and J.M. Bridger. 2007. Primary laminopathy fibroblasts display altered genome organization and apoptosis. *Aging Cell*. 6:139-153.
- Meaburn, K.J., N. Levy, D. Toniolo, and J.M. Bridger. 2005. Chromosome positioning is largely unaffected in lymphoblastoid cell lines containing emerlin or A-type lamin mutations. *Biochem Soc Trans*. 33:1438-1440.
- Meaburn, K.J., and T. Misteli. 2007. Cell biology: chromosome territories. *Nature*. 445:379-781.
- Mehta, I.S., M. Amira, A.J. Harvey, and J.M. Bridger. 2010. Rapid chromosome territory relocation by nuclear motor activity in response to serum removal in primary human fibroblasts. *Genome Biol*. 11:R5.
- Meinema, A.C., J.K. Laba, R.A. Hapsari, R. Otten, F.A. Mulder, A. Kralt, G. van den Bogaart, C.P. Lusk, B. Poolman, and L.M. Veenhoff. 2011. Long unfolded linkers facilitate membrane protein import through the nuclear pore complex. *Science*. 333:90-93.
- Meister, P., B.D. Towbin, B.L. Pike, A. Ponti, and S.M. Gasser. 2010. The spatial dynamics of tissue-specific promoters during *C. elegans* development. *Genes Dev*. 24:766-782.
- Mewborn, S.K., M.J. Puckelwartz, F. Abuisneineh, J.P. Fahrenbach, Y. Zhang, H. MacLeod, L. Dellefave, P. Pytel, S. Selig, C.M. Labno, K. Reddy, H. Singh, and E. McNally. 2010. Altered chromosomal positioning, compaction, and gene expression with a lamin A/C gene mutation. *PLoS One*. 5:e14342.
- Milner, G.R. 1969. Nuclear morphology and the ultrastructural localization of deoxyribonucleic acid synthesis during interphase. *J Cell Sci*. 4:569-582.
- Mitchell, J.M., J. Mansfeld, J. Capitano, U. Kutay, and R.W. Wozniak. 2010. Pom121 links two essential subcomplexes of the nuclear pore complex core to the membrane. *J Cell Biol*. 191:505-521.
- Morey, C., N.R. Da Silva, M. Kmita, D. Duboule, and W.A. Bickmore. 2008. Ectopic nuclear reorganisation driven by a *Hoxb1* transgene transposed into *Hoxd*. *J Cell Sci*. 121:571-577.
- Moses, M.J. 1956. Studies on nuclei using correlated cytochemical, light, and electron microscope techniques. *J Biophys Biochem Cytol*. 2:397-406.
- Nielsen, J.A., L.D. Hudson, and R.C. Armstrong. 2002. Nuclear organization in differentiating oligodendrocytes. *J Cell Sci*. 115:4071-4079.
- Nili, E., G.S. Cojocaru, Y. Kalma, D. Ginsberg, N.G. Copeland, D.J. Gilbert, N.A. Jenkins, R. Berger, S. Shaklai, N. Amariglio, F. Brok-Simoni, A.J. Simon, and G. Rechavi. 2001. Nuclear membrane protein LAP2beta mediates transcriptional repression alone and together with its binding partner GCL (germ-cell-less). *J Cell Sci*. 114:3297-3307.
- Nissan, T.A., J. Bassler, E. Petfalski, D. Tollervy, and E. Hurt. 2002. 60S pre-ribosome formation viewed from assembly in the nucleolus until export to the cytoplasm. *EMBO J*. 21:5539-5547.
- Ohba, T., E.C. Schirmer, T. Nishimoto, and L. Gerace. 2004. Energy- and temperature-dependent transport of integral proteins to the inner nuclear membrane via the nuclear pore. *J Cell Biol*. 167:1051-1062.

- Osada, S., S.Y. Ohmori, and M. Taira. 2003. XMAN1, an inner nuclear membrane protein, antagonizes BMP signaling by interacting with Smad1 in *Xenopus* embryos. *Development*. 130:1783-1794.
- Ostlund, C., J. Ellenberg, E. Hallberg, J. Lippincott-Schwartz, and H.J. Worman. 1999. Intracellular trafficking of emerin, the Emery-Dreifuss muscular dystrophy protein. *J Cell Sci*. 112:1709-1719.
- Ostlund, C., T. Sullivan, C.L. Stewart, and H.J. Worman. 2006. Dependence of diffusional mobility of integral inner nuclear membrane proteins on A-type lamins. *Biochemistry*. 45:1374-1382.
- Padmakumar VC, Libotte T, Lu W, Zaim H, Abraham S, Noegel AA, Gotzmann J, Foisner R, Karakesisoglou I. 2005. The inner nuclear membrane protein Sun1 mediates the anchorage of Nesprin-2 to the nuclear envelope. *J Cell Sci*. 118(Pt 15):3419-30.
- Pan, D., L.D. Estevez-Salmeron, S.L. Stroschein, X. Zhu, J. He, S. Zhou, and K. Luo. 2005. The integral inner nuclear membrane protein MAN1 physically interacts with the R-Smad proteins to repress signaling by the transforming growth factor- β superfamily of cytokines. *J Biol Chem*. 280:15992-16001.
- Parada, L., and T. Misteli. 2002. Chromosome positioning in the interphase nucleus. *Trends Cell Biol*. 12:425-432.
- Parada, L.A., P.G. McQueen, and T. Misteli. 2004. Tissue-specific spatial organization of genomes. *Genome Biol*. 5:R44.
- Parada, L.A., P.G. McQueen, P.J. Munson, and T. Misteli. 2002. Conservation of relative chromosome positioning in normal and cancer cells. *Curr Biol*. 12:1692-1697.
- Park, P.C., and U. De Boni. 1998. A specific conformation of the territory of chromosome 17 locates ERBB-2 sequences to a DNase-hypersensitive domain at the nuclear periphery. *Chromosoma*. 107:87-95.
- Peric-Hupkes, D., W. Meuleman, L. Pagie, S.W. Bruggeman, I. Solovei, W. Brugman, S. Graf, P. Flicek, R.M. Kerkhoven, M. van Lohuizen, M. Reinders, L. Wessels, and B. van Steensel. 2010. Molecular maps of the reorganization of genome-nuclear lamina interactions during differentiation. *Mol Cell*. 38:603-613.
- Pickersgill, H., B. Kalverda, E. de Wit, W. Talhout, M. Fornerod, and B. van Steensel. 2006. Characterization of the *Drosophila melanogaster* genome at the nuclear lamina. *Nat Genet*. 38:1005-1014.
- Polioudaki, H., N. Kourmouli, V. Drosou, A. Bakou, P.A. Theodoropoulos, P.B. Singh, T. Giannakouros, and S.D. Georgatos. 2001. Histones H3/H4 form a tight complex with the inner nuclear membrane protein LBR and heterochromatin protein 1. *EMBO Rep*. 2:920-925.
- Powell, L., and B. Burke. 1990. Internuclear exchange of an inner nuclear membrane protein (p55) in heterokaryons: in vivo evidence for the interaction of p55 with the nuclear lamina. *J Cell Biol*. 111:2225-2234.
- Prunuske, A.J., and K.S. Ullman. 2006. The nuclear envelope: form and reformation. *Current Opinion in Cell Biology*. 18:108-116.

- Rabl, C. 1885. Über Zelltheilung. *Morphol Jahrb.* 10:214-330.
- Ragoczy, T., M.A. Bender, A. Telling, R. Byron, and M. Groudine. 2006. The locus control region is required for association of the murine beta-globin locus with engaged transcription factories during erythroid maturation. *Genes Dev.* 20:1447-1457.
- Reddy, K.L., J.M. Zullo, E. Bertolino, and H. Singh. 2008. Transcriptional repression mediated by repositioning of genes to the nuclear lamina. *Nature.* 452:243-247.
- Reichart, B., R. Klafke, C. Dreger, E. Kruger, I. Motsch, A. Ewald, J. Schafer, H. Reichmann, C.R. Muller, and M.C. Dabauvalle. 2004. Expression and localization of nuclear proteins in autosomal-dominant Emery-Dreifuss muscular dystrophy with LMNA R377H mutation. *BMC Cell Biol.* 5:12.
- Reichelt, R., A. Holzenburg, E.L. Buhle, Jr., M. Jarnik, A. Engel, and U. Aebi. 1990. Correlation between structure and mass distribution of the nuclear pore complex and of distinct pore complex components. *J Cell Biol.* 110:883-894.
- Rexach, M., and G. Blobel. 1995. Protein import into nuclei: association and dissociation reactions involving transport substrate, transport factors, and nucleoporins. *Cell.* 83:683-692.
- Rolls, M.M., P.A. Stein, S.S. Taylor, E. Ha, F. McKeon, and T.A. Rapoport. 1999. A visual screen of a GFP-fusion library identifies a new type of nuclear envelope membrane protein. *J Cell Biol.* 146:29-44.
- Salpingidou, G., R. Rzepecki, E. Kiseleva, C. Lyon, B. Lane, K. Fusiek, A. Golebiewska, S. Drummond, T.D. Allen, J.A. Ellis, C. Smythe, M.W. Goldberg, and C.J. Hutchison. 2008. NEP-A and NEP-B both contribute to nuclear pore formation in *Xenopus* eggs and oocytes. *J Cell Sci.* 121:706-716.
- Sambrook, J. and Russell, D. (2001). *Molecular Cloning: A Laboratory Manual.* 3rd ed. Cold Spring Harbor Laboratory Press. New York.
- Schardin, M., T. Cremer, H.D. Hager, and M. Lang. 1985. Specific staining of human chromosomes in Chinese hamster x man hybrid cell lines demonstrates interphase chromosome territories. *Hum Genet.* 71:281-287.
- Scherthan, H., S. Weich, H. Schwegler, C. Heyting, M. Harle, and T. Cremer. 1996. Centromere and telomere movements during early meiotic prophase of mouse and man are associated with the onset of chromosome pairing. *J Cell Biol.* 134:1109-1125.
- Schirmer, E.C., L. Florens, T. Guan, J.R.r. Yates, and L. Gerace. 2003. Nuclear membrane proteins with potential disease links found by subtractive proteomics. *Science.* 301:1380-1382.
- Schirmer, E.C., and R. Foisner. 2007. Proteins that associate with lamins: many faces, many functions. *Experimental Cell Research.* 313:2167-2179.
- Schirmer, E.C., and L. Gerace. 2005. The nuclear membrane proteome: extending the envelope. *Trends Biochem Sci.* 30:551-558.
- Shimi, T., T. Koujin, M. Segura-Totten, K.L. Wilson, T. Haraguchi, and Y. Hiraoka. 2004. Dynamic interaction between BAF and emerin revealed by FRAP, FLIP, and FRET analyses in living HeLa cells. *J Struct Biol.* 147:31-41.

- Shoeman, R.L., and P. Traub. 1990. The *in vitro* DNA-binding properties of purified nuclear lamin proteins and vimentin. *J Biol Chem.* 265:9055-9061.
- Solovei, I., M. Kreysing, C. Lanctot, S. Kosem, L. Peichl, T. Cremer, J. Guck, and B. Joffe. 2009. Nuclear architecture of rod photoreceptor cells adapts to vision in mammalian evolution. *Cell.* 137:356-368.
- Solovei, I., L. Schermelleh, K. During, A. Engelhardt, S. Stein, C. Cremer, and T. Cremer. 2004. Differences in centromere positioning of cycling and postmitotic human cell types. *Chromosoma.* 112:410-423.
- Somech, R., S. Shaklai, O. Geller, N. Amariglio, A.J. Simon, G. Rechavi, and E.N. Gal-Yam. 2005. The nuclear-envelope protein and transcriptional repressor LAP2beta interacts with HDAC3 at the nuclear periphery, and induces histone H4 deacetylation. *J Cell Sci.* 118:4017-4025.
- Soullam, B., and H.J. Worman. 1993. The amino-terminal domain of the lamin B receptor is a nuclear envelope targeting signal. *J Cell Biol.* 120:1093-1100.
- Soullam, B., and H.J. Worman. 1995. Signals and structural features involved in integral membrane protein targeting to the inner nuclear membrane. *J Cell Biol.* 130:15-27.
- Stadler, S., V. Schnapp, R. Mayer, S. Stein, C. Cremer, C. Bonifer, T. Cremer, and S. Dietzel. 2004. The architecture of chicken chromosome territories changes during differentiation. *BMC Cell Biol.* 5:44.
- Steen, H.B., and T. Lindmo. 1978. Cellular and nuclear volume during the cell cycle of NHIK 3025 cells. *Cell Tissue Kinet.* 11:69-81.
- Stewart, M. 2007. Molecular mechanism of the nuclear protein import cycle. *Nat Rev Mol Cell Biol.* 8:195-208.
- Strickfaden, H., A. Zunhammer, S. van Koningsbruggen, D. Kohler, and T. Cremer. 2010. 4D chromatin dynamics in cycling cells: Theodor Boveri's hypotheses revisited. *Nucleus.* 1:284-297.
- Szczerbal, I., H.A. Foster, and J.M. Bridger. 2009. The spatial repositioning of adipogenesis genes is correlated with their expression status in a porcine mesenchymal stem cell adipogenesis model system. *Chromosoma.* 118:647-663.
- Taniura, H., C. Glass, and L. Gerace. 1995. A chromatin binding site in the tail domain of nuclear lamins that interacts with core histones. *J Cell Biol.* 131:33-44.
- Tapley, E.C., N. Ly, and D.A. Starr. 2011. Multiple mechanisms actively target the SUN protein UNC-84 to the inner nuclear membrane. *Mol Biol Cell.* 22:1739-1752.
- Theerthagiri, G., N. Eisenhardt, H. Schwarz, and W. Antonin. 2010. The nucleoporin Nup188 controls passage of membrane proteins across the nuclear pore complex. *J Cell Biol.* 189:1129-1142.
- Thomson, I., S. Gilchrist, W.A. Bickmore, and J.R. Chubb. 2004. The radial positioning of chromatin is not inherited through mitosis but is established *de novo* in early G1. *Curr Biol.* 14:166-172.
- Torrise, M.R., L.V. Lotti, A. Pavan, G. Migliaccio, and S. Bonatti. 1987. Free diffusion to and from the inner nuclear membrane of newly synthesized plasma membrane glycoproteins. *J Cell Biol.* 104:733-737.

- Turgay, Y., R. Ungricht, A. Rothballer, A. Kiss, G. Csucs, P. Horvath, and U. Kutay. 2010. A classical NLS and the SUN domain contribute to the targeting of SUN2 to the inner nuclear membrane. *EMBO J.* 29:2262-2275.
- Ulbert, S., M. Platani, S. Boue, and I.W. Mattaj. 2006. Direct membrane protein-DNA interactions required early in nuclear envelope assembly. *J Cell Biol.* 173:469-476.
- Walter, J., L. Schermelleh, M. Cremer, S. Tashiro, and T. Cremer. 2003. Chromosome order in HeLa cells changes during mitosis and early G1, but is stably maintained during subsequent interphase stages. *J Cell Biol.* 160:685-697.
- Wang, Q., X. Du, Z. Cai, and M.I. Greene. 2006. Characterization of the structures involved in localization of the SUN proteins to the nuclear envelope and the centrosome. *DNA Cell Biol.* 25:554-562.
- Watson, M.L. 1955. The nuclear envelope; its structure and relation to cytoplasmic membranes. *J Biophys Biochem Cytol.* 1:257-270.
- Wheeler, M.A., J.D. Davies, Q. Zhang, L.J. Emerson, J. Hunt, C.M. Shanahan, and J.A. Ellis. 2007. Distinct functional domains in nesprin-1alpha and nesprin-2beta bind directly to emerin and both interactions are disrupted in X-linked Emery-Dreifuss muscular dystrophy. *Exp Cell Res.* 313:2845-2857.
- Wilkie, G.S., N. Korfali, S.K. Swanson, P. Malik, V. Srsen, D.G. Batrakou, J. de las Heras, N. Zuleger, A.R. Kerr, L. Florens, and E.C. Schirmer. 2011. Several novel nuclear envelope transmembrane proteins identified in skeletal muscle have cytoskeletal associations. *Mol Cell Proteomics.* 10:M110 003129.
- Wilkie, G.S., and E.C. Schirmer. 2006. Guilt by association: the nuclear envelope proteome and disease. *Mol Cell Proteomics.* 5:1865-1875.
- Williams, R.R., V. Azuara, P. Perry, S. Sauer, M. Dvorkina, H. Jorgensen, J. Roix, P. McQueen, T. Misteli, M. Merckenschlager, and A.G. Fisher. 2006. Neural induction promotes large-scale chromatin reorganisation of the *Mash1* locus. *J Cell Sci.* 119:132-140.
- Worman, H.J., and G. Bonne. 2007. "Laminopathies": a wide spectrum of human diseases. *Exp Cell Res.* 313:2121-2133.
- Worman, H.J., J. Yuan, G. Blobel, and S.D. Georgatos. 1988. A lamin B receptor in the nuclear envelope. *Proc Natl Acad Sci U S A.* 85:8531-8534.
- Wu, W., F. Lin, and H.J. Worman. 2002. Intracellular trafficking of MAN1, an integral protein of the nuclear envelope inner membrane. *J Cell Sci.* 115:1361-1371.
- Yang, L., T. Guan, and L. Gerace. 1997. Integral membrane proteins of the nuclear envelope are dispersed throughout the endoplasmic reticulum during mitosis. *J Cell Biol.* 137:1199-1210.
- Yao, J., R.D. Fetter, P. Hu, E. Betzig, and R. Tjian. 2011. Subnuclear segregation of genes and core promoter factors in myogenesis. *Genes Dev.* 25:569-580.
- Ye, Q., and H.J. Worman. 1994. Primary structure analysis and lamin B and DNA binding of human LBR, an integral protein of the nuclear envelope inner membrane. *J Biol Chem.* 269:11306-11311.
- Ye, Q., and H.J. Worman. 1996. Interaction between an integral protein of the nuclear envelope inner membrane and human chromodomain proteins homologous to *Drosophila* HP1. *J Biol Chem.* 271:14653-14656.

- Zorn, C., C. Cremer, T. Cremer, and J. Zimmer. 1979. *Unscheduled DNA synthesis after partial UV irradiation of the cell nucleus. Distribution in interphase and metaphase. Exp Cell Res.* 124:111-119.
- Zuleger, N., D.A. Kelly, A.C. Richardson, A.R. Kerr, M.W. Goldberg, A.B. Goryachev, and E.C. Schirmer. 2011a. *System analysis shows distinct mechanisms and common principles of nuclear envelope protein dynamics. J Cell Biol.* 193:109-123.
- Zuleger, N., M.I. Robson, and E.C. Schirmer. 2011b. *The nuclear envelope as a chromatin organizer. Nucleus.* 2011 Sep 1;2(5):339-49.
- Zuleger, N. and Schirmer, E.C. (2011). *The nuclear lamina as a chromatin organizer. In: Genome organization and function in the cell nucleus. Ed Karsten Rippe. Wiley.*

APPENDIX

Algorithm for dividing the nuclear area into five concentric rings of roughly equal area

Ring macro.ipm (page #1)

```
1 Option Explicit
2 Sub Open_Image()
3
4     ret = IpMacroStop("Please open outline image", MS_MODAL)
5     ret = IpTemplateMode(1)
6     ret = IpWsLoad("C:\Documents and Settings\James\My Documents\Current Stuff\Images for sherma\c
enpB-R23b\Pos 001\DAPI000.tif", "tif")
7     ret = IpTemplateMode(0)
8
9     'performs best fit so you can see objects
10    ret = IpDrSet(DR_BEST, 0, IPNULL)
11    'loads setting file - ie clean boards
12    ret = IpBlbLoadSetting("C:\Macro ring\data.env")
13    ret = IpMacroStop("If using a sequence please move to the desired frame", MS_MODAL)
14    ret = IpMacroStop("Following this message please position the area of interest over your objec
t ", MS_MODAL)
15
16    'loads region
17    ipRect.Left = 496
18    ipRect.top = 324
19    ipRect.Right = 920
20    ipRect.bottom = 692
21    ret = IpAoiCreateBox(ipRect)
22    ret = IpMacroStop("You may want to check your threshold setting before moving onto the next Pr
ocess Image ", 0)
23
24 End Sub
25
26 Sub Process_Image()
27     ret = IpBlbCount()
28     ret = IpBlbUpdate(0)
29     ret = IpBlbSplitObjects(1)
30     'Apply filters and make mask.
31     ret = IpBlbSetFilterRange(BLEM_AREA, 1000.0, 10000000.0)
32     ret = IpBlbFilter()
33     ret = IpBlbCreateMask()
34     ret = IpFltClose(MORPHO_7x7OCTAGON, 1)
35     ret = IpFltDistance(40, 2)
36     ret = IpFltShow(0)
37     Dim NRanges As Integer, RingSize As Integer, i%
38     NRanges=10
39     RingSize=5
40     ret=IpStGetInt("Enter ring size",RingSize,5,1,100)
41     ret=IpStGetInt("Enter number of zones",NRanges,10,1,15)
42
43     'create new ranges
44     For i=1 To NRanges
45         If i>1 Then IpSegNew("Class " & i)
46             ret = IpSegSetRange(0, (i-1)*RingSize+1, i*RingSize)
47             ret = IpSegPreview(CURRENT_C_T)
48         End If
49     Next i
50     'Apply Ranges to image and save the outlines
51     ret = IpBlbSetAttr(BLOB_AUTORANGE, 0)
52     ret = IpBlbCount()
53     ret = IpBlbUpdate(0)
54     ret = IpBlbSetFilterRange(BLEM_AREA, 0.0, 10000000.0)
55     ret = IpBlbSetAttr(BLOB_OUTLINEMODE,3)
56     ret = IpBlbFilter()
57
58     ret = IpBlbSaveOutline("C:\data.scl")
59
60 End Sub
61
62
```

2-dimensional chromosome positioning algorithm

```
Ring macro.ipm (page #1)
1 Option Explicit
2 Sub Open_Image()
3
4     ret = IpMacroStop("Please open outline image", MS_MODAL)
5     ret = IpTemplateMode(1)
6     ret = IpsLoad("C:\Documents and Settings\James\My Documents\Current Stuff\Images for sherma\c
enpB-R23b\Pos 001\DAPI000.tif", "tif")
7     ret = IpTemplateMode(0)
8
9     'performs best fit so you can see objects
10    ret = IpDrSet(DR BEST, 0, IPNULL)
11    'loads setting file - ie clean boards
12    ret = IpBlbLoadSetting("C:\Macro ring\data.env")
13    ret = IpMacroStop("If using a sequence please move to the desired frame", MS_MODAL)
14    ret = IpMacroStop("Following this message please position the area of interest over your objec
t ", MS_MODAL)
15
16    'loads region
17    ipRect.Left = 496
18    ipRect.top = 324
19    ipRect.Right = 920
20    ipRect.bottom = 692
21    ret = IpAoiCreateBox(ipRect)
22    ret = IpMacroStop("You may want to check your threshold setting before moving onto the next Pr
ocess Image ", 0)
23
24 End Sub
25
26 Sub Process_Image()
27     ret = IpBlbCount()
28     ret = IpBlbUpdate(0)
29     ret = IpBlbSplitObjects(1)
30     'Apply filters and make mask.
31     ret = IpBlbSetFilterRange(BLEM_AREA, 1000.0, 10000000.0)
32     ret = IpBlbFilter()
33     ret = IpBlbCreateMask()
34     ret = IpFltClose(MORPHO 7x7OCTAGON, 1)
35     ret = IpFltDistance(40, 2)
36     ret = IpFltShow(0)
37     Dim NRanges As Integer, RingSize As Integer, i%
38     NRanges=10
39     RingSize=5
40     ret=IpStGetInt("Enter ring size",RingSize,5,1,100)
41     ret=IpStGetInt("Enter number of zones",NRanges,10,1,15)
42
43     'create new ranges
44     For i=1 To NRanges
45         If i>1 Then IpSegNew("Class " & i)
46             ret = IpSegSetRange(0, (i-1)*RingSize+1, i*RingSize)
47             ret = IpSegPreview(CURRENT_C_T)
48         End If
49     Next i
50     'Apply Ranges to image and save the outlines
51     ret = IpBlbSetAttr(BLOB_AUTORANGE, 0)
52     ret = IpBlbCount()
53     ret = IpBlbUpdate(0)
54     ret = IpBlbSetFilterRange(BLEM_AREA, 0.0, 10000000.0)
55     ret = IpBlbSetAttr(BLOB_OUTLINEMODE,3)
56     ret = IpBlbFilter()
57
58     ret = IpBlbSaveOutline("C:\data.scl")
59
60 End Sub
61
62
```

```

80 *****
81 ***   Transfers the data from the Output Window into Excel   **
82 *****
83 *****
84
85   Dim rowposition As Integer
86   Dim position As String
87
88   ret = IpIniFile(GETINT,"RowNum",rowposition)
89   position = CStr(rowposition)
90   ret = IpOutputShow(1)
91   ret = IpDde(DDE_OPEN, "excel", "system")
92   ret = IpDde(DDE_SET, "row", "position")
93   ret = IpDde(DDE_SET, "col", "2")
94   ret = IpOutputSave("", S DDE)
95   ret = IpIniFile(INICMD_SETINT,"RowNum",rowpos + 12)
96 End Sub
97 Sub Process Image()
98 *****
99 *****
100 ***   Takes the DAPI image and converts it into a binary mask filling any   **
101 ***   holes and then erodes it to make 3 AOI of equal areas. Each AOI is   **
102 ***   saved for use later in this macro   **
103 *****
104 *****
105
106 Dim TheArea As Single
107 Dim ErodeArea As Single
108 Dim x As Integer, Y As Integer
109 Dim Divider As Single
110 Dim FileNames As String
111 Dim lVal As Long
112
113   ret = IpBlbLoadSetting("\\129.215.237.150\nzuleger\Macro\maskcount.env") 'Loads measurement se
114   ttings
115
116   *** Section to create the binary mask from the DAPI image**
117   ret = IpBlbSetAttr(BLOB_AUTORANGE, 1) 'Turns on autorange
118   ret = IpBlbSetAttr(BLOB_BRIGHTOBJ, 1) 'Selects bright objects
119   ret = IpBlbCount() 'Counts bright objects
120   ret = IpBlbUpdate(0)
121   ret = IpBlbRemoveHoles() 'Removes any holes in the nucleus
122   ret = IpBlbSetFilterRange(BLBM_AREA, 10000.0, 10000000.0) 'Sets area filter ranges
123   ret = IpBlbFilter() 'Applies Filter ranges to get rid of small objects
124   ret = IpBlbCreateMask() 'Creates the binary mask
125   ret = IpFltClose(MORPHO_11x11OCTAGON, 4) ' Fills in any remaining holes/granules
126
127   *** Section to measure total area of the nucleus**
128   ret = IpBlbShow(1)
129   ret = IpBlbLoadSetting("\\129.215.237.150\nzuleger\Macro\maskcount.env")
130   ret = IpBlbSetAttr(BLOB_AUTORANGE, 1)
131   ret = IpBlbCount()
132   ret = IpBlbUpdate(0)
133   ret = IpDcUpdate(DC_RESET)
134   ret = IpDcSelect("Count_Size", "BLBM_AREA", 0)
135   ret = IpDcUpdate(DC_FETCH)
136
137   ret = IpDcGet(DC_NUMROW, -1, lVal)
138   TheArea = 0
139   For x = 0 To lVal
140     ret = IpDcSet(DC_COL, 0)
141     ret = IpDcSet(DC_ROW, x)
142     ReDim fData(10) As Single
143     ret = IpDcGet(DC_DATA, 1, fData(0))
144     TheArea = TheArea + fData(0)
145   Next x
146   ret = IpBlbSaveOutline("\\129.215.237.150\nzuleger\Macro\Outline1.scl")
147
148   *** Section to erode the total nuclear area and make the 3 equal area AOI**
149   Divider = TheArea/5
150   For x = 2 To 5
151     TheArea = TheArea - Divider 'Sets the target area size for the erode
152     **Loop continually erodes the nucleus until the target area is reached*
153     Do
154       ret = IpFltErode(MORPHO_5x5OCTAGON, 1) 'erodes the nucleus
155       ret = IpBlbSetAttr(BLOB_AUTORANGE, 1) 'Turns on autorange function
156       ret = IpBlbCount() 'Measures area
157       ret = IpBlbUpdate(0)
158       ret = IpDcSelect("Count_Size", "BLBM_AREA", 0)
159       ErodeArea = 0
160       ret = IpBlbData(BLBM_AREA, 0, 1, ErodeArea) 'Gets area measurement
161     Loop Until ErodeArea <= TheArea

```

```

.61     FileNames = "\\129.215.237.150\nzuleger\Macro\Outline" & x & ".scl"
.62     ret = IpBlbSaveOutline(FileNames) 'Saves AOI
.63 Next x
.64
.65     *** Opens the FITC Image and records its ID in a public variable so that it can be selected la
ter**
.66     ret = IpMacroStop("Please open FITC image", MS_MODAL)
.67     ret = IpTemplateMode(1)
.68     ret = IpWsLoad("\\129.215.237.150\nzuleger\backup schirmer pc\210409\New Folder","tif")
.69     ret = IpTemplateMode(0)
.70     ret = IpDocGet(GETACTDOC, 0, FITCIdToMerge)
.71     ret = IpDocGetStr(INF_FILENAME, DOCSEL_ACTIVE, FITCdescript)
.72     ret = IpWsConvertImage(IMC_GRAY12, CONV_USER, 0, 4095, 0, 4095)
.73     ret = IpDocGet(GETACTDOC, 0, FITCId)
.74
.75 End Sub
.76
.77 Sub AOI
.78 Dim NumObj As Integer, x As Integer
.79 ReDim blbpts(1000) As POINTAPI
.80 Dim numpoints As Integer, status As Integer, DupFITCId As Integer,i%
.81 Dim FileName As Variant
.82 Dim ObjCount As Integer, RingArea As Single
.83 Dim ObjCountOutput As Integer,LastObjOnLine%, TotalObjCount%
.84 Dim SegRange(1) As Single, PreviousArea As Single, PreviousIntensity As Single
.85 Dim TheBkGrd As Single, TotalMeanIntensity As Single, TotalArea As Single
.86 Dim TheArea As Single, TheMeanIntensity As Single, TheRing As Single, RingPrevious As Single
.87 Dim linenum As Integer, Y As Integer
.88 Dim Rest As Boolean
.89 ReDim fData(10) As Single
.90 Dim ObjCnt As Integer, z As Integer
.91 Dim TheAnswer As String
.92
.93     *** Load settings files for count/size and data collector **
.94     ret = IpBlbLoadSetting("F:\UserData\Nikolaj\nikisfat.env")
.95     ret = IpDcSelect("Count_Size", "BLBM AREA", 0)
.96     ret = IpDcSelect("Count_Size", "Count", 0)
.97     ret = IpDcMeasList(DC_LOAD,"\\129.215.237.150\nzuleger\Macro\WhoAteAllThePies.dcl")
.98
.99
.100
.101     *****
.102     *           Get Background Value For Subtracting           *
.103     *****
TheAnswer = InputBox("Do you want to background subtract yes/no", "Background Subtraction","yes")
.104
.105 If TheAnswer = "yes" Then
.106     ret = IpDrSet(DR_BEST, 0, IPNULL) 'performs best fit so you can see objects
.107     ret = MsgBox("Position an Ellipse over an area of background")
.108     ret = IpSegSetRange(0, 0, 4095)
.109     ret = IpSegPreview(CURRENT_C_T)
.110     ipICal(0) = 0
.111     ipICal(1) = 4095
.112     ret = IpBlbMultiRanges(ipICal(0), 1)
.113     ret = IpBlbCount()
.114     ret = IpBlbUpdate(0)
.115     ret = IpDcUpdate(DC_FETCH)
.116     ret = IpDcSet(DC_COL, 2)
.117     ret = IpDcSet(DC_ROW, 0)
.118     ret = IpDcGet(DC_DATA, 1, fData(0))
.119     TheBkGrd = fData(0)
.120     fData(0) = 0
.121     ret = IpAoiShow(FRAME_NONE)
.122 Else
.123     TheBkGrd = 0
.124 End If
.125
.126     *****
.127     *           Section to put headings into Output box ready for Excel export           *
.128     *****
.129
.130     ret = IpOutputShow(1)
.131     ret = IpOutputClear()
.132     Debug.Print ""
.133     ret = IpBlbLoadSetting("\\129.215.237.150\nzuleger\Macro\nikisfat3.env")
.134     ret = IpDcMeasList(DC_LOAD,"\\129.215.237.150\nzuleger\Macro\WhoAteAllThePies2.dcl")
.135     *****
.136     *** Get Threshold Range for spots **
.137     *****
.138     ret = IpAppSelectDoc(FITCId) 'Selects FITC image
.139     ret = IpWsDuplicate() 'Duplicates FITC image
.140     ret = IpDocGet(GETACTDOC, 0, DupFITCId) 'Gets the duplicate FITC image number
.141     ret = IpAppSelectDoc(DupFITCId) 'Selects the duplicate FITC image
.142     ret = IpOpNumberArithmetics(TheBkGrd, OPA_SUB, 0)

```



```

441   ret = MsgBox("Threshold Image")
442   ret = IpBlbCount()                               'Measures Areas
443   ret = IpBlbUpdate(0)
444   ret = IpBlbGet(GETRANGE, 0, 0, SegRange(0))      'Gets the segmentation range used to select ob
jects
445   TheFirst = SegRange(0)                          'Variable for lower segmentation range
446   TheSecond = 4095                               'Variable for upper segmentation range
447
448
449   *****
450   *** Section to get total chromosome area and intensity ***
451   *****
452
453   ret = IpBlbLoadOutline("\\129.215.237.150\nzuleger\Macro\Outlinel.scl")          'Applies 1
st AOI outline
454   numpoints = IpBlbGet(GETPOINTS, 0, 1000, blbpts(0)) 'get the outline of the object
455   ret = IpAoiCreateIrregular(blbpts(0), numpoints)
456   ret = IpAoiMultShow(1)
457   ret = IpAoiMultAppend(1)
458   ret = IpBlbSetFilterRange(BLBM_AREA, 10.0, 15000.0)
459   ret = IpBlbCount
460   ret = IpDcUpdate(DC RESET)
461   ret = IpDcSet(DC AUTO, 0)
462   ret = IpDcUpdate(DC FETCH)
463   ret = IpDcSet(DC COL, 1)
464   ret = IpDcGet(DC_DATA, 1, fData(0))
465   NumObj = fData(0)
466   For x = 1 To NumObj
467     ret = IpDcSet(DC_COL, 0)
468     ret = IpDcSet(DC_ROW, (x-1))
469     ret = IpDcGet(DC_DATA, 1, fData(0))
470     TotalArea = fData(0) + TotalArea
471     ret = IpDcSet(DC_COL, 2)
472     ret = IpDcSet(DC_ROW, (x-1))
473     ret = IpDcGet(DC_DATA, 1, fData(0))
474     TotalMeanIntensity = fData(0) + TotalMeanIntensity
475   Next x
476
477   ret = IpBlbDelete()                              'Clears measurements before outlines are placed on image
478   ret = IpDocClose()
479
480   *****
481   *          Apply Outlines to FITC image          *
482   *****
483
484   ret = IpAppSelectDoc(FITCid)                     'Selects FITC image
485   ret = IpWsDuplicate()                            'Duplicates FITC image
486   ret = IpDocGet(GETACTDOC, 0, DupFITCid)          'Gets the duplicate FITC image number
487   ret = IpAppSelectDoc(DupFITCid)                  'Selects the duplicate FITC image
488   ret = IpOpNumberArithmetics(TheBKGrd, OPA_SUB, 0)
489   FileName = "F:\UserData\Nikolaj\Outlinel.scl"    'gets filename of 1st outline to image
490   ret = IpBlbLoadOutline(FileName)                 'Applies 1st AOI outline
491   ***Turn on and set up data collector ***
492   ret = IpDcSet(DC AUTO, 1)
493   ret = IpDcUpdate(DC_RESET)
494   ret = IpDcSelect("Count_Size", "Count", 0)
495
496
497
498   *****
499   *** Outlines ***
500   *****
501   ret = IpBlbGet(GETNUMOBJEX, 0, 0, NumObj) 'Gets the number of outlined nuclei in the image
502   linenum = 5
503   FileName = "\\129.215.237.150\nzuleger\Macro\Outline" + CStr(linenum) + ".scl" 'gets file
name of 1st outline to image
504   ret = IpDcUpdate(DC_RESET)
505   ret = IpBlbLoadOutline(FileName)                 'Applies 1st AOI outline
506   Debug.Print
507   For x = 1 To 5
508     TheRing = TheRing + RingPrevious
509     RingPrevious = TheRing
510     ret = IpBlbGet(GETSTATUS, 0, 0, status)
511     '* Checks if object is in-range and visible *
512     If status >= 0 Then
513       numpoints = IpBlbGet(GETPOINTS, Y, 1000, blbpts(0)) 'get the outline of the object
514       If numpoints > 0 Then
515         ret = IpAoiCreateIrregular(blbpts(0), numpoints)
516         ret = IpAoiMultShow(1)
517         ret = IpAoiMultAppend(1)
518       End If
519     End If

```

```

320
321
322     ret = IpDcSet(DC_COL, 0)
323     ret = IpDcSet(DC_ROW, 0)
324     ret = IpDcGet(DC_DATA, 1, fData(0))
325     TheRing = fData(0)
326     TheRing = TheRing - RingPrevious
327     fData(0) = 0
328     ret = IpDcUpdate(DC_RESET)
329     ret = IpBlbSetRange(TheFirst, TheSecond)
330     ret = IpBlbSetFilterRange(BLEB_AREA, 10.0, 15000.0)
331     ret = IpBlbCount()
332     ret = IpDcSet(DC_COL, 1)
333     ret = IpDcSet(DC_ROW, 0)
334     ret = IpDcGet(DC_DATA, 1, fData(0))
335     ObjCnt = fData(0)
336
337     TheArea = 0
338     For z = 1 To ObjCnt
339         ret = IpDcSet(DC_COL, 0)
340         ret = IpDcSet(DC_ROW, (z-1))
341         ret = IpDcGet(DC_DATA, 1, fData(0))
342         TheArea = fData(0) + TheArea
343         TheArea = fData(0)
344         ret = IpDcSet(DC_COL, 2)
345         ret = IpDcSet(DC_ROW, (z-1))
346         ret = IpDcGet(DC_DATA, 1, fData(0))
347         TheMeanIntensity = fData(0) + TheMeanIntensity
348         TheMeanIntensity = fData(0)
349     Next z
350
351     TheArea = (TheArea/TotalArea)*100
352     TheArea = TheArea - PreviousArea
353     PreviousArea = TheArea + PreviousArea
354     TheMeanIntensity = (TheMeanIntensity/TotalMeanIntensity)*100
355     TheMeanIntensity = TheMeanIntensity - PreviousIntensity
356     PreviousIntensity = TheMeanIntensity + PreviousIntensity
357     Debug.Print linenum; Chr(9);
358     Debug.Print TheRing; Chr(9);
359     Debug.Print ObjCnt; Chr(9);
360     Debug.Print TheArea; Chr(9);
361     Debug.Print TheMeanIntensity;
362     Debug.Print " ";Chr(9);
363     linenum = linenum - 1
364     ret = IpAoiMultAppend(0)
365     ret = IpAoiShow(FRAME_NONE)
366     ret = IpBlbDelete()
367     ret = IpDocClose()
368     ret = IpAppSelectDoc(FITCId)           'Selects FITC image
369     ret = IpWsDuplicate()                 'Duplicates FITC image
370     ret = IpOpNumberArithmetics(TheBkGrd, OPA_SUB, 0)
371     FileName = "\\129.215.237.150\nzuleger\Macro\Outline" + CStr(linenum) + ".scl" 'gets
filename of 1st outline to image
372     ret = IpDcUpdate(DC_RESET)
373     ret = IpBlbLoadOutline(FileName)      'Applies 1st AOI outline
374     Next x
375     Debug.Print FITCdescript;
376 End Sub

```

3-dimensional chromosome positioning algorithm

```
Nik3D Rings Merged_ver3.ipm (page #1)
1 *****
2 ***
3 *** Macro takes a 2 colour deconvolved image and converts the green chromosome
4 *** image and blue dapi image into binary images. The blue dapi binary is used to
5 *** make 6 concentric rings of equal area (+/- 5%). The rings are then applied to
6 *** the chromosome image and the degree of overlap in each ring calculated to give
7 *** the amount of chromosome per ring. NOTE this will only work on 1 cell at a
8 *** time.
9 ***
10 *** Author: David Kelly
11 *****
12
13 Option Explicit
14 Public Increment(5) As Double, subsamp(10) As Double
15 Public xPix As Double, yPix As Double, zPix As Double, NObjects As Double, GreenOb As Single, Green
16 Public FirstGreen As Integer, SecondGreen As Integer, BlueRing(5) As Integer, BlueDistanceID(150) A
17 Public OriginalID As Integer, OriginalGreenID As Integer, TopAnswer As Integer, BottomAnswer As In
18 Public seqinfo As Long
19 Public TheBlue As Integer, TheGreen As Integer
20
21 Sub StartHere
22 *****
23 *** MACRO START POINT **
24 *****
25 OpenTheFile
26 PrepareImage
27 MakeColocalised
28 ret = MsgBox("Macro Finished")
29 End Sub
30 Sub OpenTheFile
31
32 *****
33 *** Subroutine to open the individual images and assign the correct **
34 *** pixel sizes to the image And capture its Image Pro ID number **
35 *****
36
37 ** Opens the Dapi Image
38 ret = MsgBox("Open the Deconvolved DAPI Image")
39 ret = IpTemplateMode(1)
40 ret = IpWsLoad("\\129.215.237.150\coil\NIKStuff\chromosome 13 human\Net37 chr13\NET37chr13-rec
heck\composites", "seq")
41 ret = IpTemplateMode(0)
42 ** pixel size declaration
43 xPix = 0.0645
44 yPix = 0.0645
45 zPix = 0.2
46 ** get number of frames and image ID
47 ret = IpSeqGet(SEQ_NUMFRAMES, seqinfo)
48 ret = IpDocGet(GETACTDOC, 0, OriginalID)
49
50 ** Opens the green chromosome image
51 ret = MsgBox("Open the Deconvolved Green Image")
52 ret = IpTemplateMode(1)
53 ret = IpWsLoad("\\129.215.237.150\coil\NIKStuff\chromosome 13 human\Net37 chr13\NET37chr13-rec
heck\composites", "seq")
54 ret = IpTemplateMode(0)
55 ** get number image ID
56 ret = IpDocGet(GETACTDOC, 0, OriginalGreenID)
57
58 ** Find top and bottom of cell to avoid rendering empty frames and input frame number
59 TopAnswer = InputBox("Find top of cell")
60 BottomAnswer = InputBox("Find Bottom of Cell")
61
62 Make2GreenBinaries
63 MakeBlueDistance
64 End Sub
65 Sub PrepareImage
66 Dim AnswerEnd As Double, AnswerStart As Double, TheStep As Double, Starting As Double
67 Dim FirstGreen As Integer, SecondGreen As Integer, x As Integer, A As Integer
68 Dim dgreen As IPDOCINFO, dblue As IPDOCINFO
69 Dim b As Long
70 Dim InitialVol As Double, Subtractor As Double, CalculatedVol As Double, zpos As Double
71 Dim CountUp As Integer
72
73 *** Section to green chromosomes to 3D Constructor **
74 ret = IpAppSelectDoc(TheGreen)
75 ret = IpRendShow(REND_VIEWER, REND_SHOW)
76 ret = IpRendSize(REND_VIEWER, 752, 607)
77 ret = IpRendSet(REND_VOXELSIZE, xPix, yPix, zPix)
```

```

78  ret = IpRendSet(REND_SUBSAMPLING, subsamp(1), subsamp(2), subsamp(3))
79  ret = IpRendSet(REND_ACTIVE_PORTION, 1, 0, 0)
80  ret = IpRendSet(REND_HI_COLOR, 1, 0, 0)
81  ret = IpRendSet(REND_RESET_OPTIONS, 0, 0, 0)
82  ret = IpRendLoad()
83  ret = IpRendShow(REND_OPTIONS, REND_SHOW)
84  ret = IpRendShow(REND_BCG_DLG, REND_SHOW)
85  ret = IpRendElem(ELEM_GET_VOLUME_INFO, 0, 0, subsamp(1)) ' Gets Sub Sampling parameters
86
87  *****
88  *** Section to add green iso-surface and get volume **
89  *****
90  ret = IpRendSet(REND_ISO_CHANNEL, REND_CH_GREEN, 0, 0)
91  ret = IpRendSet(REND_ISO_SUBSAMPLING, subsamp(1), subsamp(2), subsamp(3))
92  ret = IpRendSet(REND_ISO_FILTER, FLT_3D_None, 0, 0)
93  ret = IpRendSet(REND_ISO_CLOSE_EDGES, 0, 0, 0)
94  ret = IpRendSet(REND_ISO_COUNT, 1, 0, 0)
95  ret = IpRendSet(REND_ISO_SIMPL, ISO_SIMPL_NONE, 0, 0)
96  ret = IpRendElem(ELEM_ADD, IP_REND_ISO_SURF, 0, IPNULL)
97  ret = IpRendElemSet(ELEM_ISO_LEVEL, IP_REND_ISO_SURF, 0, 1.000000)
98
99  * Set Size limit for chromosomes *
100  ipDArray(0)=2.000000
101  ipDArray(1)=1000000000.000000
102  ret = IpRendVMeas(M_FILTER_RANGES_SET, IVM_SurfVolume, ipDArray(0))
103  ret = IpRendVMeasSet(M_UPDATE, 0, 0)
104  **** Gets Volume of green chromosomes *****
105  ret = IpRendVMeas(M_NUM_OBJECTS_GET, 0, Nobjects)
106  ReDim VolSize(Nobjects) As Double
107  ret = IpRendVMeas(M_MEAS_GET, IVM_SurfVolume, VolSize(0))
108  *Loop to get total chromosome size
109  For A = 0 To Nobjects - 1
110     GreenOb = GreenOb + VolSize(A)
111  Next A
112  ret = IpRendElem(ELEM_DELETE, IP_REND_ISO_SURF, 0, IPNULL)
113
114  *****
115  *** Insert Blue image into 3D constructor, and create a 3D distance **
116  *** map from 3d constructor. This map is thresholded prior to **
117  *** creating the 6 concentric rings of the same area **
118  *****
119  ret = IpAppSelectDoc(TheBlue)
120  ret = IpRendSet(REND_VOXELSIZE, xPix, yPix, zPix)
121  ret = IpRendSet(REND_SUBSAMPLING, subsamp(1), subsamp(2), subsamp(3))
122  ret = IpRendSet(REND_ACTIVE_PORTION, 1, 0, 0)
123  ret = IpRendSet(REND_HI_COLOR, 1, 0, 0)
124  ret = IpRendSet(REND_RESET_OPTIONS, 0, 0, 0)
125  ret = IpRendLoad()
126  ret = IpFlt3DDistance(1.000000)
127  ret = IpRendSet(REND_VOXELSIZE, xPix, yPix, zPix)
128  ret = IpRendSet(REND_SUBSAMPLING, subsamp(1), subsamp(2), subsamp(3))
129  ret = IpRendSet(REND_ACTIVE_PORTION, 1, 0, 0)
130  ret = IpRendSet(REND_HI_COLOR, 1, 0, 0)
131  ret = IpRendSet(REND_RESET_OPTIONS, 0, 0, 0)
132  ret = IpRendLoad()
133  ret = IpRendSet(REND_ISO_SUBSAMPLING, subsamp(1), subsamp(2), subsamp(3))
134  ret = IpRendSet(REND_ISO_FILTER, FLT_3D_None, 0, 0)
135  ret = IpRendSet(REND_ISO_CLOSE_EDGES, 0, 0, 0)
136  ret = IpRendSet(REND_ISO_COUNT, 1, 0, 0)
137  ret = IpRendSet(REND_ISO_SIMPL, ISO_SIMPL_NONE, 0, 0)
138  ret = IpRendElem(ELEM_ADD, IP_REND_ISO_SURF, 0, IPNULL)
139  ret = IpRendElemSet(ELEM_ISO_LEVEL, IP_REND_ISO_SURF, 0, 1.000000)
140
141  CountUp = 1
142  ** Loop to calculate the area for each concentric ring
143  IpRendVMeas(M_MEAS_GET, IVM_SurfVolume, InitialVol)
144  Subtractor = InitialVol/6
145  For x = 1 To 5
146     Increment(x) = InitialVol - (Subtractor * x)
147  Next x
148
149  *****
150  *** Loop to extract the 6 regions within the dapi nucleus **
151  *** the regions will then be overlaid with the green **
152  *** chromosomes **
153  *****
154  For x = 1 To 5
155     Do
156        IpRendVMeas(M_MEAS_GET, IVM_SurfVolume, CalculatedVol)
157        If CalculatedVol = InitialVol Then
158           ret = IpRendVMeasSet(M_CREATE_MASK_IMAGE, 0, 0)
159           ret = IpPcTint(TINT_BLUE)

```

```

160         A= 0
161         ret = IpDocGet(GETACTDOC, 0, BlueRing(A))
162         CountUp = CountUp + 2
163         ret = IpRendElemSet(ELEM_ISO_LEVEL, IP_REND_ISO_SURF, 0, CountUp)
164         IpRendVMeas(M_MEAS_GET, TVM_SurfVolume, CalculatedVol)
165     Else
166         ret = IpRendElemSet(ELEM_ISO_LEVEL, IP_REND_ISO_SURF, 0, CountUp)
167         IpRendVMeas(M_MEAS_GET, TVM_SurfVolume, CalculatedVol)
168         CountUp = CountUp + 2
169     End If
170     Loop Until CalculatedVol <= Increment(x)
171     ret = IpRendVMeasSet(M_CREATE_MASK_IMAGE, 0, 0)
172     ret = IpPcTint(TINT_BLUE)
173     ipLVal = IpSCalCreate()
174     ret = IpSCalSetStr(ipLVal, SCAL_UNITS, "microns")
175     ret = IpSCalSetLong(ipLVal, SCAL_ADD_TO_REF, 0)
176     ret = IpSCalSetSng(SCAL_CURRENT_CAL, SCAL_SCALE_X, xPix)
177     ret = IpSCalSetSng(SCAL_CURRENT_CAL, SCAL_SCALE_Y, yPix)
178     ret = IpSCalSetLong(SCAL_CURRENT_CAL, SCAL_APPLY, 0)
179     ret = IpDocGet(GETACTDOC, 0, BlueRing(x))
180     ret = IpAppSelectDoc(BlueRing(x))
181 Next x
182 ret = IpRendElem(ELEM_DELETE, IP_REND_ISO_SURF, 0, IPNULL)
183 End Sub
184 Sub Make2GreenBinaries
185
186 Dim z As Integer, MiddleFrame As Integer, TheGreentemp As Integer
187 '* Set how many frames depending on top and bottom of cell
188 TopAnswer = TopAnswer - BottomAnswer
189 MiddleFrame = ((TopAnswer - BottomAnswer) / 2) + BottomAnswer 'Frame used for thresholding
190
191 '* Select Green image and threshold the chromosomes
192 ret = IpAppSelectDoc(OriginalGreenID)
193 ret = IpBlbSetFilterRange(BLBM_AREA, 100.0, 10000000.0)
194 ret = IpSeqPlay(SEQ_FFRA)
195 ret = IpBlbSetAttr(BLOB_AUTORANGE, 0)
196 ret = IpSeqShow(1)
197 ret = IpSeqSet(SEQ_ACTIVEFRAME, MiddleFrame)
198 ret = MsgBox("Threshold the chromosomes")
199 ret = IpSeqSet(SEQ_ACTIVEFRAME, BottomAnswer)
200 *****
201 '* Make binary mask images of each selected frame *
202 '* based on the threshold values for the chromosome *
203 *****
204 For z = BottomAnswer To (TopAnswer + BottomAnswer)
205     ret = IpBlbCount()
206     ret = IpBlbUpdate(0)
207     ret = IpBlbCreateMask()
208     ret = IpDocGet(GETACTDOC, 0, GreenDistanceID(z))
209     ret = IpAppSelectDoc(OriginalGreenID)
210     ret = IpBlbDelete()
211     ret = IpSeqPlay(SEQ_NEXT)
212 Next z
213 ret = IpDocClose()
214 *****
215 '* Merge all the binary masks to make 1 image with *
216 '* multiple frames *
217 *****
218 ret = IpAppSelectDoc(GreenDistanceID(BottomAnswer))
219 For z = BottomAnswer To (TopAnswer + BottomAnswer)
220     ret = IpSeqMergeDoc(GreenDistanceID(z), 0, 1)
221 Next z
222 ret = IpPcTint(TINT_GREEN) 'Tint binary image green
223
224 '* Clean up all the binary images by closing them
225 For z = BottomAnswer + 1 To (TopAnswer + BottomAnswer)
226     ret = IpAppSelectDoc(GreenDistanceID(z))
227     ret = IpDocClose()
228 Next z
229 *****
230 '* Put the merged images into 3D constructor with the *
231 '* correct spacings *
232 *****
233
234 ret = IpDocGet(GETACTDOC, 0, TheGreentemp)
235 ret = IpRendShow(REND_VIEWER, REND_SHOW)
236 ret = IpRendShow(REND_OPTIONS, REND_SHOW)
237 ret = IpRendSet(REND_VOXELSIZE, xPix, yPix, zPix)
238 ret = IpRendSet(REND_SUBSAMPLING, subsamp(1), subsamp(2), subsamp(3))
239 ret = IpRendElem(ELEM_GET_VOLUME_INFO, 0, 0, subsamp(1)) ' Gets Sub Sampling parameters
240 ret = IpRendSet(REND_ACTIVE_PORTION, 1, 0, 0)

```

```

241 ret = IpRendSet(REND_HI_COLOR, 1, 0, 0)
242 ret = IpRendSet(REND_RESET_OPTIONS, 0, 0, 0)
243 ret = IpRendLoad()
244 ret = IpRendSet(REND_ISO_SUBSAMPLING, subsamp(1), subsamp(2), subsamp(3))
245 ret = IpRendSet(REND_ISO_FILTER, FLT_3D_None, 0, 0)
246 ret = IpRendSet(REND_ISO_CLOSE_EDGES, 0, 0, 0)
247 ret = IpRendSet(REND_ISO_COUNT, 1, 0, 0)
248 ret = IpRendSet(REND_ISO_SIMPL, ISO_SIMPL_NONE, 0, 0)
249 ret = IpRendElem(ELEM_ADD, IP_REND_ISO_SURF, 0, IPNULL)
250 ipDArray(0) = 2.000000
251 ipDArray(1) = 1000000000.000000
252 ret = IpRendVMeas(M_FILTER_RANGES_SET, IVM_SurfVolume, ipDArray(0))
253 ret = IpRendVMeasSet(M_UPDATE, 0, 0)
254 ret = IpRendElemSet(ELEM_ISO_LEVEL, IP_REND_ISO_SURF, 0, 255.000000)
255 ret = IpRendVMeasSet(M_CREATE_MASK_IMAGE, 0, 0)
256 ret = IpDocGet(GETACTDOC, 0, TheGreen)
257 ret = IpPcTint(TINT_GREEN)
258 ret = IpRendElem(ELEM_DELETE, IP_REND_ISO_SURF, 0, IPNULL)
259 ret = IpDocGet(GETACTDOC, 0, TheGreen)
260
261 ret = IpAppSelectDoc(TheGreentemp)
262 ret = IpDocClose()
263 ret = IpRendShow(REND_VIEWER, REND_HIDE)
264 End Sub
265 Sub MakeBlueDistance
266 Dim z As Integer
267
268 ret = IpAppSelectDoc(OriginalID) 'Select the original blue
269 ret = IpSeqPlay(SEQ_FFRA)
270 ret = IpBlbSetAttr(BLOB_AUTORANGE, 1) 'Set count to bright objects, no thresholding needed
271 ret = IpBlbSetAttr(BLOB_BRIGHTOBJ, 1)
272 ret = IpSeqSet(SEQ_ACTIVEFRAME, BottomAnswer)
273 *****
274 ** Make binary mask images of each selected frame *
275 ** based on the threshold values for the DAPI *
276 *****
277 For z = BottomAnswer To (TopAnswer + BottomAnswer)
278 ret = IpBlbCount()
279 ret = IpBlbUpdate(0)
280 ret = IpBlbCreateMask()
281 ret = IpFltClose(MORPHO_5x5OCTAGON, 14)
282 ret = IpDocGet(GETACTDOC, 0, BlueDistanceID(z))
283 ret = IpAppSelectDoc(OriginalID)
284 ret = IpBlbDelete()
285 ret = IpSeqPlay(SEQ_NEXT)
286 Next z
287 *****
288 ** Merge all the binary masks to make 1 image with *
289 ** multiple frames *
290 *****
291 ret = IpAppSelectDoc(BlueDistanceID(BottomAnswer))
292 For z = BottomAnswer To (TopAnswer + BottomAnswer)
293 ret = IpSeqMergeDoc(BlueDistanceID(z), 0, 1)
294 Next z
295 ret = IpPcTint(TINT_BLUE) 'Tint binary image blue
296
297 ** Clean up all the binary images by closing them
298 For z = BottomAnswer + 1 To (TopAnswer + BottomAnswer)
299 ret = IpAppSelectDoc(BlueDistanceID(z))
300 ret = IpDocClose()
301 Next z
302 ret = IpDocGet(GETACTDOC, 0, TheBlue)
303
304 End Sub
305 Sub MakeColocalised
306 Dim z As Integer, DeleteA As Integer, DeleteB As Integer, A As Integer, C As Integer
307 Dim ColocVol As Single
308 Dim Percentage As Single
309 Dim OutData(5) As String
310 Dim AreaVal(6) As Single, PercentageVal(6) As Single
311 Dim tmp As String * 100, GetTheVal As String, Output1 As String, Output2 As String
312 Dim retval As Single
313 Dim ColCount As Integer, RowCount As Integer, NewGreen As Integer
314 Dim GreenOneH As Integer, GreenOneW As Integer, BlueOneW As Integer, BlueOneH As Integer
315 Dim CorrectHeight As Single, CorrectWidth As Single
316 Dim dInfo As IPDOCINFO
317
318 ret = IpDde(DDE_OPEN, "excel", "sheet1")
319
320 **** Check Areas of masks match *****
321 C = 0
322 ret = IpAppSelectDoc(BlueRing(1))

```

```

323 ret = IpDocGet(GETDOCINFO, DOCSEL_ACTIVE, dInfo)
324 BlueOneW = dInfo.Width
325 BlueOneH = dInfo.Height
326 ret = IpAppSelectDoc(TheGreen)
327 ret = IpDocGet(GETDOCINFO, DOCSEL_ACTIVE, dInfo)
328 GreenOneW = dInfo.Width
329 GreenOneH = dInfo.Height
330
331 CorrectWidth = GreenOneW - BlueOneW
332 CorrectHeight = GreenOneH - BlueOneH
333
334 If CorrectWidth < 0 Then
335   GreenOneW = GreenOneW + Abs(CorrectWidth)
336   C = 1
337 End If
338
339 If CorrectWidth > 0 Then
340   GreenOneW = GreenOneW - Abs(CorrectWidth)
341   C = 1
342 End If
343
344 If CorrectHeight < 0 Then
345   GreenOneH = GreenOneH + Abs(CorrectHeight)
346   C = 1
347 End If
348
349 If CorrectHeight > 0 Then
350   GreenOneH = GreenOneH - Abs(CorrectHeight)
351   C = 1
352 End If
353 If C = 1 Then
354   ret = IpWsScale(GreenOneW, GreenOneH, 0)
355   ret = IpDocGet(GETACTDOC, 0, NewGreen)
356   ret = IpAppSelectDoc(TheGreen)
357   ret = IpDocClose
358 End If
359
360
361 ret = IpCmpShow( COMP_SHOW )
362 *****
363 ***   First Green Chromosome   **
364 *****
365 For z = 0 To 5
366   ret = IpAppSelectDoc(BlueRing(z))
367   ret = IpCmpNewTint( BlueRing(z), RGB(0, 0, 255) ) 'blue
368   If C = 1 Then
369     ret = IpCmpAddTint( NewGreen, RGB(0, 255, 0) ) 'green
370     ret = IpDocGet(GETACTDOC, 0, DeleteA)
371   Else
372     ret = IpCmpAddTint(TheGreen, RGB(0, 255, 0) ) 'green
373     ret = IpDocGet(GETACTDOC, 0, DeleteA)
374   End If
375
376   ret = IpCmpSet( COMP_MAKESEQUENCE, DOCSEL_ACTIVE, 0 )
377   ret = IpCmpSet( COMP_MAKESEQUENCE, DOCSEL_ACTIVE, 0 )
378   ret = IpDocGet(GETACTDOC, 0, DeleteB)
379   '* Load into 3D Constructor *
380   ret = IpRendSet(REND_CHANNEL, REND_CH_COLOR, 0,0)
381   ret = IpRendSet(REND_VOXELSIZE, xPix, yPix, zPix)
382   ret = IpRendSet(REND_SUBSAMPLING, subsamp(1), subsamp(2), subsamp(3))
383   ret = IpRendSet(REND_ACTIVE_PORTION, 1, 0, 0)
384   ret = IpRendSet(REND_HI_COLOR, 1, 0, 0)
385   ret = IpRendSet(REND_RESET_OPTIONS, 0, 0, 0)
386   ret = IpRendLoad()
387   '* Assess Blue-Green Colocalisation *
388   ret = IpRendSet(REND_ISO_CHANNEL, REND_BLUE_GREEN, 0,0)
389   ret = IpRendSet(REND_ISO_SUBSAMPLING, subsamp(1), subsamp(2), subsamp(3))
390   ret = IpRendSet(REND_ISO_FILTER, FLT_3D_None, 0, 0)
391   ret = IpRendSet(REND_ISO_CLOSE_EDGES, 0, 0, 0)
392   ret = IpRendSet(REND_ISO_COUNT, 1, 0, 0)
393   ret = IpRendSet(REND_ISO_SIMPL, ISO_SIMPL_NONE, 0, 0)
394   ret = IpRendElem(ELEM_ADD, IP_REND_ISO_SURF, 0, IPNULL)
395   ret = IpRendShow(REND_VMEAS_DATA_TABLE, REND_SHOW)
396   '* Set Size limit for chromosomes *
397   ipDArray(0)=2.000000
398   ipDArray(1)=1000000000.000000
399   ret = IpRendVMeas(M_FILTER_RANGES_SET, IVM_SurfVolume, ipDArray(0))
400   ret = IpRendVMeasSet(M_UPDATE, 0, 0)
401   ret = IpRendElemSet(ELEM_ISO_LEVEL, IP_REND_ISO_SURF, 0, 1.000000)
402   '* Calculate Volume and % of total green volume *
403   ret = IpRendVMeas(M_NUM_OBJECTS_GET, 0, NObjects)
404   ReDim VolSize(NObjects) As Double

```

```

405     ret = IpRendVMeas(M_MEAS_GET, IVM_SurfVolume, VolSize(0))
406     For A = 0 To NObjects -1
407         ColocVol = ColocVol + VolSize(A)
408     Next A
409
410     If ColocVol > 0 Then
411         Percentage = (ColocVol / GreenOb) * 100
412         Debug.Print(" Chromosome Area = " & ColocVol & " % of total chromosome = " & Percentag
e & " in nuclear area " & z);
413     Else
414         Debug.Print(" No Colocalisation For Chromosome 1 in Area " & z);
415     End If
416
417     ret = IpRendElem(ELEM_DELETE, IP_REND_ISO_SURF, 0, IPNULL)
418     ret = IpAppSelectDoc(DeleteA)
419     ret = IpDocClose()
420     ret = IpAppSelectDoc(DeleteB)
421     ret = IpDocClose()
422     AreaVal(z) = ColocVol
423     PercentageVal(z) = Percentage
424     Percentage = 0
425     ColocVol = 0
426 Next z
427 ColCount = 0
428 '* Section to find a blank cell in Excel
429 Do
430     ColCount = ColCount + 1
431     GetTheVal = "R2C" + CStr(ColCount)
432     ret = IpDde(DDE_GET, GetTheVal, tmp)
433     retval = Val(tmp)
434 Loop Until retval = 0
435 RowCount = 2
436 '* Output the Area and percentage of chromosome in the ring
437 For z = 0 To 5
438     Output1 = CStr(AreaVal(z))
439     Output2 = CStr(PercentageVal(z))
440     ret = IpDde(DDE_PUT, GetTheVal, Output1)
441     ColCount = ColCount + 1
442     GetTheVal = "R" + CStr(RowCount) + "C" + CStr(ColCount)
443     ret = IpDde(DDE_PUT, GetTheVal, Output2)
444     ColCount = ColCount -1
445     RowCount = RowCount + 1
446     GetTheVal = "R" + CStr(RowCount) + "C" + CStr(ColCount)
447 Next z
448 End Sub
449
450
451

```